MODELING AND ANALYSIS OF POWER TRANSFORMERS UNDER FERRORESONANCE PHENOMENON.

Javier Arturo Corea Araujo

Dipòsit Legal: T 1356-2015

Javier Arturo Corea Araujo

MODELING AND ANALYSIS OF POWER TRANSFORMERS UNDER FERRORESONANCE PHENOMENON

DOCTORAL THESIS

supervised by Dr. Francisco González Molina
and Dr. José Antonio Barrado Rodrigo

Department
of Electronic, Electric and Automatic Control Engineering

UNIVERSITAT ROVIRA I VIRGILI

Tarragona
2015

UNIVERSITAT ROVIRA I VIRGILI

Escola Tècnica Superior d'Enginyeria
Departament d'Enginyeria Electrònica, Elèctrica i Automàtica

Avda. Dels Països Catalans, 26
Campus Sescelades
43007 Tarragona
Tel. (+0034) 977 55 9610
Fax (+0034) 977 55 9605

We STATE that the present study, entitled "*Modeling and Analysis of Power Transformers under Ferroresonance Phenomenon*"", presented by Javier Arturo Corea Araujo for the award of the degree of Doctor, has been carried out under our supervision at the Department of Electronic, Electric and Automatic Control Engineering of this university, and that it fulfills all the requirements to be eligible for the International Doctorate Award.

Tarragona, 29th May 2015

Doctoral Thesis Supervisors

Francisco González Molina

José Antonio Barrado Rodrigo

Acknowledgments

First of all thank God in heaven, because it from HIM where all knowledge comes from.

I would like to express mi gratitude to my supervisors for leading me throughout this 'transient'. To Francisco for his patience and his gentleness when leading our research. He always found the words to say to keep me motivated and focus in the goal. To José Antonio for always being there whiling to help no matter the subject we dealt with. To you both, a sincerely thank you from the bottom of my heart.

I would like also to specially thank to Dr. Juan Martinez Velasco, for taking his own personal time to guide me through the research. Much of this work would not be possible without his knowledge. Dr. Luis Martinez and Dr. Hugo Valderrama thank you for all your support. For each project we have raised, you two always help us and never hesitate to assist us. Thank you for believe in this work.

I like to take a time to thank Dr. Luis Guasch for always being close to this work and always be ready to help and share some wisdom words.

A special metion to Dr. Abdelali El Aroudi without his valuable help all the work in nonlinear dynamics would have been impossible.

All GAEI members also deserve special mention for sharing their experiences: Freddy, Harrynson, Juan Ignacio and Daniel. Many thanks also to Josep Maria Bosque for helping with the experimentation made in the URV.

I would like to especially thank the members of high voltage grup (GRALTA), for having me during the research stage. The experience in Colombia influenced greatly the realization of this work. The professors Guillermo Aponte and Ferley Castro for giving me everything I needed for my research. A Carlos Manrique, Jorge Celis, Andres Ceron, Ricardo Cheverry, Diego Navas, William Cifuentes and Luis Esteves for their friendship and camaraderie. Special thanks to Sindy, Juan Gabriel and Juan Jose for having me in your home and make me feel like family.

There is a lot of people who has contribute this work, directly or indirectly. I'd like to thank my friend Gerardo Guerra and my friends from URV, Julian Cristiano, Victor Balderrama, Fetene Mulugueta, Ángel Ramos. And many more who have share this adventure with me. Thank you all.

There are no words to describe how grateful I am to my beautiful wife Gloria, this would have never been possible without her. My baby boy Óliver you are the keeper of my heart, watching you grow has given me hope every day during this time. This thesis is also dedicated to my mother Flor who has been there my whole life scarifying her hours to allow me to be at this point. To Carlos Murillo for always have those word of refreshment.

Last but not least, to all of those who I share every day, José, Karen, and the crew from the Friday football, Ferran, Anton, Jonathan, Fish. Thank you all.

UNIVERSITAT ROVIRA I VIRGILI
MODELING AND ANALYSIS OF POWER TRANSFORMERS UNDER FERRORESONANCE PHENOMENON.
Javier Arturo Corea Araujo
Dipòsit Legal: T 1356-2015

This work has been funded by:
- The Spanish Government Projects DPI2009-14713-C03-02 and DPI2012-31580.

- Universitat Rovira i Virgili grant URV-PDI-2011

"There are men who fight one day and are good.
There are men who fight one year and are better.
There are some who fight many years and they are better still.
But there are some that fight their whole lives,
these are the ones that are indispensable."
Bertolt Brecht

List of Publications

Journal Publications:

J.A. Corea-Araujo, F. Gonzalez-Molina, J.A. Martinez-Velasco, J.A. Barrado-Rodrigo, and L. Guasch-Pesquer, "**Tools for Characterization and Assessment of Ferroresonance Using 3-D Bifurcation Diagrams,**" *IEEE Transactions on Power Delivery*, vol.29, no.6, pp.2543-2551, Dec. 2014
doi: 10.1109/TPWRD.2014.2320599
Impact Factor: 1.657 (2013)
Position in Field 1 (2013): ENGINEERING, ELECTRICAL & ELECTRONIC - 85 of 248 (Q2)

J.A. Corea-Araujo, J.A. Barrado-Rodrigo, F. Gonzalez-Molina, and L. Guasch-Pesquer, "**Ferroresonance Analysis on Power Transformers Interconnected to Self-Excited Induction Generators**", Electric Power Components and Systems, Taylor & Francis. *Paper in revision, submitted 17-Dec-2014.*
Impact Factor: 0.664 (2013)
Position in Field 1 (2013): ENGINEERING, ELECTRICAL & ELECTRONIC - 181 of 248 (Q3)

Conference Publications:

J.A. Corea-Araujo, F. Gonzalez-Molina, J.A. Martinez-Velasco, J.A. Barrado-Rodrigo, and L. Guasch-Pesquer, **"Tools for ferroresonance characterization,"** *The European EMTP-ATP Users Group (EEUG) Conference*, Zwickau (Germany), September 2012.

J.A. Corea-Araujo, F. Gonzalez-Molina, J.A. Martinez-Velasco, J.A. Barrado-Rodrigo, and L. Guasch-Pesquer, **"An EMTP-based analysis of the switching shift angle effect during energization/de-energization in the final ferroresonance state,"** *International Conference on Power Systems Transients (IPST)*, Vancouver, July 2013.

J. A. Corea-Araujo, F. González-Molina, J. A. Martínez-Velasco, J. A. Barrado-Rodrigo, L. Guasch-Pesquer. **"Ferroresonance Analysis Using 3D Bifurcation Diagrams, "** *IEEE Power and Energy Society General Meeting*, Vancouver, July 2013.

J.A. Corea-Araujo, F. Gonzalez-Molina, J.A. Martinez-Velasco, F. Castro-Aranda, C.A. Manrique-Lemos, J.A. Barrado-Rodrigo, and L. Guasch-Pesquer, **"Three-Phase Transformer Model Validation for Ferroresonance Analysis, "** *IEEE Power and Energy Society General Meeting*, Washington DC, United States, July 2014.

J.A. Corea-Araujo, A. El Aroudi, F. Gonzalez-Molina, J.A. Martinez-Velasco, J.A. Barrado-Rodrigo, and L. Guasch-Pesquer, "**A Harmonic Balance Approach for Bifurcation Analysis of a Ferroresonant Circuit** ", *Annual Seminar on Automation, Industrial Electronics and Instrumentation (SAAEI'14),* At Tangier, Morocco. June 2014

J.A. Corea-Araujo, F. Gonzalez-Molina, J.A. Martinez-Velasco, J.A. Barrado-Rodrigo, and L. Guasch-Pesquer, "**Implementation of a Self-Excited Induction Generator Model Using TACS**", *The European EMTP-ATP Users Group (EEUG) Conference, Sardinia*, Italy, September de 2014

J.A. Corea-Araujo, F. Gonzalez-Molina, J.A. Martinez-Velasco, F. Castro-Aranda, C.A. Manrique-Lemos, J.A. Barrado-Rodrigo, and L. Guasch-Pesquer, "**Single-Phase Transformer Model Validation for Ferroresonance Analysis Including Hysteresis**" *IEEE Power and Energy Society General Meeting*; Denver CO, United States, July 2015.

Index

1 Introduction: Ferroresonance in Power Systems

1.1 INTRODUCTION

Ferroresonance is a general term applied to a wide variety of interactions between capacitors and iron-core inductors resulting in high overvoltages and causing failures in transformers, cables, and arresters. The term, first appeared in the literature in 1920, referring to oscillating phenomena occurring in an electric circuit. Such circuit must contain at least a (applied or induced) source voltage, a nonlinear inductance, a capacitance, and little damping [1], [2]. Ferroresonance in modern power systems can involve large substation transformers, distribution transformers, or instrument transformers. The capacitive effect may be in the form of capacitance of underground cables or transmission lines, capacitor banks, coupling capacitances between double circuit lines or voltage grading capacitors in HV circuit breakers. System events that may initiate ferroresonance include single-phase switching or fusing, or loss of system grounding. Ferroresonance generally occurs during a system unbalance, usually during switching events where capacitances are placed in series with transformer magnetizing impedance, although ferroresonance can be also caused by a parallel association of a capacitor and a nonlinear inductor. Ferroresonance can lead to heating of transformer, due to high peak currents and high core fluxes. High temperatures inside the transformer may weaken the insulation and cause a failure under electrical stresses. To prevent the consequences of ferroresonance, it is necessary to understand the phenomenon, predict and identify it, to finally avoid it or eliminate it. However, this complex phenomenon cannot be analyzed or predicted by computation methods based on linear approximation. Appropriate simulation tools enables predicting and evaluating ferroresonance risk in a power system, considering all possible system parameters values under any operation condition. Because of nonlinearities, the solution of a ferroresonant circuit is usually obtained using time-domain methods; typically, a computer-based numerical integration method such as the EMTP (ElectroMagnetic Transients Program) and like [3].

1.2 THE FERRORESONANCE PHENOMENON

1.2.1 *Resonance in linear circuits*

Resonance occurs in linear circuits when the capacitive reactance equals the inductive reactance at a frequency at which a circuit is driven. In this stage, the collapsing magnetic field of the inductor generates an electric current that serves to charge the capacitor. When the capacitor starts discharging it provides sufficient electric current to induce the magnetic field back into the inductor. This process is repeated continuously at the known resonance frequency. Unwanted resonance can be accompanied with the following symptoms: sustained transient oscillations, high current and high voltages, and disturbances in the operation of communications circuits. Considering the circuit in Figure 1.1a and assuming there is no damping, a general solution can be found for the case when capacitive reactance (X_C) equals inductive reactance (X_L) by means of the graphical method presented in Figure 1.1b. The resonance frequency and the inductor voltage are presented in equations (1.1) and (1.2), respectively,

$$f_0 = \frac{1}{2\pi\sqrt{LC}} \qquad (1.1) \qquad\qquad V_L = E - V_C \qquad (1.2)$$

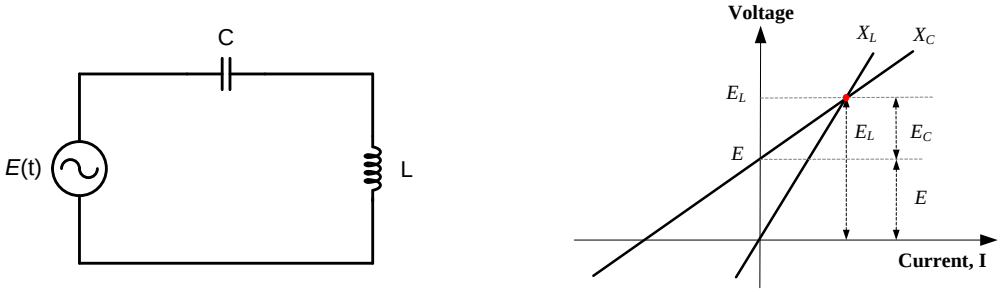

a) Circuit b) Graphical solution

Figure 1.1. Resonant circuit solution

where L and C are the inductance and capacitance of the circuit, respectively, and E is the source voltage. Because the inductance L in a resonant circuit is linear, the steady-state solution for a given frequency is the intersection of the inductive reactance line with the capacitive reactance line, yielding the current in the circuit and the voltage across the inductor. Since iron-core inductors have a nonlinear characteristic and its inductance has a range of values, there might not be a case where the inductive reactance is equal to the capacitive reactance, but yet very high and damaging overvoltages occur. Because the nonlinear nature of ferroresonance phenomenon its analysis results to be very complex. In general, ferroresonance is a series "resonance" that typically involves the saturable magnetizing inductance of a transformer and a capacitive distribution cable or transmission line connected to the transformer. Its occurrence is more likely in the absence of adequate damping.

1.2.2 *Series ferroresonance*

For this case, let's consider the case of RCL circuit having a nonlinear inductor shown in Figure 1.2a. An homologous solution to the one applied in the linear circuit is now shown in Figure 1.2b.

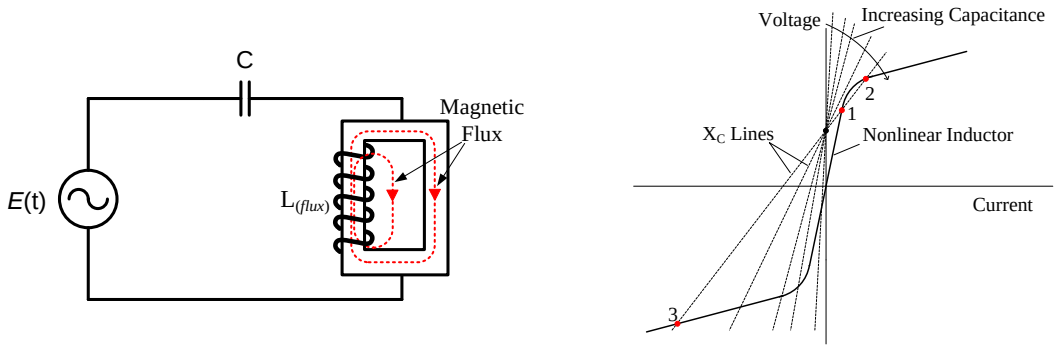

a) Circuit b) Graphical solution

Figure 1.2. Ferroresonance circuit solution

It is evident the existence of at least three intersections between the capacitor line with the nonlinear characteristic of the inductor. Intersection point 2 is an unstable operating point, and the solution will not remain there in the steady state. However, it might pass through this point during a transient. Intersections 1 and 3 are stable and will exist in the steady state. It is obvious that if the solution remains at the intersection point 3, there will be both high voltages and high currents [4]. For small capacitances, the X_C line remains steep resulting in a single intersection in the third quadrant where the capacitive reactance is larger than the inductive reactance, resulting in a leading current and higher than normal voltages across the capacitor. As the capacitance increases, multiple intersections can develop as shown in Figure 1.2b. The natural tendency then is to achieve a solution at intersection 1, which is an inductive solution with lagging current

and little voltage across the capacitor. For a slight increase in the voltage, the capacitor line would shift upward, eliminating the solution at intersection point 1. The solution would then try to jump to the third quadrant. Of course, the resulting current might be so large that the voltage then drops again and the solution point starts jumping between 1 and 3. Under such behavior, voltage and current appear to vary randomly and unpredictably. In a ferroresonance scenario involving a transformer connected to cable sections with sufficient capacitive nature, short lengths of cable have very small capacitance and there is one solution in the third quadrant at relatively low voltage. As the capacitance increases the solution point creeps up the saturation curve in the third quadrant until the voltage across the capacitor raise above normal. These operating points can be relatively stable, depending on the nature of the transient events that precipitated the ferroresonance.

In general, the main differences between a ferroresonant and a linear resonant circuit for a given frequency of the supply source may be summarized as follows:

- ferroresonance may be possible in a wide range of values of C,
- the frequency of the voltage and current waves in the nonlinear circuit may be different from that of the sinusoidal voltage source,
- there can be several stable steady state responses for a given configuration and values of parameters; one is the expected “normal” state that corresponds to the linear characteristic, whereas the other unexpected “abnormal” states are often dangerous for equipment.
- Initial conditions (initial charge on capacitors, residual flux in the core of transformers, switching instant) determine which final response will result.

1.2.3 *Ferroresonance characteristics*

The parametric variation presented in Figure 1.3 assist to better explain the features of a series ferroresonant circuit [5]:

- *Sensitivity to system parameter values:* The curve in Figure 1.3 introduces the interaction of the peak voltage V_L at the terminals of a nonlinear inductance with the peak amplitude E of the sinusoidal voltage source. By gradually varying the peak amplitude E from zero, the same test circuit can present up to three possible different behaviors. The interval between 0 and E_1 present a single solution where any value of E will lead the system to a low voltage output in the inductor. On the contrary, the values between E_4 and E_5 can develop high voltages in the inductor output. In addition, the values surrounding the *TP1* and *TP2* points are the reason why ferroresonance is often called the jumping phenomenon. At such positions, the slightly variation in a parameter system can turn a harmless output into a high overvoltage.
- *Sensitivity to initial conditions*: Ferroresonance is highly dependent on initial conditions. Values such as residual flux, initial capacitor voltage or source phase shift can affect the unfolding of the phenomenon. In Figure 1.3, the interval between E_2 and E_4 demonstrate the co-existence of three different system solutions, the occurrence of any of them is determined only by the initial state of the system. This feature of ferroresonance having co-existence of different solutions for a same set of parameters will be addressed in further chapters.

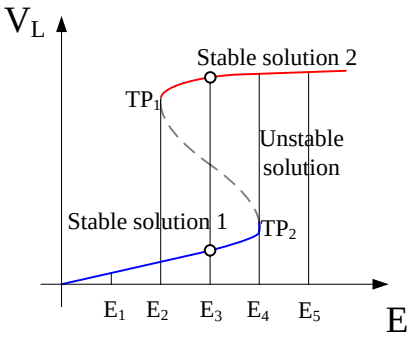

Figure 1.3. Ferroresonance tendency to parameter variation

1.2.4 *Ferroresonant modes*

The ferroresonant behavior can be identified by means of many techniques going from traditional Fourier fast transformation, obtaining the frequency spectrum, to modern nonlinear theory techniques such Poincaré maps or phase planes. This classification corresponds to the steady state condition; i.e., the condition reached once the transient process is over. Reference [6] distinguishes up to four ferroresonant modes:

- ***Fundamental mode:*** Voltages and currents are periodic with a period *T* equal to the power frequency period, and can contain a varying rate of harmonics.
- ***Subharmonic mode:*** The signals are periodic with a period *nT*, which is a multiple of the source period. This state is also known as subharmonic *n* or harmonic 1/n. Its harmonic content is normally of odd order.
- ***Quasi-periodic mode:*** This mode (also called pseudo-periodic) is not periodic and it presents a discontinuous spectrum.
- ***Chaotic mode:*** The signals show an irregular and unpredictable behavior.

Further analysis and introduction to each of the ferroresonance modes will be introduced in Chapter 3.

1.2.5 *Situations favorable to ferroresonance*

Power systems contain a vast range of capacitances and nonlinear inductances among its elements within a wide range of operating conditions. Due to these conditions situations in where ferroresonance can be ignited are almost endless. Ferroresonance may involve large substation transformers, distribution transformers, or instrument transformers. Some of the most common ferroresonance situations considered in the literature involve either a substation transformer or a voltage transformer. A list for both is presented below.

Ferroresonance caused by substation and distribution transformers

Most of ferroresonance cases related to three-phase systems occur when one or two of the source phases are lost while the transformer involved is unloaded or lightly loaded. The loss of one or two phases can happen in the following scenario [7]:

- clearing of single-phase fusing,
- operation of single-phase reclosers or sectionalizers,
- energizing or de-energizing using single-phase switching elements.

Ferroresonance is possible for any transformer core configuration. Three-phase core types provide direct magnetic coupling between phases, where voltages can be induced in the open phase(s) of the transformer. However, whether ferroresonance occurs depends on the type of switching and interrupting devices, type of transformer, the load on the secondary of the transformer, and the length and type of distribution line.

Ferroresonance caused by voltage transformers

The phenomenon is likely to occur on any case when the capacitance of the system, presented in many forms, interacts with the nonlinear inductance of the transformer whether in series or parallel connection. Some of the reported conditions until now are in the form of [8]:

- *Voltage transformer energized through the grading capacitance of an open circuit breaker:* After opening of the circuit-breaker, the grading capacitor remains in series connection with the nonlinear inductance of the transformer core. If the source delivers enough energy through the circuit-breaker grading capacitance a ferroresonance oscillation would be maintained.
- *Voltage transformers connected to ungrounded systems:* A network with ungrounded neutral can randomly switch from a balanced symmetrical operation to a ferroresonance condition and vice-versa as a consequence of a transient (e.g., a fault, a switching operation).
- *Voltage transformers connected to grounded systems:* When a phase-to-ground fault occurs on the higher voltage side, upstream from the transformer, the neutral at this side rises to a high potential. By capacitive coupling between the primary and secondary, overvoltages may appear on the lower voltage side triggering ferroresonance.

Ferroresonance may occur in a wide range of situations. Transformers of any core type and size may be involved.

Capacitive characteristic in power systems

Capacitance sources can be found either in the form of actual capacitor banks [9], or as capacitive coupling. Capacitive coupling effects can be more difficult to identify and the list of manifestations is practically endless:

- series capacitor for line compensation,
- shunt capacitor banks,
- underground cables,
- capacitive coupling,
- double circuit line,
- systems grounded via stray capacitance,
- grading capacitors on circuit breakers,
- generator surge capacitors,
- capacitive coupling internal to transformer.

1.2.6 *Symptoms of ferroresonance*

Ferroresonance is frequently accompanied by some of the following symptoms [6]:

- high permanent overvoltages of differential mode (phase-to-phase) and/or common mode (phase-to-ground),
- high permanent overcurrents,
- high permanent distortions of voltage and current waveforms,
- transformer heating (under no-load operation),
- continuous, excessively loud noise in transformers and reactances,
- damage of electrical equipment due to thermal runaway or insulation breakdown, apparent untimely tripping of protection devices.

Despite detecting many of the symptoms, it might be difficult to conclude if ferroresonance has occurred in many cases unless recording instruments are present. When recordings are not available and there are an important number of symptoms interpretations. The first step is to analyze system configuration while the event is occurring, along with any maneuver preceding it (e.g., transformer energizing, load rejection or broken phase(s)) which might initiate the phenomenon. The next step is to determine whether the conditions necessary for ferroresonance are sufficient to ignite the phenomenon or not (i.e., simultaneous presence of capacitances and non-linear inductances, lightly loaded system components). If there is no evidence of these conditions, ferroresonance is highly unlikely.

1.3 MODELING FOR FERRORESONANCE ANALYSIS

Simulations are of the used to design power systems and to study the ferroresonance phenomenon. However, simulation results have a great sensitivity to the parameters model used and errors when defining nonlinear element are common. Although much effort has been made on programs such as EMTP and like, to refine transformer models, determining nonlinear parameters is probably the biggest modeling difficulty. The transformer model has become probably the most critical element of any ferroresonance study. Different models and different means of determining the parameters are required for each type of core. The following paragraphs describe relevant information for transformer and system modeling.

Single-Phase Transformers models: The traditional *T* Steinmetz model is typically used to model and analyze single-phase transformers. The model is considered topologically correct only for the case where the primary and secondary windings are not concentrically wounded. Errors in leakage representation are not significant, however, unless the core saturates. Obtaining the linear parameters may be difficult considering that even when short circuit tests give total impedance, a judgment must be made as to how this value is divided between the primary and secondary windings.

Model performance depends mainly on the representation of the nonlinear elements, the core resistance R_c and the magnetizing inductance L_m. R_c has traditionally been modeled as a linear resistance. Previous research has shown low sensitivities to fairly large changes in R_c for single-phase transformers, but a high sensitivity for three-phase cores [10]. L_m is typically represented as a piecewise linear λ-i characteristic or as a hysteretic inductance [11], [12], [13]. The linear value of L_m (below the knee of the curve) does not much affect the simulation results [14], although great sensitivities are seen for the shape of the knee and the final slope in saturation. Since factory test data may be insufficient to determine core parameters, it is important that open circuit tests get performed with adequate care in order to extract as much data as possible. For example, the maximum voltage of the test should be as high as the conditions being simulated, otherwise the final λ-i slope of L_m would be guessed by the simulation software. Up to date research [15], [16] has proposed and alternative model also derived from duality theory and presented a specific solution for the leakage representation. This thesis will illustrate the benefits of using such model and will also presents some improvements in the hysteresis representation and modeling addition.

Three-Phase Transformer Models: A simplified model is possible for triplex core configuration by connecting together three single-phase models. However, including the

zero-sequence effects for three-phase single-core transformers is not obvious, and some of the proposed approaches are questionable. A complete transformer representation for the rest of the core types can be obtained by using a coupled inductance matrix (to model the winding characteristics) [17], to which the core equivalent is attached. The inductance matrix is obtained from standard short circuit tests involving all windings. Problems may arise for RMS short circuit data involving windings on different phases, since the current may be non-sinusoidal. The Hybrid Model presented in [18] and [19] is based on this approach. A method of obtaining topologically correct models is based on the duality between magnetic and electrical circuits [20], [21]. This method uses duality transformations, and equivalent circuit derivations reduce inconsistencies in topology. This approach results in models that include saturation in each individual leg of the core, inter-phase magnetic coupling, and leakage effects. Several topology transformer models based on the principle of duality have been presented in the literature [10], [11], [22]-[25]. Factory excitation test reports will not provide the information needed to get the magnetizing inductances for these models. Standards assume the exciting current is the "average" value of the RMS exciting currents of the three phases, which is not correct except for triplex cores, since the currents are not sinusoidal and they are not the same in each phase. Therefore, an extensive analysis of the three-phase topologically correct model will be introduced for ferroresonance analysis in further chapters.

The Study Zone: Parts of the system that must be simulated are the source impedance, the transmission or distribution line(s)/cable(s), the transformer, and any capacitance not already included. Source representation is not generally critical, unless the source contains nonlinearities, and it is sufficient to use the steady-state Thevenin impedance and open-circuit voltage. Lines and cables may be represented as RLC coupled π-equivalents, cascaded for longer lines/cables. Shunt or series capacitors may be represented as a standard capacitance, paralleled with the appropriate resistance. Stray capacitance may also be added either at the corners of open-circuited delta transformer winding or midway along each winding. Other capacitance sources are transformer bushings, interwinding capacitances, and busbar capacitances.

1.4 COMPUTATIONAL METHODS FOR FERRORESONANCE ANALYSIS

In general, the resolution of the mathematical equations describing the power system behavior requires use of computer tools. A time-domain digital simulation is the most common means to study electromagnetic transients in power systems. This approach has obvious advantages since it can confirm the results of another method for a given configuration and parameter values, and provide waveforms of voltages and currents. One of the most popular software used worldwide to analyze power systems is presented below.

1.4.1 *The Electromagnetic Transients Program*

The Electromagnetic Transients Program (EMTP) was based on the early work presented by Dr. Hermann Dommel in Germany in the mid sixties. Its development into the public domain was supported by the Bonneville Power Administration (BPA) in Portland, Oregon [3]. Originally the software target was designing and studying operation problems presented in electric power systems. Nowadays, the software main function still remains the analysis of electromagnetic transients. The name Alternative Transient Program (ATP) was first coined in 1984, right after Drs. Meyer and Liu did

not approve of proposed commercialization of BPA's EMTP motivated by DCG (the EMTP Development Coordination Group) and EPRI (the Electric Power Research Institute). Dr. Liu resigned as DCG Chairman, and Dr. Meyer, using his own personal time, started a new program from a copy of BPA's public-domain EMTP. Since then the EMTP-ATP program has been continuously developed through international contributions; several experts around contribute constantly through the user groups dispersed worldwide. The actual EMTP-ATP focuses in digital simulation of transient phenomena of electromagnetic as well as electromechanical nature and electromagnetic components modeling. Its digital implementation has extensive modeling capabilities and additional important features besides the computation of transients.

Nowadays, EMTP-ATP as wells as BPA's based version are widely used by researchers around the world. Both trends use numerical methods and modeling approaches, to provide significantly system solutions. Some of the EMTP-type programs used are: EMTP-RV, MT-EMTP, or PSCAD-EMTDC. EMTP-ATP is the only version distributed freely of charge. License is easily obtained by demanding it to regional user groups. ATPDraw is the modern graphical preprocessor to the ATP version of the Electromagnetic Transients Program (EMTP) [26]. In ATPDraw it is possible to build digital models of circuits to be simulated using the mouse and selecting predefined components from an extensive palette, interactively. ATPDraw generates the input file for the EMTP-ATP simulation in the appropriate format (FORTRAN based code). ATPDraw is most valuable to new users of ATP-EMTP and is an excellent tool for educational and research purposes. However, the possibility of multi-layer modeling makes ATPDraw a powerful front-end processor for professionals in analysis of electric power system transients, as well. Most part of the simulation and modeling presented in this thesis has been developed in ATPDraw or alternatively in hard-code implementation using EMTP-ATP.

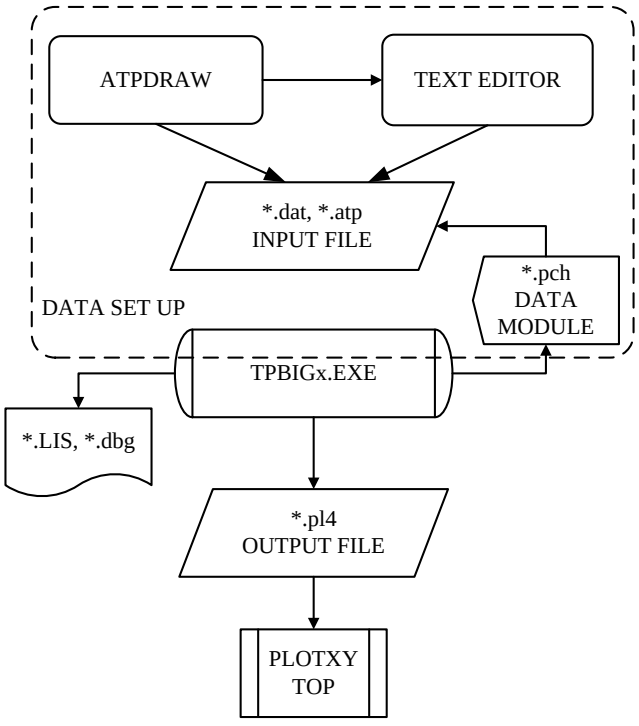

Figure 1.4. Logic sequence of EMTP-ATP

1.4.2 *Alternative solution techniques for ferroresonance analysis*

Since ferroresonance is extremely sensitive to parameter values and to initial conditions, any study performed must include each possible parameter combination. Techniques developed for analysis of nonlinear dynamical systems and chaos can be applied for this purpose [27], [28]. The most suited mathematical framework is the bifurcation theory [29]. Such technique can determine the areas at risk of ferroresonance when a parameter is varied, predicting when spontaneous jumps to dangerous operating conditions will occur. Using such techniques together with methods for direct computation of steady state; that is, methods that enable to obtain steady state solutions without requiring computation of the transient state will significantly assist ferroresonance analysis. Concepts such as attractors, Poincaré sections, bifurcations and basins of attraction provide a framework for discussion and analysis of the ferroresonance phenomenon. Recently, new nonlinear dynamics methods have been applied to the analysis of ferroresonance [30]-[32]. However, the highly complex dynamic nature of ferroresonance has only been limitedly addressed. This thesis will intend in the Chapters to come to introduce some of the methods previously explained and to propose some new analysis techniques.

1.5 MOTIVATION OF THE THESIS

Over the years, the study of ferroresonance phenomenon has presentd a vast area of research. The main focus of researchers around the world relies among four main areas of concern: (1) improving analytical and prediction methods, (2) improving transformer models, (3) analyzing case studies of system level impact and (4) developing of transformer protection and mitigation strategies. There is still a prominent amount of work towards understanding and dealing with ferroresonance. In consequence, the objectives of this Doctoral Thesis held within the first three areas of concern, having the following objectives:

- Study the feasibility to represent power systems cases under ferroresonance situation using ATPDraw.
- Explore the possibility of applying nonlinear dynamic tools in the characterization of the ferroresonance phenomenon.
- Propose new trends in the prediction assessment of ferroresonance phenomenon.
- Study the transformer models response to the ferroresonance phenomenon by determining the laboratory tests needed for its configuration.
- Validate the Hybrid three-phase transformer model for ferroresonance representation.
- Propose a model to understand the hysteresis implication in the development of ferroresonance oscillations.
- Improve the representation of single-phase transformers, by enhancing the π equivalent model including the hysteresis cycle.

1.6 OUTLINE OF THE THESIS

The document is organized as follows:

Chapter 2 introduces the bases of power systems modeling and review several cases studies presenting ferroresonance situations such as: Ferroresonance in a simple RCL circuit, ferroresonance ignited by grading capacitance in voltage transformers, ferroresonance ignited by grading capacitance in sub-station transformers, and ferroresonance in five-legged transformers.

Chapter 3 presents an extensive review of nonlinear techniques for the analysis of ferroresonance, describing its implementation on EMTP-like software. It also introduces the concepts of prediction techniques based on high dimensional maps and its implementation in simulation software.

Chapter 5 describes the experimental test to be performed to configure single- and three-phase transformer models. It also presents the experimental set up to carry out ferroresonance tests in a controlled environment. Finally it validates the Hybrid model for three-phase representation of ferroresonance cases.

Chapter 6 proposes a novel technique to calculate and represent the hysteresis cycle based on Faraday's conceptualization of the flux linked. Besides, the enhancement of the π equivalent model is presented by including the hysteresis effect to validate ferroresonance cases.

Chapter 7 presents the conclusion resulting from this doctoral thesis. It also addresses all the future work consequence of the experimentation carried out throughout the thesis.

1.7 REFERENCES

[1] M. R. Iravani, A. K. S. Chaudhary, W. J. Giewbrecht, I. E. Hassan, A. J. F. Keri, K. C. Lee, J. A. Martinez, A. S. Morched, B. A. Mork, M. Parniani, A. Sarshar, D. Shirmohammadi, R. A. Walling, and D. A. Woodford, "Modeling and Analysis Guidelines for Slow Transients: Part III: The Study of Ferroresonance," *IEEE Transactions on Power Delivery*, vol. 15, no. 1, pp. 255-265, January 2000.

[2] R. Iravani, A. K. S. Chaudhury, I. D. Hassan, J. A. Martinez, A. S. Morched, B. A. Mork, M. Parniani, D. Shirmohammadi, R. A. Walling, "Modeling Guidelines for Low Frequency Transients," Chapter 3 of *Modeling and Analysis of System Transients Using Digital Programs*, A. Gole, J.A. Martinez-Velasco and A. Keri (eds.), IEEE Special Publication TP-133-0, IEEE Catalog No. 99TP133-0, 1998.

[3] H. W. Dommel, S. Bhattacharya, V. Brandwajn, H.K. Lauw, and L. Marti, *EMTP Theory Book*, 2nd ed. Vancouver, BC, Canada: Microtran Power System Analysis Corporation, May 1992.

[4] A. Greenwood, *Electrical transients in power systems*, 1991.

[5] CIGRE Working Group C4.307, Resonance and Ferroresonance in Power Networks and Transformer Energization, *Cigre Technical Brochure no. 569*, February 2014.

[6] P. Ferracci, *Ferroresonance*, Cahier Technique no. 190, Groupe Schneider, 1998.

[7] D. A .N. Jacobson, "Field Testing, Modelling and Analysis of Ferroresonance in a High Voltage Power System", Ph.D. Thesis, The University of Manitoba, 2000.

[8] J. A. Corea-Araujo, F. Gonzalez-Molina, J. A. Martinez-Velasco, J. A. Barrado-Rodrigo, and L. Guasch-Pesquer, "Tools for ferroresonance characterization", *EEUG Conference*, Zwickau, Germany, September 2012.

[9] J.A. Martinez-Velasco, J.R. Martí: *Electromagnetic Transients Analysis, Chapter 12 in Electric energy systems: analysis and operation, Antonio Gomez-Exposito (Ed.)*, Boca Raton, CRC Press, 2008.

[10] B.A. Mork, "Ferroresonance and chaos—Observation and simulation of ferroresonance in a five-legged core distribution transformer," North Dakota State University, Ph.D. dissertation, Publication no. 9227588, UMI Publishing Services, Ann Arbor, MI 48106, (800) 521-0600, May 1992.

[11] J.A. Martinez and B. Mork, "Transformer modeling for low- and mid-frequency transients - A review," *IEEE Transactions on Power Delivery*, vol. 20, no. 2, pp. 1625-

1632, April 2005.

[12] J.A. Martinez, R. Walling, B. Mork, J. Martin-Arnedo, and D. Durbak, "Parameter determination for modeling systems transients. Part III: Transformers," *IEEE Trans. on Power Delivery*, vol. 20, no. 3, pp. 2051-2062, July 2005.

[13] F. de León, P. Gómez, J. A. Martinez-Velasco, and M. Rioual, "Transformers," Chapter 4 of *Power System Transients. Parameter Determination*, J.A. Martinez-Velasco (ed.), CRC Press, 2009.

[14] E. Brenner, "Subharmonic response of the ferroresonance circuit with coil hysteresis," *AIEE Trans.*, vol. 75, pp. 450-456, September 1956.

[15] F. de Leon, A. Farazmand, P. Joseph, "Comparing the T and π Equivalent Circuits for the Calculation of Transformer Inrush Currents", *IEEE Transactions on Power Delivery*, vol.27, no.4, pp.2390-2398, October 2012.

[16] S. Jazebi, A. Farazmand, B. P. Murali, F. de Leon, "A comparative study on π and T equivalent models for the analysis of transformer ferroresonance", *IEEE Transactions on Power Delivery*, vol.28, no.1, pp.526-528, January 2013.

[17] V. Brandwajn, H.W. Dommel, and I.I. Dommel, "Matrix representation of three-phase n-winding transformers for steady-state and transient studies," *IEEE Trans. on Power Apparatus and Systems*, vol. 101, no. 6, pp. 1369-1378, June 1982.

[18] B.A. Mork, F. Gonzalez, D. Ishchenko, D.L. Stuehm, and J. Mitra, "Hybrid transformer model for transient simulation: Part I: Development and parameters," *IEEE Trans. on Power Delivery*, vol. 22, no. 1, pp.248-255, January 2007.

[19] B.A. Mork, D. Ishchenko, F. Gonzalez, and S.D. Cho, "Parameter estimation methods for five-limb magnetic core model," *IEEE Trans. on Power Delivery*, vol. 23, no. 4, pp. 2025-2032, October 2008.

[20] E.C. Cherry, "The duality between interlinked electric and magnetic circuits and the formation of transformer equivalent circuits," *Proc. of the Physical Society*, pt. B, vol. 62, pp. 101–111, 1949.

[21] G.R. Slemon, "Equivalent circuits for transformers and machines including non-linear effects," *Proc. IEE*, vol. 100, Part IV, pp. 129-143, 1953.

[22] C.M. Arturi, "Transient simulation and analysis of a three-phase five-limb step-up transformer following an out of phase synchronization," *IEEE Trans. on Power Delivery*, vol. 6, no. 1, pp. 196-207, January 1991.

[23] A. Narang and R.H. Brierley, "Topology based magnetic model for steady-state and transient studies for three-phase core type transformers," *IEEE Trans. on Power Systems*, vol. 9, no. 3, pp. 1337-1349, August 1994.

[24] B.A. Mork, "Five-legged core transformer equivalent circuit," *IEEE Trans. Power Delivery*, vol. 4, no. 3, pp. 1786–1793, July 1989.

[25] B.A. Mork, "Five-legged wound-core transformer model: Derivation, parameters, implementation, and evaluation," *IEEE Trans. on Power Delivery*, vol. 14, no. 4, pp. 1519-1526, October 1999.

[26] H. K. Høidalen, L. Prikler, J. Hall, "ATPDraw- Graphical Preprocessor to ATP. Windows version", *International Conference in Power Systems Transients (IPST)*, Budapest, 1999

[27] B.A. Mork and D.L. Stuehm, "Application of nonlinear dynamics and chaos to ferroresonance in distribution systems," *IEEE Trans. Power Systems*, vol. 9, no. 2, pp. 1009-1017, April 1994.

[28] R.G. Andrei and B.R. Halley, "Voltage transformer ferroresonance from an energy standpoint," *IEEE Trans. Power Delivery*, vol. 4, no. 3, pp. 1773-1778, July 1989.

[29] P. S Bodger, D. A. Irwin, D. A. Woodford, and A. M. Gole,"Bifurcation Route to Chaos for a Ferroresonant Circuit Using an Electromagnetic Transients Program". *IEEE proceedings of Generation, Transmission and Distribution*, Vol. 143, No. 3, pp. 238-232, May 1996.

[30] S. Mozaffari, M. Sameti, and A. C. Soudack, "Effect of Initial Conditions on Chaotic Ferroresonance in Power Transformers", *IEEE proceedings of Generation, Transmission and Distribution*, Vol. 144, No. 5, pp. 456-460, September 1997.

[31] J. H. B. Deane, "Modelling the Dynamics of Nonlinear lnductor Circuits", *IEEE Transactions on Magnetics*, Vol. 130, No. 5, pp. 2795-2801, September 1994.

[32] B. A. Mork, and D. L. Stuehm, "Application of Nonlinear Dynamics and Chaos to Ferroresonance in Distribution Systems", *IEEE Transactions on Power Delivery*, Vol. 9, No. 2, pp. 1009-1017, April 1994.

2. Practical Ferroresonance case studies

2.1. INTRODUCTION

Modern electrical power systems are constantly growing not only in size but also in complexity. The integration of power electronics and the continuous advances in the generation and transport equipment has turn power systems into a complex large scale grid. Power systems analysis is used as the basic and fundamental gauge to study planning and operating problems [1]. In just a few decades, electrical power researchers have been embarked on the generation of technological advancements on research and development areas. A significant progress in theoretical analysis and numerical calculation has been made. But still, deregulation and increasing demand of energy force power systems most of the time to operate in stress conditions and be subjected to higher risks of instability and more uncertainties [2]. Consequently, power system analysis and simulation tasks have become gradually more difficult and requiring more advanced techniques. Simultaneously, developments of digital computer technology have notably improved enhancing the performance of hardware and software. Nowadays, complex problems can easily be dealt with; for example, load flow issues with large number of nodes and optimal load flow analysis, which were once considered hard problems to solve, have attained practical solutions [3].

After transmission lines, transformers are the most important components of transmission and distribution systems. Its accurate modeling is essential when transients are present in systems to be studied. Many transient phenomena require proper modeling of the nonlinear behavior of the transformer iron-core; magnetization and hysteresis, for example, are fundamental when studying cases such as: ferroresonance in transformers after connection or disconnection maneuvers. Other transients require adequate representation of the frequency-dependent elements such leakage and/or nonlinear parameters. Very high-frequency transients require the accurate representation of all capacitances: to ground, between windings, intersection and even inter-turns. Only after the component models and the overall system representation have been verified, one can confidently proceed to run meaningful simulations. This is an iterative process. If there are some transient events recorded to be compared, more model benchmarking and adjustment may be required. Some useful modeling guidelines can be found for subjects such: power components representation for transient phenomena studies [4], insulation coordination studies when using numerical simulation [5], modeling and analysis of system transients using digital programs [6].

EMTP-like software contains several built-in models that can be directly used for digital simulation of transient phenomena analysis [7], [8]. Using digital programs, complex networks and control systems of arbitrary structure can be efficiently simulated. EMTP extensive modeling capabilities include for example: transformer models, machine models, cable and line models, sources and switches, etc. All together, they may be enough for building a power system network and doing system studies such as steady-state and transient analysis. The goal of this chapter is to present efficient methods and models for different power system situations involving ferroresonance. The key feature is presenting the modeling of non-linear inductances and transformers using different types of embedded EMTP models such as Type-94 inductance, Saturable transformer routine and BCTRAN transformer component.

2.2. MODELING TRANSFORMERS FOR POWER SYSTEM STUDIES: FERRORESONANCE

Among all components in a power system, transformers are unquestionably the equipment demanding the most detailed modeling due to its nonlinear nature. The parameters used in the transformer model should as well be adequate specifically for the type of study to be performed, other way, the simulation may not reproduce the real behavior of the system. The intrinsic difficulty in transformer modeling is due to several factors, among them the type of study to be performed. For ferroresonance analysis, it should be considered that the phenomenon is characterized as a low frequency transient. Thus, the parameters to be considered: core configuration, self and mutual inductances between windings, leakage fluxes and magnetic core saturation [9].

A transformer model can be separated into two parts: representation of windings and representation of iron core. The first part is linear, the second one is nonlinear, and both of them are frequency dependent. Each part plays a different role, depending on the study for which the transformer model is required. For instance, core representation is critical in ferroresonance simulations, but it is usually neglected for load-flow and short-circuit calculations [10].

General step-by-step guidelines where introduced by [11]. The following list can be addressed when selecting models and the system area for simulation of electromagnetic transients:

1. Select the system zone taking into account the frequency range of the transients; the higher the frequencies, the smaller the zone to be modeled.
2. Minimize the part of the system to be represented. An increased number of components do not necessarily mean an increase in accuracy, since there could be a higher probability of insufficient or wrong modeling. In addition, a very detailed representation of a system will usually require longer simulation time.
3. Implement an adequate representation of losses. Its impact for maximum peak voltages and high frequency oscillation is limited. Because of that, they do not play a critical role in many cases. There are, however, some cases for which losses are critical, for example, when defining the magnitude of ferroresonance overvoltage.
4. Consider an ideal representation of some components if the system to be simulated is too complex. Such representation will facilitate the simulation.
5. Perform a sensitivity study if one or several parameters cannot be accurately determined. Results derived from such studies will show which parameters are of concern.

Several criteria can be used to classify transformer models: number of phases, behavior (linear/nonlinear, constant/frequency- dependent parameters), and mathematical models. In this chapter, a brief explanation about transformer model existing in EMTP software is addressed. In addition, the implementation of the models is tested using four different case studies involving: RLC ferroresonant circuit, Voltage transformers, Substation transformers, and Three-phase five-legged transformers.

2.2.1. Transformer modeling

Traditionally, in computational implementation, a two-winding single-phase transformer can be represented by the Steinmetz model or, as has recently proved, by an analogous π shaped equivalent model. Both models are presented in Figure 2.1. The π model has been used to study different transients providing more accuracy when facing highly saturated phenomena such as ferroresonance [12], [13].

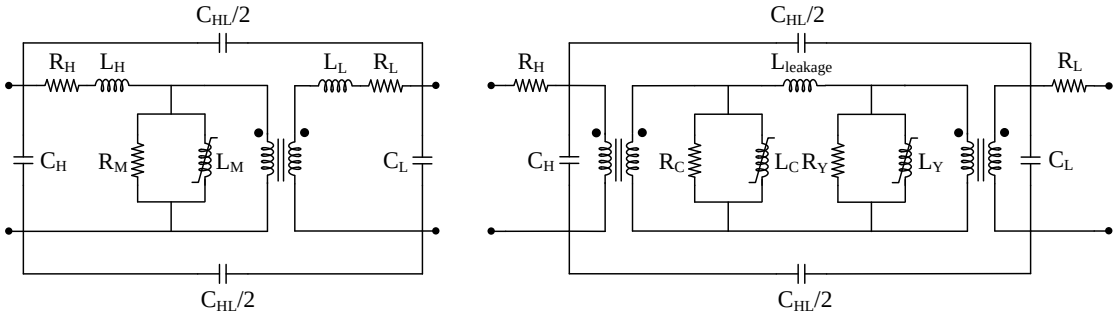

a) T 'Steinmetz' model b) π model

Figure 2.1. Single-phase transformer models.

In EMTP-like software, besides using built-in models it is possible to implement transformer models by simply using general purpose components. In this way, it is also possible, for example, implementing three-phase transformer models. Several papers have been presented describing the correct topologies for a three-legged and five-legged core transformers [14], [15], [16]. In ATPDraw [17], the graphical pre-processor created for ATP, implements an interactive drag-and-drop method, making simpler the design. It will be enough just to collect the components required to draw the circuit. Figure 2.2 presents a circuit representation of a five-legged transformer. A categorized list of the EMTP elements will be described in the coming pages, being its purpose to give an initial introduction of the main components of a power system or a transformer model.

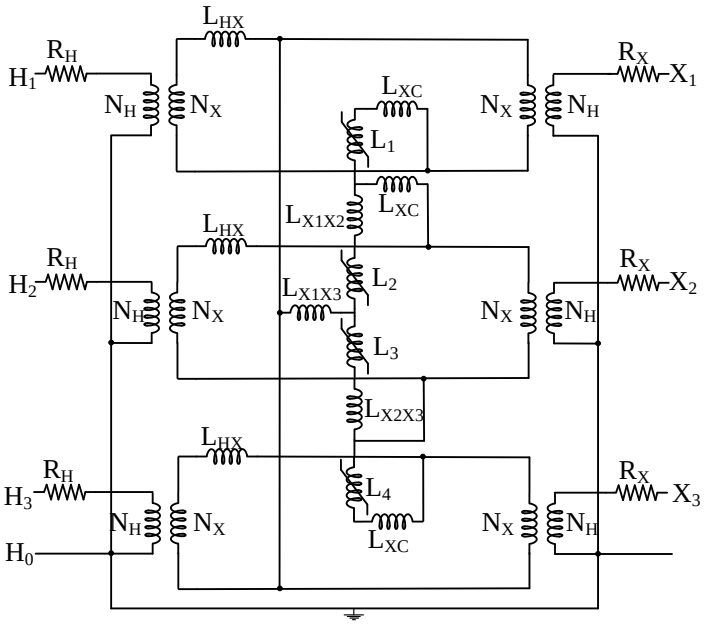

Figure 2.2. Circuit representation of a five-legged transformer.

Table 2.1: EMTP network components

Sources	Switches
• DC source, current or voltage • AC source, current or voltage • Ungrounded AC or DC voltage source • AC source, 3 phase, current or voltage • Ramp source, current or voltage • Two-slope ramp source, current or voltage • Double exponential source • TACS controlled source, current or voltage	• Single phase time controlled • Three-phase time controlled • Voltage controlled • TACS (external) controlled • Statistic (random, based on predefined distribution functions) • Systematic (periodic)

Table 2.1 introduces some of the basic components to assemble power networks. In addition, sources driven by arbitrary signals can be also created by using the transient Analysis of Control Systems (TACS) components, TACS were introduced in EMTP in 1976 to develop model control for HVDC converters. Nowadays, TACS are widely used to model interactions between power systems and control systems. TACS components also assist implementation of harmonics and symmetrical components analysis. EMTP also has some specialized switches that can be externally controlled. It is important to introduce the concept of the current threshold 'I_{mar}'; this feature forces ATP to immediately perform a commutation or to wait a time-step period (Δt).

Table 2.2: EMTP distribution system components

Lines, cables	Transformers

• ***Lumped***
  o RLC equivalent 1, 2, 3 phases
  o RL coupled non-symmetric 2, 3, 2x3 phases
  o RL coupled, symmetric 3, 2x3 phases
• ***Distributed***
  o Transposed 1, 2, 3, 6, 2x3, 9 phase, untransposed 2, 3 phases
• ***LCC line/cable***
  o defined by the geometrical and material data of the line/cable 1…9 phases
  o Bergeron, J-Marti, Noda and Semlyen type of transmission line models
	• Ideal, 1 phase (only the turn ratio can be given)
	• Ideal, 3 phases (only the turn ratio can be given)
	• Saturable, 1 phase (2 windings)
	• Saturable, 3 phases (2 or 3 windings, the winding connection and phase shift can be chosen)
	• Saturable, 3 phases, 3-leg core type (Y/Y only) with high homopolar reluctance
	• BCTRAN
	• Hybrid model

From the elements presented in Table 2.2, probably the most complete component for cable representation is the LCC model where the geometrical and material data of the line/cable have to be provided. Skin effect, bundling and transposition can automatically be taken into consideration. On the other hand, three-phase transformers can be implemented in two different approaches: assembling single-phase transformers or using the built-in models. To use the existent transformer models it is needed, in general, to define the parameters of the magnetizing branch, the voltage, the resistance and the inductance of the windings. The non-linear characteristic can also be provided. Two of the most useful components presented in Table 2.3 are the capacitor and inductor with initial voltage/current features. This allows working with initial conditions, a feature really important when facing dynamic phenomena such as ferroresonance, where the impact of the initial conditions can vary the behavior of the final waveform.

Table 2.3: EMTP RLC components

Linear Elements	Non-linear Elements
• Resistor • Capacitor with damping resistor • Inductor with damping resistor • Series RLC branch, 1 phase • Series RLC branch, 3 phases • Parallel RLC branch, 1 phase • RLC in series, 1 phase • RLC in series, 3 phases • RLC branch 3 phase Y-connected • RLC branch 3 phase D-connected • Capacitor with initial voltage • Inductor with initial current	• Resistor, time-dependent • Resistor, current-dependent • Resistor, TACS (external) controlled • Inductor, current dependent • Inductor, current dependent with initial flux • Hysteresis inductor • Hysteresis inductor with initial flux

2.2.2. Saturable transformer

The Saturable Transformer Component (STC Model) is a single-phase *N*-winding transformer model based on a star-circuit representation [18]. Figure 2.3 presents the circuit.

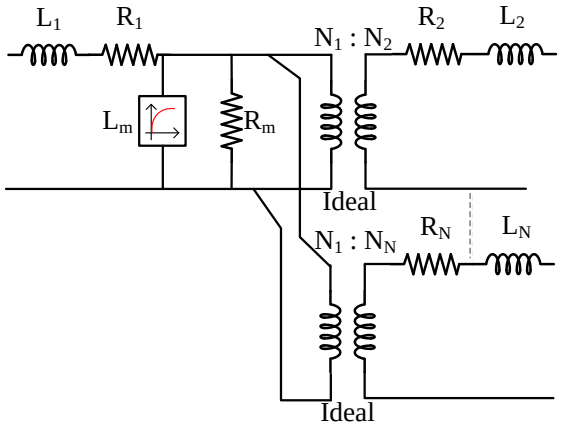

Figure 2.3. Star-circuit representation of single-phase transformer.

The equation of a single-phase N-winding transformer, without including the core, has the form:

$$\left[\frac{di}{dt}\right] = [L]^{-1}[v] - [L]^{-1}[R][i] \tag{2.1}$$

where *[L]*,*[v]*,*[i]*, and *[R]* are the matrix representation of the circuit elements. The primary branch is treated as an uncoupled R-L branch, any additional windings is handled as a two winding ideal transformer. However, the matrix product $[L]^{-1}[R]$ is symmetric, which is not true in for most case [18]. Saturation and hysteresis effects can be modeled by adding an extra nonlinear inductor at the star point. The STC model can be extended to three-phase units through the addition of a zero-sequence reluctance parameter, but its usefulness is limited. The input data consist on the values of each star branch, the turn ratios, and the information for the magnetizing branch. This model has some important limitations: it cannot be used for more than three windings, since the star circuit would not be valid; the magnetizing inductance with resistance, in parallel, is connected to the star point, which is not always the correct topological connecting point; apart from that, numerical instability has been reported for the three-winding case [19], [20].

2.2.3. Matrix Representation (BCTRAN Model)

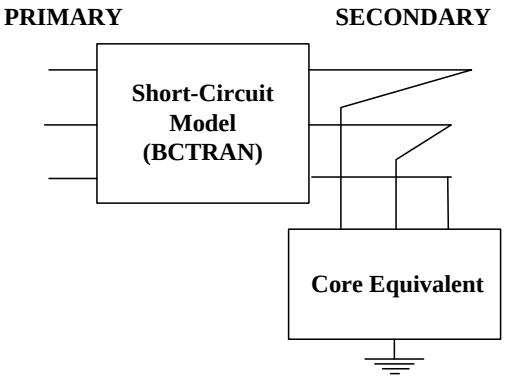

Figure 2.4. Basic BCTRAN model.

The BCTRAN transformer component is a direct EMTP implementation of the transformer matrix modeling. It works supporting the routines developed by Brandwajn [21]-[23], where the steady-state equations represent the multi-phase, multi-winding transformer and are expressed using the branch impedance matrix:

$$[V] = [Z][I] \tag{2.2}$$

In transient calculations, (1) must be rewritten as:

$$[v] = [R][i] + [L][\frac{di}{dt}] \tag{2.3}$$

where *[R]* and *jω[L]* are, respectively, the real and the imaginary part of the impedance matrix *[Z]*, whose elements can be derived from excitation tests. This approach includes phase-to-phase coupling, models terminal characteristics, but does not consider differences in core or winding topology since all core designs receive the same mathematical treatment [24]. There could be some accuracy problems with the previous calculations since the branch impedance matrix *[Z]* can become ill-conditioned either for very small exciting currents or when these currents are totally ignored [25]. To solve these problems, an admittance matrix representation should be used;

$$[I] = [Y][V] \tag{2.4}$$

where *[I]* does always exist and its elements can be obtained directly from standard short-circuit tests. For transient studies, the matrix must be splited up into resistive and inductive components. The transformer can be also described by the following equation:

$$\left[\frac{di}{dt}\right] = [L]^{-1}[v] - [L]^{-1}[R][i] \tag{2.5}$$

All of these models are linear; however, for many transient studies, it is necessary to include saturation and hysteresis effects. The non-linear behavior may not be included directly in the BCTRAN model. This behavior (saturation and/or hysteresis) may be taken into account with the inclusion of an external magnetizing branch connected to the appropriate transformer terminals [9] as seen in Figure 2.4. Such an externally attached core is not always topologically correct, but good enough in many cases. Although this model is theoretically valid only for the frequency at which the nameplate data were obtained, they are reasonably accurate for frequencies below 1 kHz.

2.2.4. The Hybrid Transformer Model

The Hybrid Transformer is a model adequate for low- and mid-frequency transient simulations; it was presented in [26] and [27]. It uses the strength of the inverse inductance matrix for the leakage representation, the principle of duality for core representation, and incorporates capacitive effects and the frequency-dependency of coil resistances.

The modeling of the transformer is based on the magnetic circuit transformed to its electric dual [28], [29]. The leakage and main fluxes are then separated into a core model for the main flux and an inverse inductance matrix for the leakage flux. The copper losses and coil capacitances are added at the terminals of the transformer,

The model is topologically correct, reflecting actual core structure, and including leakages between cores and coils. Since the model represents the actual internal core and coil arrangements, it is a universal model independent of winding connections, which are made up as external jumper connections at the model's terminals. Figure 2.5 shows the main data-entry window for the model as implemented in ATPDraw [17].

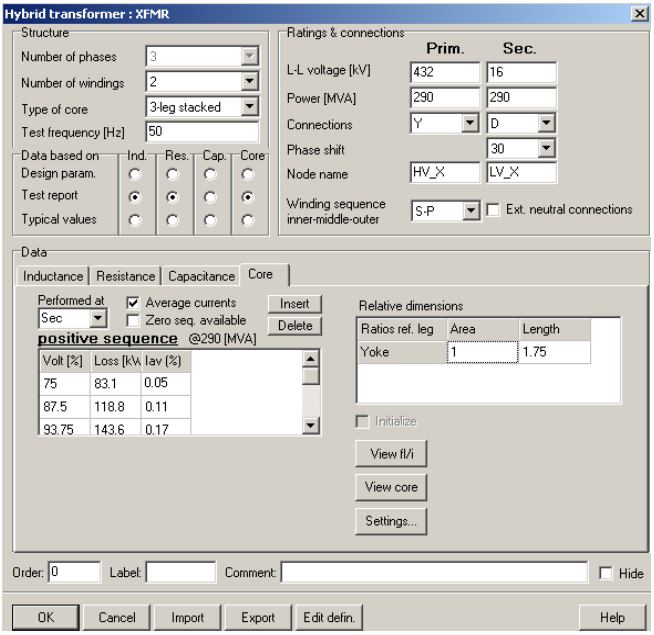

Figure 2.5. Hybrid transformer model in ATPDraw.

Modeling of a transformer using the Hybrid Model can be based on three different data sources: typical values, test report, and design information. The three sources can be selected independently for resistance, inductance, capacitance, and core. Test report input is based on standard open and short circuits tests, with capacitance measurements as an additional option. This is the normal choice of data source for existing transformers. Design data requires the geometry and material parameters of the windings and the core. Such data are rarely available so this option is more for research purposes.

The Typical Value option uses available text book tabulated values of leakage impedance, copper and core losses, and magnetizing current to estimate the transformer model. This is suitable when the transformer is not purchased yet, or data is unavailable in an initial study. However, such option must be used with caution.

2.2.5. Case Study A: Ferroresonant circuit

The ideal starting point for ferroresonance analysis is to consider a simple RLC circuit such as the one presented in Figure 2.6 [24]. Generally speaking, the fundamental requirements for ferroresonance existence are a voltage source, a non-linear inductance, some capacitance and a little damping. Therefore, there are many situations in which a simplified power system network may address the RLC set up. Some examples can be in the form of transformers with: ungrounded neutral, small power demand or no load at all, one or two switch poles open, power supply made through a cable providing the capacitance, etc.

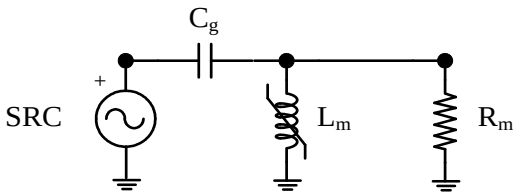

Figure 2.6. Diagram of the test circuit.

The system main parameters are listed below:

- Power Source: 25 kV, 50 Hz, Phase Shift 0^0
- Capacitor (variable): 0.01 - 0.1 - 1 µF
- Resistance: 40 kΩ

Figure 2.7 shows the magnetizing characteristic of the non-linear inductance, and the attached table presents the voltage–current rms curve.

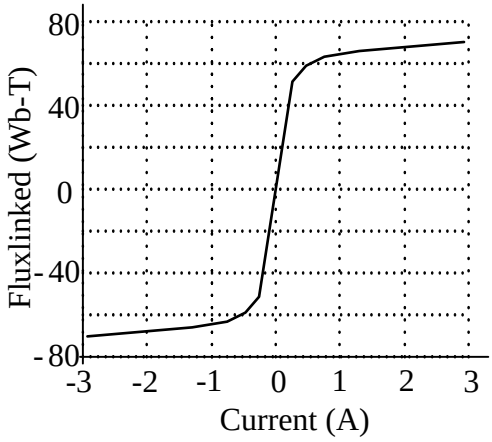

I (Amps)	Fluxlinked(Wb-T)
0.25733	51.4998
0.47475	58.7901
0.75493	63.111
1.30383	65.905
2.91546	70.2259

Figure 2.7. Non-linear inductance characteristic.

The goal of this example is to analyze the influence that the series capacitance and the parallel resistance can have on ferroresonant final conditions. The study will consist in changing the capacitance value and checking its influence on the ferroresonance waveform. The influence of the capacitance will be tested under two possible scenarios: (1) infinite losses ($R_m=\infty$), and (2) normal steady state losses ($R_m=40\ k\Omega$).

Although ferroresonance can be seen as a steady-state phenomenon started after some system failure, in this example all calculations begins with all initial conditions set to zero. This means that no residual flux or initial capacitance voltage are considered. Three different values for the series capacitance have been used for the two cases studied. The results were obtained using an integral the step set to $\Delta t = 1\mu s$.

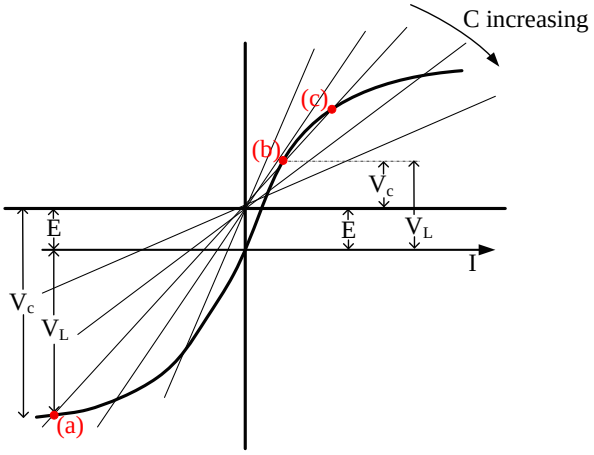

Figure 2.8. Ferroresonance possible operation points.

Figure 2.8 presents the graphic interaction of capacitive V_c and inductive V_L voltages. The analysis is homologous to that [25] showing how higher capacitive values matches highly saturated points. In this study the analysis consists merely on gradually varying the values of the capacitor going from C = 0.01 to C = 0.1 μF and to C = 1 μF, while the rest of parameters remain constant. It also simulates the effect of varying core losses. In a most general way, it is also attempted to corroborate the theory approached in [24] and [30], regarding the operation points of ferroresonance as capacity effect increases.

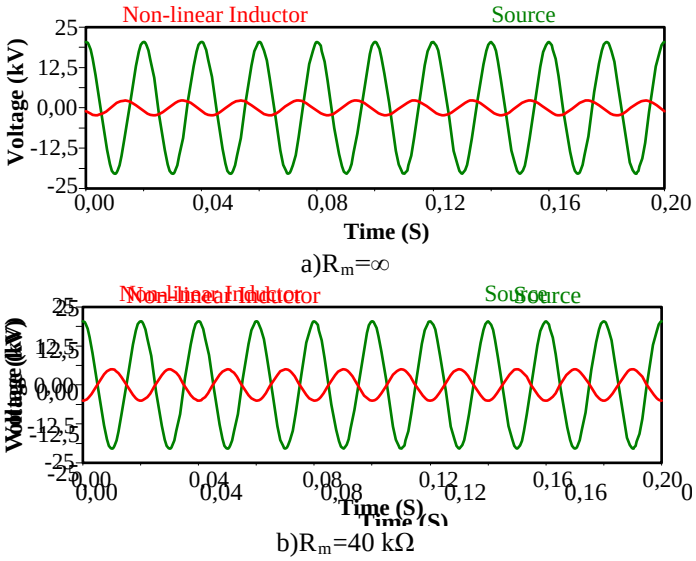

Figure 2.9. Ferroresonance signal response for C=10 nF.

There are few details that must be taken into account when reproducing ferroresonance studies in general. Data such as the phase shift angle is not often available and have a significant impact over the simulation results. In this case, for example, the value used was 0º. It should be kept in mind that ATP sources have been created to work as a function of cosinusoidal signals. Thus, if a purely sinusoidal source is needed to be used, a value of -90º should be used in any ATP source. All the waveforms are sampled during the first 200 ms. The signals presented in Figure 2.9 show the non-linear inductor voltage overlapped to the source voltage. This will allow a clear understanding of the severity of the ferroresonance event. Low capacitance values as 10 nF does not affect the response of the system in a destructive way. The signal presented for both cases cannot be considered as ferroresonance, since only a small sinusoidal induction is obtained. For these cases, the capacitive reactance line represented in Figure 2.8 is

crossing the saturation curve of the inductor at a point where the value of V_L is very low as compared to the source voltage E.

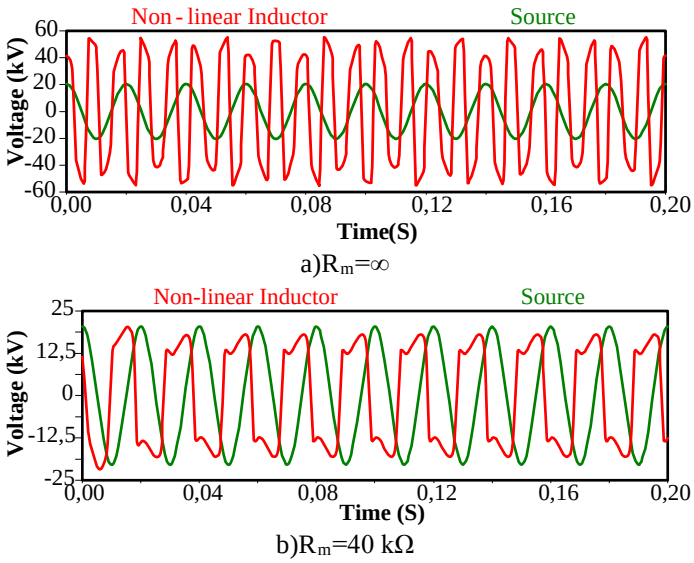

Figure 2.10. Ferroresonance signal response for C=0.1 μF.

Once the capacitance is increased by a factor of ten, C = 0.1 uF, ferroresonance appears. Previous studies suggest a classification for ferroresonance waveform types [30]. According to that classification, Figures 2.10a and 2.10b correspond to quasi-periodic and fundamental modes, respectively. Now, the study continues by analyzing the changes caused by increasing the capacitance values, again, by a factor of ten. Figure 2.11 presents the signal response to a new value of C = 1 μF.

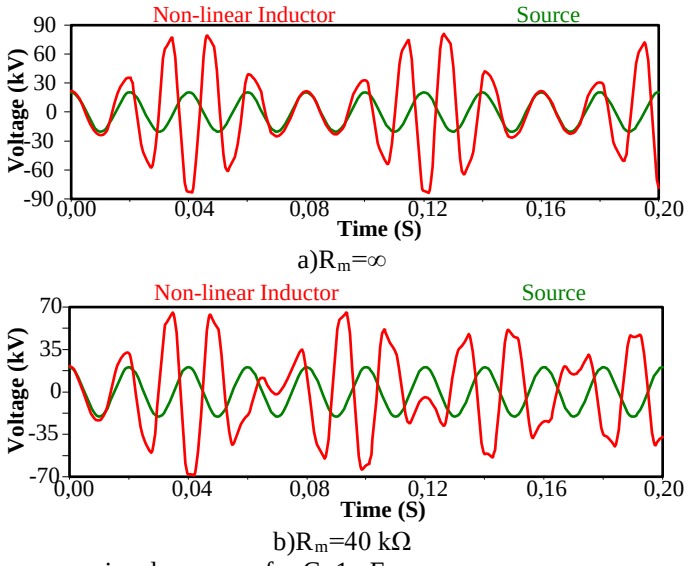

Figure 2.11. Ferroresonance signal response for C=1 μF.

From Figure 2.11, it can be seen that the results are similar in magnitude despite the presence of the core resistance. However, comparing to the classification presented in [30], it is evident that Figure 2.11b presents a chaotic state. From this simply study, two conclusions can be made: (1) Capacitance affects directly the way ferroresonance appears, shaping its form and magnitude; (2) It is important to properly design a transformer core model due to the high impact that the core losses can present in the formation of ferroresonance.

2.2.6. Case study B: Ferroresonant Behavior of a Substation Transformer

One of the most significant modern studies of the phenomenon of ferroresonance was presented by David Jacobson [31]. That work discusses the ferroresonance event occurred to Dorsey transformation station, located in the northern side of Winnipeg, Manitoba (Canada). The relevance of this study lies in the opportunity to model a real ferroresonant situation by using electromagnetic analysis software such EMTP-ATP.

The work explains in detail how ferroresonance phenomenon can be ignited when having an open three-phase switch connected to grading capacitance. Grading capacitors are commonly used in combination with High Voltage circuit breakers with different purposes, for example, to ensure uniform voltage distribution across all contact points during normal and switching system operation. In addition, the work presented by Jacobson provides a vast analysis using nonlinear dynamics [32], [33]. Figure 2.12 shows a complete scheme of the Dorsey station.

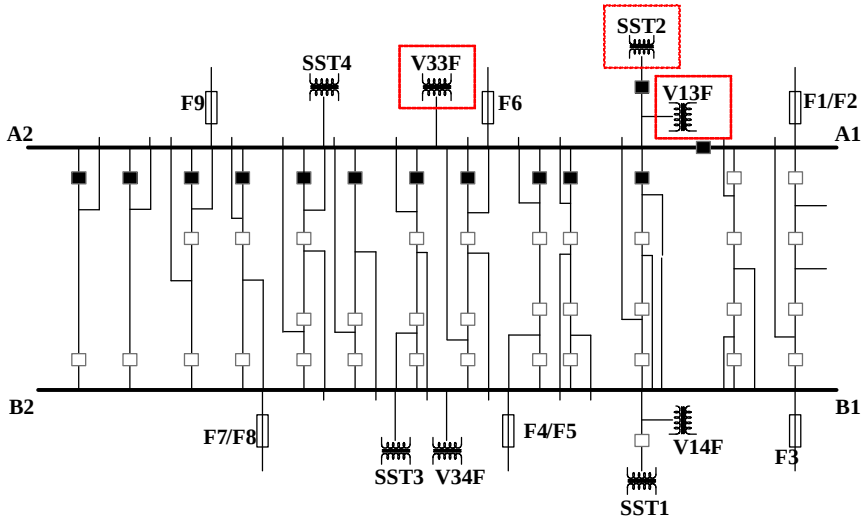

Figure 2.12. Dorsey Power Station, bus configuration.

According to Figure 2.12, the elements of the system are: two high voltage parallel lines of 443m represented by the capital letters A and B, which are responsible for carrying energy to small power stations (buses A and B from now on); Filters to control the stability of signals, numbered from F1 to F9; Small transformer stations (SS standing for sub-station and V standing for voltage transformers); The small squares represent interconnection switches between lines A and B, being the shaded ones the open switches at the moment of the failure.

In order to perform a routine maintenance, all switches shaded (black) in Figure 2.12 were opened to completely disconnect the bus A. Those operations in the network changed the circuit configuration providing the necessary elements for ferroresonance phenomenon appearance. Finally, SST2 went to no load condition producing a catastrophic failure in the voltage transformers V13F and V33F that eventually lead them to explode. In order to understand the new topology of the system, Figure 2.13 shows the equivalent circuit.

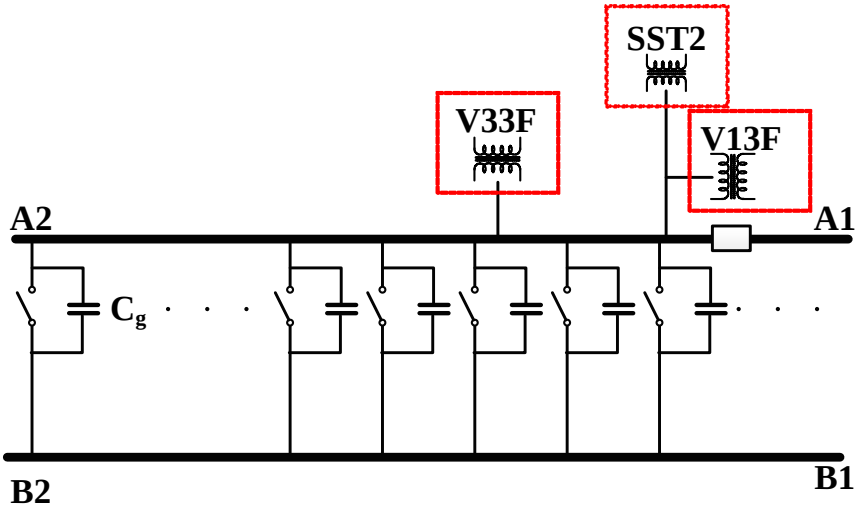

Figure 2.13. Dorsey Power Station, grading capacitance representation.

Figure 2.13 presents in detail the switches configuration, each of them composed by a normal three-phase switch connected in parallel to a grading capacitance (C_g); these capacitor elements have a solid physical connection and are often used to ensure having the same voltage levels and both buses, avoiding external stress in the lines due to current arcs when the contacts are getting opened or closed.

Now, the topology of the system is simpler and understanding the causes of the ferroresonance ignition is less complicated: the opening of the switches between the bus A and bus B, rather than disconnecting the lines, actually made a direct path leading to a series resonant circuit through the grading capacitances; since the bus A will still energizing the transformers V33F, V13F and SST2, from the bus B. Finally, the circuit became prone to ferroresonance when the transformer SST2 got disconnected, decreasing the inductive load in the circuit. At this point, the relationship between all capacitances and inductances surely ignited the ferroresonance phenomenon. Jacobson analyzed this case using the EMTP model shown in Figure 2.14.

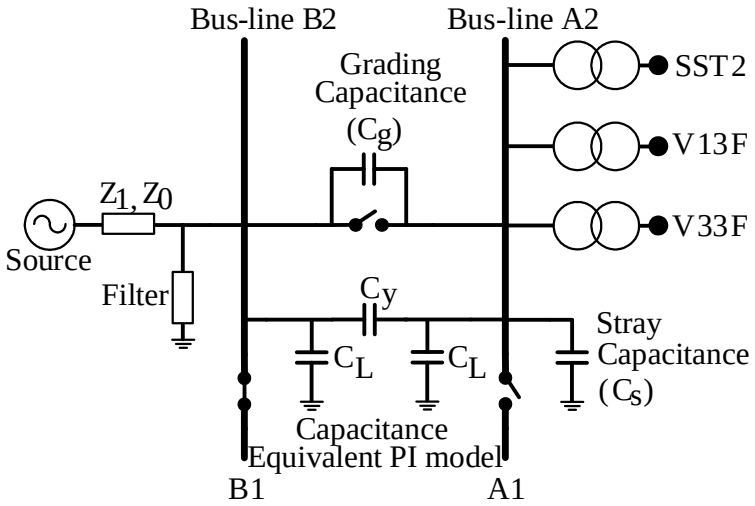

Figure 2.14. Dorsey Power Station, EMTP equivalent circuit.

The EMTP model designed for the ferroresonance study of the Dorsey Station includes all the elements shown in Figure 2.14: source, transformers, system filters, one switch with grading capacitance and the rest of switches between buses represented by an equivalent PI arrangement of capacitance. It is important to note that the cable of the buses is not modeled in any way and only its capacitive effect is considered being concentrated in a single three-phase capacitance representation C_s. All data used in the model are presented below:

- **Power source**: L-L Voltage = 230 kV; Frequency = 60 Hz; Per phase short-circuit impedance = 0.2116 Ω + j4.3801 Ω.
- **Bus-line B1-B2**: Per phase values:
    - Line Filter 1: R = 2.17 Ω; X = 16.72 Ω; C = 0.938 μF.
    - Line Filter 2: R = 1.84 Ω; X = 16.74 Ω; C = 1.31 μF.
- **Bus-lines interconnections**: Represented by a PI arrangement of capacitances with the following values:
    - Series capacitance C_Y = 0.001108 μF.
    - Parallel capacitance C_L = 0.005316 μF.
- **Circuit breaker**: Represented by a grading capacitance, C_g, with variable value.
- **Bus-line A1-A2**: It is represented by a stray capacitance, C_s, with variable value.
- **Voltage transformers (V13F, V33F):**
    - YNyn0 three-phase two-winding transformers.
    - Rated voltages: 230/0.115 kV.
    - Short-circuit test: $R_{sh,1w}$ = 7490 Ω, $X_{sh,1w}$ = 0.001 Ω; $R_{sh,2w}$ = 0.0463 Ω, $X_{sh,2w}$ = 0.1642 Ω.
    - No load test (steady state): Current = 0.00478 A; Flux = 0.38 W-T; Core loss resistance R_m = 9.52 MΩ.
    - Saturation curve shown in Fig. 15.
- **Substation transformer (SST2):**
    - YNy0 Three-phase two-winding transformer, grounded through a 2.4 Ω impedance.
    - Rated voltages = 230/4.16 kV.
    - Short-circuit test: $R_{sh,1w}$ = 12 Ω, $X_{sh,1w}$ = 322.69 Ω; $R_{sh,2w}$ = 0.0012 Ω, $X_{sh,2w}$ = 0.1056 Ω.
    - No load test (steady state): Current = 0.02485 A; Flux = 0.04 W-T; Core loss resistance: R_m = 3.11 MΩ.
    - Saturation curve shown in Fig. 16.
- **Load (connected to V13F and V33F):** Per phase values R = 163.2 Ω and X = 0.268 Ω.

Figure 2.15 and Figure 2.16 presents the saturation curves used for the transformers representation.

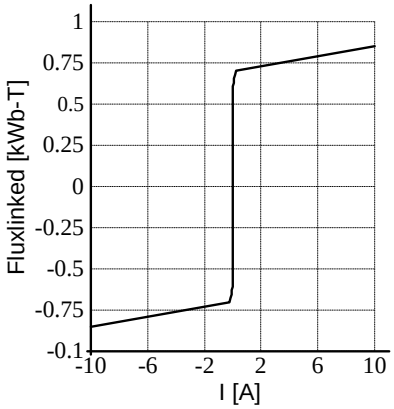

Current (A)	Flux (WB-T)
0.00478023	450.38324
0.00582715	495.42156
0.00995685	539.94220
0.01645366	562.72021
0.02425828	584.98053
0.03498387	607.75853
0.05153677	630.01885
0.07600783	652.79685
0.12093922	675.05717
0.21079611	702.49431
10	850

Figure 2.15. Saturation curve of the voltage transformers (V13F, V33F).

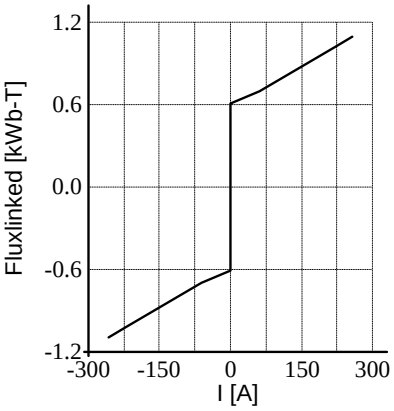

Current (A)	Flux (WB-T)
0.02484975	390.04167
0.06467868	424.9113
0.12967085	458.28649
0.21305588	483.19337
0.26390417	498.13752
0.42907889	537.98848
0.54855853	555.42321
0.76131575	582.82045
1.1461796	607.72742
62.047277	692.41084
221.37816	1016.2005
257.98675	1095.9024

Figure 2.16. Saturation curve of the substation transformer (SST2).

The Dorsey case will be reviewed below. All the results obtained in [34] will be replicated. In addition, an explanation to the discrepancies when simulating the initial transient will be introduced. An extra study on the implication of the switch shift angle will be added. The real-time measurements of phase B, captured for the Dorsey case is presented in Figure 2.17.

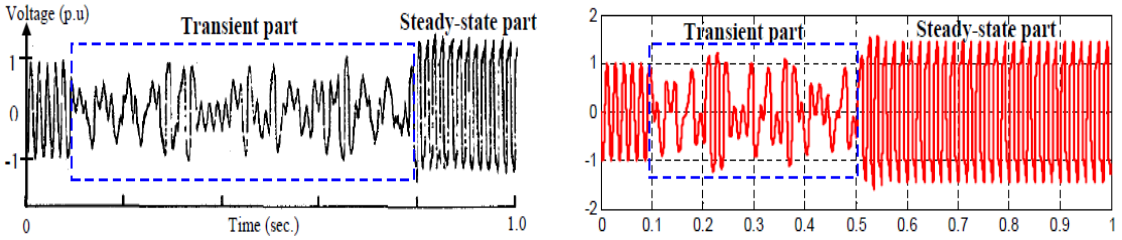

a) Real event measurement b) Dorsey study simulation

Figure 2.17. Comparison between ferroresonance waveforms.

In Figure 2.17 the effect of ferroresonance in power transformers for phases A is shown. It also compare the field measured sample (Figure 2.17a) against the EMTP generated (Figure 2.17b). It is observed that even when the transitional stage between steady state and ferroresonant state is not equal in duration, the mode of ferroresonance and its magnitude is the same.

The discrepancy in the waveform and duration of transient may be attributed to many factors: the transfomer model used, the two piecewise representation of the exitation curve, the capacitance values not included, and the uncertainty of the correct shit angle of the switch at the momment of the fault. This last concern reinforces the importance of studying the effects of the shift angle of the swicth.

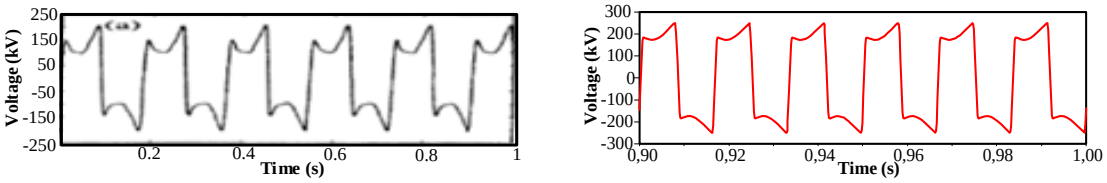

a) Dorsey model b) EMTP model

Figure 2.18. Comparison between ferroresonance waveforms.

Figure 2.18a shows a screenshot of the results provided by Jacobson, and this is compared to the result obtained in this work using EMTP-ATP simulation in Figure 2.18b. It can be seen from the comparision that the final stage of ferroresonance presents the same fundamental mode, and in extention, it also conserves agrement to the measurements performed at Manitoba Hydro. An extensive study of the waveform analysis can be found in [33]. The EMTP model created for this study preserves most of the accuracy obtained with the model originally used by Jacobson. A first validation of the whole waveform can be done by comparing the similarities on the signals in Figure 2.19.

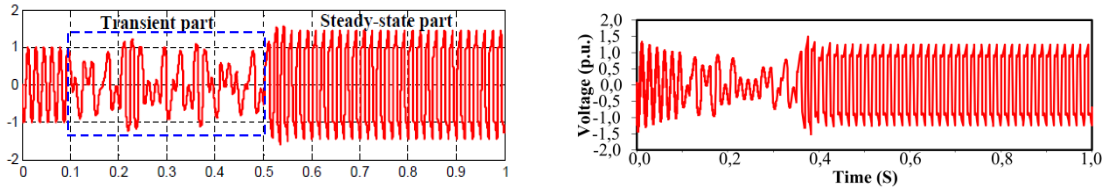

a) Dorsey model b) EMTP model

Figure 2.19. Comparison between ferroresonance waveforms dynamics.

There are some discrepancies when comparing the initial transient from this study against the presented by Jacobson. A shorter length of the transient was obtained with the EMTP model, and this, according to previous studies [35] it can be due to the simplification used when representing the equivalent π capacitances. However, the result is quite accurate. Now, after verifying the correct response of the model using the initial conditions described in [31], the study continues with the aim of analyzing the behavior of ferroresonance waveforms with respect to the shift angle of the switch.

Figures 2.20 to 2.23 are presented as an introduction to the analysis of the changes occurring to the ferroresonance phenomenon when varying the shift angle at which the switch is commutated. For this, the opening of the three-phase switch is centralized using the pole of phase Bas reference and a complete time cycle has left pass prior the commutation to have a zero crossing reference before controlling the shift angle. Some of the effects obtained for the shift angle change are shown below:

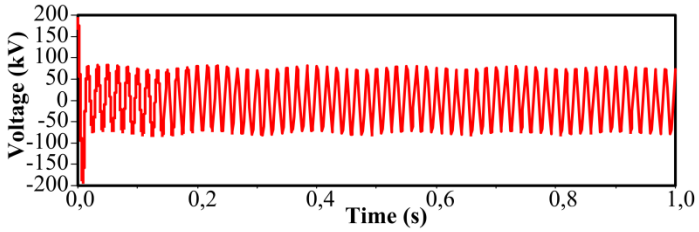

a) Phase A

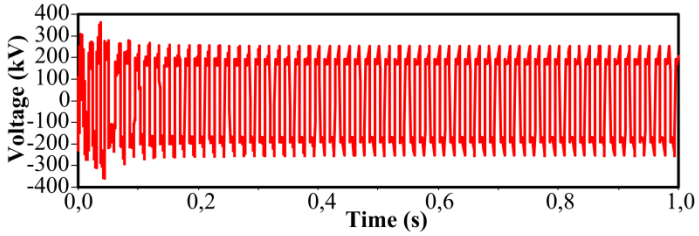

b) Phase B

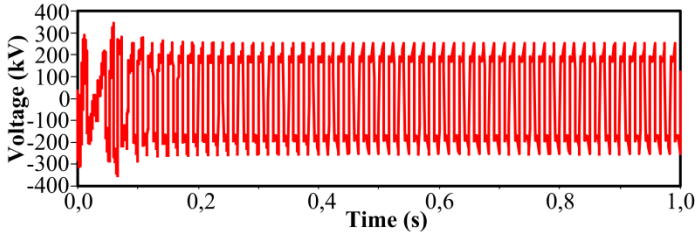

c) Phase C

Figure 2.20. Ferroresonance waveforms: Switch shift angle 0º.

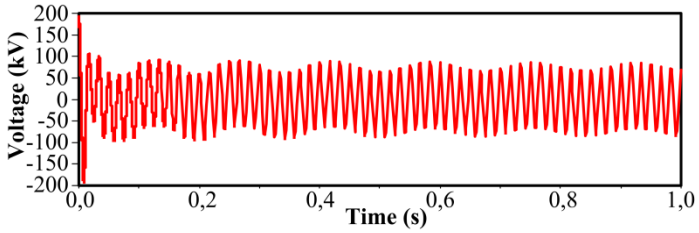

a) Phase A

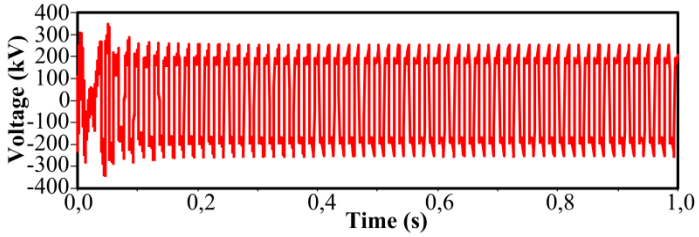

b) Phase B

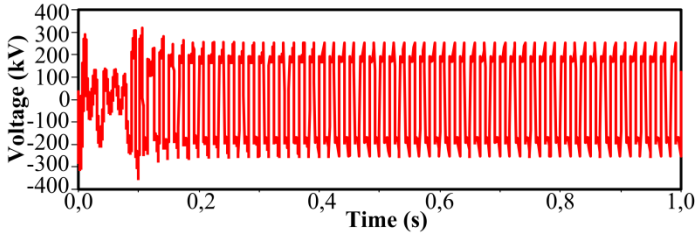

c) Phase C

Figure 2.21. Ferroresonance waveforms: Switch shift angle 15º.

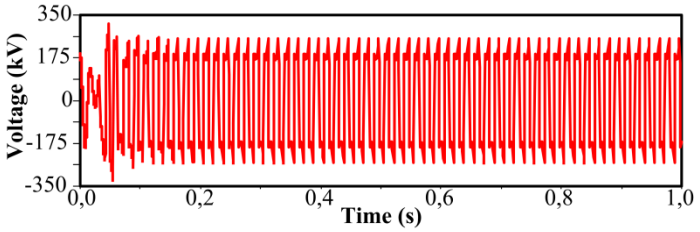

a) Phase A

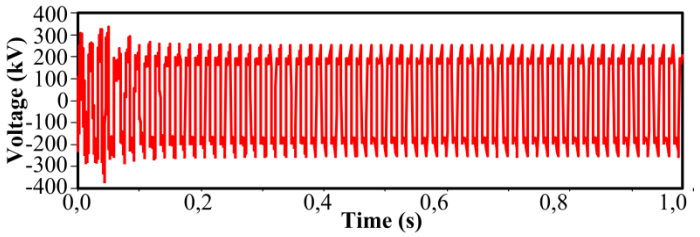

b) Phase B

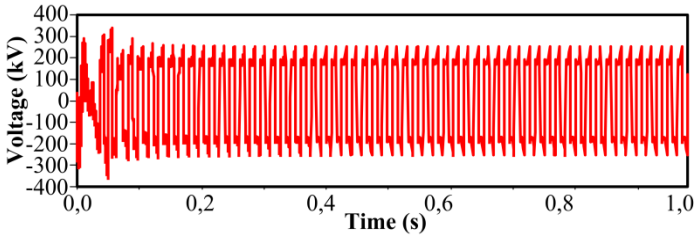

c) Phase C

Figure 2.22. Ferroresonance waveforms: Switch shift angle 30º.

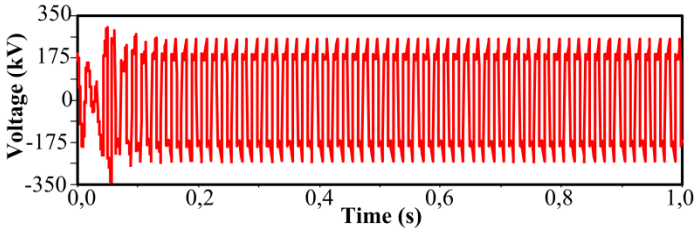

a) Phase A

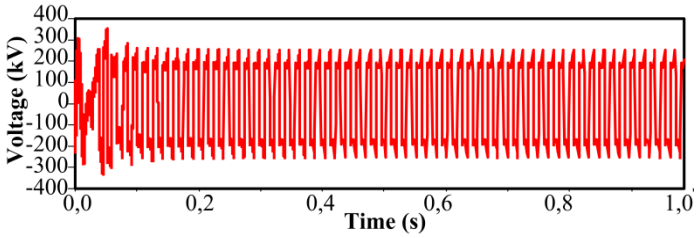

b) Phase B

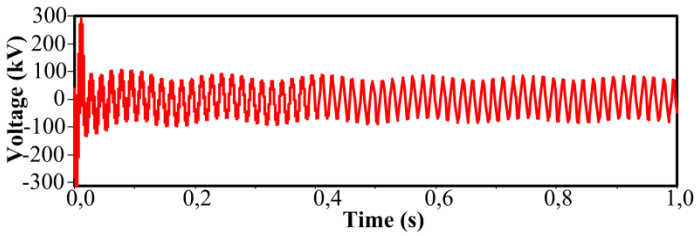

c) Phase C

Figure 2.23. Ferroresonance waveforms: Switch shift angle 45º.

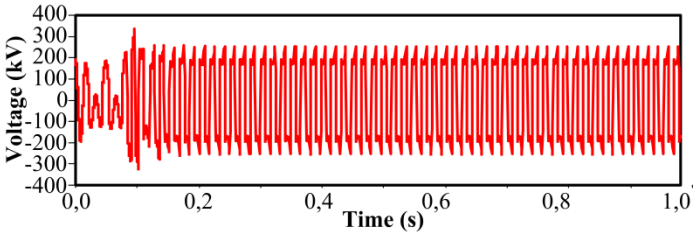

a) Phase A

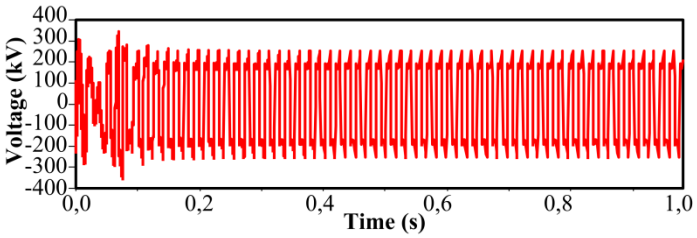

b) Phase B

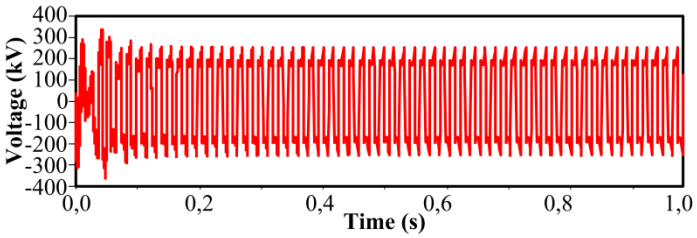

c) Phase C

Figure 2.24. Ferroresonance waveforms: Switch shift angle 60º.

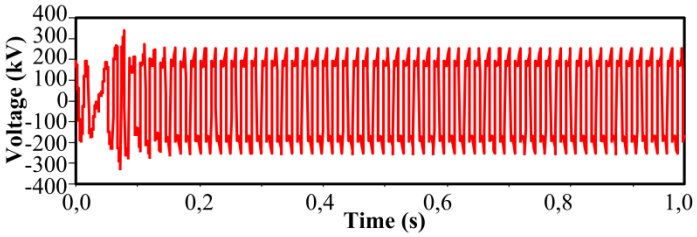

a) Phase A

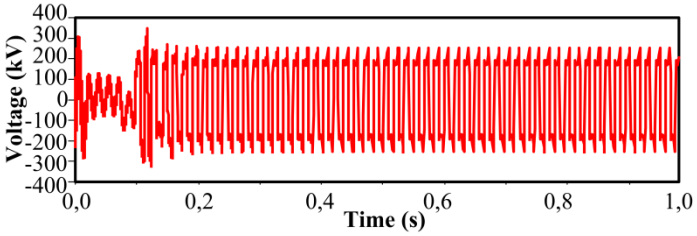

b) Phase B

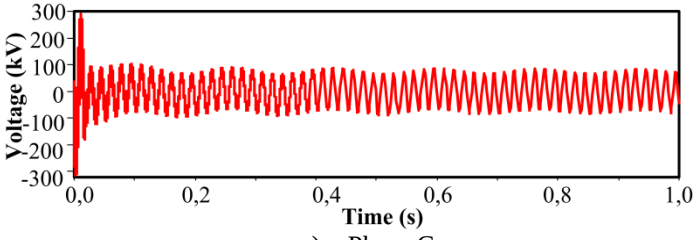

c) Phase C

Figure 2.25. Ferroresonance waveforms: Switch shift angle 90º.

It can clearly be observed there is a dynamic displacement affecting both transient duration and ferroresonance steady state part. This gives a first intuition over the impact the shift angle has. Indeed, it could have affected the Dorsey model when representing the transient experimentally measured at Dorsey Station. There is also a mitigation effect depending on the shift angle causing ferroresonance appearing or vanishing when the angle varies. Figures 2.24 and 2.25 show the damping effect in the Phase *C*. The behavior of the system remains rather similar in all three phases, although there are some variations in the transient length and randomly damped responses. It is interesting to think that even though the actual event in Dorsey was severe, it could have been even worse taking in to account that there are values of angles for which the ferroresonance is present in all 3 phases simultaneously (i.e. 30º and 60º). In this study, Figure 2.26 presents a time length in the transient in Phase *B*, closer to what happened in Dorsey.

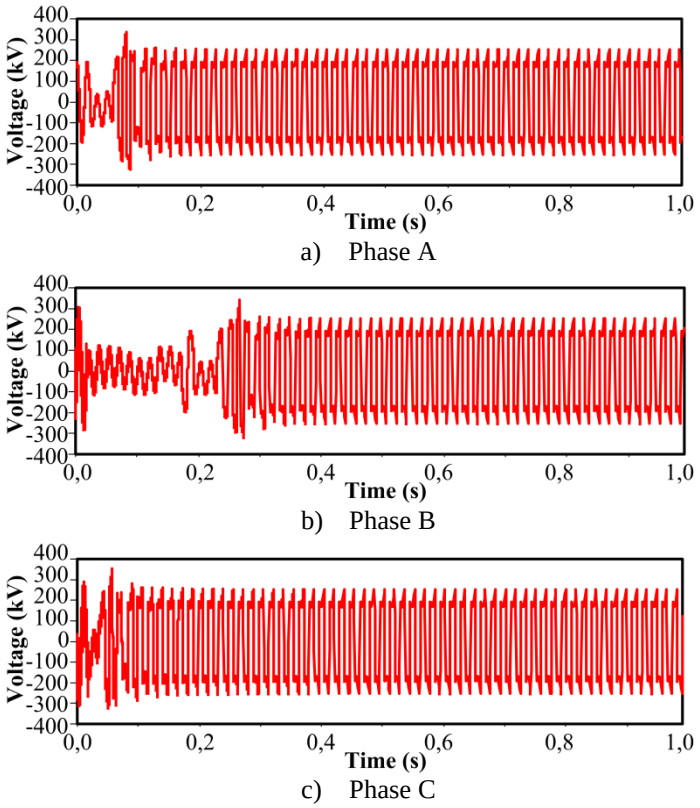

Figure 2.26. Ferroresonance waveforms: Switch shift angle 135º.

It can be assumed that the transient between steady state and ferroresonant state depends on the time when the switch was open. Although there is little difference between the matrix capacitance representation used in the original Dorsey model and the simplified π capacitance model used for this study [31]. It is also true that, if the model for the buses A and B is improved, for example, by using models such as the LCC component, the transient response might be more accurate. These types of models take into account the capacitance effect of the cable, which is a function of the length and the type of insulation.

It can be concluded that ferroresonance may occur even in situations in which it is thought that a system has been completely disconnected. Ferroresonance cases ignited by grading capacitance commonly affect the three phases of the system and their result is a destructive event.

2.2.7. Case C: Ferroresonant Behavior of a Voltage Transformer

This case study was originally presented by Val Escudero and Dudurych [36][37]. Its development is similar to that presented by Jacobson in the 90's. The ferroresonant phenomenon was caused by the implication of grading capacitances connected in parallel with power breakers. The scenarios are completed by a three-phase disconnection maneuver and by disconnecting the major part of the load supplied by transformers. Both Val Escudero and Jacobson cases represent real events having data collected during ferroresonance appearance. The line circuit of this case study is presented in Figure 2.27.

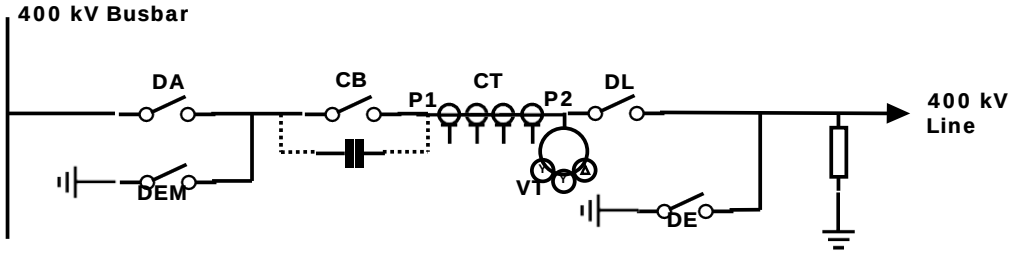

Figure 2.27. 400 kV Substation.

The events occurred with the launch of a new 400 kV substation in Ireland, in the test phase; The line switch *DL* was turned off, then, it was intended o de-energize the voltage transformers bank *VT* by switching off the 'circuit breaker' *CB* while having the bus main switch *DA* close. The ferroresonance phenomenon appeared due to the grading capacitance connected to the circuit breaker and its interaction with the non-linear inductance of the transformer bank. Distortions in the voltage signal were reported, having peaks up to 2 times the nominal value. The simplified circuit describing the ferroresonance phenomenon during the failure is shown in Figure 2.28.

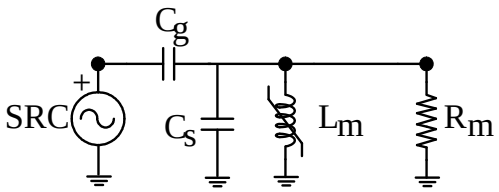

Figure 2.28. 400 kV Substation, ferroresonant equivalent circuit.

In the simplified circuit C_g represents the grading capacitance, C_s the stray capacitance of the cable and L_m and R_m the magnetic core of the transformer. From the network information a detailed model has been created to represent the sections of the substation involved in the event. Figure 2.29 shows the EMTP circuit.

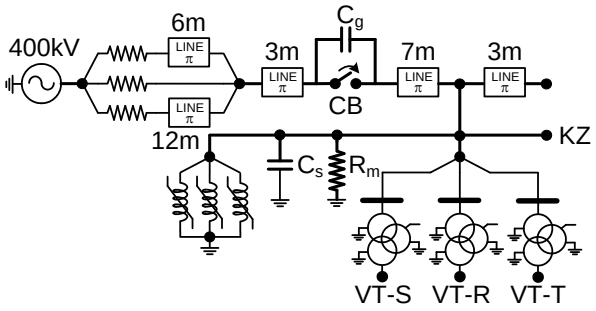

Figure 2.29. 400 kV Substation, EMTP representation.

The EMTP model most of the sections of the original system: The overhead lines, all switches, transformer bank, grading capacitance (C_g) and the shunt capacitive effects of the cables near the transformers (C_s). Detailed information of the model is presented below.

- **Power source (ideal):** L-L Voltage = 400 kV; Frequency = 50 Hz.
- **Cables:** Represented by constant-parameters PI models. Their lengths vary between 3 and 12 m.
    - **Single Phase cable (3m and 6m sections):** R = 0.0001659 Ω/m, C = 3.09E-6 mH/m, L = 6.08E-5 μF/m
    - **Three-phase cable (all sections):** Phase Resistance R11 = 0.00019355 Ω/m, Resistance between phases R21 = 6.916E-8 Ω/m, Phase Inductance L11= 3.605E-6 mH/m, Inductance between phases L21= 2.2306E-6 mH/m, Capacitance between phase and ground C11= 7.096E-5 μF/m, Capacitance between phases C21= 1.07E-5 μF/m.
- **Circuit breaker:** Represented by a grading capacitance, C_g= 600 pF and T_{open}= 0.256 s.
- **Stray capacitance (C_s):** 460 pF.
- **Voltage transformers (VTs):** Main characteristics
    - Single-phase three-winding transformer.
    - Ratings: 400/0.1/0.033 kV, 0.1/0.1/0.05 kVA.
    - Short-circuit test values: $Z_{sh,1w\text{-}2w}$ = 13.46 %, $Z_{sh,1w\text{-}3w}$ = 20 %, $Z_{sh,2w\text{-}3w}$ = 20 %.
    - No load test losses: R_m = 182 MΩ.
    - Saturation curve shown in Figure 2.30.

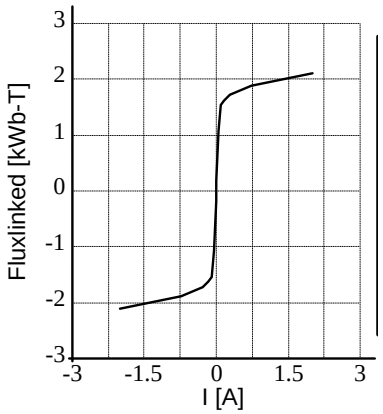

Current (A)	Flux (WB-T)
0.0007348	180.058
0.00578	1080.139
0.00838	1530.284
0.0154	1620.729
0.0273	1710.55
0.07416	1890.608
0.2	2100

Figure 2.30. Saturation curve of the voltage transformers (VTs).

The purpose of the EMTP model is not just to reproduce the single destructive event of the system, but also to find the allowed values of cable length. For this purpose, a capacitor C_s has been used to perform a sensitivity analysis proving the sufficient data to establish a stable zone. In addition, the variation of the capacitance allows simulating up to 3 of the 4 ferroresonance modes. This feature made the model itself a significant contribution to ferroresonance analysis since it is difficult to observe the 4 waveform modes for the same model. Figure 2.31 shows the data originally obtained with the model used in [36] against the simulation results of the EMTP model created for this study.

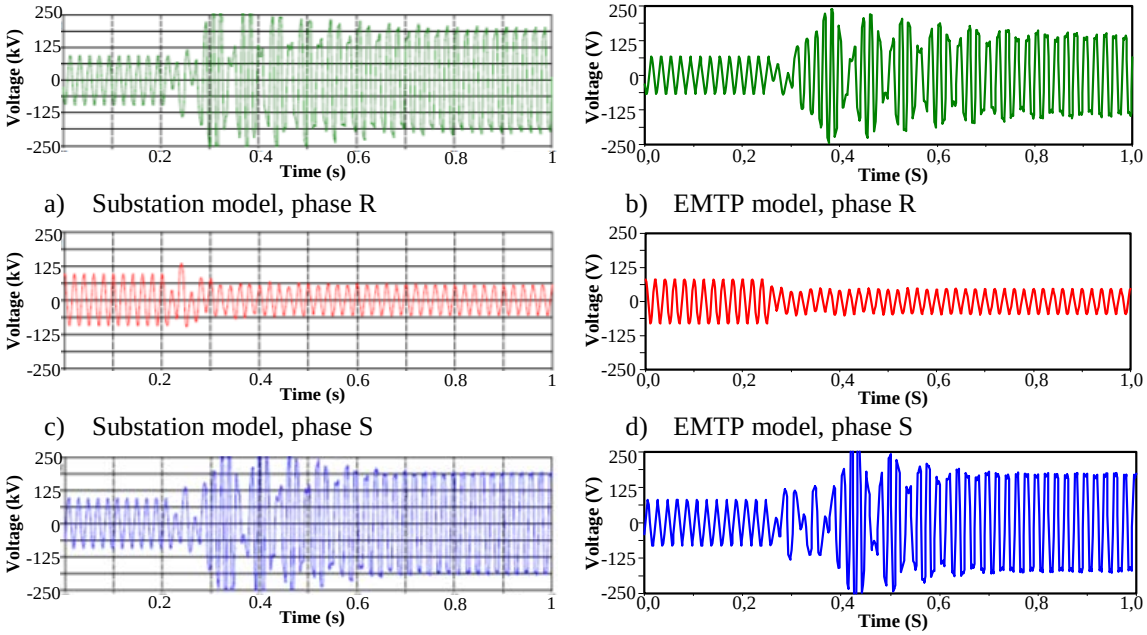

a) Substation model, phase R b) EMTP model, phase R

c) Substation model, phase S d) EMTP model, phase S

e) Substation model, phase T f) EMTP model, phase T

Figure 2.31. Ferroresonant event in the 400 kV Substation.

From the figures, it can be seen that the results of the model implemented in EMTP are very close to the ones provided with the original analysis. For the EMTP model, the BCTRAN transformer component was used, cables were represented by a RLC equivalent, and a general three-phase power source was used for the feeder. The most interesting part of the study comes when checking the responses of the system to different values of C_s. Up to three different modes of ferroresonance were reported in the original study. Figure 2.32 introduces a C_s value that leads the system to fundamental mode.

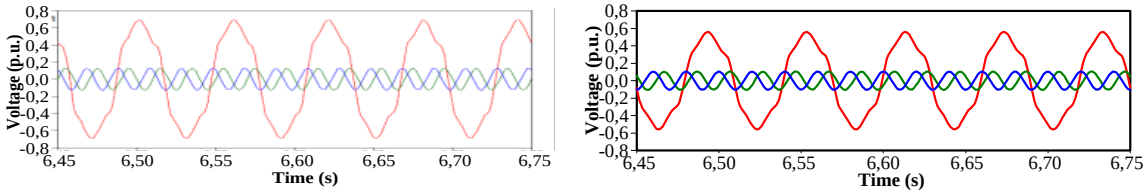

a) Substation model b) EMTP model

Figure 2.32. Ferroresonant fundamental mode, C_s=4040 pF and C_g=600 pF.

In the original study, a variation of the ground shunt capacitance (C_s) was performed to analyze the dynamic of the ferroresonance. Since usually the shunt value is related to cables lengths, by, changing the capacitance parameter gives an insight idea of possible effects resulting with cable length variations. For the case of C_s=4040 pF a fundamental behavior is observed. Figure 2.33 presents the waveform obtained for a C_s = 2320 pF.

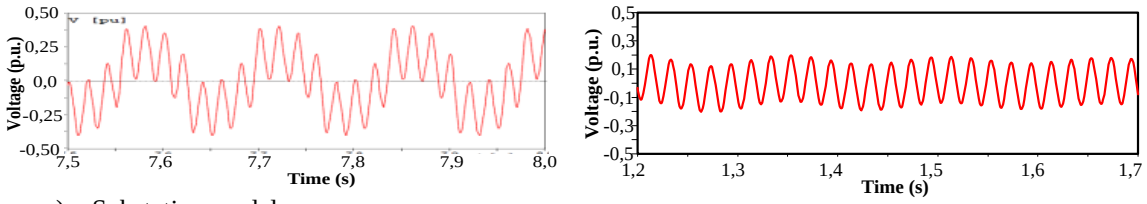

a) Substation model b) EMTP model

Figure 2.33. Ferroresonant quasi-periodic mode, C_s=2320 pF and C_g=600 pF.

Regarding the modeling, the results obtained with the EMTP model are very similar to the ones obtained by Val Esducero and Dudurych. Nevertheless, both models could be always improved. The data provided includes only a pseudo-lineal saturation curve, thus, improving this representation to a hysteretic one could, perhaps, improve the simulation results. Figure 2.34 presents the model comparison for a chaotic signal.

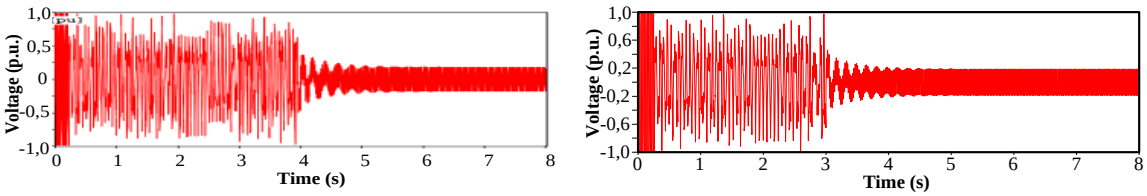

a) Substation model b) EMTP model

Figure 2.34. Ferroresonant chaotic mode, C_s=2590 pF and C_g=600 pF.

It is interesting to observe the different dynamics presented in this case study. The existence of "*jumps*" between ferroresonance states is a characteristic not easy to see in most systems. One of the important considerations that give relevance to the study of Val Escudero is the fact of modeling every part of the conductor lines. It is well known that the capacitive effects included in the underground cable and the shunt capacitance of π equivalent overhead lines directly affects the behavior of ferroresonance [38]. Even thou, the sudden *"jumps"* from one state to another cannot be attributed to a single parameter, the final state of ferroresonance depends on the interaction of all system parameters together.

A few things can be concluded for this study. First, the destructive nature of ferroresonance phenomenon becomes evident once again. It is clear from the study that there are settings that could be very unfavorable. It reconfirms the usefulness of nonlinear dynamics in the study and understanding of systems under ferroresonance. Finally, it proves the importance of modeling every component able to provide capacitive, resistive and inductive effect.

2.2.8. Case D: Ferroresonance in a Five-Legged Transformer

This case is based on a series of studies conducted in the early 90's. Those researches synthesize the experimental work, modeling and analysis of a five-legged wounded core transformer driven into a ferroresonance stage. Originally, The National Rural Electric Cooperative Association (NRECA) financed a study in 1986 and 1987 to assess the problem on rural electric cooperative systems. Five-legged core transformer operating under the grounded-wye connection reported operating problems such as overvoltages [39]. This situation induced the need to develop a transformer model that would efficiently allow analyzing the origins of the transient state [40]. After a large validation work the overvoltage was categorized as ferroresonance phenomenon [41].

Later, Bruce Mork in 1992 [42] presented an EMTP model for a five-legged core transformer. That study was aimed to analyzing the ferroresonant response of the transformer to changes in the capacitance characteristic of the cable feeding the transformer from the source. The contribution of that work was also considered as the first approach to the non-linear analysis applied to power systems, and it is still widely studied [43][44].

The case presented here reproduces the work done by Mork on the cable capacitance modeling and extends it to inquiry on the effects in the ferroresonance final stage provoked by the phase shift angle variation and the source voltage regulation (±10%). Figure 2.35 presents the transformer model scheme.. More information about the test system is provided below.

- **Power source:** L-L Voltage = 480 V; Frequency = 60 Hz;
- **Three-phase transformer:**
  - YNy0 Three-phase two-winding transformer, grounded through a 2.4 Ω impedance.
  - Rated voltages = 12470/7200Yn - 480/277Yn V.
  - Rated power = 75 kVA.
  - High Voltage side data: R_h = 4.7 Ω, L_{hx} = 0.118 Ω.
  - Low voltage side data: R_x = 0.0224 Ω, L_{xc} = 0.08 Ω.
  - Saturation curves shown in Figures 2.36 to 2.39.
  - Core resistance: R_1 = 411 Ω, R_2 = 337 Ω, R_3 = 372 Ω, R_4 = 395.6 Ω.
- **Load:** R = 1E11 Ω (non load condition).
- **Shunt capacitance C:** Variable through the study going from 0 to 30 μF.

Since the ferroresonant situation starts along with the simulation, the switch between the source and the transformer phase A is left open. Additionally, since ferroresonance is highly dependent of the initial condition of the system all experiments have been homogenized by setting to zero the initial voltage in the shunt capacitances and the residual flux in the core. After running a series of simulations, it was possible to understand that the switching angle, the capacitance value and the source voltage were directly affecting the final state of the ferroresonance [45].

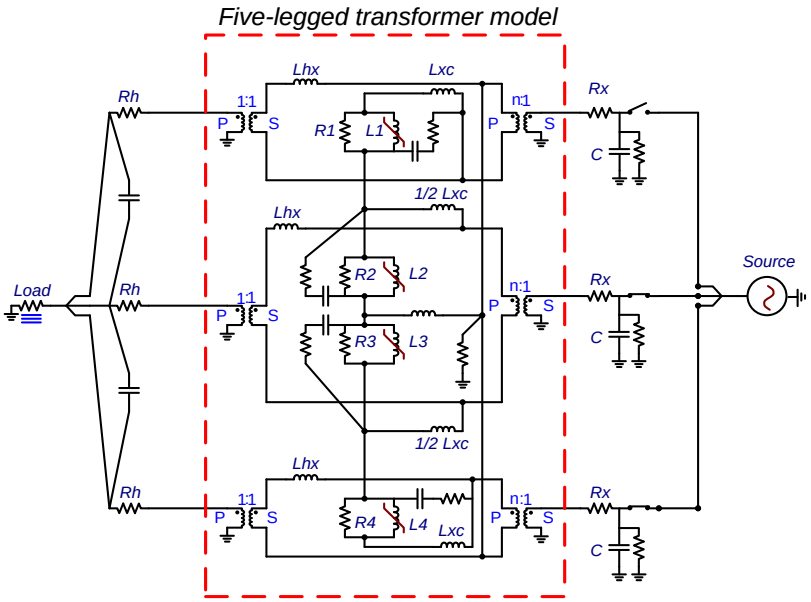

Figure 2.35. EMTP five-legged transformer model.

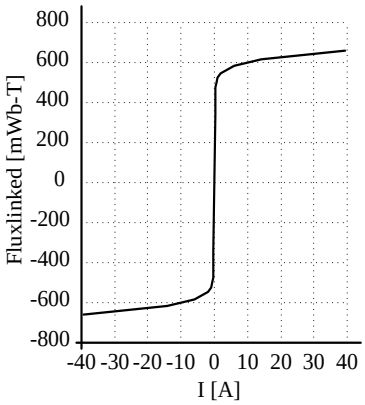

Current (A)	Flux (WB-T)
0.2048	0.3423
0.3253	0.4330
0.4611	0.4726
0.6594	0.4975
1.0484	0.5223
1.9703	0.5470
5.9339	0.5810
14.299	0.6147
39.3920	0.6573

Figure 2.36. Saturation curve of the inductance L_1.

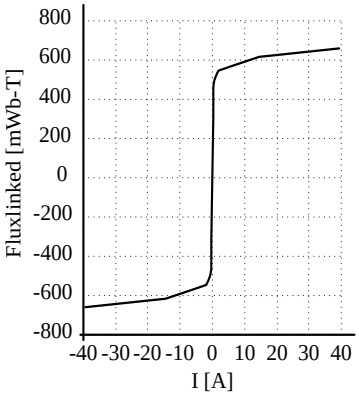

Current (A)	Flux (WB-T)
0.1950	0.3136
0.3100	0.4133
0.4550	0.4646
0.6581	0.4936
1.1030	0.5204
2.0099	0.5423
5.6543	0.5687
14.3230	0.6147
39.4180	0.6573

Figure 2.37. Saturation curve of the inductance L_2.

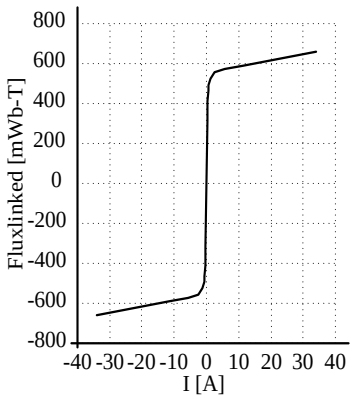

Current (A)	Flux (WB-T)
0.2000	0.3109
0.3200	0.4103
0.4976	0.4643
0.7182	0.4930
1.2090	0.5231
2.4080	0.5562
5.5097	0.5742
11.3310	0.5897
34.1210	0.6592

Figure 2.38. Saturation curve of the inductance L_3.

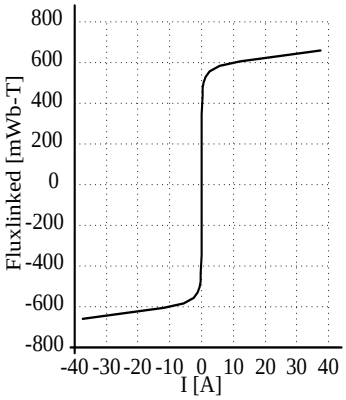

Current (A)	Flux (WB-T)
0.0264	0.3433
0.3308	0.4348
0.4041	0.4767
0.6844	0.5005
1.1574	0.5274
2.3642	0.5541
5.6238	0.5820
11.9063	0.6043
37.4722	0.6591

Figure 2.39. Saturation curve of the inductance L_4.

Once the transformer model has been designed and validated against experimental data, Bruce Mork used the capacitors connected between each switch and ground to represent the capacitive effect of the cable connecting the transformer to the power supply. In this way, it would ensure having a ferroresonant circuit by forcing a direct interaction between capacitance and nonlinear inductance. Some examples of the results can be seen in [45]; the former FORTRAN-coded model implemented in the traditional version of EMTP is compared to the one implemented for this work using ATPDraw:

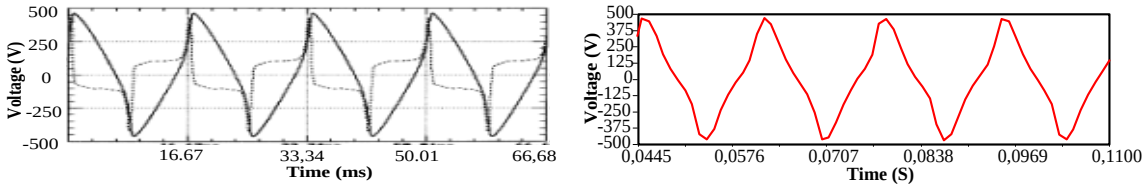

a) Mork model b) EMTP model

Figure 2.40. Ferroresonance waveform, C=5 µf, phase A.

Figure 2.40 presents the first 65 ms of a fundamental waveform. The voltage have been measured in phase A having a shunt capacitor of 5 µF. The next study occurs before a period bending, as known in nonlinear dynamics, the signal presents more than one response each period. Figure 2.41 presents the comparison for the first 160ms.

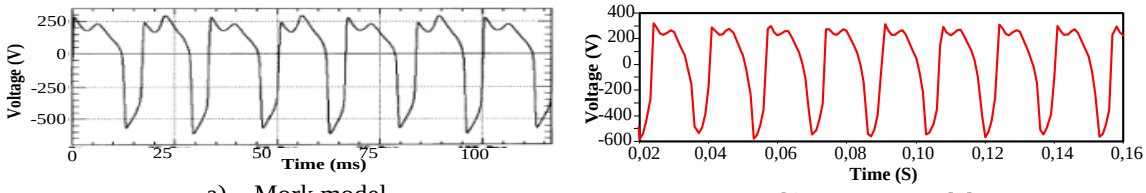

a) Mork model b) EMTP model

Figure 2.41. Ferroresonance waveform, C = 10 µf, phase A.

Figure 2.42, presents a clearly chaotic stage obtained whit a capacitance value of 15µF. The first 400 ms are presented in the figure.

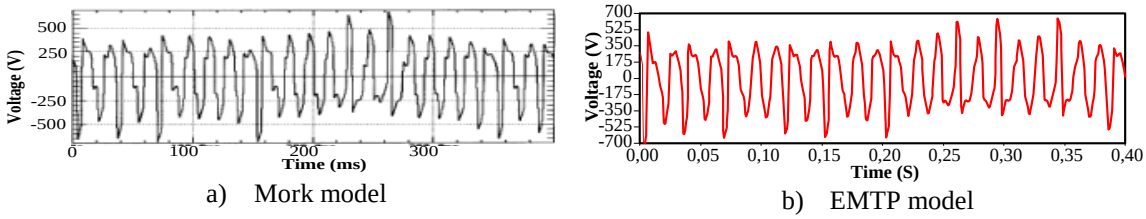

a) Mork model b) EMTP model

Figure 2.42. Ferroresonance waveform C = 15 µf, phase A.

Some extra simulation results, with different capacitance values, are presented in Figures 2.43 and 2.44.

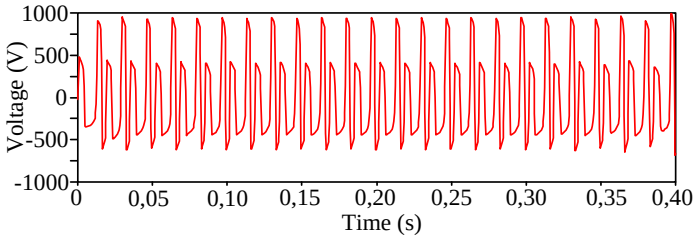

Figure 2.43. Ferroresonance waveform C = 25 µf, phase A.

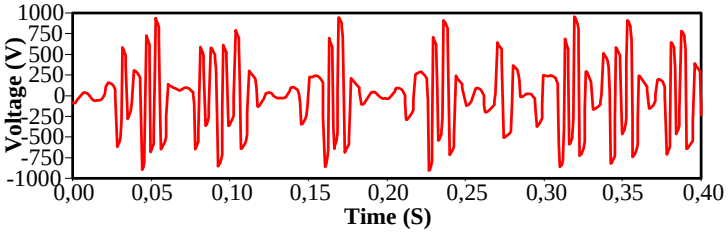

Figure 2.44. Ferroresonance waveform C = 30 µf, phase A.

The study presented here has been probably one of the most famous in the ferroresonance analysis field. Besides, it presented a vast variety of ferroresonance modes, being the focus of attention for many years, because five-legged transformers were commonly used in Y-Y three-phase connections. This original study presented by Mork helped, not only to better understand ferroresonance but to generate awareness among power system designers. Nowadays, for power system engineers it is a splendid test system to start modeling ferroresonance situations and also to develop techniques to better understand its global behavior.

2.3. CHAPTER SUMMARY

Different power systems have been simulated to prove the possibility to represent ferroresonance phenomenon in different situations using EMTP software. There exist diverse approaches to model real systems using the components and built-in models included in such program. It has been found that with sufficient care when modeling, it is possible to replicate ferroresonance real events with precision enough to perform larger parametric analysis.

The models replicated here present different system topologies and different set ups for ferroresonance ignition. Further use of these models enables a wide range of potential new scenarios to study ferroresonance. Areas such as dynamic behavior, parameter dependency or fault prediction can be deeply studied.

It was also possible to conclude that the graphical version of EMTP facilitates the implementation of existing system models. This generates a trustable bond in the software for the generation of brand new models. In conclusion, ATPDraw can be used to implement and analyze transformer and electric system models under the ferroresonance phenomenon.

2.4. REFERENCES

[1] Z. Dong, and P. Zhang, *Emerging techniques in power system analysis*, Springer Science and Business Media, 2010.

[2] X. F. Wang, Y. Song, and M. Irving, *Modern power systems analysis*, Springer Science and Business Media, 2010.

[3] S. A. H. Soliman, and A. A. H. Mantawy, *Modern optimization techniques with applications in electric power systems*, Springer Science and Business Media, 2011.

[4] CIGRE WG 33.02, Guidelines for Representation of Network Elements when Calculating Transients, CIGRE Brochure 39, 1990.

[5] IEC TR 60071-4, Insulation Co-ordination—Part 4: Computational Guide to Insulation Co-ordination and Modeling of Electrical Networks, IEC, 2004.

[6] A. Gole, J. A. Martinez-Velasco, and A. Keri (eds.), Modeling and Analysis of Power System Transients Using Digital Programs, *IEEE Special Publication TP-133–0*, IEEE Catalog No. 99 TP133-0, 1999.

[7] H. W. Dommel, "Digital Computer Solution of Electromagnetic Transients in Single- and Multiphase Networks", *IEEE Transactions on Power Apparatus and Systems*, vol. 88, no. 4, pp. 388-398, 1969.

[8] ATP, "Alternative Transients Program - Rule Book", Leuven EMTP Center Belgium, (LEC), 1987.

[9] L. B. Viena, F. A. Moreira, N. R. Ferreira, A. C. de Castro, and N. C. de Jesus, "Analysis and application of transformer models in the ATP program for the study of ferroresonance", *IEEE/PES Transmission and Distribution Conference and Exposition: Latin America (T&D-LA)*, pp. 738-744, November 2010.

[10] J. A. Martinez, J. Mahseredjian, and R. A. Walling, "Parameter determination for modeling system transients", *IEEE Power Energy Magazine*, vol. 3, no. 5, pp. 16–28, September/October 2005.

[11] J. A. Martinez, "Parameter determination for power systems transients", *IEEE Power and Energy Society General Meeting*, Tampa, June 2007.

[12] F. de Leon, A. Farazmand, and P. Joseph, "Comparing the T and π equivalent circuits for the calculation of transformer inrush currents", *IEEE Transactions on Power Delivery*, vol. 27, no. 4, pp. 2390-2398, October 2012.

[13] S. Jazebi, A. Farazmand, B.P. Murali, and F. de Leon, "A comparative study on π and T equivalent models for the analysis of transformer ferroresonance", *IEEE Transactions on Power Delivery*, vol. 28, no. 1, pp. 526-528, January 2013.

[14] B. A. Mork, "Five-legged wound-core transformer model: derivation, parameters, implementation and evaluation", *IEEE Transactions on Power Delivery*, vol. 14, no. 4, pp. 1519-1526, October 1999.

[15] X. Chen, "A three-phase multi-legged transformer model in ATP using the directly-formed inverse inductance matrix", *IEEE Transactions on Power Delivery*, vol. 11, no 3, pp. 1554-1562, July 1996.

[16] B. A. Mork, D. Ishchenko, F. Gonzalez, and S. D. Cho, "Parameter estimation methods for five-limb magnetic core model", *IEEE Transactions on Power Delivery*, vol. 23, no 4, pp. 2025-2032, September 2008.

[17] H. K. Høidalen, L. Prikler, and J. Hall, "ATPDraw- Graphical Preprocessor to ATP. Windows version", *International Conference in Power Systems Transients (IPST)*, Budapest, Hungary, June 1999.

[18] H. W. Dommel, *EMTP Theory Book*, Portland, OR: Bonneville Power Admin., August 1986.

[19] X. Chen, "Negative inductance and numerical instability of the saturable transformer component in EMTP", *IEEE Transactions on Power Delivery*, vol. 15, no. 4, pp. 1199–1204, October 2000.

[20] T. Henriksen, "How to avoid unstable time domain responses caused by transformer models", *IEEE Transactions on Power Delivery*, vol. 17, no. 2, pp. 516–522, April 2002.

[21] C. M. Arturi, "Transient simulation and analysis of a five-limb generator step-up transformer following an out-of-phase synchronization", *IEEE Transactions on Power Delivery*, vol. 6, no. 1, pp. 196–207, January 1991.

[22] F. de León and A. Semlyen, "Complete transformer model for electromagnetic transients", *IEEE Transactions on Power Delivery*, vol. 9, no. 1, pp. 231–239, January 1994.

[23] V. Brandwajn, H. W. Dommel, and I. I. Dommel, "Matrix representation of three-phase n-winding transformers for steady-state and transient studies", *IEEE Transactions on Power Apparatus and Systems*, vol. PAS-101, no. 6, pp. 1369–1378, June 1982.

[24] J. A. Martinez-Velasco and J. R. Martí, "Electromagnetic Transients Analysis", Chapter 12 in *Electric Energy Systems: Analysis and Operation*, A. Gomez-Exposito, A. Conejo, and C. Canizares (Eds.), CRC Press, Boca Raton, 2008.

[25] A. Greenwood, *Electrical transients in power systems*, Wiley 1991.

[26] B. A. Mork, F. Gonzalez, D. Ishchenko, D.L. Stuehm, and J. Mitra, "Hybrid transformer model for transient simulation-Part I: Development and parameters," *IEEE Trans. on Power Delivery*, vol. 22, no. 1, pp. 248-255, January 2007.

[27] H. K. Høidalen, B. A. Mork, F. Gonzalez, D. Ishchenko, and N. Chiesa, "Implementation and verification of the hybrid transformer model in ATPDraw," *Electric Power Systems Research*, vol. 79, no. 3, pp. 454-459, March 2009, Special issue: papers from the 7th Int. Conf. Power Systems Transients (IPST).

[28] E. C. Cherry, "The duality between interlinked electric and magnetic circuits and the formation of transformer equivalent circuits," *Proc. of the Physical Society. Section B* 62.2 (1949), 101.

[29] G. R. Slemon, "Equivalent circuits for transformers and machines including non-linear effects," *Proc. of the IEE-Part IV: Institution Monographs* 100.5 (1953): 129-143.

[30] P. Ferracci, "Ferroresonance", Cahier Technique no. 190, Groupe Schneider, 1998.

[31] D. A .N. Jacobson, "Field Testing, Modelling and Analysis of Ferroresonance in a High Voltage Power System", Ph.D. Thesis, The University of Manitoba, 2000.

[32] D. A. N. Jacobson, P. W. Lehn, and R. W. Menzies, "Stability domain calculations of period-1 ferroresonance in a nonlinear resonant circuit", *IEEE Transactions on Power Delivery*, vol. 17, no.3, pp. 865- 871, November 2002.

[33] D. A. N. Jacobson, "Examples of ferroresonance in a high voltage power system", *IEEE Power and Energy Society General Meeting*, Toronto, July 2003.

[34] D. A. N. Jacobson, and R. W. Menzies. "Investigation of station service transformer ferroresonance in manitoba hydro's 230-kv dorsey converter station", *International Conference on Power Systems Transients*, Rio de Janeiro, Brazil, June 2001.

[35] Z. Emin, B. A. T. Al Zahawi, D. W. Auckland, and Y. K. Tong, "Ferroresonance in electromagnetic voltage transformers: a study based on nonlinear dynamics", *IEE Proceedings-Generation, Transmission and Distribution*, vol. 144, no 4, pp. 383-387, 1997.

[36] M. Val Escudero, I. Dudurych, and M. A. Redfern, "Characterization of ferroresonant modes in HV substation with CB grading capacitors", *Electric Power Systems Research*, vol. 77, no. 11, pp. 1506-1513, September 2010.

[37] M. Val Escudero, I. Dudurych and M. A. Redfern, "Characterization of Ferroresonant Modes in HV Substation with CB Grading Capacitors", *International Conference on Power Systems Transients*, Montreal, Canada, June 2005.

[38] G. Buigues, I. Zamora, V. Valverde, A. J. Mazón, and J. I. San Martín, "Ferroresonance in Three-Phase Power Distribution Transformers: Sources, Consequences and Prevention", *19th International Conference on Electricity Distribution*, CIRED, Vienna, May 2007.

[39] D. D. Mairs, D.L. Stuehm, B. A. Mork, "Overvoltages on five-legged core transformers on rural electric systems," *IEEE Transactions on Industry Applications*, vol. 25, no. 2, pp. 366-370, March/April 1989.

[40] D. L. Stuehm, B. A. Mork, and D. D. Mairs, "Five-legged core transformer equivalent circuit," *IEEE Transactions on Power Delivery*, vol. 4, no. 3, pp. 1786-1793, July 1989.

[41] D. L. Stuehm, B. A. Mork, and D. D. Mairs, "Ferroresonance with Three-Phase Five-Legged Core Transformers", Minnesota Power Systems Conference, Minneapolis, MN, October 1988.

[42] B. A. Mork, "Ferroresonance and Chaos - Observation and Simulation of Ferroresonance in a Five Legged Core Distribution Transformer", Ph.D. Thesis, North Dakota State University, 1992.

[43] B. A. Mork, "Five-legged wound-core transformer model: derivation, parameters, implementation and evaluation", *IEEE Transactions on Power Delivery*, vol.14, no. 4, pp. 1519-1526, October 1999.

[44] IEEE Slow Transients TF, "Modeling and analysis guidelines for slow transients – Part III: The study of ferroresonance", *IEEE Transaction on Power Delivery*, vol. 15, no. 1, pp. 255-265, January 2000.

[45] B. A. Mork: "Understanding and Dealing with Ferroresonance", Minnesota Power Systems Conference, Minneapolis, MN, October 2006.

3 Ferroresonance Identification Methods: Analysis and Prediction Tools

3.1 INTRODUCTION

Nowadays, design and operation of power systems relies more on simulations and computational tools. Advances in software development and the ever-growing improvements in computational hardware, imply a significantly increase in the accuracy of virtual representation for physical systems [1]. Today, the application of simulations tools to the analysis of electromagnetic transient phenomena has become a common task. Simulation software is used in a wide variety of situations such as: determination of component ratings, designing and optimizing process; testing and controlling protection systems; and power systems analysis under various scenarios [2].

In ferroresonance analysis, despite the extensive literature available, prediction methods and behavior characterization still remain widely unknown. Ferroresonance has been present in power systems for more than a century. The first analytical works were presented in the 50's [3], [4]. Later on, during the 70's and 80's, digital simulators began to replace traditional transient network analyzers (TNA). A pioneering work in digital computer solution methods was presented by Dommel [5]. That work settles the foundations to solve system equations by using nodal analysis and numerical integration. It was in the late 70's after the breakthrough of nonlinear dynamics and chaos theory that a new door for ferroresonance analysis was open. This connection allowed upgrading the expertise in waveform analysis that lastly enabled the first classification of ferroresonance possible states [6]. The first formal work linking up ferroresonance with non-linear analysis was published in 1992 [7]. That work presented a three-phase transformer leading to a chaotic state. Since then, Topics such as bifurcation theory, global dynamic behavior or the Galerkin method were common in ferroresonance analysis [7],[8]. However, it was not until 2000 when several techniques obtained from the merge with nonlinear dynamics were developed [9]. One of the first significant contributions was presented in [10]. That work demonstrated the existence of stability domains in ferroresonance cases. Today, research topics such as ferroresonance behavioral patterns [11], hysteresis impacts [12], transformer core studies [13] or derivation of new transformer models [14], are frequently followed by words related to chaos theory such as 'stability domain', 'dynamic behavior' or 'harmonic balance' [15], [15].

Increasing speed of computers and advances on computational methods allowed electromagnetic transient software to be capable of, for example, efficiently include the analysis of electromechanical phenomena. In fact, such transients can be studied with higher precision, as compared to traditional positive-sequence-based methods. Modern computers can efficiently establish links between several software tools for multi-task procedures; for instance, EMTP-like software can be used to model and analyze electrical systems while any other mathematical software (e.g., MATLAB) can be used to perform complex signal processing. In this chapter, several techniques will be introduced and implemented to assist the ferroresonance analysis. Areas such as waveform analysis, system global behavior and fault predictions would be addressed. Methods such as Poincaré maps or Bifurcation Diagrams are not presented as new techniques. In fact, those tools have been extensively used during the last 20 years in different areas of expertise. However, its implementation assisting the study of dynamic phenomena such as ferroresonance must be explained in an easy-to-follow way.

3.2 FERRORESONANCE ANALYSIS TOOLS

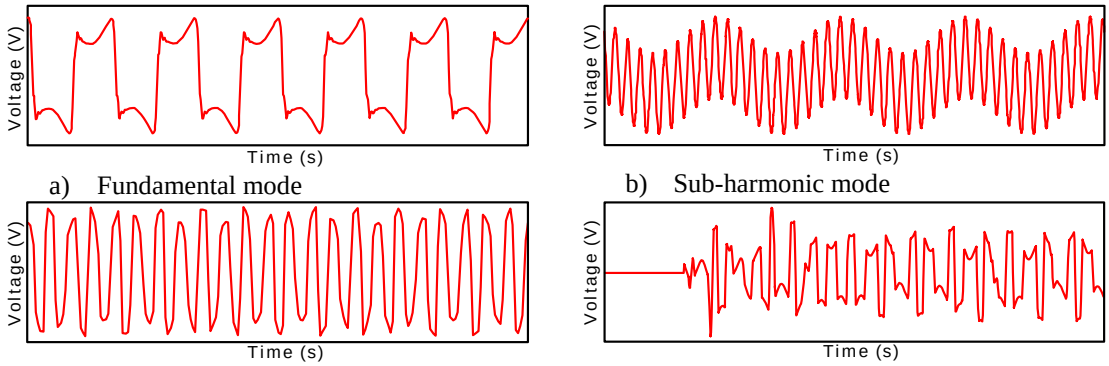

a) Fundamental mode
b) Sub-harmonic mode
c) Quasi-periodic mode
d) Chaotic mode

Figure 3.1. Ferroresonance possible modes.

Modeling electrical system components has been a critical part of any ferroresonance study. There exist different models and different means of determining the parameters required to represent each element. In addition, determining non-linear parameters is still an on-going challenge. Simulation results have been proved to have a great sensitivity to the applied mathematical models, and most errors of convergence are directly related to imprecise modeling of non-linear components. In general, the main study zone for ferroresonance cases involved all system elements being replicated to obtain a study system model [2]: transformers, source impedance, transmission or distribution line(s)/cable(s), and any external capacitance source. In addition, the shift angle of the switch and the phase shift of the source commonly are undervalued parameters although they play an important role in the resulting final state in case of ferroresonance and in the length of the initial transient.

Commonly, once a proper system model has been built, parametric analyses are performed to analyze its dynamic behavior. Usually, these analyses consist on performing an exhausting number of simulations to check the waveform variation, for example, voltage or current measured on a fixed node while a system parameter is being changed. This task becomes more complex when facing phenomena such as ferroresonance where waveforms are jumping from fundamental-frequency to sub-harmonic, quasi-periodic or even chaotic oscillations. Distinguishing and categorizing the different states of ferroresonance signal can turn into a complicated work. For these reasons, it is important to have on-hand-tools for optimizing this type of studies. A standard guide of waveform classification is presented in Figure 3.1.

Tools for discerning, classifying and predicting ferroresonance are collected in the following sections: Poincaré maps are used to describe the time behavior of a system; Bifurcation Diagrams are used to detail the locations of all the abrupt changes in a parametric study; The Harmonic Balance method is presented as an approach to predict the dynamics of a ferroresonant system; 3D Bifurcation Diagrams are used to predict ferroresonance appearance and to assist finding safety zones for power system parameter design; 4D Maps can be implemented to generalize a complex system behavior assisting engineers designing over a proved safe zone. Finally, the Shift Angle Switching Study validates the impact of initial conditions when performing large parametric analysis.

3.2.1 *Poincaré Maps*

The French scientist Jules Henri Poincaré was the first person to consider the possibility of chaos in a deterministic system [17]. The *Poincaré map* is identified as the portrait '*S*' drawn by the marks of a periodic signal when a flat plane intersects its orbit. Figure 3.2 shows the pattern of a Poincaré section.

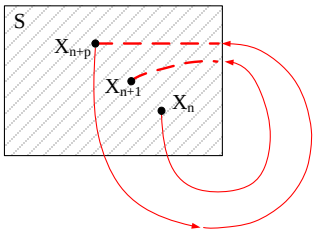

Figure 3.2. Poincaré map.

Reading the possible sketches drawn in a Poincaré map is simple: *Fundamental signals* shows a single point moved far away from the steady state point. *Sub-harmonic signals* present *n* points as orbit produced by the oscillation. *Quasi-periodic signals* have several points forming a closed path. *Chaotic signals* show several points with not fixed pattern. Poincaré maps can be implemented in any simulation software that allows output signal storage because is based on a sampling technique consisting mainly in plotting the saved samples. Figure 3.3 presents an organized method to obtain the map.

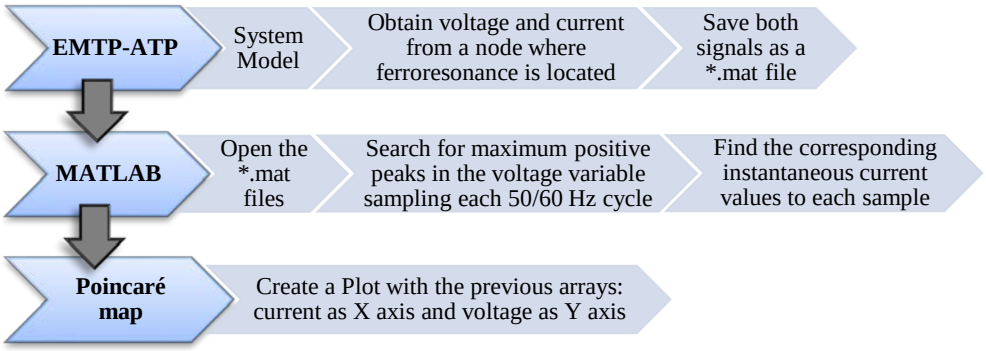

Figure 3.3. Poincaré map flow chart.

There are some concepts to be guaranteed in order to correctly implement a Poincaré map. By definition, a signal orbit refers to the trajectory a system waveform walks-through every amount of time [18]. In electricity, this concept represents the curve described by voltage or current every cycle. Figure 3.4 shows an example of a data sampling.

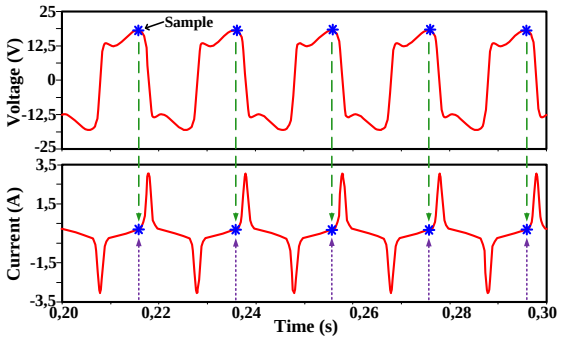

Figure 3.4. Poincaré map data selection.

```
MODEL POINCARE
DATA   freq     -- Base frequency

INPUT x         -- Monitored voltage
          y                       -- Monitored current
VAR
      cycles, peak, peaktime, yout                    -- Internal variables
      tau, i, sample, num_ciclos
            tiempo, tau2, xout
INIT
  xout:=0         -- Initial conditions
  yout:=0
  peak:=0
ENDINIT
EXEC
  cycles:=1/freq
  num_cycles:=round(stoptime/cycles)
  time:=t
  sample:=x

  IF sample>peak THEN              -- Conditioning one sample per cycle
     peak:=sample
     peaktime:=t
     yout:=y
  ENDIF

  FOR i:=1 TO num_cycles BY 1 do
         tau2:=(cycles*i)
                IF tau2=t THEN       -- Recording the values
                        xout:=peak
                        peaktime:=peaktime
                        yout:=yout
                        write('BEGIN WRITE @UseAS')
                        write1(xout,' ', yout,' ',peaktime)
                        write('END WRITE @UseAS')
                        peak:=0
                endif
  endfor
ENDEXEC
ENDMODEL
```

Figure 3.5. MODELS code example.

For ferroresonance waveforms, the flat plane introduced can be obtained by matching voltage and current measured in a network node. Thus, every period a sample should be taken, capturing the instantaneous values of the voltage and current. Each pair of values will further draw the map. The implementation of Poincaré maps under ATP-EMTP software can also be performed using a straight forward strategy based on a general-purpose language called MODELS [19]. This tool supports the study of time-domain systems providing mathematical function analysis and control theory implementation. Figure 3.5 presents an example to create a Poincaré map using the MODELS language.

The objective of the code is to avoid external post-processing of the measured signals. Hence, the code will assist the calculation of the maximum peaks of the voltage and the corresponding current values. It is important to remark that the code structure is an example of how the peak detection can be achieved. However, any simplification or change can be made and it will only depend on the coding expertise. The code presented in Figure 3.5 saves into an external text file all the data calculated. This file can be exported easily to a mathematical processor such as MATLAB. Since most of the post-processing has been carried out using MODELS, the Poincaré map will be created by simply plotting the vectors exported to MATLAB. A series of case studies is presented below, demonstrating the application of the Poincaré map in real power systems.

3.2.1.1 Case study A: Ferroresonant circuit

The best way to illustrate the capabilities of a Poincaré map is by applying it to a basic ferroresonant circuit, and examining some of its waveforms. The ferroresonance system studied here is based on a practical RC with a nonlinear inductance. Details on the circuit model can be found in Chapter 1. Figure 3.6 presents the circuit used.

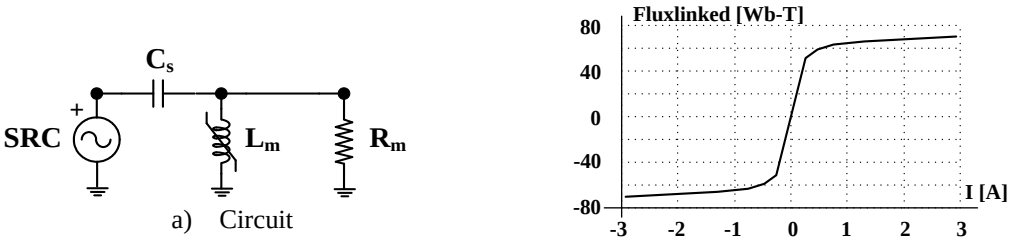

a) Circuit b) Saturation curve

Figure 3.6. Ferroresonance case study.

Ferroresonance signals cannot be easily characterized; Note that it is not possible to directly distinguish between chaotic or quasi-periodic states. According to theory, the Poincaré map results in a closed shape when a quasi-periodic behavior is represented and a cloud of points when having chaotic behavior. Figure 3.7 shows the voltage waveform in the non-linear inductor when the resistor value is considered to be infinite; that is, assuming a lossless circuit with a capacitance value of 0.1 μF.

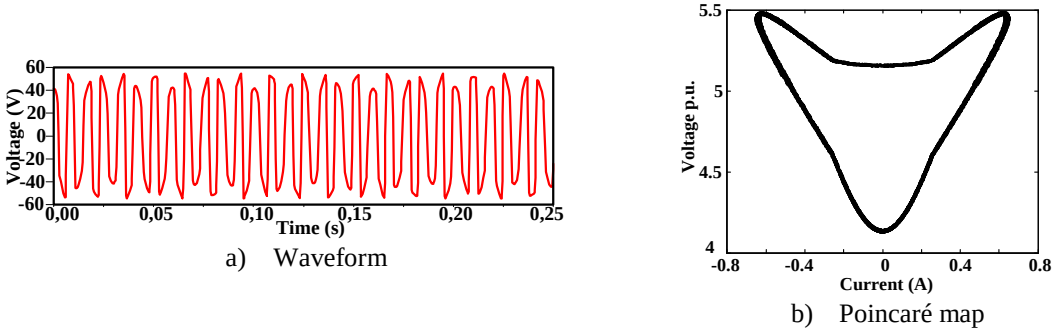

a) Waveform b) Poincaré map

Figure 3.7. Ferroresonance waveform analysis, $R_m=\infty$ and $C_s= 0.1$ μF.

Figure 3.7b allows directly concluding that the ferroresonance signal presents a quasi-periodic behavior. When extensive simulations are being performed, and ferroresonance waveforms are in and out of a chaotic stage, a tool such as Poincaré map can be helpful to rapidly discern among stages. Figure 3.8 shows a new time-domain waveform and a new Poincaré map when the capacitance value changes to a 1 μF.

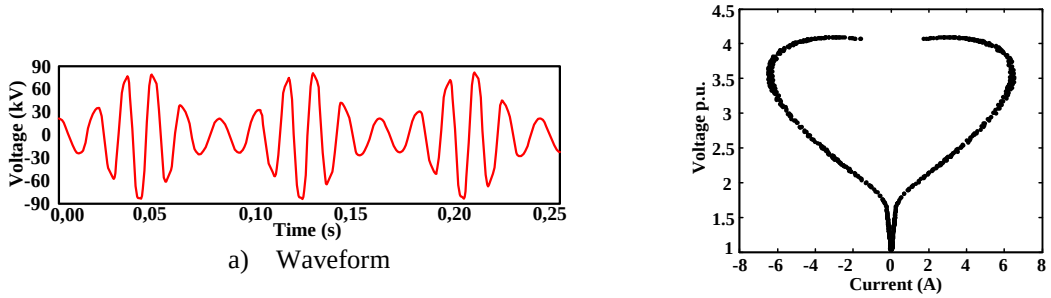

a) Waveform

b) Poincaré map

Figure 3.8. Ferroresonance waveform analysis, $R_m=\infty$ and $C_s=1$ µF.

The signal being analyzed differs in shape from the signal in Figure 3.7a, however, both represents a quasi-periodic stage. The Poincaré map in Figure 3.8b confirms the periodicity of the signal. Regardless of the studied waveform dynamic, Poincaré maps responses are constant. Closed curves represent quasi-periodic signals, cloud of points represents chaotic signals, single points depict periodic solutions and *n* points stands for sub-harmonic behaviors.

3.2.1.2 Case study B: Ferroresonance in a five-legged distribution transformer

Consider the five-legged transformer presented in the previous chapter. Since there is up to four different nonlinearities included in the model, the possibilities of obtaining all different types of ferroresonance are in favor. All waveform samples have been taken when energizing the transformer having the phase *A* open from the start of the simulation. Figure 3.9 presents the test circuit, already used in Chapter 2, to obtain ferroresonance.

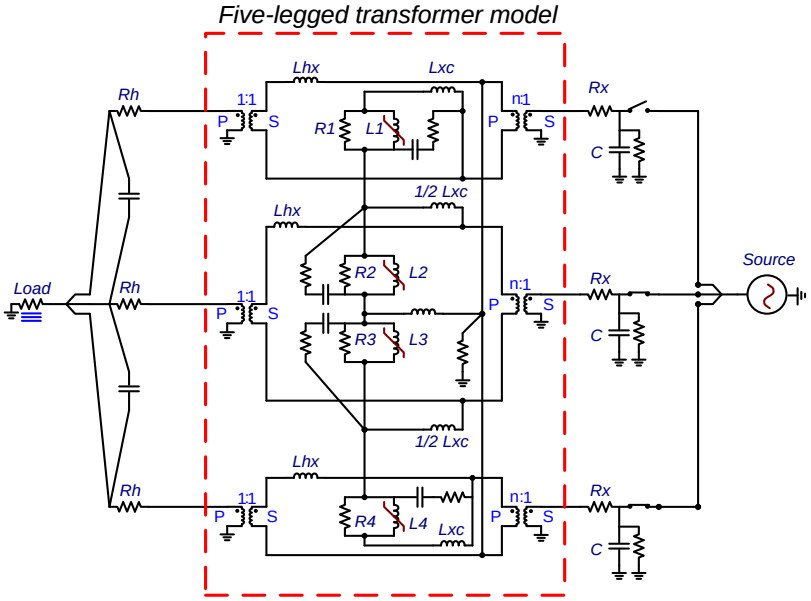

Figure 3.9. Five-legged transformer model.

In this section, a Poincaré map is used to identify the nature of two of the ferroresonance waveforms obtained from the test circuit. The first ferroresonance signal is the classic case of chaotic behavior having a vast range of frequencies. The waveform has been obtained using a capacitance value of $C = 15\ \mu F$. Figure 3.10b presents a cloud of points indicating the existence of a chaotic signal; this collection of dots if often called *attractor*, and it is believed that represents a numerical value toward which a system tends to evolve, for a wide variety of initial conditions [17].

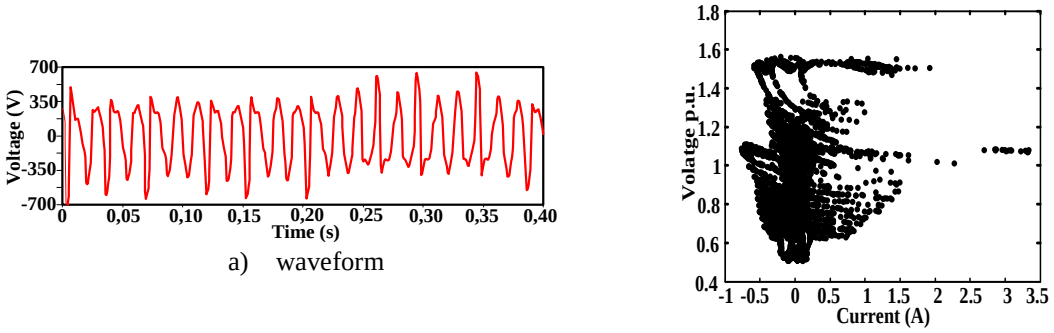

a) waveform b) Poincaré map

Figure 3.10. Ferroresonance chaotic waveform.

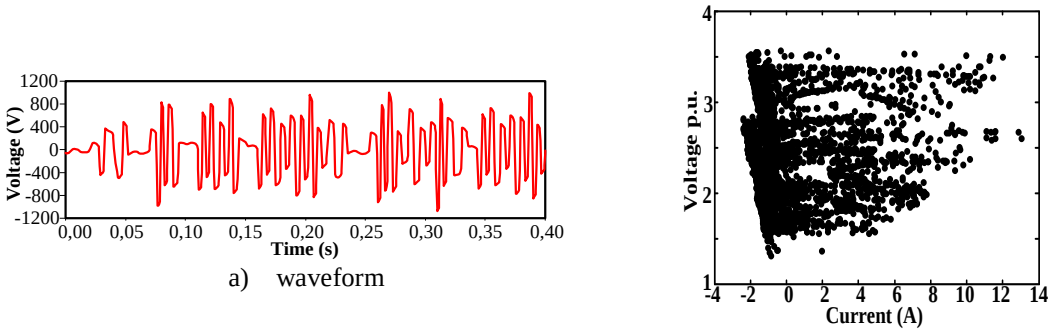

a) waveform b) Poincaré map

Figure 3.11. Ferroresonance chaotic waveform.

The importance of Poincaré maps resides on its easy to understand presentation, in contrast with common FFTs where a collection of frequencies can appear making almost impossible to differentiate a chaotic signal from a quasi-periodic one [18]. Figure 3.11 presents a different case obtained for a capacitance value of $C = 40\ \mu F$, showing also chaotic behavior. Despite the change in the waveform, the Poincaré map is similar to the previous one describing also a chaotic behavior. No matter which shape a chaotic signal presents, a cloud of points will always be present in the Poincaré map.

3.2.1.3 Case study C: Ferroresonance in a Sub-station Transformer

In this study, one of the most well-known ferroresonance cases is considered. The detailed information of the model was already introduced in Chapter 2. The reason why this case has been widely studied relies on the facility of obtaining different dynamics in the ferroresonance waveforms. Figure 3.12 presents the schematic of the analyzed circuit.

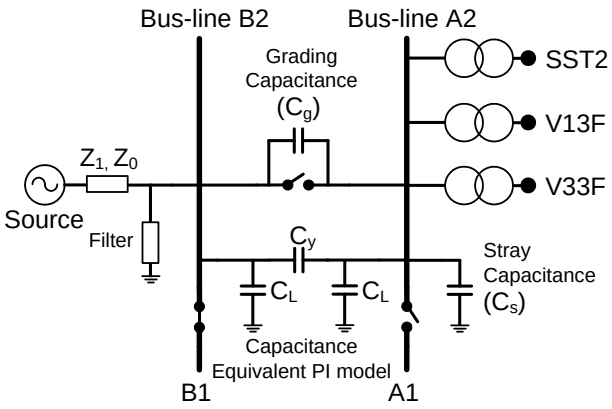

Figure 3.12. Sub-station transformer model.

Different types of ferroresonance can be obtained from the same circuit due to the combination of different capacitive effects distributed along the circuit. In this section, two scenarios are being analyzed. Figure 3.13 presents the first ferroresonance waveform obtained with capacitive values of C_s=*8 nF* and C_g=*5061 pF*.

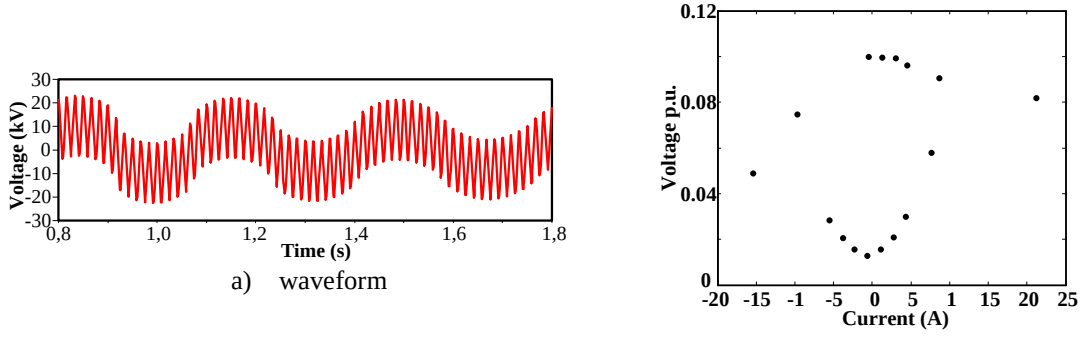

a) waveform b) Poincaré map

Figure 3.13. Ferroresonance sub-harmonic waveform.

A sustained sub-harmonic oscillation is presented. According to theory, a small quantity of points should be distributed along the map indicating the sub-harmonic behavior. The second waveform shows a fundamental case, Figure 3.14 has been obtained using capacitive values of C_g = *6580 pF* and C_s = *4000* pF.

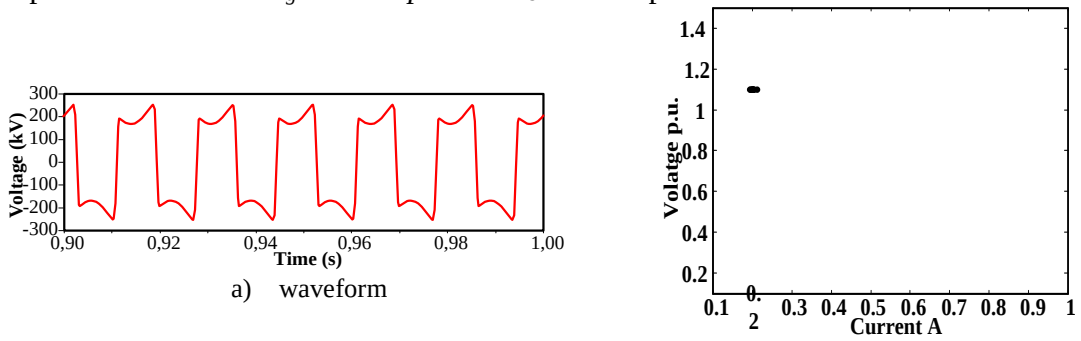

a) waveform b) Poincaré map

Figure 3.14. Ferroresonance fundamental waveform.

The fundamental mode of ferroresonance is the most common waveform obtained when involving voltage transformers. Despite that fundamental mode is easily recognized at glance, a Poincaré map still assists its classification and also gives relevant information about its maximum peaks.

3.2.2 *Bifurcation Diagrams*

Parametric analyses may involve thousands of simulations taking a significant amount of time. However, there are tools that allow summarizing large quantities of information. One of the most useful ones is the Bifurcation diagram. This technique consists on recording in a 2D plane the locations of all abrupt changes occurring to the final operating state of a signal, while in the test system one or more parameters are quasi-statically varied [20].

In simple words, a Bifurcation diagram is a portrait indicating all changes in the steady-state behavior of a system over a range of parameter values as it seen in Figure 3.15. This technique was adopted in ferroresonance analysis to intent for understanding

system behaviors. It has been proved to be an effective method to summarize long parametric analyses consolidating all the information into a single easy-to-read plot.

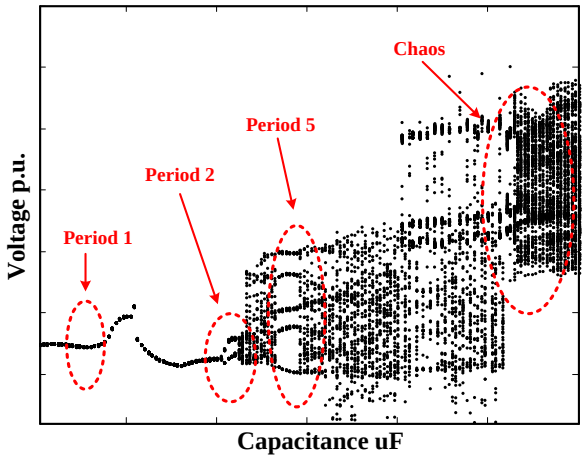

Figure 3.15. Bifurcation diagram scheme.

There are two methods to build a bifurcation diagram: The continuation method and the experimentation method. The first one is based on a mathematical solution of a system; and the last one is based on time-domain analysis [11]. Regardless the method used, the map computed is a simplistic and easy-to-read drawing where straight lines represent fundamental mode situations and broken lines symbolize outputs going from period-2 to chaotic mode. A general procedure to implement a bifurcation diagram by using an EMTP – MATLAB link is described in Figure 3.16.

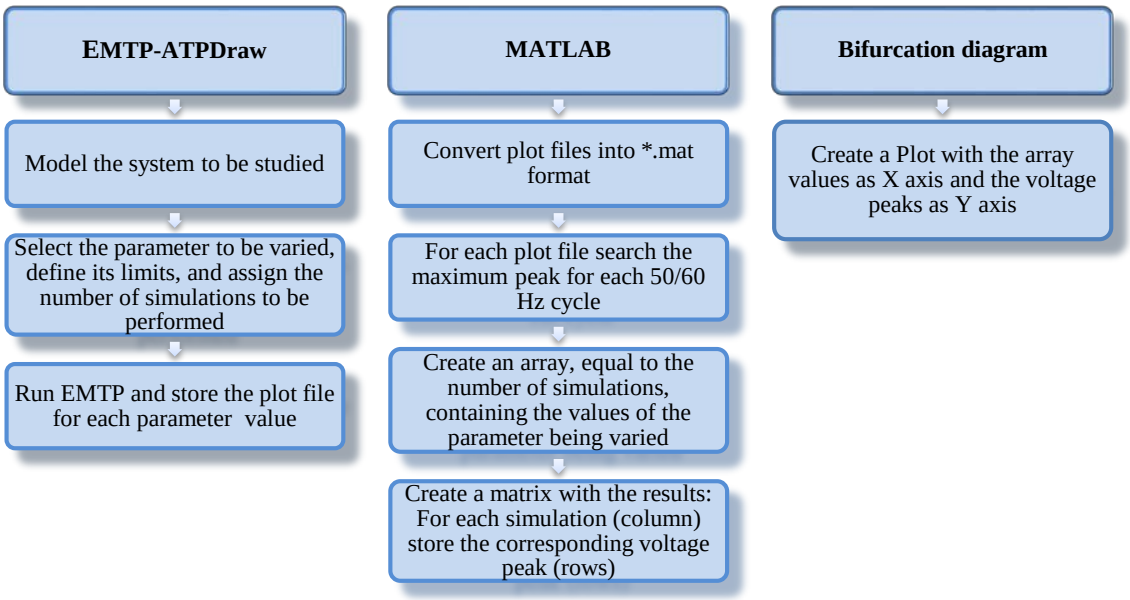

Figure 3.16. Bifurcation diagram construction flow chart.

The 2D bifurcation diagram is an alternative to traditional parametric and sensitivity methods and can be used to better understand ferroresonant systems. Its implementation in EMTP-like software can be assisted using MODELS, enabling pre-processing waveforms in real time. In this way, the work done by any external software will be significantly reduced. Figure 3.17 presents an example.

```
MODEL BIFURCATION
DATA  freq            -- base frequency
      PARAM1          -- Parameter being varied
INPUT x               -- monitored signals
VAR
     cycles, peak, peaktime, i                    --internal variables
     sample, num_cycles, time, tau2, xout
INIT
 xout:=0              --initial conditions
 peak:=0
ENDINIT
EXEC
 cycles:=1/freq
 num_cycles:=round(stoptime/cycles)
 time:=t
 sample:=x

 IF sample>peak THEN                  --conditioning one sample per cycle
    peak:=sample
    peaktime:=t
 ENDIF

 FOR i:=1 TO num_cycles BY 1 do
            tau2:=(cycles*i)
            IF tau2=t THEN
                  xout:=peak
                  peaktime:=peaktime
                  write('BEGIN WRITE @UseAS')
                  write(xout,' ',peaktime,' ', PARAM1)
                  write('END WRITE @UseAS')
                  peak:=0
            endif
 endfor
ENDEXEC
ENDMODEL
```

Figure 3.17. Example of MODELS code to create Bifurcation diagrams.

Since MODELS are a line-to-line language, for every execution of the example presented there are some hierarchical order to fulfill. First, all the external inputs and data needed should be declared. This will allow the real-time connection to external electric circuits. Second block of instructions consist on declaring all the temporal variables to be used an address all its initial conditions. The main block of the code is that presented between the EXEC and ENDEXEC instructions. There, the main purpose of the MODEL must be set, that is, the number of cycles to analyze must be computed and the peak selection should be performed once per cycle. Finally, the '*write*' instructions store all the information in an external txt document. A series of studies have been created, showing the potential of using bifurcation diagrams to summarize large parametric analyses when studying power systems under ferroresonance phenomenon.

3.2.2.1 Case study A: Ferroresonant Circuit

A large parametric analysis is performed to the ferroresonant circuit in case study *A* introduced in Chapter 2. The experimentation method has been used to compute a bifurcation diagram while varying the C_s value from 0.1 to 1 μF. The ferroresonance voltage has been measured across the non-linear inductor, and the 2D bifurcation diagram obtained is presented in the Figure 3.18.

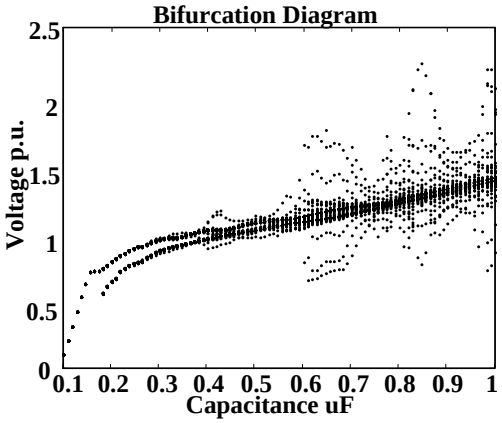

Figure 3.18. Bifurcation diagram for C_s analysis.

This diagram clearly demonstrates the behavior of the ferroresonant voltage for each value of C_s between 0.1 to 1 μF, and shows the stable and chaotic zones. In addition, the magnitude of the ferroresonant voltage is known for each value of C_s as a per unit value based on the normal steady state voltage. According to this plot, there is a period-2 between 0.2 and 0.4 μF where the plot draw two individual lines, a possible quasi-periodic state between 0.4 and 0.6 μF where the diagram shows multiple lines and a chaotic behavior in the 0.6 – 1 μF interval where a collection of points is gather for each *C* value. In a second example, the resistance value has been varied from infinite (lossless case 0 Ω) to 40 kΩ. The result of the parameter variation is presented in Figure 3.19 while having a C_s = 0.1 μF.

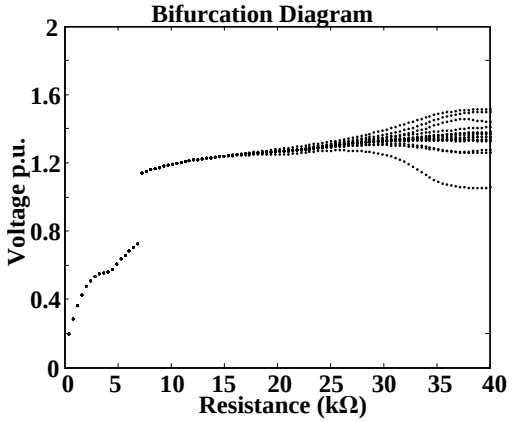

Figure 3.19. Bifurcation diagram for R_m analysis.

This plot allows understanding how the losses presented in a transformer core directly affect the occurrence of ferroresonance phenomenon. It is easy to see how after the value of 5 kΩ the magnitude of the voltage peaks start to increase.

Bifurcation diagrams clearly prove to be a powerful tool assisting the behavior analysis of ferroresonance signals upon the parameter variation. On the other hand, it proves that it is possible to summarize a long simulation study in just one diagram.

3.2.2.2 Case study B: Ferroresonant Behavior of a Voltage Transformer

The work based on the ferroresonant experience of the 400kV substation presented in Chapter 2 is one of the most interesting cases to be studied using large parametric analyses. The effect produced by circuit breaker grading capacitors and stray capacitance over inductive voltage transformers (VT's) is a very interesting case to be analyzed. The resume of the parametric analysis performed by changing the stray capacitance C_s value is shown in Figure 3.20.

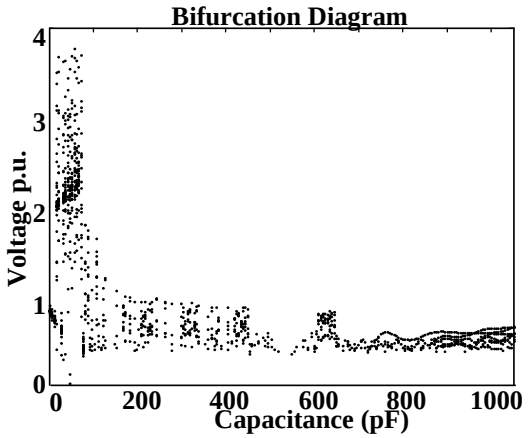

Figure 3.20. Bifurcation diagram for C_s analysis.

The values of the stray capacitance C_s and the grading capacitance C_g are both recognized as major influence parameters in the ferroresonant circuit because they are the greatest capacitance affecting the nonlinear inductance in the system. In this example, the values of C_s and C_g are 490 pF and 600 pF, respectively. According to the above diagram the voltage in the transformer has a chaotic behavior for C_s values lower than 100 pF. The study of the impact of the grading capacitance on the final ferroresonance state is collected in Figure 3.21.

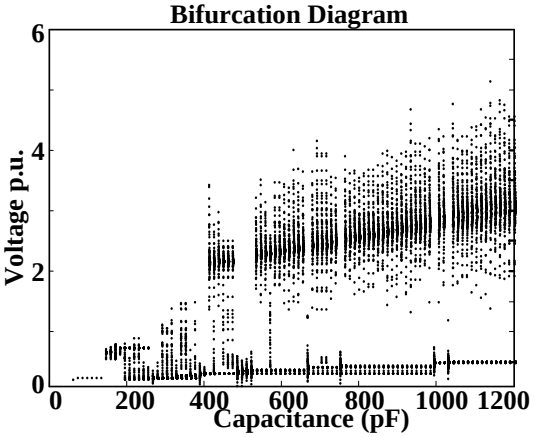

Figure 3.21. Bifurcation diagram for C_g analysis.

The diagram provides a clear insight of the system behavior. Values below 200 pF result in non-high overvoltages. It is important to remember that the fixed grading capacitance value of the system was 600 pF, and according to [21] the ferroresonance event terminated into a catastrophic event. Although the values of the capacitance remained fixed in normal operation, both bifurcation diagrams show the impact caused by any possible variation. Therefore, the bifurcation diagram can be used to select a safe set of grading capacitances.

3.2.2.3 Case study C: Ferroresonant Behavior of a Five-Legged Transformer

This study is based on the five-legged transformer presented in Chapter 2, and it is aimed to analyze the ferroresonant response to changes in the capacitance value that represents the cable between the source and the transformer. Signal analysis has demonstrated that the system is capable of having different modes of ferroresonance. The bifurcation diagram in Figure 3.22 summarizes the implication of the capacitance value in the system dynamics.

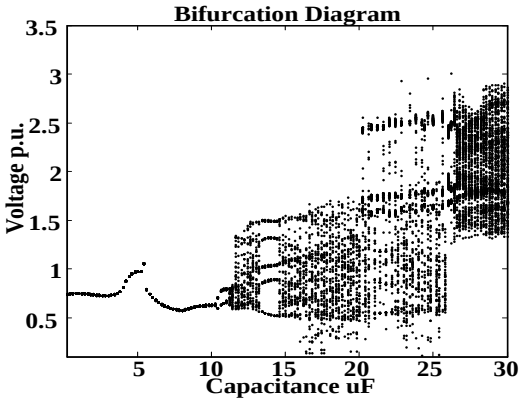

Figure 3.22. Bifurcation diagram for C_s analysis.

The diagram presents different responses for the system obtained when the value of the capacitance C_s is varied from 1 to 30 μF. The case of the five-legged transformer is probably one of the most canonic studies nowadays in the ferroresonance field, since most of the distribution transformers are built using this type of core and its studies have been present since the 80's. Several dynamics can be seen in the diagram going from fundamental mode, in the interval below 5 μF to period-2 and period-5, in the interval between 10 to 15 μF. Chaotic mode is present in the interval going from 15 to 30 μF. It is important to point out that in order to identify the different chaotic dynamics presented, a deeper analysis is needed and a tool such a Poincaré map can be used. A second study has been carried out to inquiry in the effect caused by the source phase shift. Figure 3.23 presents a bifurcation diagram obtained from the variation of C_s, however, the source phase shift has been set to 0 degrees; the original study was performed with a -90º.

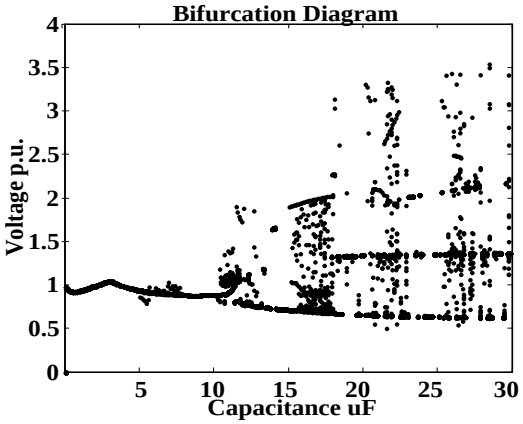

Figure 3.23. Bifurcation diagram for C_s analysis with source phase shift 0º.

The diagram obtained resembles the one previously studied. However, a significant decrease in the chaotic intervals can be seen. This type of phenomenon demonstrates the huge impact that initial conditions of the system have over ferroresonance.

3.3 FERRORESONANCE PREDICTION TOOLS

3.3.1 *3D Bifurcation Diagrams*

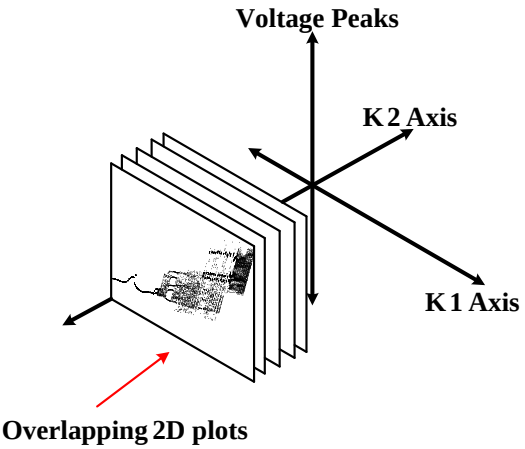

Figure 3.24. 3D Bifurcation diagram concept.

Traditional two dimensional bifurcation diagrams have introduced a roadmap for ferroresonance analysis. Such diagrams generate a map concentrating all information coming from large parametric analyses. Its application has been widely studied [22] - [30]. However, ferroresonance characterization and prediction requires analyzing countless possible scenarios, mainly when more than one parameter may significantly affect the behavior of a ferroresonant nonlinear circuit. Therefore, a novel technique has been proposed by applying 3D bifurcation diagrams for complementing ferroresonance characterization [31].

The 3D bifurcation diagram conceptually is based on a quasi-statically variation of two system parameters (K1 and K2). The variation of the first system parameter generates individual 2D planes while the stacking of planes corresponds to the variation of the second system parameter. The final output of a 3D bifurcation map consists on a colored point cloud revealing areas where the parameters under study lead to less dangerous ferroresonance states. This feature allows a better comprehension of the behavior of a power system while driven into ferroresonance. In addition, it is providing general insights for system design in order to know where safe zones are located.

The implementation of 3D Bifurcation diagrams uses the experimentation method, also known as brute-force method, and it consists on repeating time-domain simulations over a system followed by frequency-domain sampling of the same output to determine its periodicity. Figure 3.24 shows the scheme for 3D planes construction. In this study, an EMTP-based analysis is applied to solve system transients, while MATLAB is used for signal processing.

The general logic procedure developed to obtain 3D bifurcation diagrams is shown in Figure 3.25. The first three blocks of the scheme (inside the dashed-box) are entirely processed in EMTP, and the resulting outputs are exported to MATLAB (notice that there is one output for every value of parameter K1). Data sampling is performed each duty cycle in order to create individuals 2D planes. The plane stacking is developed by means of a 3D matrix; where each matrix layer contains a 2D plane. In such manner, the

stacked planes when plotted generate a volume, with K1 and K2 as X and Y axes, respectively, and the ferroresonant voltage value expressed in per unit value as Z axis. The base for the *per unit* calculation will always be the source voltage; in this way, it is easy to understand that every XY match describes the state of the ferroresonant voltage signal. The resulting 3D map is easy-to-read and maintains several features of the 2D diagrams: Straight lines will represent a fundamental mode and broken lines any period different than period-1 or in chaotic mode [7]. Whenever high precision is required to recognize a ferroresonance mode among the bifurcation diagram, a Poincaré map can be performed from a time domain simulation to determine the exact mode of the signal.

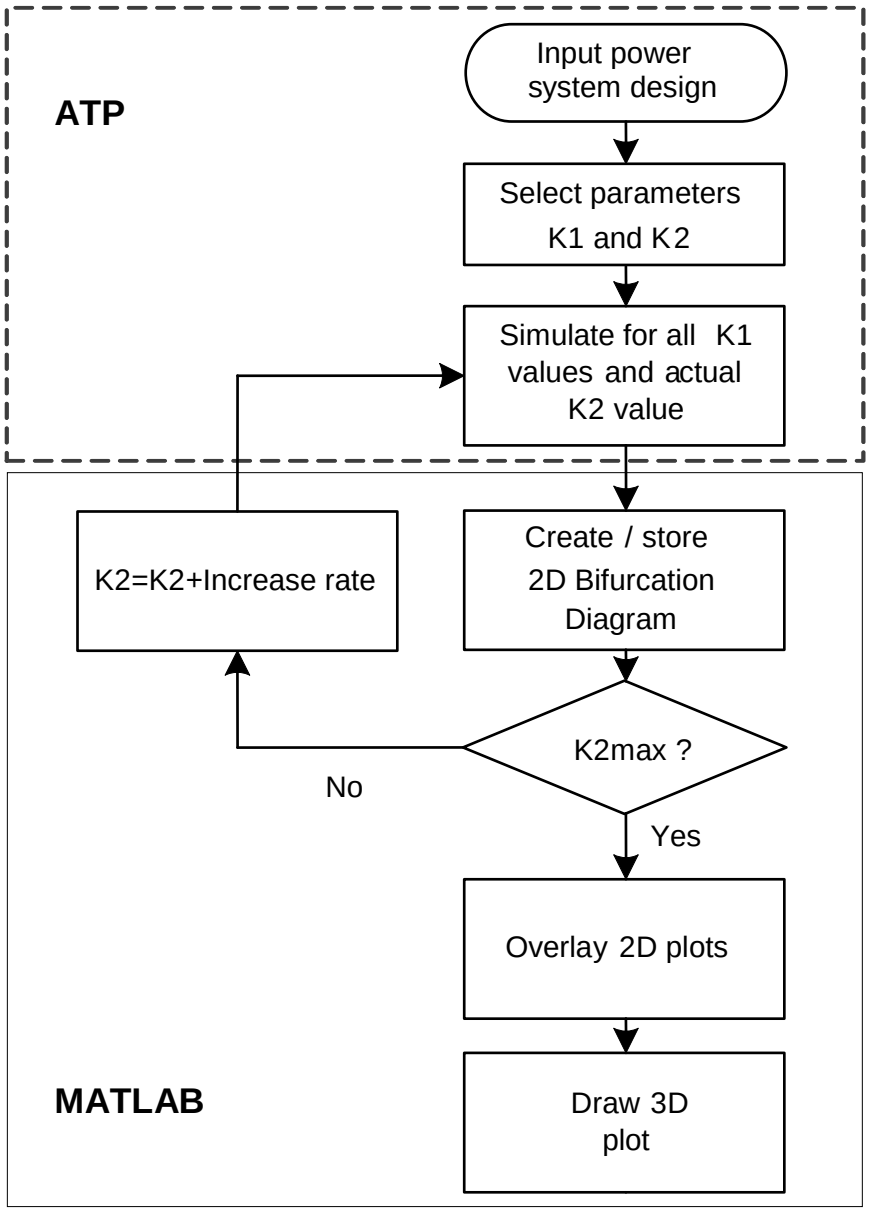

Figure 3.25. Sequence for generating 3D bifurcation diagrams.

3.3.1.1 Case study A: Ferroresonant Circuit

The simplest way to explain the 3D mapping approach is using the basic ferroresonant system presented in Chapter 1. The circuit is composed of a 25 kV/50 Hz power source, a capacitance of 0.1 µF, and a saturable inductance in parallel with a resistance of 40 kΩ.

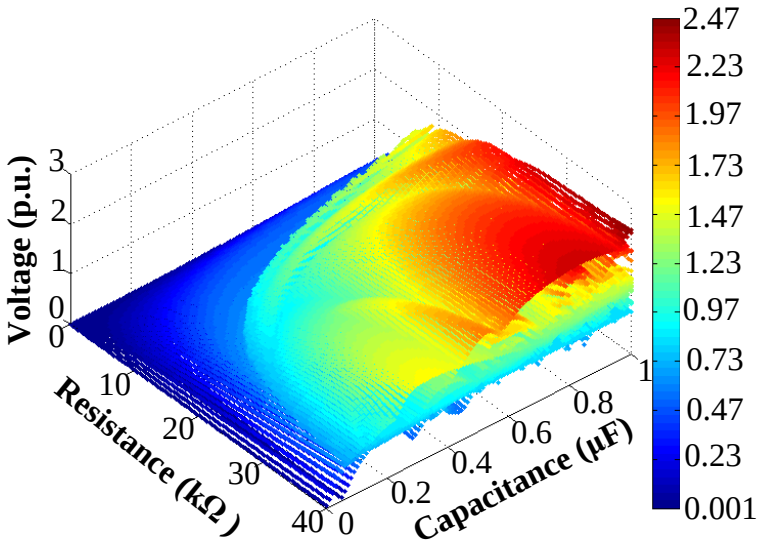

Figure 3.26. Case A: 3D Bifurcation diagram.

Assuming that the ferroresonance voltage has been measured across the nonlinear inductor, it is possible to perform a parametric analysis by changing the value of C_s from 0.1 to 1 µF. By applying the procedure presented in Figure 3.25 and slowly varying parameter C_s (parameter K1) and R_m (parameter K2). The intervals used goes from 0 to 1 µF, and 0 to 40 kΩ, respectively. It is possible to obtain a single 3D plot as the one shown in the Figure 3.26. The influence over the ferroresonant output made by the two main parameters of the circuit, C_s and R_m, is described by means of the 3D map, being the Z axis the per unit value based on the source voltage rate. Even though ferroresonance is present in almost any match C_s-R_m, there are two intervals (i.e., C_s = 0 - 0.2 µF and $R_m \leq 10$ kΩ) in which the signal is completely damped.

Notice also that the surrounded light blue area remains below the nominal voltage. The 3D bifurcation diagram summarizes a parametric analysis and can be used to select design parameters for newer systems and predict, beforehand, whether in a ferroresonant event the values will remain or not in a non-destructive zone. Note also that the diagram can be easily applied for analyzing the impact on given equipment by indicating in a chosen color (e.g., red color) the range of values for which equipment failure could occur. For example, cases affecting arresters commonly occur in power systems involving underground cables. In such cases, the ferroresonance voltage on the open line is usually much higher than the voltage feeding the transformer. In most cases that voltage is high enough to stress the lightning arresters and cause them to fail. By using a 3D map, it is possible to estimate the ferroresonance peak rate for a given system configuration, and comparison can be made to the failure rate for lightning arresters. Then, steps can be taken to properly coordinate the arresters operating range. Figure 3.27 presents two different perspectives of the 3D map, demonstrating how this type of graph gives relevant information to design systems.

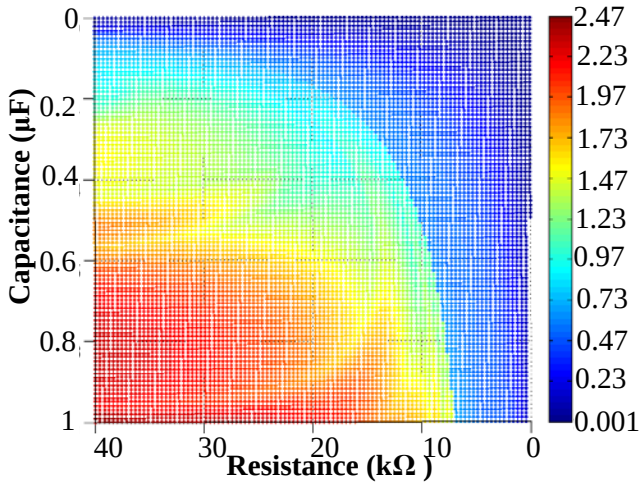

a) Top view

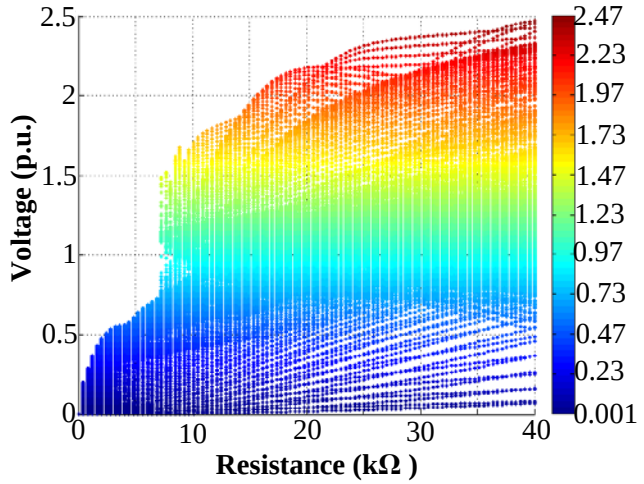

b) Side view

Figure 3.27. Case A: 3D bifurcation diagram views.

3.3.1.2 Case Study B: Voltage transformer

This case study is based on a work presented in 2010 [21]. The power system is composed with a 400 kV busline and a branch feeding a transformer bank.

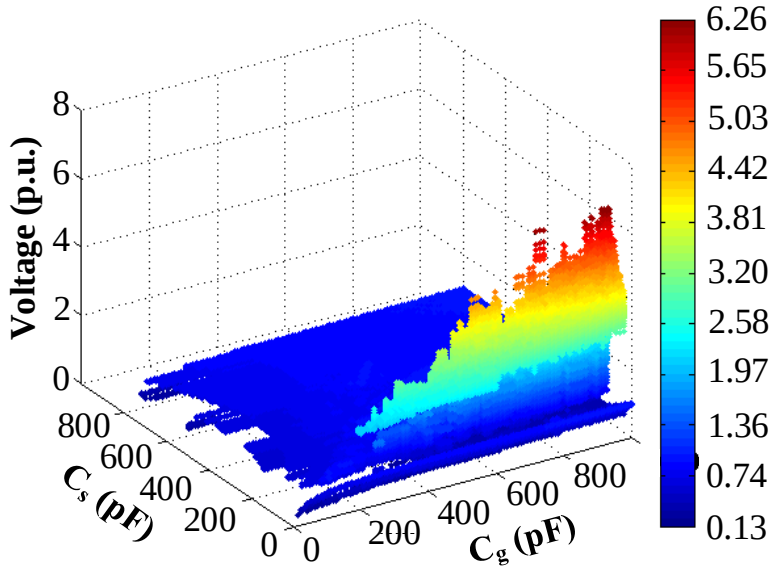

Figure 3.28. Case B: 3D bifurcation diagram.

The length of the branch cables and switches are included, and also the grading capacitance of the switch CB. The circuit and its data appeared in Chapter 2. Figure 3.28 resumes an extensive parametric analysis involving the main two capacitances implicated in the formation of ferroresonance. In steady-state, the values of the cable capacitance C_s and the grading capacitance C_g are 490 and 600 pF, respectively. Those values are recognized as major influence parameters in the ferroresonant system. The 3D diagrams show the impact of any system variation and describe the behavior of the ferroresonance effect with respect to those changes.

The 3D map was built according to the flow chart presented in Figure 3.25 and using C_s and C_g as K1 and K2, respectively. Since the Z axis is the per-unit value based on the source voltage, it is easy to identify that in most combinations of C_s and C_g, the resulting mode of ferroresonance will not exceed the 1 p.u. value, with exception of those values of C_s lower than 200 pF, interval that could unfold a chaotic mode with values up to 6 p.u..

In Figure 3.29 two different views of the map are shown. From the figures, it is easy to understand the effect that every individual C_s-C_g pair has over the final state of ferroresonance.

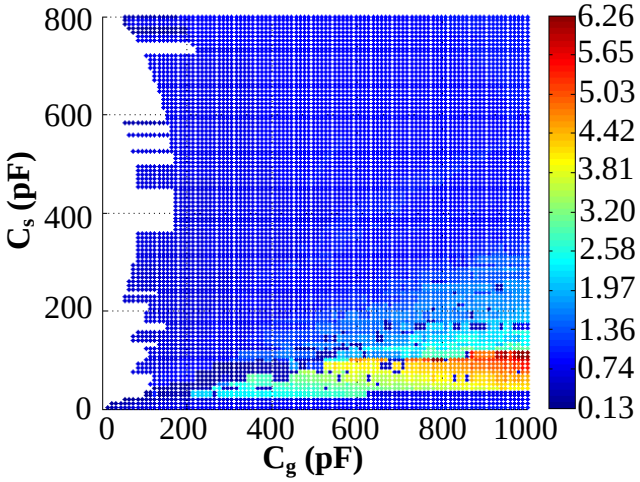

a) Top view

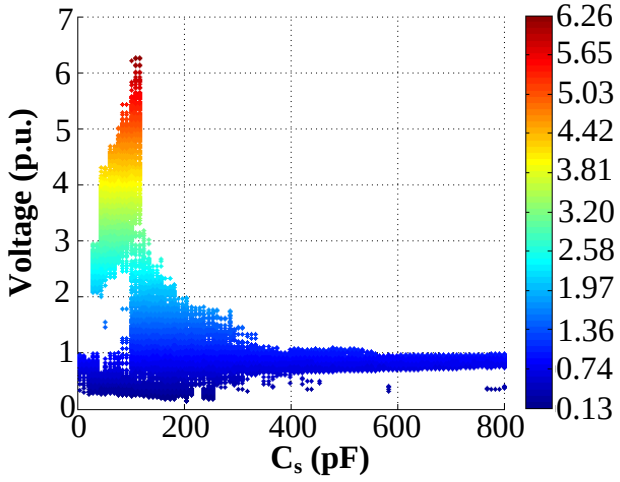

b) Side view

Figure 3.29. Case B: 3D bifurcation diagram views.

3.3.1.3 Case Study C: Sub-station transformer

The last case studied is based on the Dorsey Conversion Station located in Manitoba [10], [11]. The detailed information of the circuit can be found in Chapter 1. The system consists on two bus-lines delivering 230 kV, two power transformers, and a sub-station transformer.

The values of both the stray capacitance C_s and the grading capacitance C_g are also recognized here as major influence parameter in the ferroresonant system. Under steady-state, their values are 6000 and 6580 pF, respectively. A parametric analysis has been performed using both capacitances with the results shown in Figure 3.30.

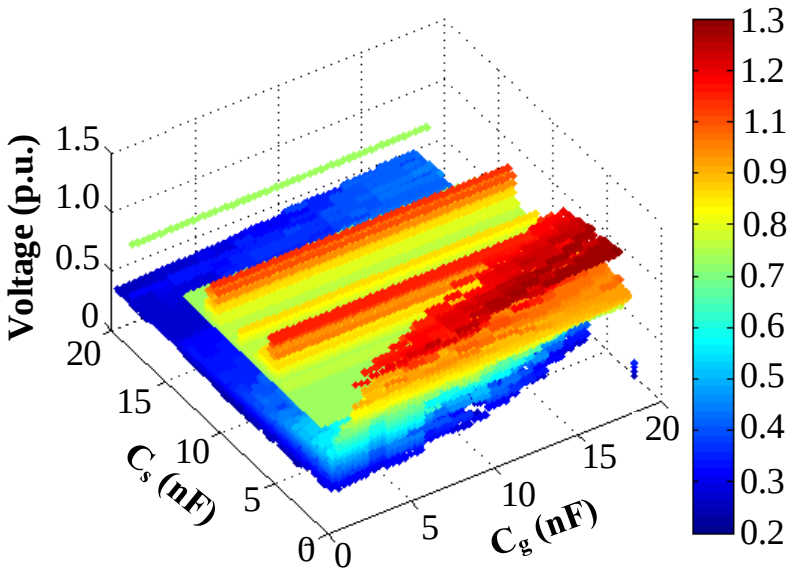

Figure 3.30. Case C: 3D Bifurcation diagram.

The 3D Bifurcation diagram analyzes both values of capacitances and show the response to any variation on the fixed values. The description of the system given in [11] clearly concludes that the typical values of the grading capacitance are in the range of 325 to 7500 pF, and perhaps, the one installed was around 6580 pF. Under this circumstance, following what is shown in Figure 3.30, it is possible to assume that if the value of the grading capacitance installed would have remained below 2000 pF, the ferroresonance voltage in the final state would have been smaller than the source voltage and, in the best case scenario, it would have been damped as shown in the map.

In order to have a better perspective of the matching between C_s and C_g, Figure 3.31 introduces the top view and the viewpoint from one of the sides. In general, the 3D map clearly shows that for most C_g - C_s combinations the final ferroresonance state will have 1 p.u. Remember that the blue zones represent the safe design zones. Even in the worst case scenario, the final state of ferroresonance will remain under 0.6 p.u. It is worth to remark that the red areas should be avoided from the designing point of view, since they normally represent chaotic behavior.

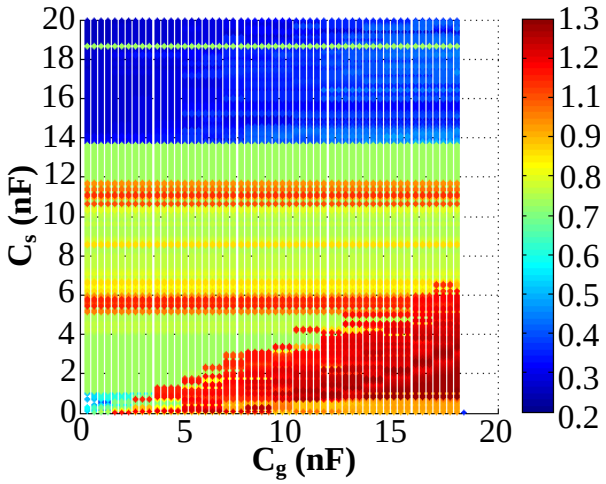

a) Top View

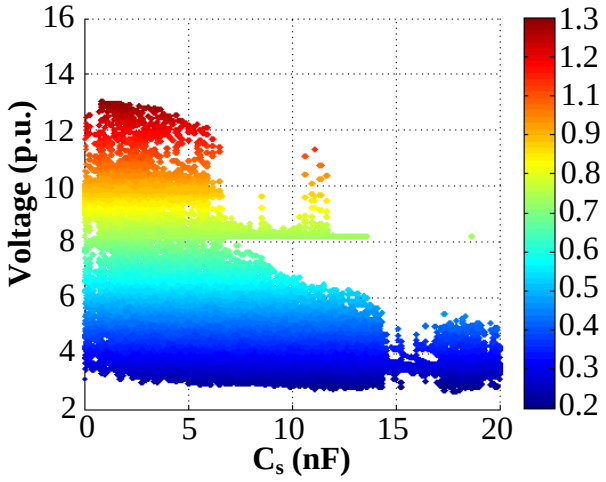

b) Side view

Figure 3.31. Case B: 3D Bifurcation diagram views.

3.3.2 *3D bifurcation Diagrams using Parallel Computing*

The 3D bifurcation diagrams have shown to be a versatile tool when attempting to characterize ferroresonance situations. However, the generation of such diagrams is a very tedious task since a high number of simulations has to be run in order to obtain a rigorous representation of the whole phenomenon; that is, a complete parametric study of a ferroresonant scenario can require thousands of iterations. In addition, a rather small time step (i.e. less than 10 μs.) has usually to be considered due to the nonlinearities involved in this phenomenon. This means that for a rather small system model more than one week of computer time could be necessary for completing the parametric study. A simple solution to this problem is the application of parallel computing. Indeed, several parametric studies can be simultaneously run using a multicore installation to cover the whole range of the parameter values of concern. Following the approach presented in the last section, a MATLAB procedure has been developed to drive ATP within a multicore installation and collect the information generated to obtain the bifurcation diagram characterizing the behavior of the test system. Figure 3.32 presents a diagram for the procedure implemented in MATLAB to run ATP in a multicore environment.

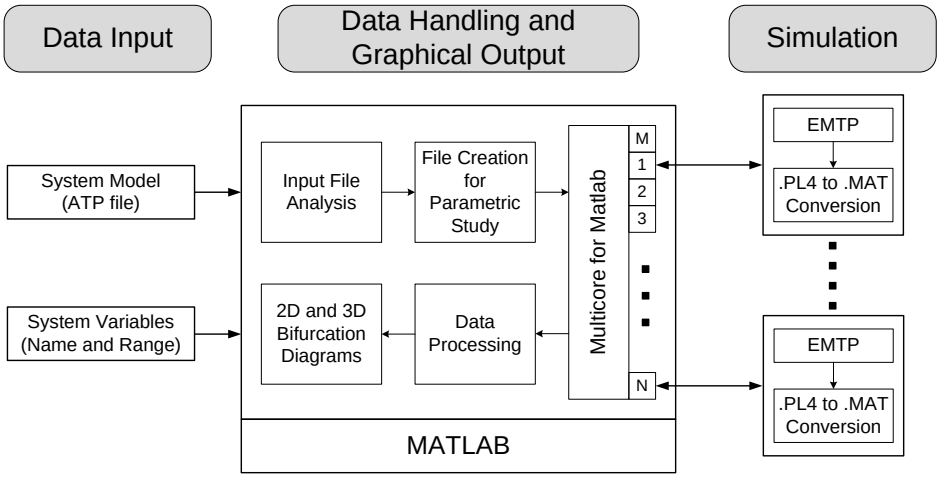

Figure 3.32. Procedure for generating bifurcation diagrams using a multicore installation.

A template of the input file corresponding to the test case is firstly elaborated. This template includes the ATP feature POCKET CALCULATOR VARIES PARAMETERS (PCVP), normally used to perform parametric analyses. By means of a MATLAB procedure the first parameter is written in the PCVP section and varied as many times as its range requires; while PCVP is used to vary the second parameter while the first one remains constant in each iteration. The user has to specify the range of values and the number of iterations for each parameter. The diagram presented in Figure 3.32 shows the procedure covering the three main parts: (1) data input preparation (aimed at editing input files); (2) data handling and generation of plots; (3) conversion of simulation results produced by ATP (i.e. the so-called PL4 files) to MATLAB format (i.e. MAT files). Notice the directions in which the information is flowing: the MATLAB code generates the final input files, distributes them between cores, controls the ATP iterations and the data conversion, reads and manipulates simulation results once they have been translated into MATLAB code, and finally takes care of the bifurcation diagrams generation. Another important aspect to be considered is the size of the files generated by ATP when using PCVP. Since a PL4 file for each combination of the two parameters to obtain the 3D diagram is needed, the size of the manipulated information is huge (e.g. if every parameter is varied 200 times, up to 40000 PL4 files will have to be read). To avoid the storage and manipulation of such a quantity of information, the simulations are progressively made; for instance, if 200 iterations are to be controlled from PCVP, since individual iterations do not depend to one another, the same file can be executed 4 times and using different parameter ranges, this way, the PCVP controls only 50 iterations within each execution. Remember that the ultimate goal is to obtain both 2D and 3D bifurcation diagrams for ferroresonance characterization.

3.3.2.1 Case A: 3D Bifurcation Diagram of a Five-Legged Transformer

The case presented uses the test system presented in Chapter 1 to analyze the effects in the ferroresonance final stage provoked by the cable capacitance and the source voltage regulation (±10%): the capacitance has been varied from 0 to 30 μF, and the source voltage has been varied from 432 to 528 V. The 3D map created compress up to 90000 simulations, performed in a total simulation time of 35558 s. An integration time step of $\Delta t = 1$ μs. has been used and the parallel computing has been done by means of 50 external cores. Figure 3.33 and 3.34 presents different views of the map.

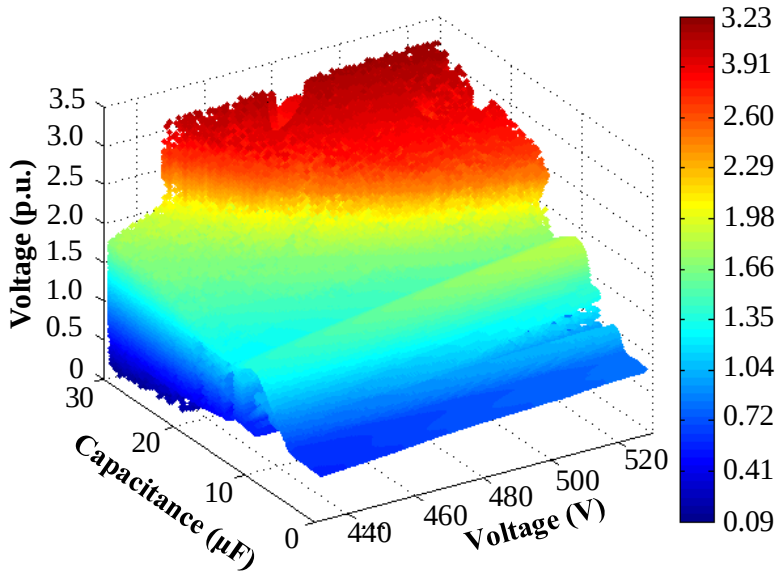

Figure 3.33. Case A: 3D bifurcation diagram.

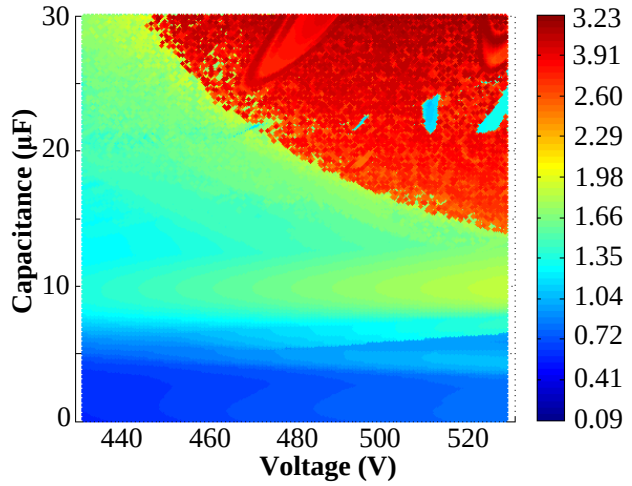

a) Top View

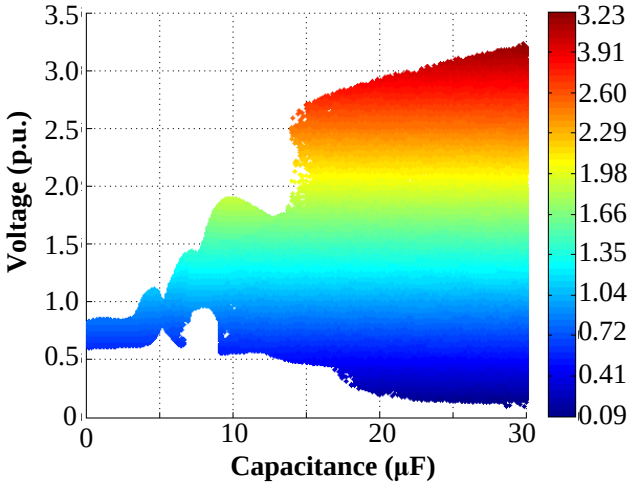

b)Side view

Figure 3.34. Case A: 3D bifurcation diagram views.

3.3.3 *4D bifurcation map*

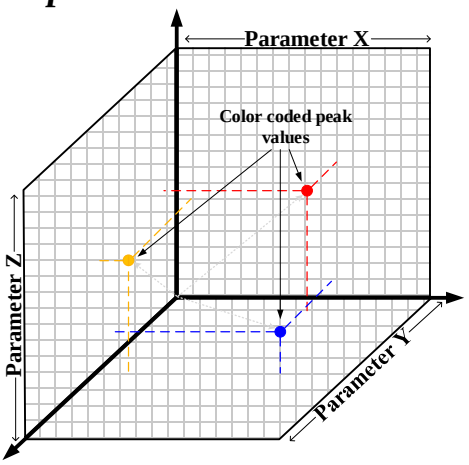

Figure 3.35. 4D Bifurcation diagram concept.

One of the most problematic features of ferroresonance is its unpredictability. According to dynamic systems theory, a probabilistic system like ferroresonance would be easily predicted if all initial conditions where known or at least controlled [18]. As a consequence, the need of determining the most influential parameters in ferroresonance ignition has been exposed during the last few decades. Throughout the years several system parameters have been pointed out to directly contribute to ferroresonance phenomenon. For this reason, the pursuit of a general tool to characterize and predict any ferroresonance case is still the main goal. By exploiting the great computational power offered by parallel computing, it has been possible to create a high dimensional tool that will summarize millions of simulations in a reasonable amount of computational time. Figure 3.35 introduces the idea of a 4D diagram. It consists on varying three individual parameters and collecting the voltage peaks resulting of the induced ferroresonance. The peaks selected are then colored coded according to its severity; this will enhance the map by avoiding the use of an axis representing the peaks. Figure 3.36 presents a simple flow chart explained such process.

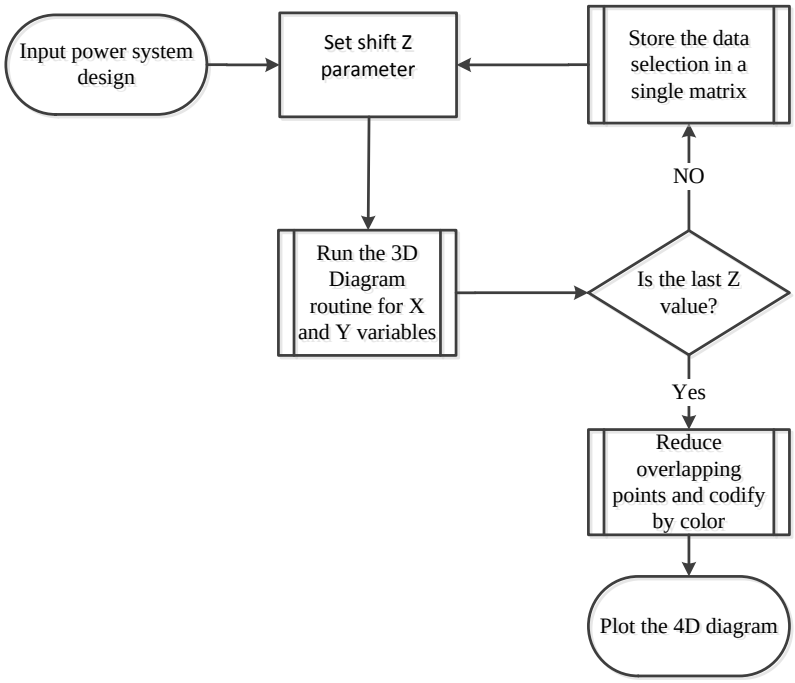

Figure 3.36. Sequence for generating 4D bifurcation diagrams.

3.3.3.1 Case study: 4D Diagram of a Ferroresonant Circuit.

The example selected to implement the 4D diagram is based on a simple 25kV ferroresonance circuit presented in Chapter 1. The parameters to be evaluated here are: The resistance R_m, capacitance C_s, and the power source variation (±10%). The fourth axis is depicted as the color coded range given to the output voltage. Figure 3.37 shows the 4D map.

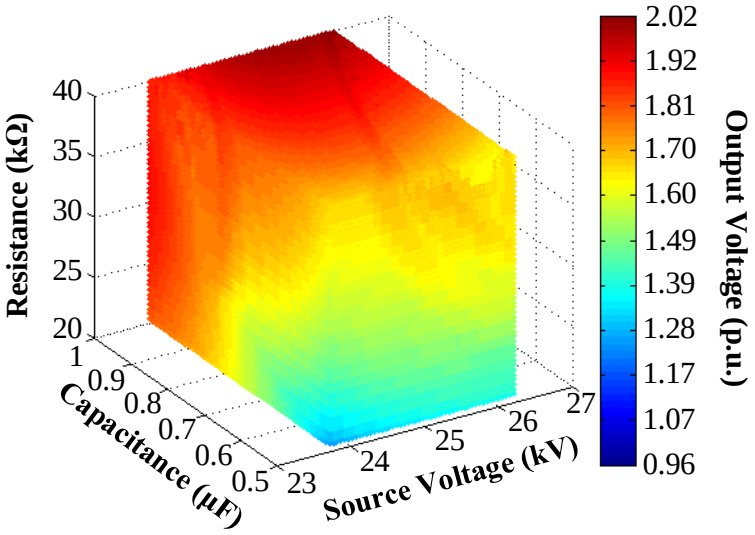

Figure 3.37. Case A: 4D Diagram.

The 4D map has been obtained after 125000 simulations and contains up to 6125000 points. The total simulation time was around 6 hours. A 3D map comprising an equivalent amount of simulations will be around the same time having more resolution, nevertheless, covering a smaller range of analysis zone. It is important to pointing out the factors influencing the duration of the total simulation time, which are: The amount of simulations, the time being simulated and the integration time step. Despite the amount of information condensed, the reading and understanding of the map sill remains simple. A color bar has been conveniently attached to the map to assist the reading, as it was in 3D maps, but in this case representing the range values of a forth axis. Dark red areas represent zones with high ferroresonance peaks up to 2 times the above normal operation value.

To simplify the interpretation, the map can be separated in sub-plots containing the range of values of interest. Figure 3.38a shows the map section corresponding to all those peaks bigger than 1 p.u. but lower than 2 p.u.. Figure 3.38b introduces the section of the map for those peaks colored in red and corresponding to high voltage ferroresonance. It is important to stand out the versatility of the diagram obtained. Different areas can be plotted individually allowing a better interpretation. By selecting a range of values among the fourth axis (i.e. the output voltage) a sub-plot can be created, the map will include all the parameter combinations within the *XYZ* axis resulting in the desired output range.

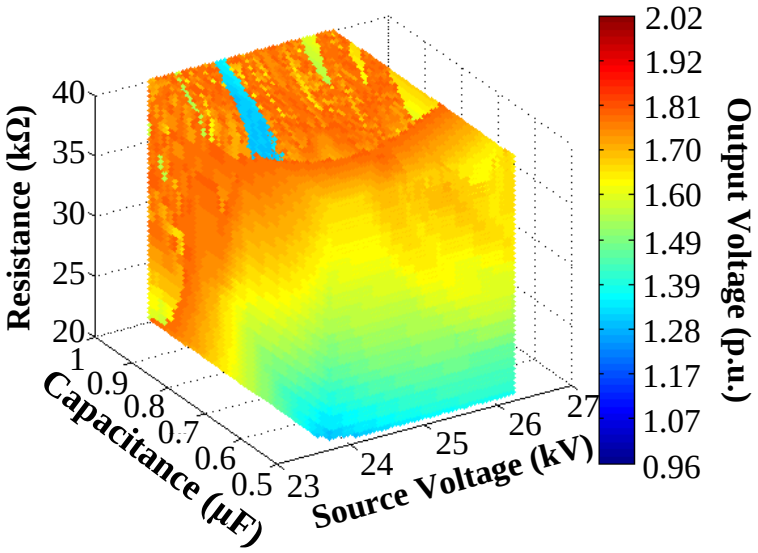

a)Medium voltage segment

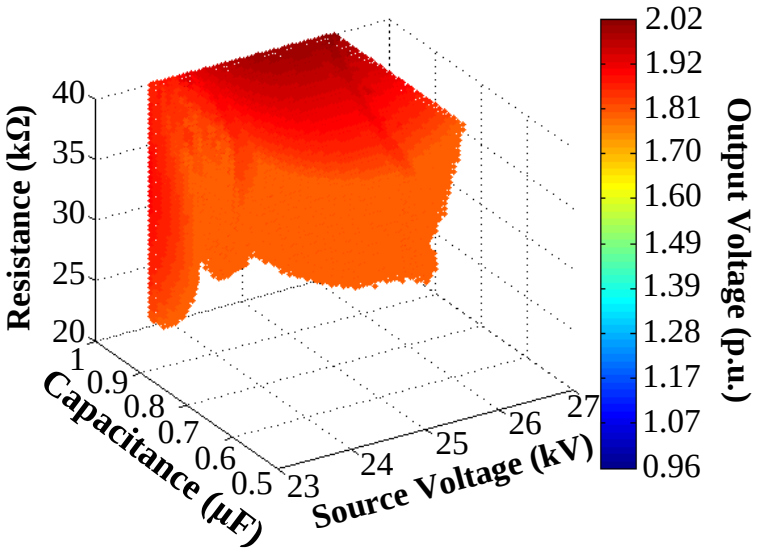

b)High voltage segment

Figure 3.38. Case A: 4D Diagram segments.

3.4 CONVENIENT STRATEGIES FOR LARGE PARAMETRIC ANALYZES

3.4.1 *An EMTP-based analysis of the switching shift angle*

Many conditions prone to initiate ferroresonance on a three-phase system are related to any manner of transformer energization/de-energization [4]. Some typical cases are [32]: Load rejection and transformer energized accidently on one or two phases while the transformer remains unloaded or lightly loaded (below 10-20% rated load). For more than a century a high number of ferroresonance cases have been reported, modeled and studied [4] - [7].

In most cases, research focuses in long parametric analysis involving the system principal components such capacitances, inductance or transformer load. However, exist

some cases where the veracity of those large parametric can be significantly affected just by changing the set up in the switch event, so much of the responsibility of the transient relies on the shift angle. Besides, there are commonly found research works where oscillations prior to the steady-state ferroresonant condition were almost impossible to be replicated. It was suggested then this was due to a random combination of parameters such as switching time or pre-switching voltage [21].

To date a serious study of the implication of the energization/de-energization shift angle into the final ferroresonant state cannot be easily found. This section tries to illustrate such implication by providing a case study aimed at understanding the ferroresonance behavior and presenting an alternative method to more accurately reproduce real ferroresonance cases [11], [21]. The implication of the switching shift angle in the final ferroresonant state is analyzed. Bifurcation diagrams are also applied to summarize ferroresonance behavior and to analyze the possible divergence in parametric analysis results due to the switching shift angle effect.

3.4.1.1 Test System

The test system studied in this section contains the principal elements in a classical ferroresonance parametric analysis [33]. In this study, the shift angle in switch *S1* used for the energization/de-energization will be the priority. The system zone presented in Figure 3.39 interconnects a transmission system to a distribution network by means of a substation transformer. The parameters of the power system components are detailed below:

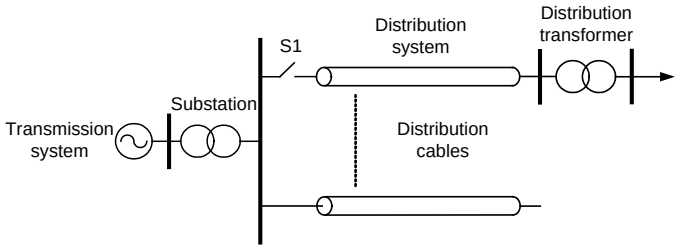

Figure. 3.39. Diagram of the system under study.

3.4.1.2 High Voltage Transmission System

The HV transmission system is represented by a 110 kV, 1500 MVA power source with X/R = 10, X_0/X_1 = 1.1, and a 110/25 kV, 35 MVA, 12%, Yd11, triplex core substation transformer grounded through a zig-zag reactance with 75 Ω per phase. The characteristics of the transformer are given by:

- No load test (positive sequence, MV side): V_0 = 100 %; I_0 = 0.296 %; W_0 = 18.112 kW.
- Short circuit test (positive sequence, HV side): V_{sh} = 12 %; I_{sh} = 83.34 %; W_{sh} = 348.263 kW.

3.4.1.3 Medium Voltage Distribution System

The MV distribution system is represented by two of the main components involved in a ferroresonance phenomenon: A distribution insulated cable and a distribution transformer. The main characteristics of the underground cable are: Al RHV, 3x(1x240 mm), 18/30 kV. Figure 3.40 presents a scheme of the cable representation.

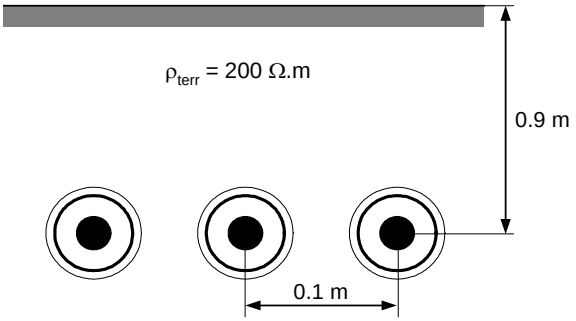

Figure 3.40. Underground cable configuration.

The distribution transformer is a 25/0.4 kV, 1 MVA, 6%, Dyn11 three-legged stacked core with internal characteristics given by:

- Short-circuit test (positive sequence, MV side): V_{sh} = 6 %; I_{sh} = 100 %; W_{sh} = 12 kW.
- No load test (homopolar sequence, LV side): V_h = 100 %; I_h = 0.5 %; W_h = 1.8 kW.
- Saturation curves are shown in Figure 3.41.

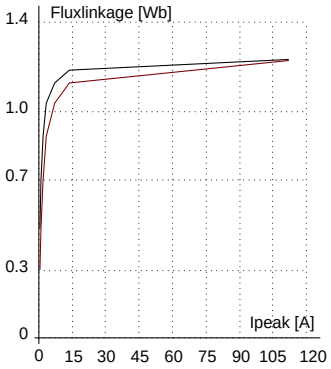

Figure 3.41. Saturation curve of the distribution transformer.

The study has been performed using EMTP-ATP [34]. Considering the system configuration and data, ATP built-in components (LCC for cables and the hybrid model for transformers) are accurate enough for analyzing the ferroresonant behavior of the system and for estimating the shift angle effect. The system modeled in ATPDraw is shown in Figure 3.42.

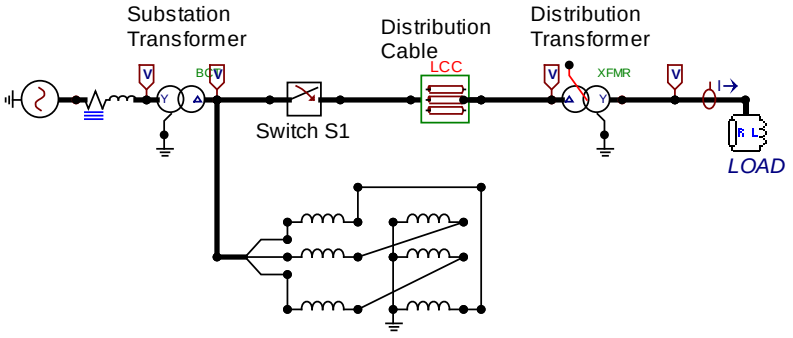

Figure 3.42. ATPDraw network model of the test system.

3.4.1.4 Shifting Angle Representation

The angle of the voltage feeding at the moment of the commutation is rarely known during the energization/de-energization of a transformer while performing a ferroresonance analysis. This has been normally due to the fact that this parameter is unknown or not considered important. In any case, the set up for switches in simulation software is given in time values not in degrees, leading to the common mistake of thinking in seconds and not in the amount of volts. Figure 3.43 shows a normal sinusoidal signal over the shifting angle.

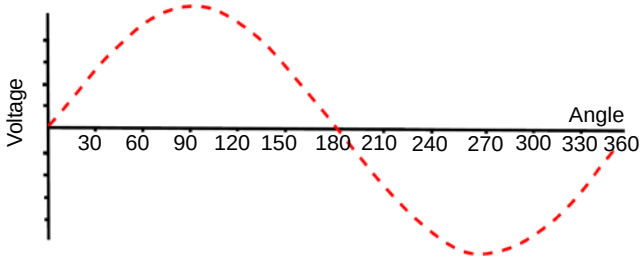

Figure 3.43. Sinusoidal signal.

Since any angle value corresponds to a different instantaneous value of the voltage signal, it is easy to understand that for different values of voltage, the transformer has different saturation points. The saturation curve is the cornerstone in the appearance of ferroresonance. There are previous works dealing with the impact of ferroresonance behavior due to the source phase angle [35], [36], but yet not explaining its dynamical and overall influence. In order to calculate any possible angle for the sinusoidal signal, assume that:

$$v = \sqrt{2} \cdot V_{rms} \cdot \sin \omega t \tag{3.1}$$

Since ωt represents the angle in this case, it is allowed to assume:

$$\theta = \omega t \tag{3.2}$$

$$t = \frac{\theta}{2\pi f} \tag{3.3}$$

By using this simple expression, it is possible to have the time for any studied angle. However, it is recommended to leave at least one duty cycle before setting the switch to have a zero crossing reference. Since the period of a cycle is equal to the inverse of the frequency, this value will be equal to 0.02 s for 50 Hz signals and 0.01667 s for 60 Hz. The shift angle time then can be defined as:

$$t_{shf} = k + \frac{\theta}{2\pi f} \tag{3.4}$$

where θ is the angle or set of angles under study, k is the period of one duty cycle in seconds and f is the power system frequency. This analysis could seem too simple, but it grows in relevance due to the great development in computational software. Current EMTP-like software allows users to edit variable parameters in which a simple value such the open/close time of a switch can respond to an elaborated equation. For that reason, it is simple to obtain the whole behavior of a signal under the phase shift effect by implementing the expression (3.4).

3.4.1.5 Case Study

The basis of the proposed analysis relies on two principal premises:

- A power system is prone to ferroresonance when a transformer is energized/de-energized accidently on one or two phases while the transformer remains unloaded or lightly loaded (below 10-20% rated load).
- The switching time (shift angle) of the energized/de-energized action can be undetermined but it affects the final state of the ferroresonance signal.

Considering the test system configuration shown in Figure 3.42, ferroresonance will be induced into the distribution transformer by accidentally opening the phase *A* pole of the switch S_1 connected to the primary side while the transformer remains lightly loaded; the other two phases remain closed. Two operating conditions are taken into consideration: 0.1%, and 2% of the transformer load. For both cases the shift angle will be varied in order to see whether there is any change in the state of ferroresonance. Only the de-energization is performed assuming that the energization maneuver will be affected in the same manner.

3.4.1.6 De-energizing a 0.1% Loaded Transformer

Taking into account that the full load for the distribution transformer is 1 MVA, the load applied will be around 1 kW. Initially, it is important to know the shape of ferroresonance under such operating conditions. Figures 3.44, 3.45 and 3.46 show the behavior of the ferroresonant voltage measured in the phase *A* at the medium voltage side of the distribution transformer, considering three different angles. It can be easily seen that, apart from the high values of the voltage, the switching shift angle has a major implication, not only in the final overall behavior of the signal but also in the initial transient between the normal stable state and the ferroresonance state. The whole influence of the shift angle for the ferroresonance condition in a 0.1% loaded transformer can be resumed using a bifurcation diagram as shown in Figure 3.47 [20], [30]. The diagram presents three important states: damped zones in which the voltage drops to almost 0.1 p.u., dangerous chaotic zones with voltage peaks up to 4.5 p.u., and repeatedly quasi-periodic zones oscillating between 2.5 and 3 p.u..

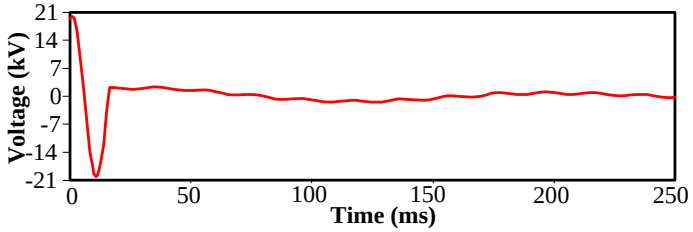

Figure 3.44. Ferroresonance signal for a 0^0 shift angle - 0.1% load.

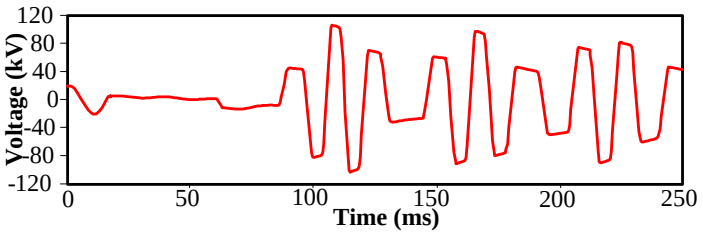

Figure 3.45. Ferroresonance signal for a 15^0 shift angle - 0.1% load.

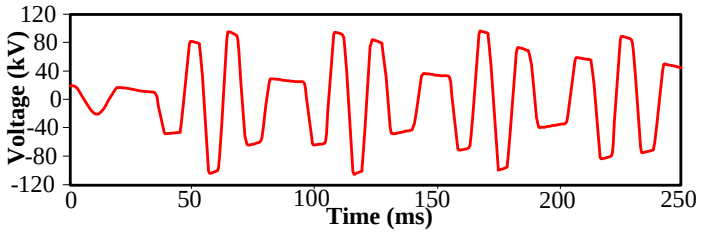

Figure 3.46. Ferroresonance signal for a 60^0 shift angle - 0.1% load.

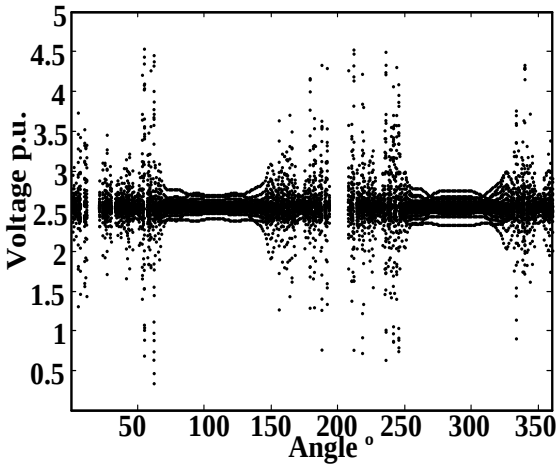

Figure 3.47. Bifurcation diagram for 0.1% load connected.

3.4.1.7 De-energizing a 2% Loaded Transformer

Once it has been seen that the shift angle can affect the behavior of ferroresonance, it is necessary to assure that assumption. For that purpose, the load of the transformer is increased to 5 kW. The shape of ferroresonance at different shift angles with the new operating condition is shown in Figures 3.48, 3.49 and 3.50. The pattern shown by the new plots is similar to the situation with 0.1% load, which means again that the shift angle has a direct implication on the way ferroresonance is going to be unfolded. However, from the bifurcation diagram shown in Figure 3.51, it is evident that now there are more damped areas than in the previous case.

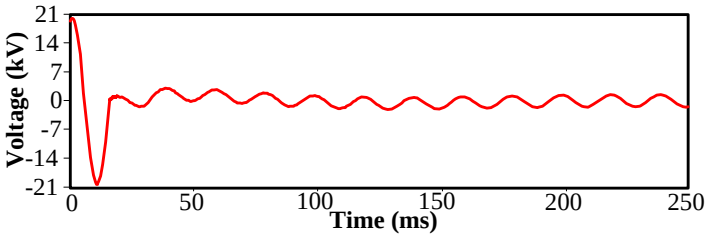

Figure 3.48. Ferroresonance signal for a 0^0 shift angle - 2% load.

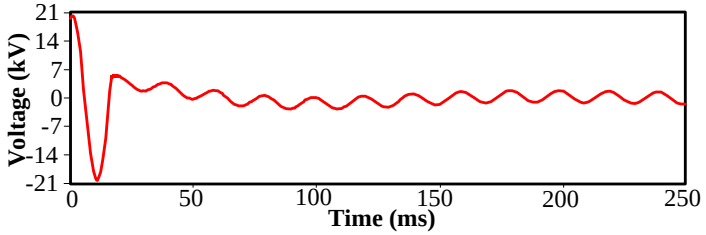

Figure 3.49. Ferroresonance signal for a 15^0 shift angle - 2% load.

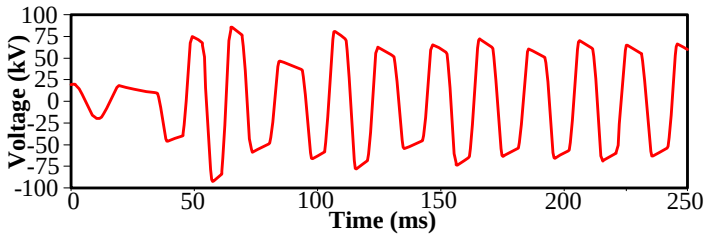

Figure 3.50. Ferroresonance signal for a 60^0 shift angle - 2% load.

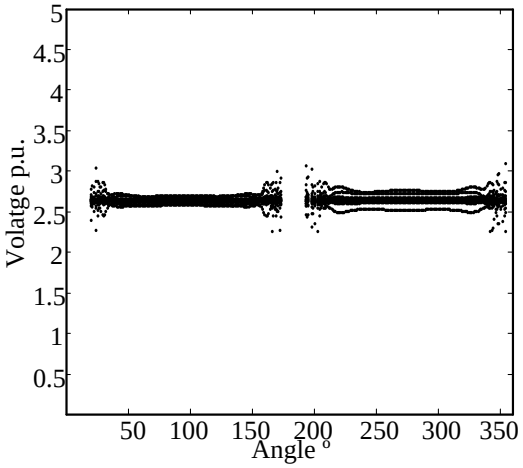

Figure 3.51. Bifurcation diagram for 2% load connected.

3.4.1.8 Parametric Analysis

The previous section has proved that the switching shift angle is a parameter to be taken into account in ferroresonance studies. To extend the results shown here, a parametric analysis aimed at exploring the effect of the load has been performed and repeated for different values of the shift angle. The resulting effect is important because besides the load, there are no other critical parameter changes (capacitance or saturation) in the power system.

The result shown in Figure 3.52 follows the typical shape in which ferroresonance theory is described [6]; that is, ferroresonance has a significant attenuation, normally referred to as damping, when the load increases in the secondary side of the transformer.

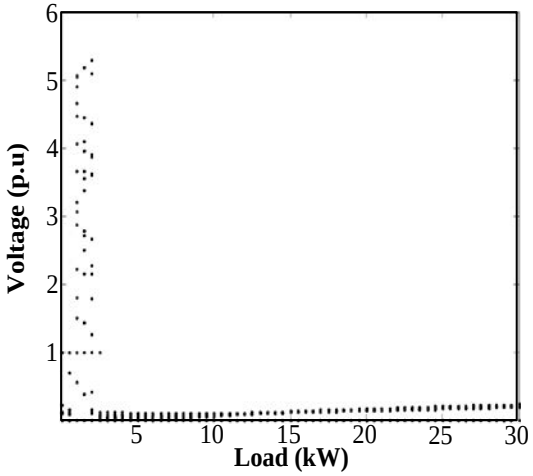

Figure 3.52. Bifurcation diagram for 15^0 shift angle.

The dynamic of the diagram shown in Figure 3.53 goes from chaotic mode to a damped signal. The importance of the shift angle becomes here more evident and realistic. In contrast with the results from Figure 3.52, the dangerous behavior remains even if the load reaches more than 5% of the nominal value.

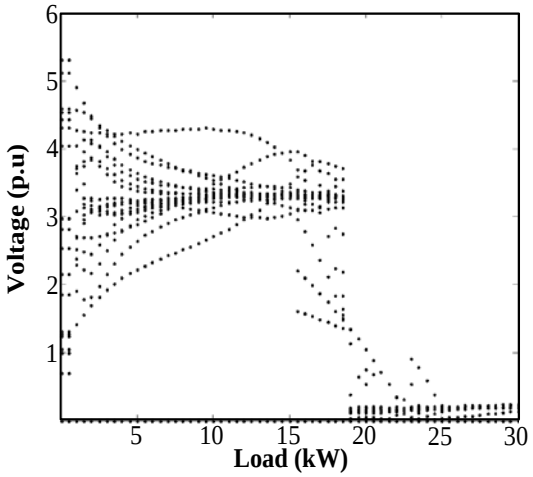

Figure 3.53. Bifurcation diagram for 60^0 shift angle.

The result shown in Figure 3.54 confirms that the possibility of obtaining a misleading response in a parametric analysis can be high if the shift angle is not well defined. That is, the dynamic behavior of ferroresonance can be misrepresented having a different result when comparing with Figure 3.53.

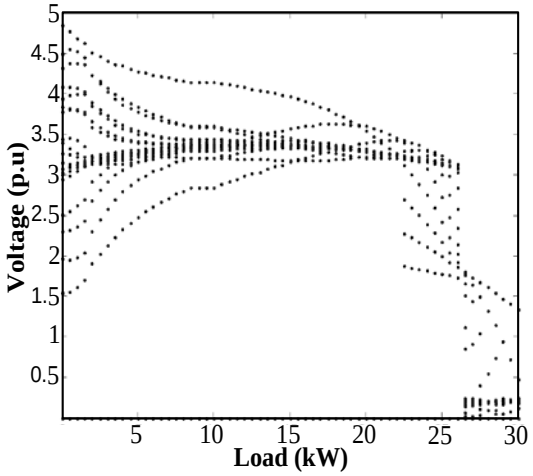

Figure 3.54. Bifurcation diagram for 90^0 shift angle.

The analysis developed has shown that in addition to the parameters usually considered in ferroresonance analysis (i.e., series capacitance, transformer core reactance, load), it is important to consider the shift angle of the switch with which the commutation action is performed. There are some cases in which a long transient is established between the steady state voltage signal and the ferroresonant final state. It has been proved that the veracity of a parametric analysis involving any system value related to load or capacitances, among others, can be significantly affected just by changing the set up in the switch event, so much of the responsibility of the transient relying on the shift angle. In order to obtain the most precise representation of such cases, some effort should be addressed to approach the correct moment of the energization/de-energization event.

3.4.2 *A Harmonic Balance Approach for Ferroresonant Analysis*

In this section, a predictive analysis is presented to locate stability domains for a period-1 ferroresonance. This prediction is made by using the Harmonic Balance method to solve the differential equation of the system. The order of polynomial expression representing the non linearity has been strategically selected to approach the physical characteristic of the inductor. The solution technique used in the harmonic balance allows comparing the procedure with the widely studied Duffing's equation solution [11].

The implication of initial conditions in the final ferroresonant state will also be analyzed. Bifurcation diagrams are obtained to depict the path in which the phenomenon will move and to predict the critical points where ferroresonance occurs. Stability regions for the test system are also located.

3.4.2.1 Test System

To explain the approach of this section, the basic circuit shown in Figure 3.55, will be analyzed. The circuit is composed of a 25 kV/50 Hz power source, a capacitance of 5 μF and a saturable inductance in parallel with a resistance of 40 kΩ representing the core losses [33].

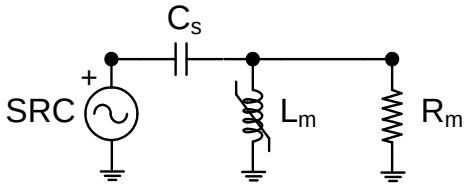

Figure 3.55. Diagram of the test circuit.

A proper representation of the transformer saturation is considered vital in ferroresonance studies [37]. Hence, when a mathematical equivalence of a transformer circuit is developed, the expression representing the saturation effect must be close-fitted to actual test data. Several approaches have been used throughout the years, being the two most accurate the trigonometric approximation based on the hyperbolic arctangent properties [38], and the polynomial approximation, whose strength relies on its simple implementation and the easy calculation of its coefficients [11], [39]. In this analysis, the polynomial approximation has been used due to its suitability on the harmonic balance resolution. Expression (3.5) shows the polynomial form.

$$i_L(t) = \mathrm{a}\lambda(t) + \mathrm{b}\lambda(t)^{\mathrm{n}} \tag{3.5}$$

where i_L represents the magnetizing current, λ represents the fluxlinked, and *a* and *b* the coefficients for the curve fitting. Selecting a proper value of *n* in the polynomial expression will significantly mark the accuracy of the representation. Figure 3.56 shows different curves corresponding to (3.5) with different *n* values and the actual test data. The figure proves that higher values of *n* approach better to the real nature of magnetization curve and its utilization will make the modeling more realistic. From Figure 3.56, the differential equation representing the mathematical behavior of the system is as presented below:

$$\ddot{\lambda} + k\dot{\lambda} + C_1\lambda + C_2\lambda^n = G\cos(\omega t) \tag{3.6}$$

where $k= 1/R_mC_s$, $C_1= a/C_s$, $C_2= b/C_s$ and $G=\omega V_{rms}$. In order to best approach the physical reality of the saturation curve '*n*' is set to 11. The coefficients are obtained following the technique presented in [11], [39]: $a = 43.59 \times 10^{-4}$ and $b = 7.415 \times 10^{-21}$.

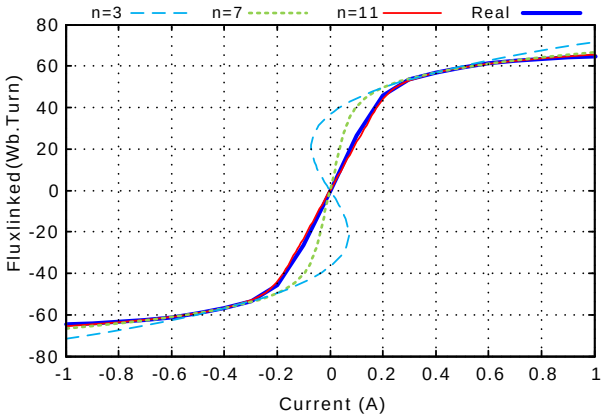

Figure 3.56. Non-linear inductance characteristic.

3.4.2.2 The Harmonic Balance Method

The harmonic balance is a method for the study of non-linear oscillating systems which are defined by non-linear ordinary differential equations [40]. Few approaches has been made in the ferroresonance field, most of them only consider the sinousoidal approximation or consider a low order polynomial approximation [41], [42]. In general terms, the method consists on substituting the unknown variable in the equation by an assumed solution so approximate periodic solutions can be found. The forced solution can be selected to behave as a steady state solution using a truncated Fourier series [18]:

$$\lambda = \lambda_0 + \sum_{k=0}^{K} A_N \cos(k\omega t) + B_N \sin(k\omega t) \tag{3.7}$$

In this study, the dc component can be neglected due to the sinusoidal state of the source signal. Here *k* sets the number of the harmonic component *N*. Normally this value depends on the oscillations considered or expected. For this work, *k* is set to 1 to obtain a first order approximation. Thus, the equation (3.7) will have the form:

$$\lambda = A\cos(\omega t) + B\sin(\omega t) \tag{3.8}$$

In order to substitute (3.8) into (3.6), the first and second derivatives should be found. These are:

$$\dot{\lambda} = -\omega A \sin(\omega t) + B\,\omega\cos(\omega t) \tag{3.9}$$

$$\ddot{\lambda} = -A\,\omega^2\cos(\omega t) - B\,\omega^2\sin(\omega t) \tag{3.10}$$

Substituting the expression for the flux and its derivatives in (3.6) and having the value '*n*' as 11, will significantly change the expression (3.6) in size and complexity. Once the simplification is performed, and the third and higher harmonics are neglected, a set of expressions are obtained for the first-order solution of the parameters *A* and *B*. These are given as follows:

$$A\left((C_1-\omega^2)+\frac{231}{512}C_2(A^2+B^2)^5\right)+Bk\omega=G \tag{3.11}$$

$$B\left((C_1-\omega^2)+\frac{231}{512}C_2(A^2+B^2)^5\right)-Ak\omega=0 \tag{3.12}$$

A general expression can be found by using the polar solution of the flux:

$$\lambda=A\cos(\omega t)+B\sin(\omega t)=r\cos(\omega t+\varphi) \tag{3.13}$$

where

$$r=\sqrt{A^2+B^2} \tag{3.14}$$

Thus, *r* by convenience provides also the magnitude of the flux. Then, (3.11) and (3.12) merges in a single expression:

$$\rho(r)=r^2\left((C_1-\omega^2)+\frac{231}{512}C_2r^{10}\right)+k^2\omega^2=G^2 \tag{3.15}$$

According to [9], real values of *r* that satisfy (3.15) correspond to the periodic solutions for the original differential equation (3.6). A graphical explanation of (3.15) can be made using a bifurcation diagram. It is obtained by finding the analytically solution for (3.6) while a system parameter is varied (source voltage). Figure 3.57 shows the result for the system. It can be deduced from this figure that, when the bifurcation parameter increases, the response of the flux suddenly jumps when it approaches the first turning point (TP1). The same will happen when the bifurcation parameter is slowly decreased; the flux will abruptly drop while approaching the second turning point (TP2). This type of behavior is usually referred as hysteretic-type pattern and it is associated to a saddle-node bifurcation [9]. The frontier at which the jumps in Figure 3.58 occur can be determined by finding the threshold of the change just when (3.14) has only one solution instead of two. This occurs when $\frac{d\rho}{dt}=0$. The derivative of (3.15) will give solution for (3.6) at the turning points.

$$2r\left(k^2\omega^2+((C_1-\omega^2)+\frac{231}{512}C_2r^{10})^2\right)+\frac{1155}{128}r^{11}((C_1-\omega^2)+\frac{231}{512}C_2r^{10})C_2=0 \tag{3.16}$$

If different capacitance values are tested, the corresponding values of voltage for the turning points can be calculated evaluating (3.17) for V_{rms}, and using the pairs (r,C_s) obtained from (3.16) [13].

$$r^2\left((C_1-\omega^2)+\frac{231}{512}C_2r^{10}\right)+k^2\omega^2=(\omega V_{rms})^2 \tag{3.17}$$

The graphical representation of equation (3.17) is known as bifurcation line or stability domain boundary [11]. The 2D bifurcation map from Figure 3.58 has a significant

meaning for ferroresonance analysis: it allows predicting where the boundary between sinusoidal and ferroresonance response is located. For instance, every *XY* combination of values at the right of the TP1 curve will have a high flux peak response (i.e. the *r* value is solved from equation (3.17)) while the left side combinations could have both: Low flux values for TP1 and high flux values response due to the coexistence with TP2 conditions.

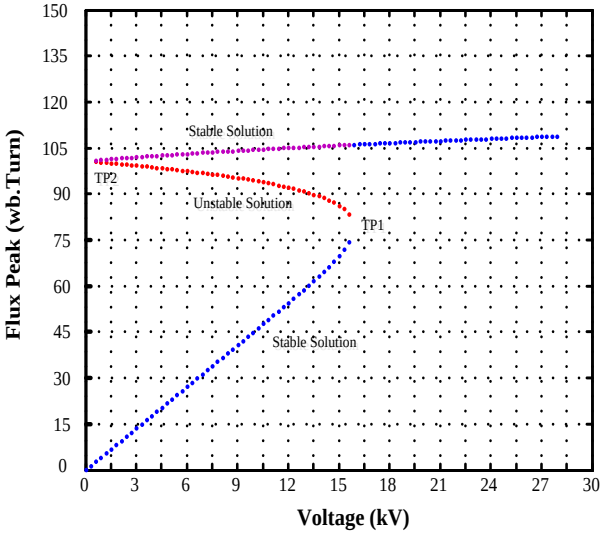

Figure 3.57. 2D bifurcation diagram for $C_s=5\mu F$.

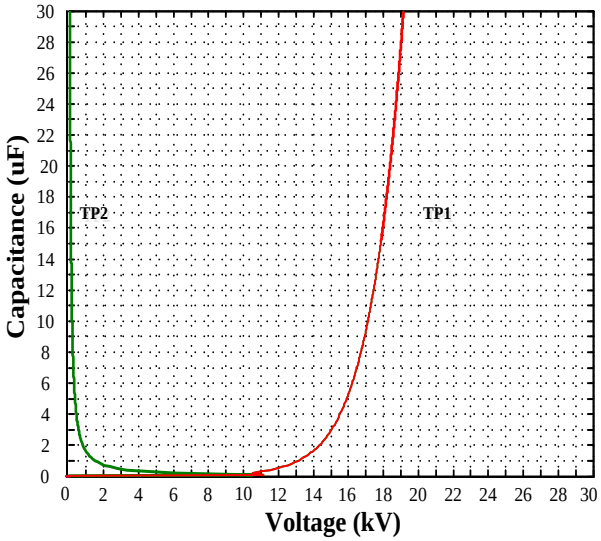

Figure 3.58. 2D bifurcation diagram.

3.4.2.3 Bifurcation Diagrams

In order to benchmark the Harmonic Balance Method, a set of bifurcation maps will be presented using the test system. Time domain simulations will be carried out under MATLAB environment to validate the mathematical analysis and the veracity in the harmonic balance approximation. Figure 3.59 shows the bifurcation diagram obtained from time domain simulation. This result proves the two different solutions predicted by the harmonic balance. Both solutions are obtained by increasing and decreasing the voltage, respectively. It is important to emphasize the co-existence of the two solutions, which reinforces the influence that initial conditions have over the behavior of a

ferroresonant system. To demonstrate the advantages of the result obtained with the harmonic balance analysis, an EMTP simulation study has been performed. Figure 3.60 presents the 2D bifurcation diagram originated from the EMTP-ATP simulation and applying the brute-force method. The results are significantly close to the harmonic balance prediction. A small discrepancy can be detected on the upper stable solution when comparing Figure 3.57 against Figures 3.59 and 3.60. However, it is important to keep in mind that the harmonic balance prediction is based on a first-order harmonic approach, which implies that only the sinusoidal stage is considered whereas computational systems include all the harmonic series in their solution. It is important remarking that the EMTP-ATP simulation can take several hours without including the post-processing task. On the other hand, harmonic balance can take no more than an hour.

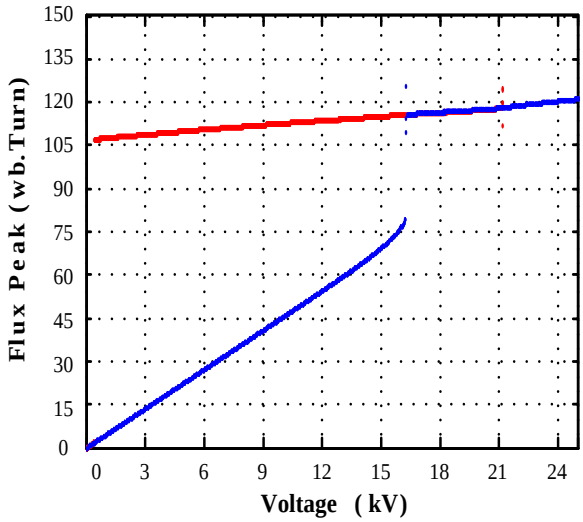

Figure 3.59. 1-D bifurcation diagram obtained using MATLAB for C_s=5μF.

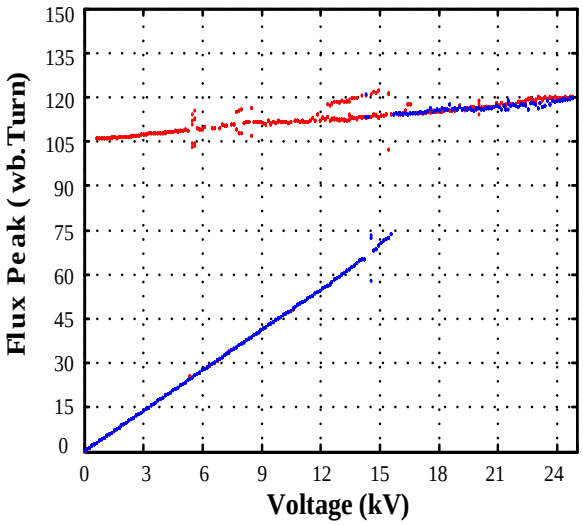

Figure 3.60. 1-D bifurcation diagram obtained using EMTP-ATP for C_s=5μF.

From Figure 3.58 it is easy to differentiate the regions for the systems stability. Any match of parameters selected at the right of the TP1 boundary will result into an undesirable solution, that is, in a ferroresonant state. A time-domain simulation has been performed to prove the previous statement.

Figure 3.61 validates the prediction for the undesirable region. However, the region at the left of TP1 in Figure 3.58 is totally dependent on the initial condition of the system.

Two different stages could occur. On one hand, the system could work in a sinusoidal state, normally for initial conditions set to zero. On the other hand, due to initial conditions (i.e., remanent flux and initial capacitance voltage), the response of the system could be unstable; in other words, ferroresonant. Figure 3.62 shows the co-existence of the two responses for the same set of parameters.

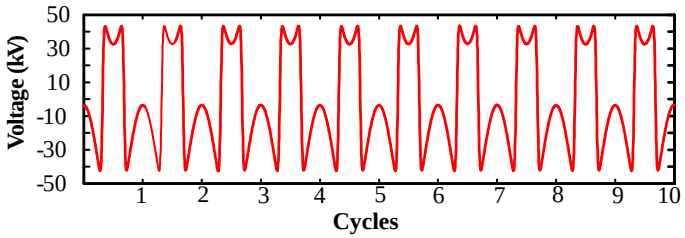

Figure 3.61. System response for $V_{rms}=25\ kV$ and $C_s=10\ \mu F$.

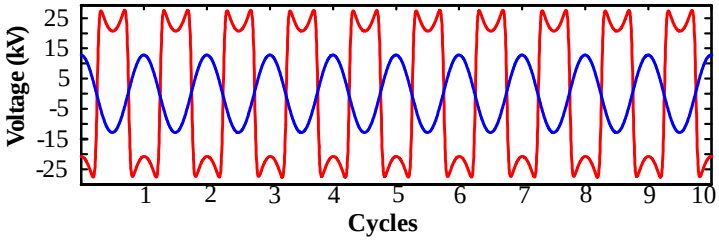

Figure 3.62. System response for $V_{rms}=9\ kV$ and $C_s=10\ \mu F$.

This section has presented the application of the Harmonic Balance Method for ferroresonance analysis using a simplified transformer model and by respecting the true nature of the magnetic saturation. The solutions were derived from a high-order polynomial so the results are close to the physical reality of a transformer. Comparisons of time-domain simulations using MATLAB and EMTP-ATP were presented. The analysis presented in this work has remarked the influence of the initial conditions in ferroresonance representation; the proper characterization can be vital for a well developed analysis.

The main contribution of applying the harmonic balance as a prediction tool is the capability to describe the behavior tendency of a system prone to ferroresonance making it a powerful technique. At the same time its simplicity makes it suitable to substitute large parametric analysis avoiding extensive time-domain simulations. Finally, bifurcation maps resulting from harmonic balance analysis provides clear paths for system design that could avoid hypothetical ferroresonance conditions.

3.5 CHAPTER SUMMARY

Several techniques for ferroresonance characterization have been introduce, explained and implemented. Such techniques address relevant subjects such identification of ferroresonance behavior and summarization of large parametric studies.

High dimensional techniques have been implemented to identify the safe zones in extensive parametric analyses. The maps resulting from those techniques are capable of summarizing millions of simulations, however, it reading remains simple and its contribution to understanding ferroresonance behavior is undeniable. 3D maps have been the subject of a publication product of this thesis. The 4D map is an approach to

globalize the whole behavior of ferroresonance systems for an extensive range of parameters.

The switching shift angle study and the harmonic balance method presents in detailed information for the preparation of parametric analysis. The impact of initial conditions and its impact in the final result of ferroresonance are put in evidence. Also the Harmonic Balance presents an interesting discussion whether simple ferroresonance circuits should be analyzed through time-domain simulations or by analytical techniques.

3.6 REFERENCES

[1] H. K. Høidalen, L. Prikler, and J. Hall, "ATPDraw- Graphical Preprocessor to ATP. Windows version", *International Conference in Power Systems Transients (IPST)*, Budapest, Hungary, June 1999.

[2] J. A. Martinez, R. Walling, B. Mork, J. Martin-Arnedo, D. Durbak, "Parameter Determination for Modeling Systems Transients. Part III: Transformers", *IEEE Transactions on Power Delivery*, vol. 20, no. 3, pp. 2051-2062, 2005.

[3] R. Rüdenberg, *Transient Performance of Electric Power Systems*, McGraw-Hill, New York, 1950.

[4] R. H. Hopkinson, "Ferroresonance during single-phase switching of 3-phase distribution transformer banks", *IEEE Transactions on Power Apparatus and Systems*, vol. 84, no. 4, pp. 289-293, 1965.

[5] H. W. Dommel, "Digital computer solution of electromagnetic transients in single- and multiphase networks", *IEEE Transactions on Power Apparatus and Systems*, vol. 88, no. 4, pp. 388-398, 1969.

[6] P. Ferracci, *Ferroresonance*, Cahier Technique no. 190, Groupe Schneider, 1998.

[7] B. A. Mork, "Ferroresonance and Chaos - Observation and Simulation of Ferroresonance in a Five Legged Core Distribution Transformer", Ph.D. Thesis, North Dakota State University, 1992.

[8] A. E. A. Araujo, A. C. Soudack and J. R. Marti, "Ferroresonance in power systems: chaotic behavior", *IEE Proceeding C (Generation, Transmission and Distribution)*, Volume 140, no. 3, pp. 237 -240, May 1993.

[9] S. Mozaffari, S. Henschel, and A.C. Soudack, "Chaotic ferroresonance in power transformers", *IEE Proceeding C (Generation, Transmission and Distribution)*, vol.142, no. 3, pp. 247-250, May 1995.

[10] D. A .N. Jacobson, "Field Testing, Modelling and Analysis of Ferroresonance in a High Voltage Power System", Ph.D. Thesis, The University of Manitoba, 2000.

[11] D. A. N. Jacobson, P. W. Lehn, and R. W. Menzies, "Stability domain calculations of period-1 ferroresonance in a nonlinear resonant circuit", *IEEE Transactions on Power Delivery*, vol. 17, no. 3, pp. 865-871, July 2002.

[12] V. Valverde, G. Buigues, E. Fernandez, A. J. Mazon, and I. Zamora, "Behavioral patterns in voltage transformer for ferroresonance detection", *16th IEEE Mediterranean Electrotechnical Conference* (MELECON), Tunisia, March 2012.

[13] P. S. Moses, M. A. S. Masoum, H. A. Toliyat, "Impacts of hysteresis and magnetic couplings on the stability domain of ferroresonance in asymmetric three-phase three-leg transformers", *IEEE Transactions on Energy Conversion*, vol. 26, no. 2, pp. 581-592, June 2011.

[14] A. Rezaei-Zare and R. Iravani, "On the transformer core dynamic behavior during electromagnetic transients", *IEEE Transactions on Power Delivery*, vol. 25, no. 3, pp. 1606-1619, July 2010.

[15] S. Jazebi, A. Farazmand, B. P. Murali, and F. de Leon, "A comparative study on π and T equivalent models for the analysis of transformer ferroresonance", *IEEE Transactions on Power Delivery*, vol. 28, no. 1, pp. 526-528, January 2013.

[16] T. Van Craenenbroeck, D. Van Dommelen, C. Stuckens, N. Janssens, and P. A. Monfils, "Harmonic balance based bifurcation analysis of three-phase ferroresonance with full scale experimental validation", *IEEE Transmission and Distribution Conference*, April 1999.

[17] S. H. Strogatz, *Nonlinear Dynamics And Chaos: With Applications To Physics, Biology, Chemistry, And Engineering (Studies in Nonlinearity)*. Westview Press, 2001.
[18] R. Hilborn, *Chaos and Nonlinear Dynamics: An Introduction for Scientists and Engineers*, Oxford University Press, USA, 2001.
[19] L. Dubé, *MODELS in ATP*, Language manual, February 1996.
[20] T. S. Parker and L. O. Chua, *Practical Numerical Algorithms for Chaotic Systems*, Springer, 1989.
[21] M. Val Escudero, I. Dudurych, and M. A. Redfern, "Characterization of ferroresonant modes in HV substation with CB grading capacitors", *Electric Power Systems Research*, vol. 77, no. 11, pp. 1506-1513, 2010.
[22] C. Kieny, "Application of the bifurcation theory in studying and understanding the global behavior of a ferroresonant electric power circuit", *IEEE Transactions on Power Delivery*, vol. 6, no. 2, pp. 866-872, April 1991.
[23] C. Kieny, G. Le Roy, and A. Sbai, "Ferroresonance study using Galerkin method with pseudo-arclength continuation method", *IEEE Transactions on Power Delivery*, vol. 6, no. 4, pp. 1841-1847, October 1991.
[24] D. A. N. Jacobson, "Examples of ferroresonance in a high voltage power system", *IEEE Power and Energy Society General Meeting*, Toronto, July 2003.
[25] P. S. Bodger, G. D. Irwin, D. A. Woodford, and A. M. Gole, "Bifurcation route to chaos for a ferroresonant circuit using an electromagnetic transients program", *IEE Proceeding C (Generation, Transmission and Distribution)*, vol. 143, no. 3, pp. 238- 242, May 1996.
[26] A. Ben-Tal, D. Shein, and S. Zissu, "Studying ferroresonance in actual power systems by bifurcation diagram", *Electric Power Systems Research*, vol. 49, no. 3, pp. 175-183, April 1999.
[27] F. Wörnle, D. K. Harrison, and C. Zhou, "Analysis of a ferroresonant circuit using bifurcation theory and continuation techniques", *IEEE Transactions on Power Delivery*, vol. 20, no. 1, pp. 191-196, January 2005.
[28] A. Rezaei-Zare, R. Iravani, and M. Sanaye-Pasand, "Impacts of transformer core hysteresis formation on stability domain of ferroresonance modes", *IEEE Transactions on Power Delivery*, vol. 24, no. 1, pp. 177-186, January 2009.
[29] F. Ben Amar and R. Dhifaoui, "Study of the periodic ferroresonance in the electrical power networks by bifurcation diagrams", *Electrical Power and Energy Systems*, vol. 33, pp. 61-85, 2011.
[30] J. A. Corea-Araujo, F. Gonzalez-Molina, J. A. Martinez-Velasco, J. A. Barrado-Rodrigo, and L. Guasch-Pesquer, "Tools for ferroresonance characterization", *EEUG Conference*, Zwickau, Germany, September 2012.
[31] J. A. Corea-Araujo, F. González-Molina, J. A. Martínez, J. A. Barrado-Rodrigo, and L. Guasch-Pesquer, "Tools for characterization and assessment of ferroresonance using 3-D bifurcation diagrams", *IEEE Transactions on Power Delivery*, vol. 29, no. 6, pp. 2543-2551, December 2014.
[32] J. A. Martinez-Velasco and F. Gonzalez-Molina, Temporary Over-voltages in Power Systems, Chapter 5 in *Power Systems Transients*, J.A. Martinez-Velasco (Ed.), Ref. 6.39.59, The Encyclopedia of Life Support Systems (EOLSS-UNESCO), 2012.
[33] J. A. Martinez-Velasco and J. R. Martí, Electromagnetic Transients Analysis, Chapter 12 in *Electric Energy Systems:Analysis and Operation*, A. Gómez-Expósito, A. Conejo and C. Cañizares (Eds.), Boca Raton, CRC Press, 2008.
[34] K. U. Leuven EMTP Center, *Alternate Transients Program Rule Book*. Heverlee, Belgium: Leuven EMTP Center, 1987.
[35] M. Roy and C. K. Roy, "A study on ferroresonance and its dependence on instant of switching angle of the source voltage", *3rd International Conference on Power Systems*, ICPS, India, December 2009.
[36] P. Sakarung and S. Chatratana, "Application of PSCAD/EMTDC and chaos theory to power system ferroresonance analysis", *6th International Conference on Power Systems Transients*, IPST, Montreal, Canada, June 2005.
[37] M. R. Iravani, A. K. S. Chaudhary, W. J. Giewbrecht, I. E. Hassan, A. J. F. Keri, K. C. Lee, J. A. Martinez, A. S. Morched, B. A. Mork, M. Parniani, A. Sarshar, D. Shirmohammadi, R. A. Walling, and D. A. Woodford, "Modeling and analysis guidelines for slow transients: Part III: The study of ferroresonance", *IEEE Transactions on Power Delivery*, vol. 15, no. 1, pp. 255-265, January 2000.

[38] A. Rezaei-Zare, R. Iravani, M. Sanaye-Pasand, H. Mohseni, and S. Farhangi, "An accurate hysteresis model for ferroresonance analysis of a transformer", *IEEE Transactions on Power Delivery*, vol. 23, no. 3, pp. 1448-1456, January 2008.

[39] T. Van Craenenbroeck, D. Van Dommelen, J. Driesen, and R. Belmans, "Application of the harmonic balance method to study ferroresonance in voltage transformers", *11th International Symposium on High Voltage Engineering*, London, United Kingdom, August 1999.

[40] M. Moradi and A. Gholami, "Harmonic balance based stability domain analysis of period-1 ferroresonance", *Electric Power Components and Systems*, vol. 39, no. 12, August 2011.

[41] A. Bardhi, P. Cipo, and M. Braneshi, "Study of a ferroresonant circuit using analytic harmonic balance, numerical integration of nonlinear ODE and experimental methods", *14th Int. Power Electronics and Motion Control Conference* (EPE/PEMC), Ohrid, Macedonia, September 2010.

[42] N. A. Janssens, "Magnetic cores modeling for ferroresonance computations using the harmonic balance method", *IEEE Power and Energy Society General Meeting*, Toronto, Canada, July 2003.

4 Improvements of analytical techniques and transformers modeling for ferroresonance situations

4.1 INTRODUCTION

VALIDATING power system models for transient analysis imply the use of actual data from either field measurements or laboratory tests. This task can be particularly difficult when the transient process is quite nonlinear, as it occurs in ferroresonance phenomena. For transformers core, highly saturated stages are reached [1] - [3]. The goal of this chapter is to compare simulation results to actual measurements from routine and special tests of transformers and propose a manner for performing a ferroresonance essay under a controlled environment. Several approaches for representing transformers in transients are documented in the literature [4], [5]. The principle of duality is a very common approach for transformer core representation [6], [7], and has been used in the implementation for the models studied in this chapter.

For single-phase transformers an up-to-date research presented in [8] and [9] proved that the π model can be more accurate than the classical T model for representing the transient response of transformers with a high level of saturation. In addition, hysteresis effects should be included in the transformer representation for a better benchmarking with laboratory results [10]-[12]. This chapter will also focus the analysis on three-phase transformers under ferroresonance phenomenon. For this, the Hybrid Transformer model, implemented in ATPDraw [13]-[15] will be configured and tested. It is important to remark that few works analyze the behavior of the Hybrid model under transient state, however, it has never been tested for ferroresonance analysis.

Although an actual test for ferroresonance measurements has not been yet considered by international standards, it is possible, however, to find within literature some authors who describe precisely the ferroresonance path and the prone conditions for ferroresonance ignition. It is therefore possible to prepare a sort of tests to measure and capture ferroresonance signals in a controlled environment for both single- and three-phase transformers [9], [16].

The goal of this chapter is to validate the representation of a single-phase transformer by using the π model for core representation and the Hybrid model for three-phase transformers. In addition, other ferroresonance cases involving high saturated phenomena will be also analyzed including self-excited generator and other non-linear sources. All simulations presented in the chapter have been implemented using ATPDraw [17].

4.2 SINGLE-PHASE AND THREE-PHASE TRANSFORMERS MODELING AND FERRORESONANCE ANALYSIS

The experimental work presented in the following pages is the result of a three month research period carried out in the high voltage laboratory in Universidad del Valle, Cali, Colombia.

4.2.1 Laboratory Tests

The use of transformers in power systems has been and will longer remain the mainstay for both transmission and distribution systems. Its study means not only having the

ability to ensure proper operation in the conversion of energy, but at the same time, to ensure that energy quality will be held in desirable rates of efficiency. In practice, to certify that a new transformer or repaired one meet the standards to maintain the stability of power systems, it is necessary to perform a sort of experiments called routine tests. This procedure is done to confirm that the fundamental parts of the transformer are in good condition: mechanical, electrical and magnetic parts. Tests being used in this chapter:

- Insulation resistance (R-A)
- Transformation ratio (R-T)
- Winding resistance (R-D)
- No-load losses (P-V)
- Load losses (P-C)

Once these tests have been performed, a decision can be made whether the transformer is suitable for operation or not. A technical report is prepared containing the internal information of the transformer in accordance with the IEC and IEEE [10], [11], having a standardized temperature rate of: a) 85º for load-losses, windings resistance, and load-losses impedance, reactance and resistance b) 20 ° for no-load losses and currents.

4.2.2 Special tests

In order to obtain more than only the typical transformer physical information, three extra tests have been performed to acquire relevant information for modeling. Since these tests are not covered by any international standard, they receive the label of special tests. Even if those tests are not significant to be presented in a common technical transformer report, they do have a great significance for computational modeling. The tests are:

- Saturation curve extraction (SAT)
- Zero-sequence test (S-C)
- Transformer internal capacitive effects (CAP)

Table 4.1: Summary of tested transformers

	kVA	Condition	R-A	R-T	R-D	P-V	P-C	SAT	S-C	CAP
Tri_1	45	Repaired	√	√	√	√	√	√	√	
Tri_2	75	Repaired	√	√	√	√	√	√	√	
Tri_3	112.5	Repaired	√	√	√	√	√	√	√	
Tri_4	112.5	Repaired	√	√	√	√	√	√	√	
Tri_5	45	Repaired	√	√	√	√	√	√	√	
Tri_6	112.5	Repaired	√	√	√	√	√	√	√	√
Tri_7	75	Repaired	√	√	√	√	√	√	√	√
Tri_8	112.5	Repaired	√	√	√	√	√	√	√	√
Tri_9	75	Repaired	√	√	√	√	√	√	√	√
Tri_10	112.5	Repaired	√	√	√	√	√	√	√	√
Tri_11	500	New	√	√	√	√	√	√	√	√
Tri_12	45	New	√	√	√	√	√	√	√	√
Tri_13	400	New	√	√	√	√	√	√	√	√
Mono_1	25	Repaired	√	√	√	√	√	√	N.A	
Mono_2	25	Repaired	√	√	√	√	√	√	N.A	
Mono_3	3	Repaired	√	√	√	√	√	√	N.A	√
Mono_4	37.5	Repaired	√	√	√	√	√	√	N.A	√
Mono_5	5	Nuevo	√	√	√	√	√	√	N.A	√

Table 4.1 presents a summary containing the detailed information for all the transformers tested and presented in this chapter. It should be noted that the tests are the same for both single- and three-phase transformers. In the Table 4.1, each transformer is labeled for further reference. The 'Tri_' prefix is given to three-phase transformers, while the 'Mono_' prefix to single-phase transformers. Once it has been confirmed the proper state condition of the transformer, any other tests can be performed. For this study, it proceeded to perform ferroresonance tests.

4.2.3 Ferroresonance tests

The tests presented in this section should be performed with caution due to the destructive nature of ferroresonance phenomenon. In all cases, the experiments were carried out in the low voltage winding, being common in transformers within the range of 214-240 V. Using the low voltage side allows having some control over the severity of the phenomenon since the high voltage side (13.2 kV in all cases) remains in open circuit and properly isolated. Sufficient precautions were taken: switches were used to separate the transformer from the power supply, and fuses were placed to protect the power source from the rest of the network. The general criterion to ignite ferroresonance is based on the configurations studied in [16]. For the case of three-phase transformers, the main configurations are shown in Figure 4.1.

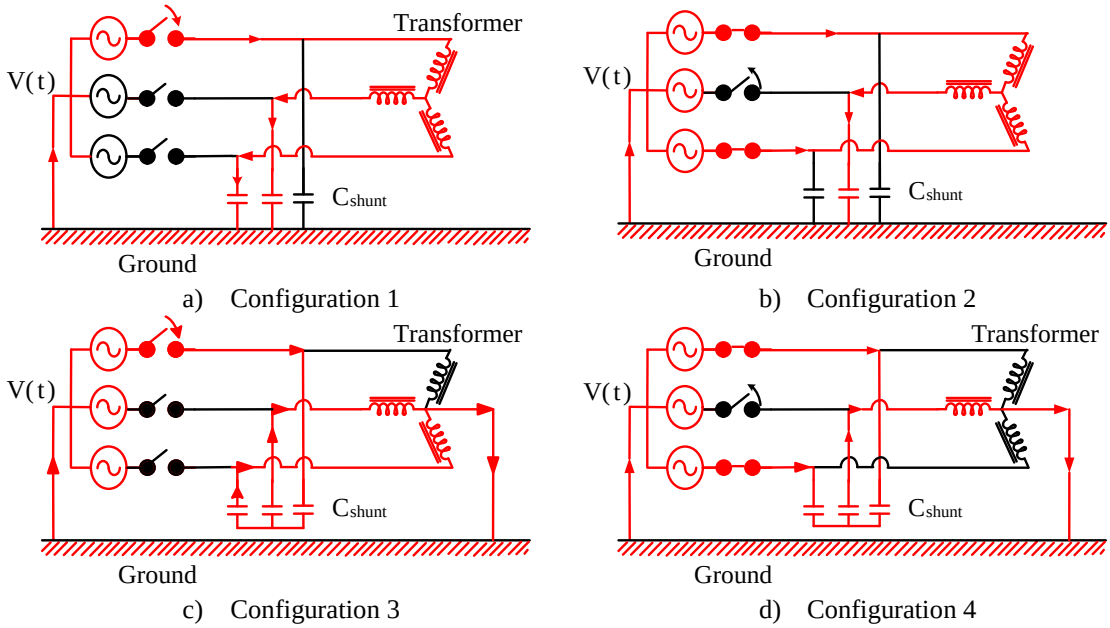

Figure 4.1. Three-phase transformer test circuit for ferroresonance experiments.

The configurations in Figure 4.1 can be used to ignite ferroresonance when one or two of the source phases are lost while the transformer is unloaded. In the Figures the sections in color red show the ferroresonance path. The phase-to-phase and phase-to-ground capacitances represent the capacitance of the underground cable or the overhead line supplying a transformer whose low voltage windings are wye connected with isolated or grounded neutral. Because the most common configuration for distribution transformers used by the Colombian National Grid corresponds to *Dyn*, no records of ferroresonance phenomenon induced into delta winding connection were taken. It is important to remark again that all tests were performed on the low voltage winding. In addition, ferroresonance was ignited and recorded using both energization and de-energization maneuvers and the fault condition arise with one or two phase's misconnection. For single-phase transformers, the criteria suggested in [5] – [7] were

followed. From those works, it was possible to extract the configurations shown in Figure 4.2. The point of using these set ups was to cover all the possible situations prone to ferroresonance phenomenon, where the capacitance effects which interacts with the transformer could be found in parallel (C_s) for Configuration 1, in series (C_g) for Configuration 2, or a combination of both in Configuration 3. Finally, the Configuration 4 which is in fact a variation of Configuration 1, is used to represent the real connection of a transformer to the electrical network. It is based on the fact that most of the distribution transformers generally are fed through two phases, instead of one phase and the neutral as shown in Configuration 1. In this case, there will be a capacitance (C_s) connected in parallel to each phase. Table 4.2 summarizes the most meaningful data obtained during the experimental ferroresonance testing. In such table, each column represents the possible ferroresonance modes obtained during the experimentation for each transformer.

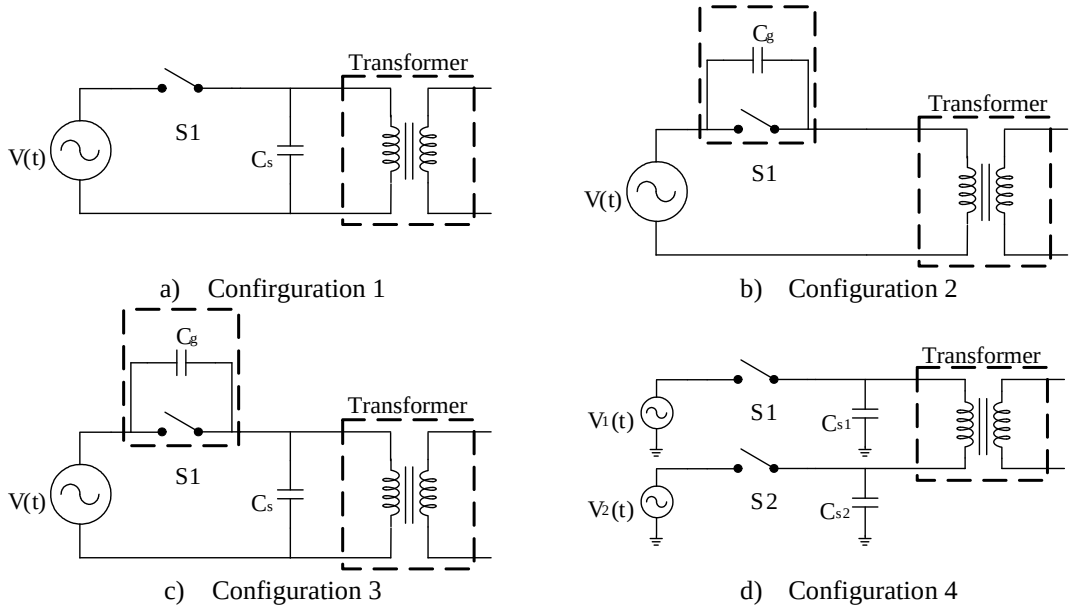

Figure 4.2. Single-phase transformer test circuits for ferroresonance experiments.

Table 4.2: Summary of ferroresonance tests

	kVA	Estado	Validation	Fundamental	Quasi-periodic	Sub-harmonic	Chaotic
Tri_1	45	Repa.		√			√
Tri_2	75	Repa.		√			
Tri_3	112.5	Repa.		√	√		
Tri_4	112.5	Repa.		√	√		
Tri_5	45	Repa.		√			√
Tri_6	112.5	Repa.		√			
Tri_7	75	Repa.		√			
Tri_8	112.5	Repa.	√	√	√		
Tri_9	75	Repa.		√	√		√
Tri_10	112.5	Repa.		√			
Tri_11	500	New	√	√	√		
Tri_12	45	New	√	√	√		√
Mono_1	25	Repa.		√			
Mono_2	25	Repa.		√			
Mono_3	3	Repa.	√	√			
Mono_4	37.5	Repa.	√	√			
Mono_5	5	New	√	√			

It should be remembered that for each transformer an average of thirty waveforms were recorded, providing results going from damped sinusoidal waveforms to different ferroresonance behaviors. The waveforms obtained for the single-phase transformers were compared to those ones obtained using the models:

- T model: the classic Steinmetz [18] model used in most textbooks.
- π model: the original model presented by Slemon [19], recently retaken for transient analysis due to its greater physical sense [20].
- Saturable model: the built-in model, one of the model solutions provided by EMTP for representing transformers.

All cases obtained for three-phase transformers have been validated using the Hybrid model.

4.2.4 Tests validation for single-phase transformers using the π model

The principle of duality for core representation was presented by Cherry in 1948 [21]. It established the foundations allowing transforming a magnetic circuit into its electric dual. It was Slemon in 1952 [19] who presented the equivalent circuit for a single-phase transformer. That model was including both electrical and magnetic circuits, and it was called π model. In up-to-date research [20], [22], it has been proposed that π model's response is better to transients with a high level of saturation, such inrush or ferroresonance, than using the classical T representation. Figure 4.3 presents both classical T and π models. Values for T model were obtained from typical test reports (short-circuit and excitation factory tests). Winding capacitances are also added at the terminals of the transformer, for a better representation. Those effects are of relevant importance in transients such ferroresonance. C_L represents the capacitive effect between the low voltage winding and the ground, C_H the capacitive effect between the high voltage winding and the ground, and C_{HL} the capacitive effect between windings. The π model is implemented here using ATPDraw. Figure 4.4 shows such representation.

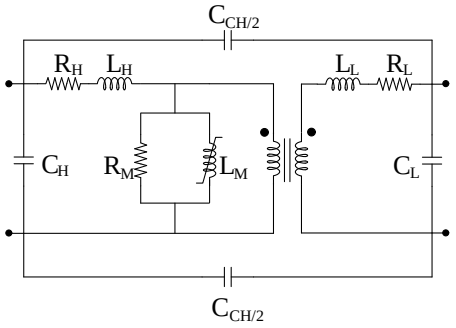

a) T model

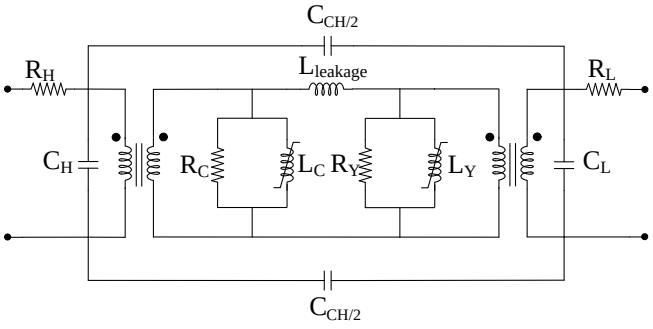

b) π model

Figure 4.3. Transformer's model representation.

The relationship between both models according to [20] is as follows:

$$L_{leakage} = L_H + L_L \tag{4.1}$$

$$R_C = 2R_M \tag{4.2}$$

$$L_C = 2L_M \tag{4.3}$$

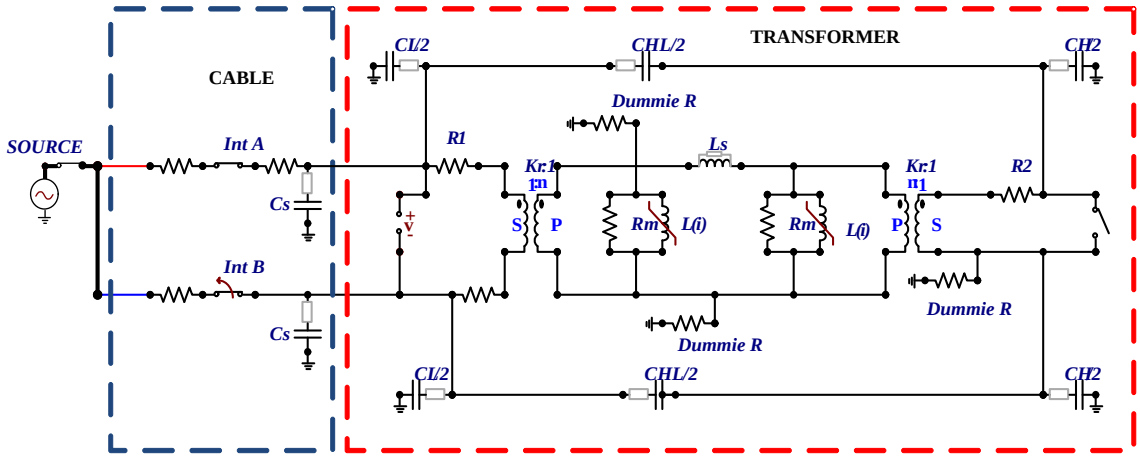

Figure 4.4. Transformer's model in ATPDraw.

It is important to clarify that 'dummie resistances' presented in the ATP circuit are used to improve system's stability; generally, their value is very high and they are used as grounding reference.

This study is divided into two parts: a) present actual waveforms experimentally measured in some of the essays, and b) waveforms comparison between computational simulations and actual laboratory test. A total of five single-phase transformers were tested. However, it was only been possible to simulate three cases. Two experimental cases have been discarded because of the low quality of the captured data, not sufficient to configure a computational model. In addition, some errors were detected in one of the cases while performing the ferroresonance test.

4.2.4.1 Experimental Results

The first single-phase transformer allowed observing the first experimental ferroresonance waveforms. The plate data information for the transformer labeled as Mono_1 is presented in Table 4.3:

Table 4.3: Transformer Mono_1 main data

Phases	Single	Power (kVA)	25	High Voltage side (V)	13200
Year	2012	Main TAP	2	Low Voltage side (V)	240

Figure 4.5 shows the waveform obtained, which signal corresponds to an energization case using Configuration 1, with the series capacitance (C_S) value being 2 μF.

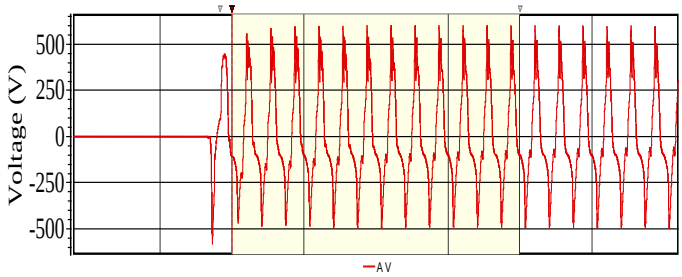

Figure 4.5. Experimental Case 1: Configuration 1, energization with C_s= 2μF.

Figure 4.6 shows the second measurement obtained; for this case, Configuration 2 was used with a grading capacitance (C_g) equal to 40 μF.

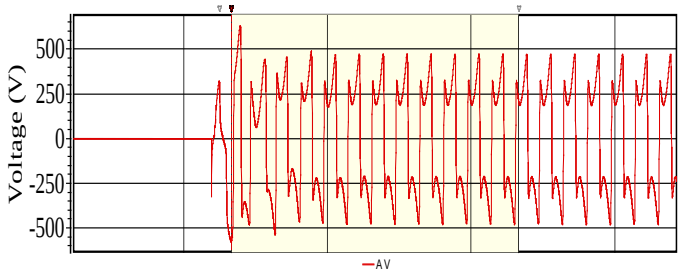

Figure 4.6. Experimental Case 2: Configuration 2, de-energization with C_g= 40μF.

The last measurement was obtained for a de-energization maneuver using Configuration 3. The cable capacitance (C_s) was equal to 20 μF, while the switch grading capacitance (C_g) was equal to 30 μF. Figure 4.7 presents that result.

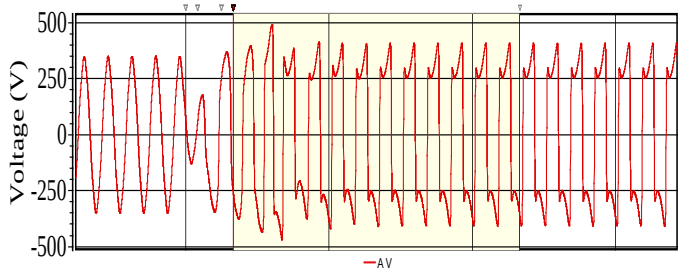

Figure 4.7. Experimental Case 3: Configuration 3, de-energization with C_g= 30μF and C_s= 20μF.

4.2.5 π Model Benchmarking

Criteria suggested in [5] – [7] were followed up to test single-phase transformers. A considerably amount of experimental data was collected for transformer model validation. The configurations used for this validation are the same of those presented in Figure 4.2. As it was stated previously, the principal objective of those configurations is to include all possible situations prone to the ferroresonance phenomenon. For all configurations, the phenomenon will be initiated either by energizing or de-energizing the transformer. Three different case studies have been documented here to illustrate different ferroresonance stages:

(i) Case 1: Four tests were carried out on a 3 kVA 7.62-0.240 kV single-phase transformer: a) Configuration 2 de-energizing the transformer, with C_g = 5 μF; b) Configuration 1 energizing the transformer from steady state, with C_s = 5 μF; c) Configuration 2 de-energizing the transformer from steady state, with C_g = 40 μF; d) Configuration 3 de-energizing the transformer with C_s= 20 μF and C_g= 20 μF.

(ii) Case 2: Four tests were carried out on a 37.5 kVA 7.62-0.240 kV single-phase transformer: a) Configuration 4 de-energizing the transformer from steady state by switching off S2, with C_{s1} and C_{s2} equal to 80 μF; b) Configuration 1 energizing the transformer from steady state, with C_s = 40 μF; c) Configuration 2 de-energizing the transformer from steady state, with C_g = 10 μF; d) Configuration 3 a de-energizing the transformer with C_s= 20 μF and C_g= 10 μF.

(iii) Case 3: Four tests were carried out on a 5 kVA 7.62-0.240 kV single-phase transformer: a) Configuration 4 energizing the transformer by switching on S2, with C_{s1} and C_{s2} equal to 5 μF; b) Configuration 4 energizing the transformer from steady state, with C_{s1} and C_{s2} equal to 5 μF; c) Configuration 2 de-energizing the transformer from steady state, with C_g = 2 μF, d) Configuration 4 a de-energizing the transformer with C_{s1} and C_{s2} equal to 20 μF.

4.2.5.1 Case Study 1

Table 4.1 shows the transformer data plate, the typical information that a tranformer should have. Tables 4.4 and 4.5 present the data required to implement the transformer using the T and π models, respectively; that is, leakage inductance ($L_{leakage}$), winding resistances (R_H, R_L), and core losses (R_{core}). Table 4.6 includes the measured values of capacitances between windings. Figure 4.8 presents for both models the magnetization curve for the core.

Table 4.4: Case 1, transformer data plate

Phases	Single	Power (kVA)	3	High voltage side (V)	7620
Year	2012	Main TAP	3	Low voltage side (V)	240

Table 4.5: Case 1, data for *T* model implementation

Resistances and linear inductances				
R_H (Ω)	R_L (Ω)	L_H (mH)	L_L (mH)	R_{core} (Ω)
224,160057	0,167507	439,3912	0,435877	2753353,8160

Table 4.6: Case 1, data for π model implementation

Resistances and linear inductances			
R_H (Ω)	R_L (Ω)	$L_{leakage}$ (mH)	R_{core} (Ω)
224,160057	0,167507	439,827165	5506707,632
Interwinding capacitances			
Windings			C(nF)
HV - LV (C_{HL})			0.2292
HV - GND (C_H)			0.3256
LV - GND (C_L)			0.126

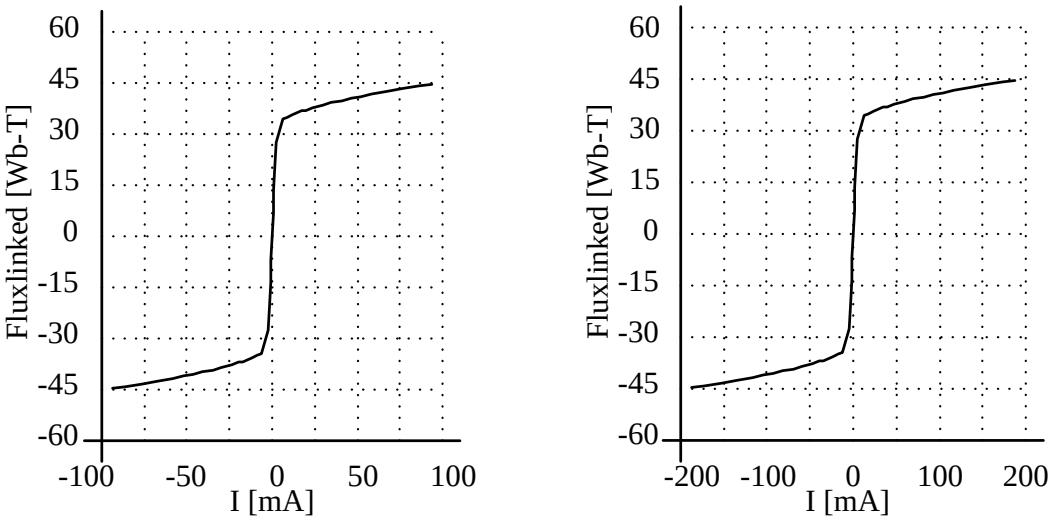

a) π Model b) T model

Figure 4.8. Case 1: Transformer's magnetization curve.

To begin the validation process a series of scenarios were studied and analyzed. The structure of the analysis follows the coming guidelines: First, the π transformer model is validated through overlapping and comparing its output waveforms against the experimental measurements. Then, the π model will be also compared against both, T and SATURABLE models. Subsequently, a brief analysis of the internal capacitive effects of the transformer will be presented, and finally, different cases involving the other configurations are studied using the same transformer to complete the π model benchmarking.

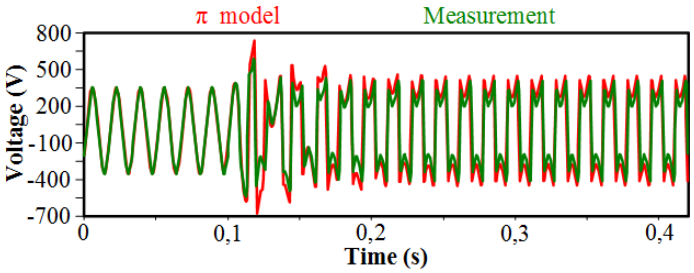

Figure. 4.9. Case 1 - Configuration 2: Waveforms comparison (meaurement vs π model simulation).

To obtain the signals presented in Figure 4.9 the Configuration 2 was used. The waveform presented shows the contrast between the simulated signal and the experimental measurement. The test was performed using a capacitance value (C_g) of 5 μF and the de-energization maneuver was executed opening the Switch S1 at 0.11 seconds of the simulation time. The effects of internal capacity were not considered for this first essay. The same settings were used in Figure 4.10, and in this case, the responses for the T model and the Saturable model were included. By overlapping the signals, little difference can be perceived between models. Nevertheless, according to [21], significant differences can appear when transformer saturation is reached.

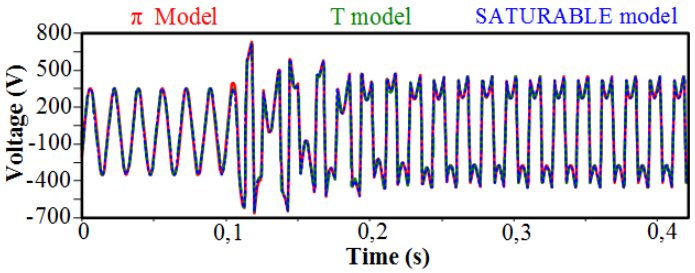

Figure 4.10. Case 1 - Configuration 2: Waveforms comparison between simulation models.

To continue the analysis, the same settings were used to analyze the transformer model response whether including or not the internal capacitive effects. Figure 4.11 shows the comparison between the measured and simulated waveforms. For a more precise comparison, two different areas are separately presented: Figure 4.12 is focused in the initial transient, while Figure 4.13 shows the behavior when ferroresonance reaches the stable state. In general, once the stable state is reached, there is basically no influence from the internal capacitive effects of the transformer. On the other hand, although simulated and measured signals are not identical, the match is quite acceptable, since the global and dynamic behavior is similar.

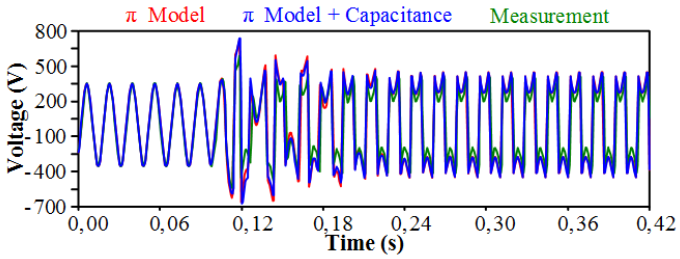

Figure 4.11. Case 1 - Configuration 2: Waveforms comparison.

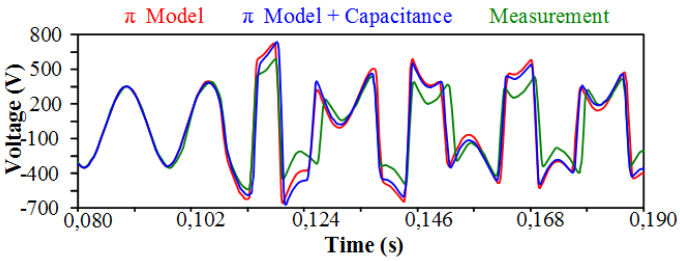

Figure 4.12. Case 1 - Configuration 2: Ferroresonance initial transient.

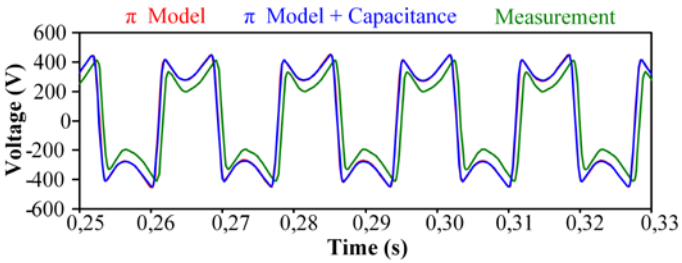

Figure 4.13. Case 1 - Configuration 2: Ferroresonance stable state.

To complete the analysis, the internal capacitive effects will continue being included for all other cases. Three extra experiments will be addressed presenting different saturation conditions. The next case presents the energization of a transformer using Configuration

1 and a parallel capacitance of 5 μF. Internal capacitive effects of the transformer, shown in Table 4.6, were considered.

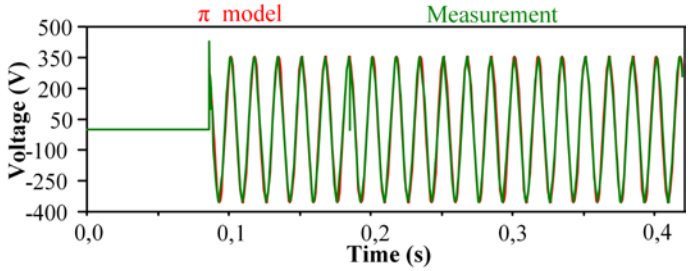

Figure 4.14. Case 1 - Configuration 1: Waveforms comparison.

Figure 4.14 shows the comparison between measured and simulated waveforms. Although ferroresonance is not obtained in this case, the example is used to verify that the model react properly to the captured signal regardless any system changes. The next case uses the Configuration 2 with a different grading capacitance (C_g), a value of 40 μF for a de-energization maneuver. Figure 4.15 presents the comparison between signals.

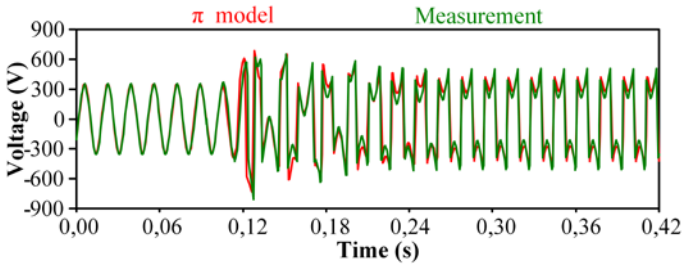

Figure 4.15. Case 1 - Configuration 2: Waveforms comparison.

As shown above, the π model reacts quite well. The graphic representation provided by the model is acceptable and very similar to the real one. The validation process will consider now the de-energization of a transformer using Configuration 3. This is a more complex case since ferroresonance will depend not only on the transformer's capacitance, but also on the capacitance of the circuit breaker (C_g), and the cable capacitance (C_s). Figure 4.16 shows both measured and simulated waveforms.

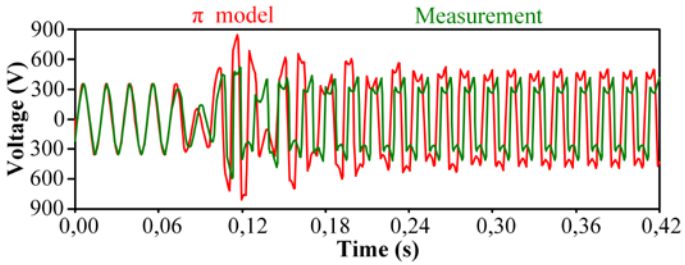

Figure 4.16. Case 1 - Configuration 3: Waveforms comparison.

Finally, to finish this case's validation, as an example, primary's transformer current behavior is presented. This current measurement was obtained using the same setting as the one presented in Figure 4.15. Figure 4.17 shows this comparison.

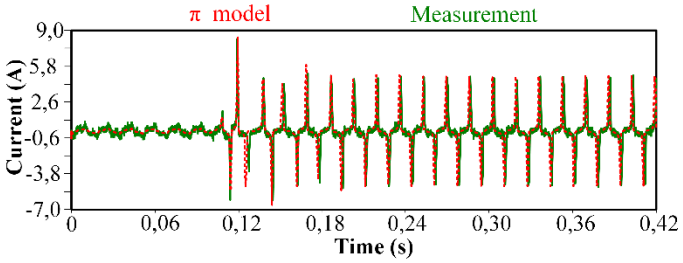

Figure 4.17. Case 1 - Configuration 2: Low voltage side excitation current.

In general, the model's response in every case exhibits a great versatility to face dynamic complexities. The results are acceptable since the general behavior of both experimental and simulated waveforms are similar. The plots show, however, that the signal representation at times differs both in peak and phase values. Differences between them can be due, among others, to the fact that: (i) the model for the voltage source used in the simulations did not consider any saturation degree, being assumed ideal; (ii) the hysteresis effect was not included in the transformer magnetization curve [23] - [27]; (iii) the temperature's effect of the core, when ferroresonance occurs the temperature conditions can be completely different from that when the magnetization curve and internal parameters were estimated.

4.2.5.2 Case Study 2

Table 4.7 shows the transformer data plate. Tables 4.8 and 4.9 present the data required to implement the transformer using the T and π models, respectively. Figure 4.18 shows the magnetization curve for the core.

Table 4.7: Case 2, transformer data plate

Phases	Single	Power (kVA)	37.5	High voltage side (V)	7620
Year	2006	Main TAP	3	Low voltage side (V)	240

Table 4.8: Case 2, data for *T* model implementation

Resistances and linear inductances				
R_H (Ω)	R_L (Ω)	L_H (mH)	L_L (mH)	R_{core} (Ω)
7,101834	0,004732	64,716762	0,064199	537777,4253

Table 4.9: Case 2, data for π model implementation

Resistances and linear inductances			
R_H (Ω)	R_L (Ω)	$L_{leakage}$ (mH)	R_{core} (Ω)
7,101834	0,004732	64,780962	1075554,851
Interwinding capacitances			
Windings			C(nF)
HV - LV (C_{HL})			1
HV - GND (C_H)			0.5
LV - GND (C_L)			0.57

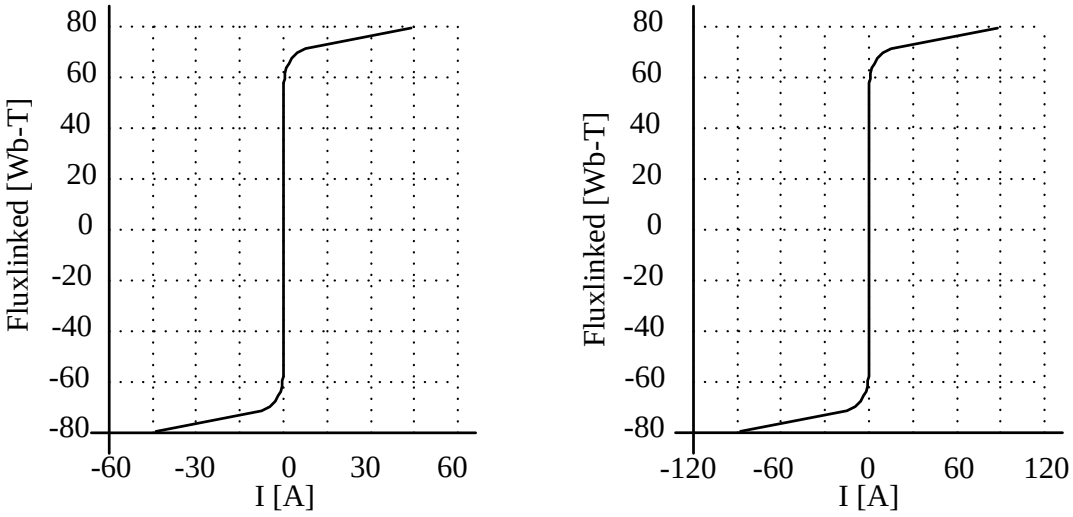

a) π Model b) T model

Figure 4.18. Case 2: Transformer's magnetization curve.

To analyze the ferroresonance phenomena a de-energization process using Configuration 4 is presented. The Switch S2 is open at 0.08 s, disconnecting the transformer from steady state. Figure 4.19 shows the comparison between measured and simulated waveforms. Simulations considered capacitive effects with C_s=80 μF.

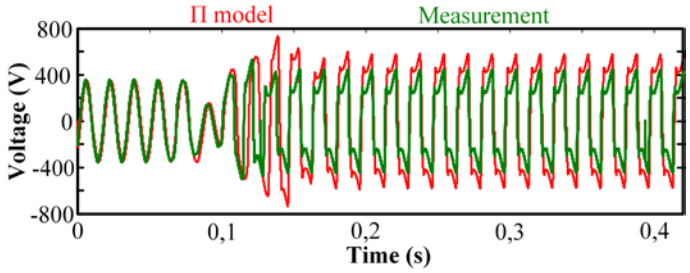

Figure. 4.19. Case 2 - Configuration 4: Waveforms comparison (meaurement vs π model simulation).

The waveforms dynamics represented in the plot are similar to one another, even during the variation in the transient part. The only significant difference comes in the amplitude of the ferroresonance steady state. There exist many reasons for this difference, for example, simulation systems often do not consider power source saturation and are simply modeled by ideal power sources. The signal obtained using the π model was also been compared to the T and the SATURABLE models. Figure 4.20 presents the detail.

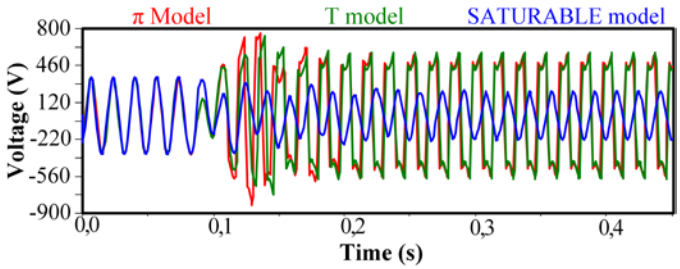

Figure 4.20. Case 2 - Waveforms comparison between simulation models.

For this specific case, the SATURABLE transformer response is not correct and its representation is completely erroneous. This is an important detail to be remarked when finding the best single-phase model for representing ferroresonance. Defects like the

one presented for the SATURABLE model can lead to incorrect conclusions. Therefore, when simulating ferroresonance cases, the model selected should be validated in various scenarios prior using it for larger analysis.

To test the internal capacitive effects using the π model, two different areas were separately studied: Figure 4.22 focused in the initial transient, while Figure 4.23 show the behavior when ferroresonance reached the stable state. Again, once the stable state is reached, there is no influence from the internal capacitances of the transformer, basically, as shown in the plot, not affecting the voltage signals. In the same line to the results obtained in the previous case study, although the global behavior is similar while comparing the calculated response using the model to the one obtained from lab measurements, main variation is located during the transient initial state. Differences between waveforms may be the ones already explained in the previous case.

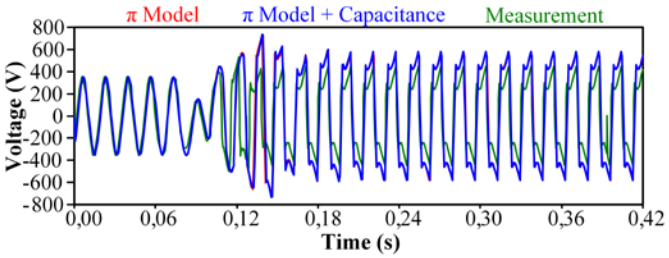

Figure 4.21. Case 2 - Configuration 4: Waveforms comparison.

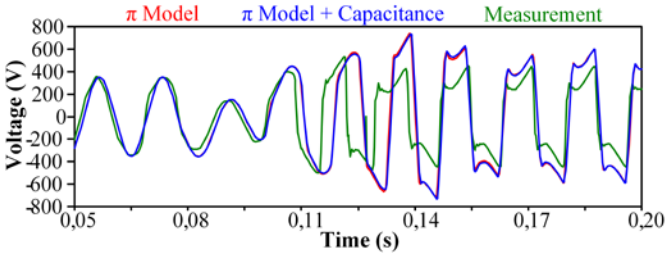

Figure 4.22. Case 2 - Configuration 4: Ferroresonance initial transient.

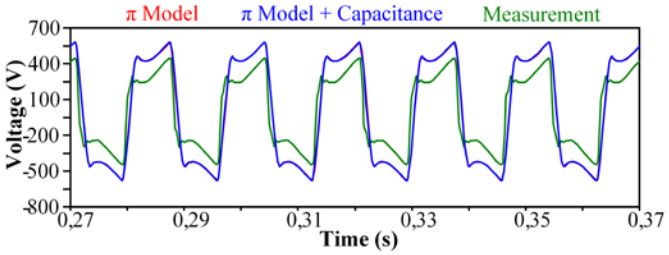

Figure 4.23. Case 2 - Configuration 4: Ferroresonance stable state.

To continue with the analysis, it is needed to study the π model under different situations. Configuration 1 is used again closing the switch at 0.057 s. The settings used here considered a shunt capacitance C_s = 40 μF. Figure 4.24 shows those results.

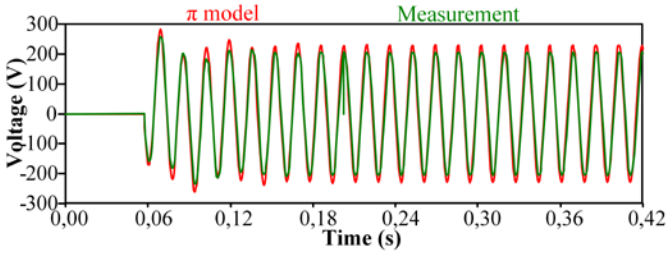

Figure 4.24. Case 2 - Configuration 1: Waveforms comparison.

Despite the small difference in amplitude during the first oscillations of the signals, the computational representation is quite accurate. It is worth to mention that when using Configuration 1 was not possible to obtain ferroresonance distortion and most of the results resumed in only damped oscillations. To follow with the validations, a de-energization case was considered, the switch opening time was t= 0.094 s. The set up of the test circuit corresponds to the Configuration 2 with a grading capacitance value C_g = 10 μF. Figure 4.25 presents the results.

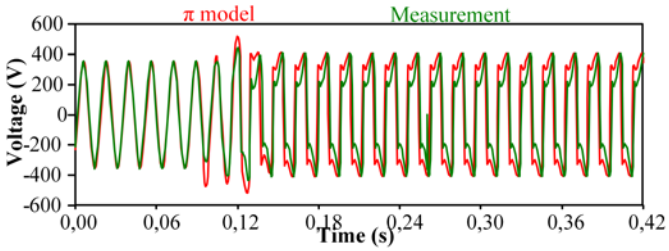

Figure 4.25. Case 2 - Configuration 2: Waveforms comparison.

For this case, the maximum peak reached in the ferroresonance steady state part of the signal is the same, however the shape of the waveform differs a little. Yet the general representation of the event is correct. The last analysis performed for this transformer consisted on using the test circuit presented in Configuration 3 with an opening time at t = 0.084 s. The settings of the circuit included a shunt capacitance C_s = 20 μF and a grading capacitance C_g = 10 μf. Figure 4.26 shows the matching between the waveforms.

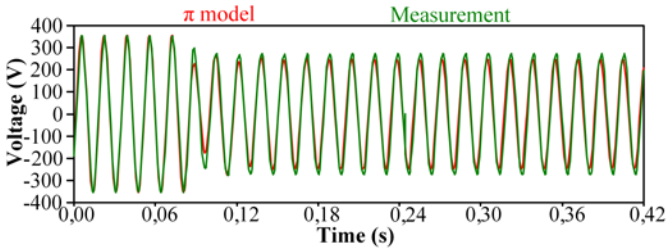

Figure 4.26. Case 2 - Configuration 3: Waveforms comparison.

Once again, the resulting signal is not considered as ferroresonance, although it is still an important perturbation to the system. Besides the fact that the model keep representing correctly the results of the test circuit is a plus. Despite the change in the signal dynamic, the simulation result was maintained accurate. Finally, to conclude the validation study, the magnetizing current in the low voltage side is presented. The setting of the systems corresponds to the one used in Figure 4.25. Figure 4.27 presents the current signal.

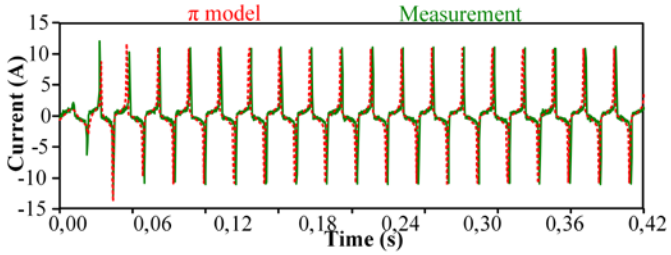

Figure 4.27. Case 2 - Configuration 2: Low voltage side excitation current.

It can be concluded from the analysis that the internal capacitive effects have only a small influence in the formation of the initial transient of the signal, however, the final state of the ferroresonance depends more on other important capacitive effects such series or parallel capacitances coming from cable or switches.

4.2.5.3 Case Study 3

The data plate extracted from the transformer is presented in Table 4.10. Tables 4.11 and 4.12 introduce relevant information for the transformer modeling. The data used to represent the nonlinear characteristic of the core is presented in Figure 4.28.

Table 4.10: Case 3, transformer data plate

Phases	Single	Power (kVA)	5	High voltage side (V)	7620
Year	2013	Main TAP	3	Low voltage side (V)	240

Table 4.11: Case 3, data for *T* model implementation

Resistances and linear inductances				
R_H (Ω)	R_L (Ω)	L_H (mH)	L_L (mH)	R_{core} (Ω)
86.038966	0.077426	386.601295	0.383509	1974557.2784

Table 4.12: Case 3, data for π model implementation

Resistances and linear inductances			
R_H (Ω)	R_L (Ω)	$L_{leakage}$ (mH)	R_{core} (Ω)
86.038966	0.077426	386.984804	3949114.557

Interwinding capacitances	
Windings	C(nF)
HV - LV (C_{HL})	1
HV - GND (C_H)	0.125
LV - GND (C_L)	0.07

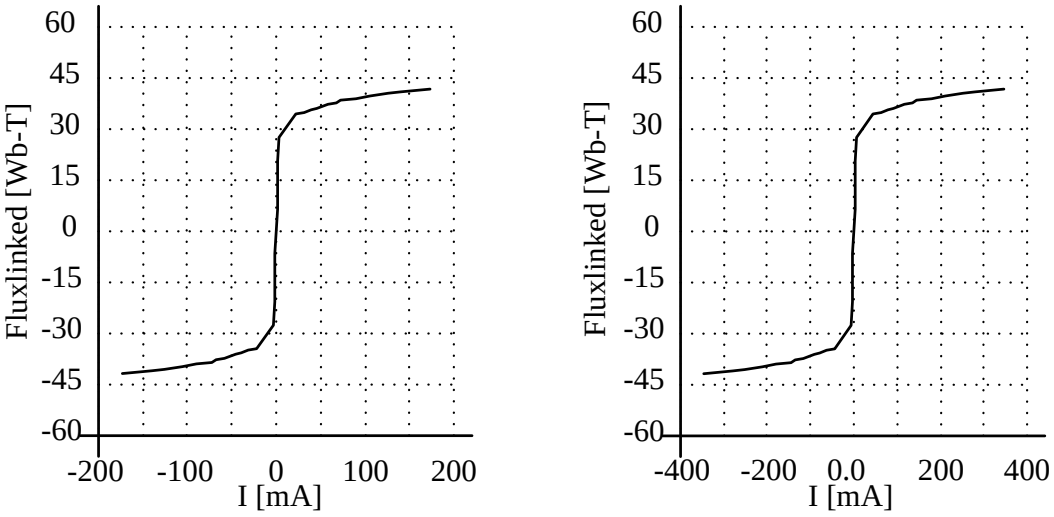

a) π Model b) T Model

Figure 4.28. Case 3: Transformer's magnetization curve.

Configuration 4 is used for the first validation considering a de-energization by switching off S2 at t=0.009 s. Figure 4.29 shows the comparison between measured waveform and the simulated one using the π model. The capacitance C_s is equal to 5 μF. Simulations considered the transformer without any internal capacitive effects.

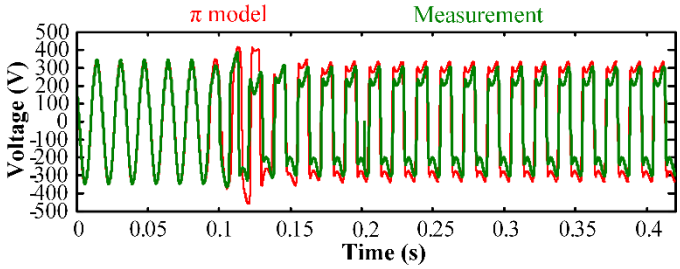

Figure 4.29. Case 3 - Configuration 4: Waveforms comparison (meaurement vs π model simulation).

Similar results were obtained in this case compared to the previous ones. The degree of accuracy provided by the π model is quite acceptable, even during the initial transient state. In Figure 4.30 a comparison between models can be seen.

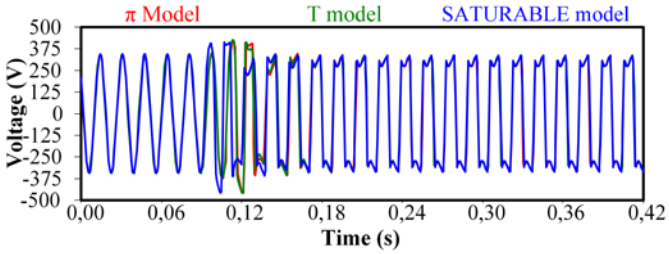

Figure 4.30. Case 3 - Waveforms comparison between simulation models.

For this specific case, the results from all models are quite accurate, since no significant differences were found in the ferroresonance steady state of the signal, and the discrepancies during the initial transient are not conclusive to select one model over the others. Following the analysis, once more, the π model will be used to study the possible impact the internal capacitance effects may have over a ferroresonance phenomenon. Figure 4.31 presents such comparison.

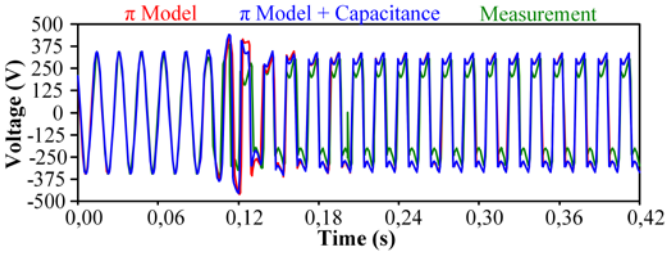

Figure 4.31. Case 3 - Configuration 4: Waveforms comparison.

Figure 4.32 shows a close up over the initial transient.

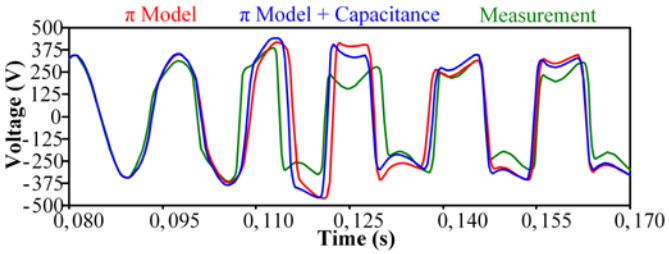

Figure 4.32. Case 3 - Configuration 4: Ferroresonance initial transient.

Figure 4.33 presents only the steady state part of the ferroresonance as an approach to see the effects of including the internal capacitances in a computational model.

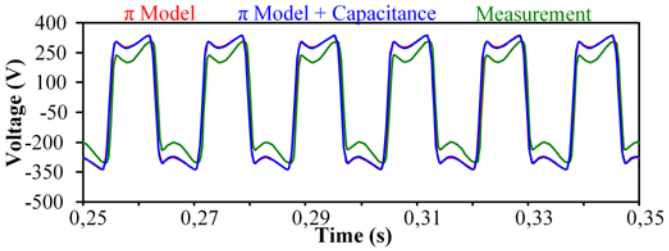

Figure 4.33. Case 3 - Configuration 4: Ferroresonance stable state.

As presented in the previous cases, there is no indication that the presence of internal capacitances in the model affects directly the final stage of the ferroresonance. However, it exists a little effect over the initial transient when the internal capacitances are included in the model. After evaluating the results, it is important to reconsider whether the internal capacitance is a main parameter for modeling single-phase transformers when studying ferroresonance. It may seem that there is too little impact over the ferroresonance waveforms in spite of the complex methods required for its experimental calculation. The cable and switches capacitances have bigger capacive values compared to those internal ones, being the first one in the order of *micro* farads while any internal capacitance are not bigger than a few *nano* or *pico* farads. Following the validation steps, one more case is considered. The main settings used in the next test circuit corresponds to the Configuration 4 closing the switch at t=0.077 s. The shunt capacitance value C_s is set to 5 μF. Figure 4.34 presents the results.

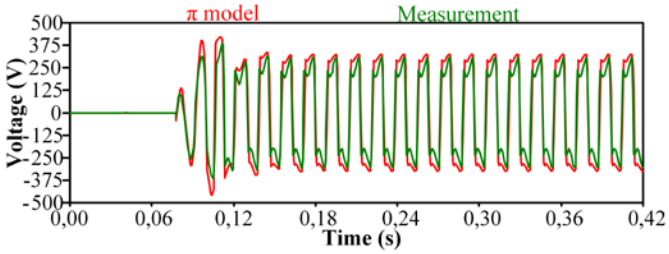

Figure 4.34. Case 3 - Configuration 4: Waveforms comparison.

The π model has an accurate general response despite its initial variations. The amplitude mismatch, as mentioned before, can be due to saturations effects in the power source during the experimental measurements. The second case to consider uses the Configuration 2 with a grading capacitance C_g of 2 μF. Figure 4.35 presents the waveform comparison for a de-energization maneuver with an opening time of the switch of t=0.084 s.

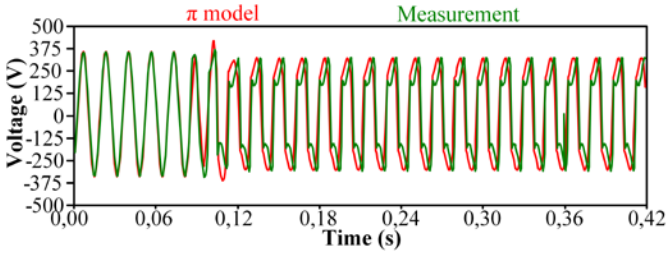

Figure 4.35. Case 3 - Configuration 2: Waveforms comparison.

The representation made by the π model shows a general agreement in the dynamic behavior of the signal. The time length of the initial transient and the changes to ferroresonance are always precise. However, the waveform shape representation is not completely accurate, the magnitude is correct but the outline of the wave seems to be different. The next validation presents a de-energization using the Configuration 4, having a cable capacitance of C_s = 60 μF and a t_{open} = 0.16 s. Figure 4.36 presents the results.

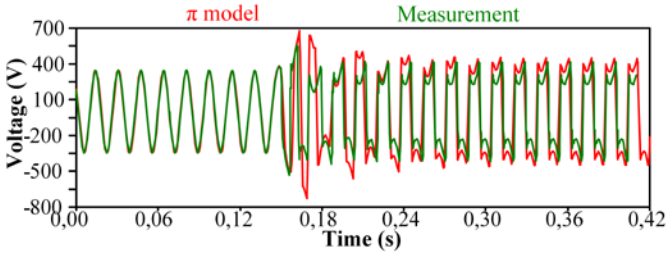

Figure 4.36. Case 3 - Configuration 4: Waveforms comparison.

In this case, the differences in amplitude for the ferroresonance steady state and in the transient state are bigger than in the previous cases; this may probably be due to the bigger capacity value used here, so, the ferroresonance operating point may have reached a higher saturation value for both the transformer and the power supply. Finally, to conclude the validation, the current behavior is presented when the transformer is subject to ferroresonance. The waveform presented in Figure 4.37 has been obtained using the same test system for the de-energizing case presented in Figure 4.35.

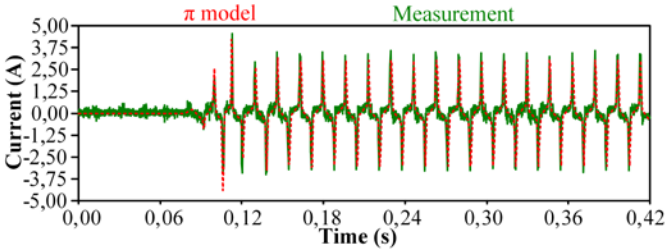

Figure 4.37. Case 3 - Configuration 2: Low voltage side excitation current.

The conclusions of this study prove that ferroresonance accurate validation is highly dependent on the models used for representing the main system components, being the transformer the most critical one. This Section has compared the results obtained by means of simulation to actual lab measurements (routing tests, special tests, ferroresonance tests). The π model, implemented in ATPDraw, has been used here to represent single-phase transformers. This work has provided some insights on how ferroresonance can appear through energization and de-energization processes, and demonstrated the general correctness of the π model behavior for ferroresonance analysis. Comparison between measured and simulated waveforms show for all the cases studied that, although there can be some differences between waveforms mainly for the initial transient state, the global and dynamic behavior has been found to be similar, and stable ferroresonant states are quite precisely represented. Differences between measurements and simulation results may be mainly due to: (i) the no consideration of any saturation degree for the voltage source used in the simulations; (ii) the no consideration of the hysteresis effect in the transformer magnetization curve; (iii) the differences between temperature of the core during ferroresonance tests and, at the beginning, during excitation tests for estimating internal core parameters. Improvements considering the addition of the hysteresis effect will be presented later in this thesis. A first approach for hysteresis major loop implementation in the π model is presented in the coming sections; in addition, the last chapter presents an extensive study of the π model using a full hysteresis cycle for ferroresonance representation.

4.2.6 Three Phase Transformer Testing and modeling

A total of twelve three-phase transformers have been tested obtaining a large amount of experimental data. An average of 35 waveforms measurements has been made on each transformer, obtaining different ferroresonance modes. Table 4.2 has presented a summary of the results. Some of the experimental measurements have been used to validate the Hybrid transformer model implemented in ATPDraw. The theory backing up the model is presented, and then experimental testing is presented to confirm the methods used to ignite ferroresonance in a controlled laboratory environment. Finally, a series of validations are presented overlapping computational simulation results to actual experimental measurements to benchmark the use of the Hybrid model in the representation of the ferroresonance phenomenon.

Among the extensive variety of existing transformer models, the topology-based models are considered to be the ones which provide the most accurate representations of the iron core [8], [28], [29], [30]. The use of Duality Transformations to obtain equivalent circuits is a method based on the theory that relates magnetic to electrical circuits. It was originally developed by Cherry [20] in 1949 and Slemon [19] in 1953. At the beginning, these methods did not receive much attention, presumably since computers were not available. Researchers have recently begun to use duality to provide equivalent electric

circuits which are more topologically correct [31]-[38]. This approach includes the effects of saturation in each individual leg of the core, inter-phase magnetic coupling, and leakage effects. Two of the most remarkable works were carried out to obtain the equivalent model for a five-legged wound-core transformer [31],[34].

More recently a model has been developed sponsored by Bonneville Power Administration (BPA); the model is usually referred in literature as XFMR [10], [39], [40]. Officially, the model was named as the Hybrid model due to its capability to unify the matrix representation from BCTRAN for the winding modeling, with the duality principle for the representation of the core magnetization in legs and yokes. The model supports three-phase, two- and three-winding transformers, autotransformers, and wye and delta couplings. Its recent implementation in ATPDraw has been also sponsored by the BPA. The component support three different ways of input data: (1) Design parameters, using winding and core geometry and material properties; (2) Test reports, based on standard test data, like in BCTRAN, with the addition of capacitances and frequency-dependent resistances; (3) Typical values, based on typical text book data from transformer ratings.

The principles behind such model construction are its topologically correct derived core model with an external connection to an artificial winding on the core surface. Individual magnetizing branches are established for the yokes and legs depending on their relative length and area, normally values within limited range. The magnetization is assumed to follow the Frolich equation which is fitted to Test Report data using the Gradient Method optimization. This improves extremely the saturation behavior since it avoids linear extrapolation to points further than the date given in test reports. The leakage inductance is modeled using an inverse inductance matrix, following the BCTRAN approach. Shunt capacitances and frequency-dependent winding resistances are also considered. This Hybrid model combines the strengths of different approaches, creating a universal model that can be adapted to specific core and coil configurations. Besides, it is independent of coil connection as delta, wye, auto, and zig–zag configurations are made by jumpering the external connections. The transformer model consists on four parts, as shown in Figure 4.38, and described as follows:

- Leakage reactance: Matrix representation with the addition of core-to-coil couplings,
- Frequency-dependent winding resistances,
- Shunt capacitances: Matrix representation including capacitive effects externally attached to the bushing terminals of the model
- Core: Individual magnetization and losses for legs and yokes used with a nonlinear duality-based topologically correct representation.

Although it is considered to be an extremely powerful model, it is still seldom used by the scientific community, in part due to its complexity, and in part due to the quantity of requested data.

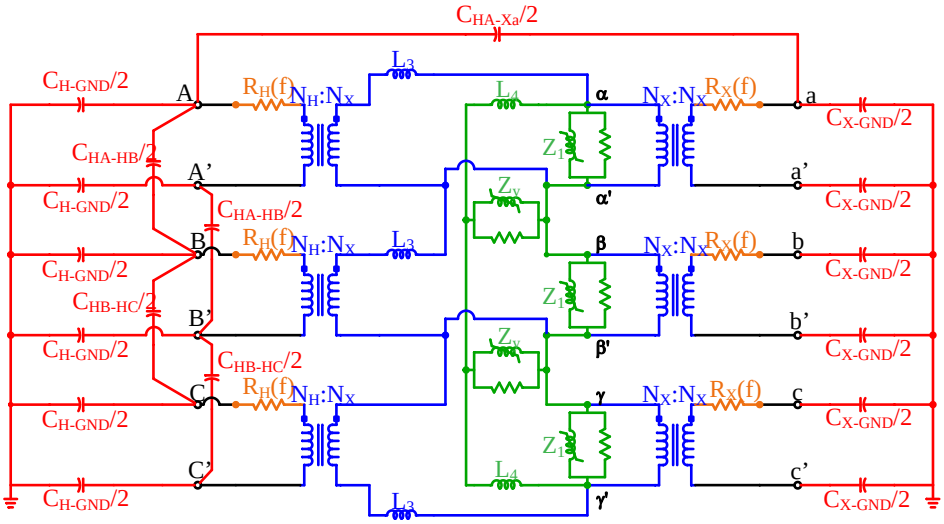

Figure 4.38. The Hybrid transformer model internal topology.

4.2.6.1 Experimental Waveform Analysis

The main characteristics of each transformer and some of the experimental waveforms obtained are presented in the coming pages.

4.2.6.1.1 Experimental Case 1

The first transformer tested has been labeled as Tri_1 in Table 4.13. It has the characteristics shown below:

Table 4.13: Transformer Tri_1 main data

Phases	Three	*Power(kVA)*	45	*High Voltage side (V)*	13200
Core type	5-legged	*Conecction Grup*	Dyn5	*Low Voltage side (V)*	214

Following the procedure described in the initial sections (see Figure 4.1), it was possible to obtain waveforms under quasi-periodic ferroresonance mode. The setting during the essay corresponds to a de-energization using Configuration 2 and with a capacitance value of 50 μF.

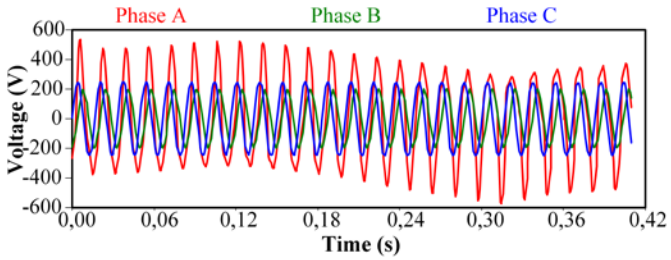

Figure 4.39. Three-phase transformer experimental case 1: Waveform analysis.

Figure 4.39 shows how Phase *A* is in ferroresonance quasi-periodic mode, while Phases *B* and *C* (green and blue color, respectively) are subjected to a significant angular displacement due to the flux induction through the transformer core.

4.2.6.1.2 Experimental Case 2

For the three-phase transformer labeled as Tri_4, the plate characteristics are presented below:

Table 4.14: Transformer Tri_4 main data

Phases	Three	*Power(kVA)*	112,5	*High Voltage side (V)*	13200
Core type	5-Legged	*Connection Grup*	Dyn5	*Low Voltage side (V)*	214

The transformer was driven to ferroresonance using Configuration 2 with a capacitance value in the cables of 30 μF while de-energizing the Phase *A*. During the phenomenon it was possible to witness audible noise, vibration and overheating in the transformer terminals and the measuring equipment. The waveforms obtained are shown below:

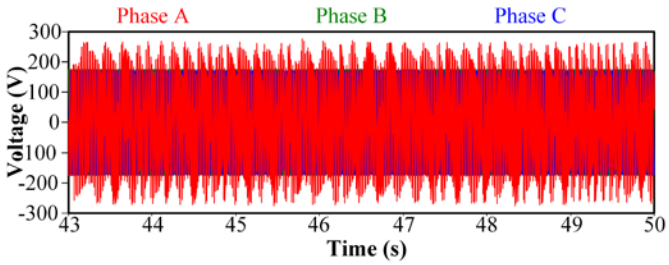

Figure 4.40. Three-phase transformer experimental case 2: Waveform analysis.

Figure 4.40 presents a sustained oscillation in chaotic mode. Such events can produce a severe vibration that happens to be audible and can physically move a transformer. In addition, damage to isolation material can occur if the phenomenon is not soon damped.

4.2.6.1.3 Experimental Case 3

The main parameters for the transformer Tri_5 are presented below:

Table 4.15: Transformer Tri_5 main data

Phases	Three	*Power(kVA)*	45	*High Voltage side (V)*	13200
Core type	5-Legged	*Connection Grup*	Dyn5	*Low Voltage side (V)*	214

In this case, the transformer is settled using Configuration 1, while is energized through the Phases *B* and *C* (green and blue color, respectively), Phase *A* remains open. The value of the cable capacitance is 40 μF. Figure 4.41 displays the waveform obtained:

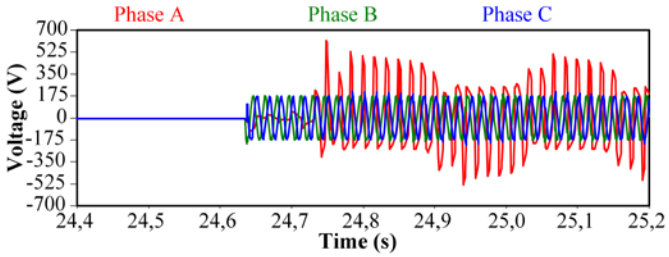

Figure 4.41. Three-phase transformer experimental case 3: Waveform analysis.

Figure 4.41 presents the effect in the open Phase *A* (red color), behaving as a ferroresonance signal labeled as quasi-periodic mode. The other two phases are

operating normally. The signal peaks reach values up to three times its nominal value, demonstrating the severity of the ferroresonance phenomenon.

4.2.6.1.4 Experimental Case 4

The transformer label as Tri_9 presents one of the most interesting cases obtained in experimentation. The basic transformer data is attached below:

Table 4.16: Transformer Tri_9 main data

Phases	Three	*Power (kVA)*	75	*High Voltage side (V)*	13200
Core type	5-Legged	*Connection Grup*	DY5	*Low Voltga side (V)*	214

The test system presents a Configuration 4 and uses a two-phase de-energization, i.e. when disconnecting the transformer while one of the phases remains closed. The cables capacitance value is 90 μF.

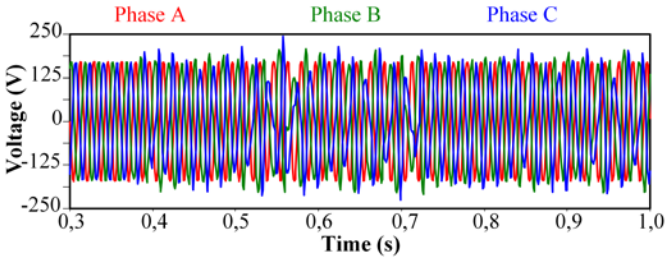

Figure 4.42. Three-phase transformer experimental case 4: Waveform analysis.

Figure 4.42 shows the signal behavior of Phases *B* and *C* (green and blue color, respectively). Right after the de-energization starts, it is driven to a quasi-periodic stage, thereby producing an atypical case: usually in such disconnection the phases take a very similar behavior, while in this case the phases oscillate independently.

Finally, to conclude this section, it should be stressed that the quality of the data obtained in the experimental tests, reaffirms the legitimacy of the test systems used to ignite ferroresonance.

4.2.7 Data Validation and the Hybrid model Configuration in ATPDraw

Once it has been proved that experimental ferroresonance data can be obtained with sufficient quality, it is essential to check that all the laboratory tests performed to the transformers are able to deliver enough information to set accurate simulation models and thereby making possible to carry out software validation against those experimental data. Below are shown, one by one, the validated transformers.

4.2.7.1 Validation 1

The transformer tested has been labeled as Tri_4, its plate data is presented in Table 4.17.

Table 4.17: Transformer Tri_4 main data

Phases	Three	*Power (kVA)*	112,5	*High Voltage side (V)*	13200
Core type	5-Legged	*Connection Grup*	Dyn5	*Low Voltage side (V)*	214

The configuration data for transformer simulation is presented in Table 4.18 containing the data required for core configuration and setting up the magnetization curve:

Table 4.18: Case 1- Hybrid transformer configuration data

V%	Loss kW	Iav %
20.1694888	0.012520	0.05963489
39.6860863	0.045580	0.10850695
59.5210357	0.097140	0.16319973
79.7606699	0.174400	0.2178925
99.2287051	0.311500	0.381861
101.440982	0.335200	0.4949806
103.35649	0.371600	0.67300668
105.541788	0.401200	1.0394922

Saturation

IMP(%)	POW(MVA)	PLOSS(kW)
2.491	0.112500	1.126268

Resistance and Inductance

IMP(%)	POW(MVA)	PLOSS(kW)
12.97	0.112500	0.00182

Zero sequence

V(%)	Loss (kW))	Iav(%)
1	0.00182	0.2735

Zero sequence

The data presented in Table 4.18 fulfill that required by the Hybrid model in ATPDraw. The saturation curve is obtained through the excitation test, where voltage values are expressed in percent (V%), non-load losses in kilowatts (Loss kW) and current excitation as a percentage of the nominal current (Iav%). In addition, the values for resistance and inductance of the core are defined by the short-circuit impedance IMP (%), the load-losses Ploss (kW) and the transfomer power defined in MVA. (POW (MVA)). Finally, the zero sequence values corresponding to the zero sequence impedance, zero sequence losses, and zero sequence voltage and current are introduced. For this transformer, in specific, no data has been calculated for the internal capacitance, thus, some details in the transitions between the steady sinusoidal state and the ferroresonance final state may not be well represented. The analysis was conducted having settled the Configuration 2 and de-energizing the Phase *A*; Phases *B* and *C* remain closed; the cable capacitance is set to 30 μF. The comparison between the experimental and the simulated signals are presented in Figure 4.43.

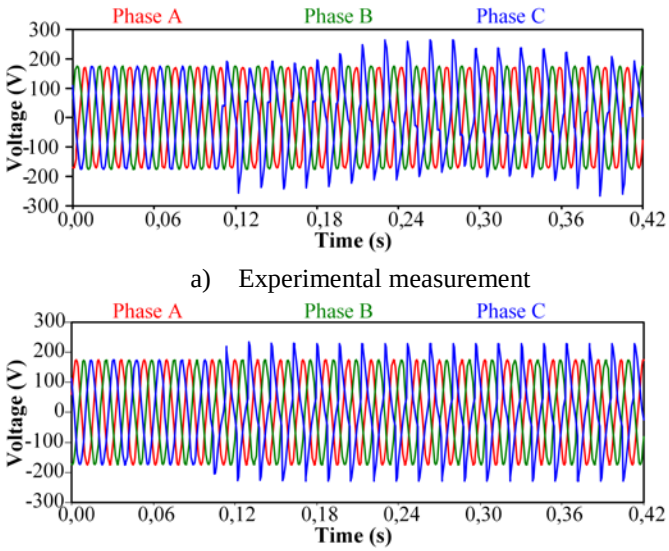

a) Experimental measurement

b) Hybrid model simulation

Figure 4.43. Three-phase transformer validation case 1: Waveform analysis.

Phases *A* and *B* do not suffer any distortion thus a more detailed analysis can be avoided. In this case, the focus is on Phase *C*. The state of the experimental signal shows a clearly quasi-periodic behavior while the behavior of the simulated one is more complex to identify, since it has less oscillations and can be confused with the fundamental mode. Expanding the plot and isolating the phase C, Figure 4.44 is obtained:

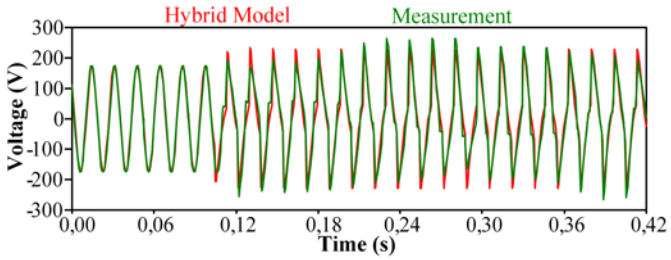

Figure 4.44. Three-phase transformer validation case 1: Phase C.

Even when the waveforms are not completely identical, there are a few details to consider in this particular case. In favor of the validation, the global dynamic behavior of the signal is the same, i.e. it also has a quasi-periodic behavior. The drawbacks and the justifications are separated in two parts: First, the internal capacities of this transformer were not considered and could influence the model; Second, and perhaps a more critical aspect, it is the fact that the Hybrid model in the core configuration box, presented in Figure 4.45, despite allows introducing three individual excitation currents (one per winding), it only admits an individual value for the core losses (see *Loss [kW]* in Figure 4.45), so the model is actually using only one saturation curve for each leg.

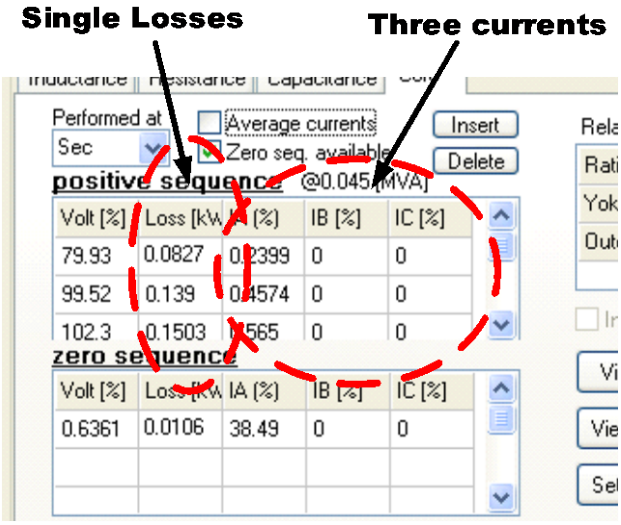

Figure 4.45. Hybrid model internal core configuration dialogue box.

This error will generate a mismatching when creating the magnetization branches and when selecting the individual currents option in ATP, returning always an error suggesting that the currents do not match the average losses. So the user will be forced to use the option of *Average currents*, which, at the end will set the same magnetic behavior for all legs.

4.2.7.2 Validation 2

The second validation is based on the transformer coded in Table 4.1 as Tri_7. The characteristics of this transformer are shown below.

Table 4.19: Transformer Tri_7 main data

Phases	Three	*Power(kVA)*	75	*High Voltage side (V)*	13200
Core type	5-Legged	*Connection Grup*	Dyn5	*Low Voltage side (V)*	214

The data used for the configuration of the Hybrid model in ATPDraw is shown in the following set of tables.

Table 4.20: Case 2 - Hybrid transformer configuration data

V%	Loss kW	Iav %
19.2764845	0.009030	0.07693231
39.1330171	0.064410	0.12882455
57.068646	0.073170	0.19290736
78.3038047	0.145600	0.8055653
98.5272515	0.252000	2.87944292
100.145991	0.269000	3.5369094
102.54712	0.286300	3.78022637
104.13888	0.300000	4.3243536
106.324178	0.316700	4.87902403
107.673127	0.331800	5.284113

Saturation

IMP(%)	POW(MVA)	PLOSS(kW)
2.99	0.075000	1.127286

Resistance and Inductance

IMP(%)	POW(MVA)	PLOSS(kW)
12.57	0.075000	1.127286

Zero sequence

V(%)	Loss(kW)	Iav(%)
0.157	0.002617	16.57

Zero sequence

HV-LV(nF)	HV-GND(nF)	LV-GND(nF)
2	0.2	1

Internal Capacitance

The validation process was conducted using the test Configuration 1 while Phase *A* was energized, and with the cable capacitance having a value of 40 µF. The comparison is presented in Figure 4.46.

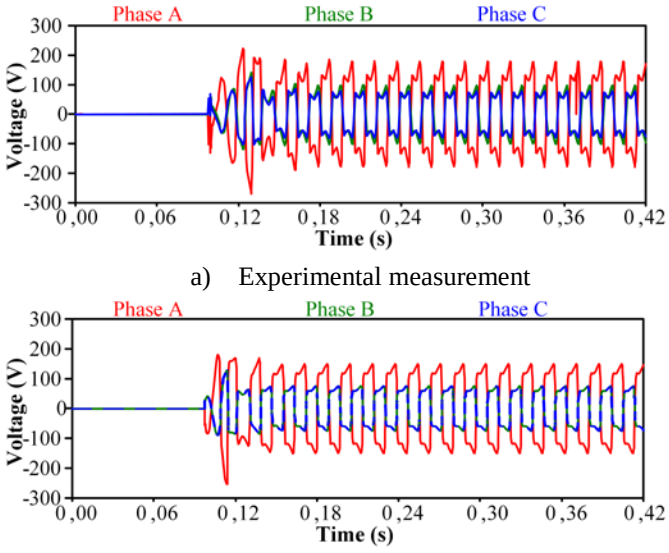

a) Experimental measurement

b) Hybrid model simulation

Figure 4.46. Three-phase transformer validation case 2: Waveform analysis.

In this case, ferroresonance is obtained in fundamental mode affecting the open Phases *B* and *C*. it is important to remark that Phase A should continue having sinusoidal behavior although significant distortion is presented, forcing it to take the form of fundamental ferroresonance. The representation of the simulation has a fairly high accuracy; a detailed one by one plot is presented in Figures 4.47 to 4.49 comparing the experimental signals to the simulation.

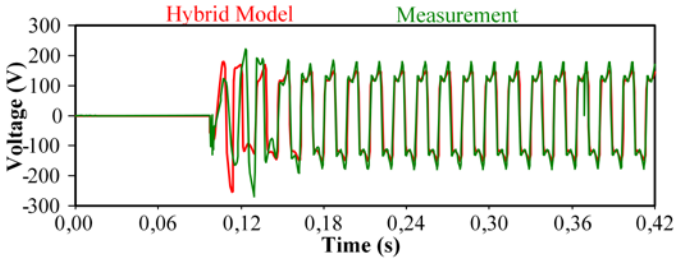

Figure 4.47. Three-phase transformer validation case 2: Phase A

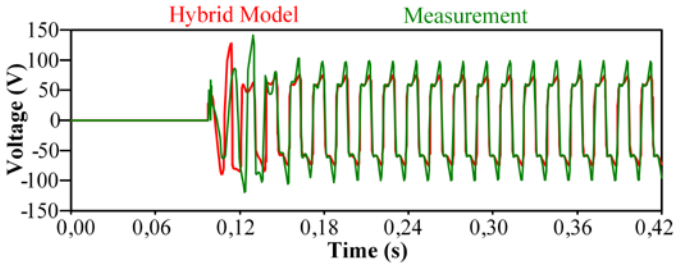

Figure 4.48. Three-phase transformer validation case 2: Phase B

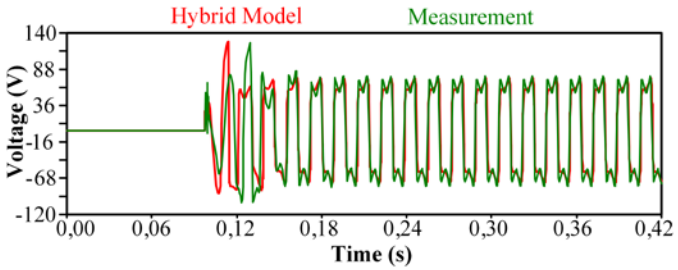

Figure 4.49. Three-phase transformer validation case 2: Phase C.

From the plots, it can be concluded that even though the initial transient presents some differences, the stable state of the ferroresonance is quite well represented by the Hybrid model.

4.2.7.3 Validation 3

The third transformer used for validation, corresponds to the transformer coded as Tri_8. General data is displayed below.

Table 4.21: Transformer Tri_8 main data

Phases	Three	*Power(kVA)*	112.5	*High Voltage side (V)*	13200
Core type	5-Legged	*Connection Grup*	Dyn5	*Low Voltage side (V)*	214

The data used to configure the Hybrid model are shown below:

Table 4.22: Case 3 - Hybrid transformer configuration data

V%	Loss kW	Iav %
19.2306202	0.013420	0.07303353
38.6581869	0.051560	0.1286049
58.9221022	0.119700	0.20603142
78.4629807	0.220700	0.48564549
98.5812095	0.378000	1.62430953
100.307865	0.397000	1.8632884
102.088478	0.419600	2.0988627
103.653259	0.433000	2.35080091
105.892514	0.464400	2.7617655

Saturation

IMP(%)	POW(MVA)	PLOSS(kW)
2.894	0.112500	1.886238

Resistence and Inductance

IMP(%)	POW(MVA)	PLOSS(kW)
14.8	0.112500	0.00971

Zero sequence

V(%)	Loss(kW)	Iav(%)
0.1532	0.00971	10.86

Zero sequence

HV-LV(nF)	HV-GND(nF)	LV-GND(nF)
2.2	0.3	1.29

Internal Capacitance

The validation process is performed for a de-energization case settled in test Configuration 2, with a total of 50 μF being used to represent the line capacitance. The switch opens the Phase *A* while the other two phases continue in normal operation. The waveform comparison is presented in Figure 4.50.

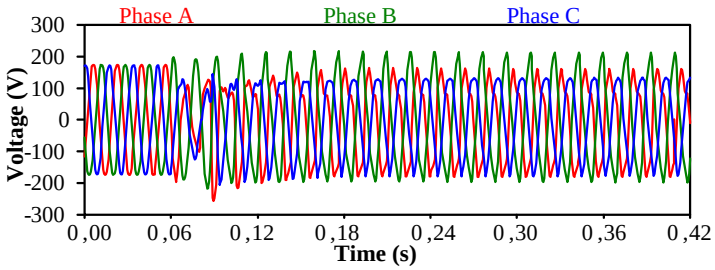

a) Experimental measurement

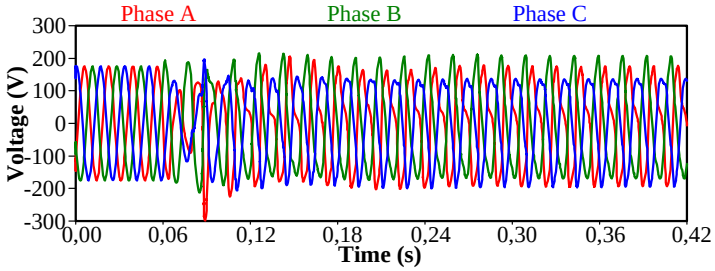

b) Hybrid model simulation

Figure 4.50. Three-phase transformer validation case 3: Waveform analysis.

In this case, the dynamic response of the simulated signal is really similar to the experimental one. Closer detail for each phase is presented in Figures 4.51 to 4.53.

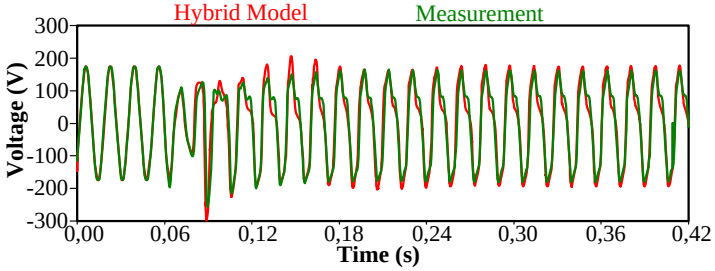

Figure 4.51. Three-phase transformer validation case 3: Phase A.

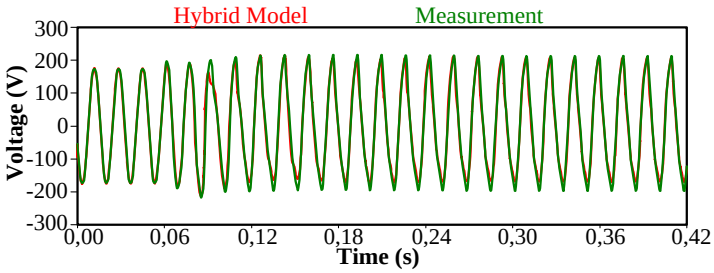

Figure 4.52. Three-phase transformer validation case 3: Phase B.

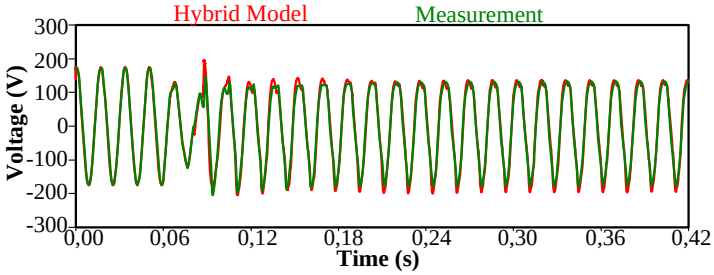

Figure 4.53. Three-phase transformer validation case 3: Phase C.

It is quite clear that the simulated model responses are very close to the actual event, even during the initial transient. Any small noticeable differences can be attributed to the use of an ideal source in the simulated model, while the experiment used a toroidal adjustable source.

4.2.7.4 Validation 4

The fourth validation case is carried out using the transformer encoded as Tri_9. The main parameters are shown below:

Table 4.23: Transformer Tri_9 main data

Phases	Three	*Power (kVA)*	75	*High Voltage side (V)*	13200
Core type	5-Legged	*Connection Grup*	Dyn5	*Low Voltage side (V)*	214

The parameters used to configure the Hybrid model ATPDraw are the following:

Table 4.24: Case 4 - Hybrid transformer configuration data

V%	Loss kW	Iav %
40.1690101	0.038530	0.14480407
60.5705182	0.090590	0.22832587
79.6986182	0.171400	0.56850835
100.361822	0.310200	2.12840566
101.575877	0.331300	2.35360152
103.599301	0.355000	2.75193626
104.975229	0.371700	3.12028882
106.8098	0.405000	3.65881499
108.806245	0.427000	4.40721645
111.477164	0.482000	5.65790189
116.792024	0.658000	9.61571504

Saturation

IMP(%)	POW(MVA)	PLOSS(kW)
1.176	0.075000	0.78449

Resistence and Inductance

IMP(%)	POW(MVA)	PLOSS(kW)
1.176	0.075000	0.78449

Zero sequence

IMP(%	POW(MVA)	PLOSS(kW)
1.176	0.075000	0.78449

Zero sequence

HV-LV(nF)	HV-GND(nF)	LV-GND(nF)
2.52	1.15	0.2

Internal Capacitance

Once the model was properly configured, the test system was connected following the Configuration 4, where cable capacitance is settled as ungrounded wye connection. A de-energization on Phases *B* and *C* was performed and ferroresonance was ignited into quasi-periodic mode; the capacitance value of the cable used was 50 μF. The results are presented in Figure 4.54.

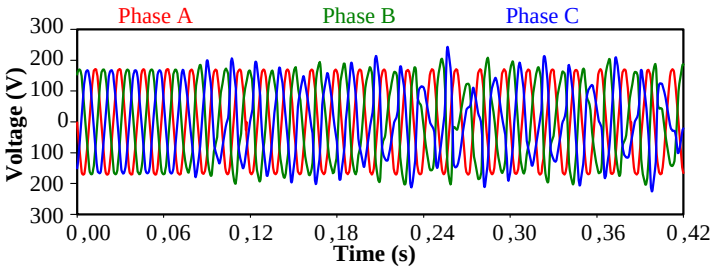

a) Experimental measurement

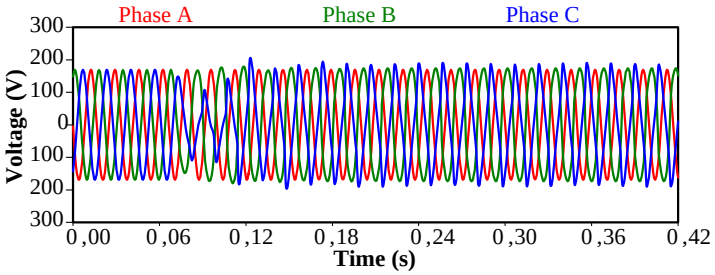

b) Hybrid model simulation

Figure 4.54. Three-phase transformer validation case 4: Waveform analysis.

In these plots, as in previous cases, the computational representation is acceptable, the waveform dynamics and the peaks magnitude are correctly represented. Any discrepancies in this case may be due to the saturation of the power supply; in the real experiment, the source may be suffering significant saturation stress causing the signal to have a non constant oscillation. A close up of the three waveforms is presented in Figures 4.55 to 4.57.

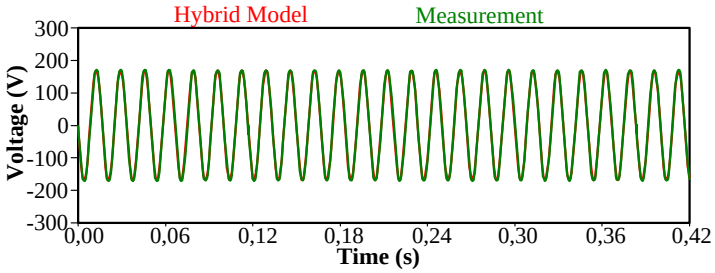

Figure 4.55. Three-phase transformer validation case 4: Phase A.

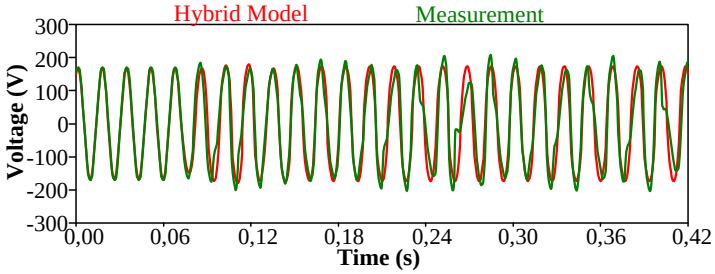

Figure 4.56. Three-phase transformer validation case 4: Phase B.

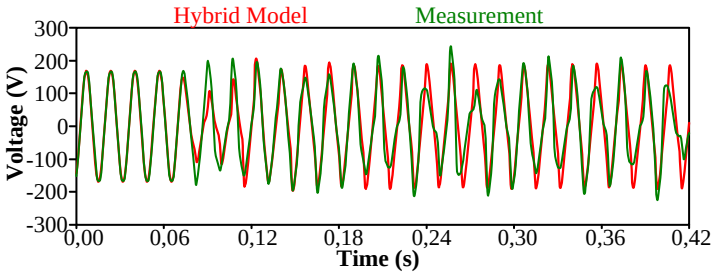

Figure 4.57. Three-phase transformer validation case 4: Phase C.

This is perhaps one of the cases worth to highlight because of the intensity of the ferroresonance phenomenon, affecting two of the phases and having a complex oscillation in quasi-periódic mode. Yet the response of the model approaches quite well to the experimental data; it is important to remark once again that the Hybrid model uses an *average current* value for the magnetization curve representation. If individual curves where considered for each leg the result may have been closer in accuracy.

4.2.7.5 Validation 5

The next test validation was performed on the transformer coded as Tri_11. The main parameters are shown below:

Table 4.25: Transformer Tri_11 main data

Phases	Three	*Power(kVA)*	500	*High Voltage side (V)*	13200
Core type	3-Legged	*Connection Grup*	DYn5	*Low Voltage side (V)*	214

The data used for configuration of the magnetic branch is presented below:

Table 4.26: Case 5 - Hybrid transformer configuration data

V%	Loss kW	Iav %
18.5821253	0.012200	0.12263003
39.8398415	0.046150	0.15319089
61.4664203	0.095250	0.18067645
79.6609726	0.160000	0.21951042
101.59761	1.090000	0.69472142
101.811443	1.436000	0.98706111
103.735944	2.026000	1.33936024
105.125862	2.470000	1.65586828
106.221758	2.893000	1.98883773

Saturation

IMP(%)	POW(MVA)	PLOSS(kW)
6.45	0.5	5.44375275

Resistence and Inductance

IMP(%)	POW(MVA)	PLOSS(kW)
29.21	0.5	0.04399

Zero sequence

V(%)	Loss(kW)	Iav(%)
0.005	0.04399	0.029

Zero sequence

HV-LV(nF)	HV-GND(nF)	LV-GND(nF)
0.1385	1.126	0.627

Internal Capacitance

This essay is much more accurate than the previous one, possibly due to the large amount of data obtained. Besides, the computational resolution of a three-legged core is simpler compared to a five-legged. It should also be noted that the ferroresonance oscillation is the fundamental mode, so from the viewpoint of mathematics software resolution the system is less prone to erroneous calculation. The result for a de-energization using Configuration 2 and having a capacitance value of 60 μF is shown in Figure 4.58.

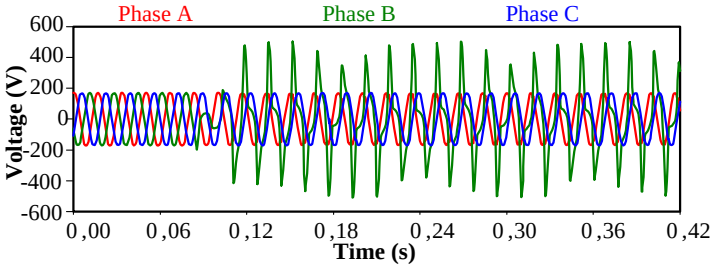

a) Experimental measurement

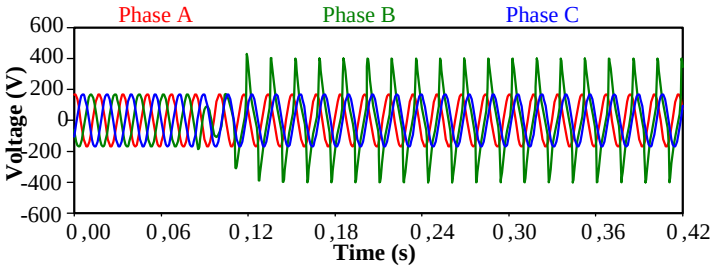

b) Hybrid model simulation

Figure 4.58. Three-phase transformer validation case 5: Waveform analysis.

Figure 4.58 shows how the Phase *B* is driven into ferroresonance after being disconnected. In this case, the signal obtained from the simulation is considered good, although the experimental signal peaks have higher amplitude. The general dynamics of the waveforms are similar, even the initial transient shows the same behavior. Figures 4.59 to 4.61 present detailed information of the waveforms.

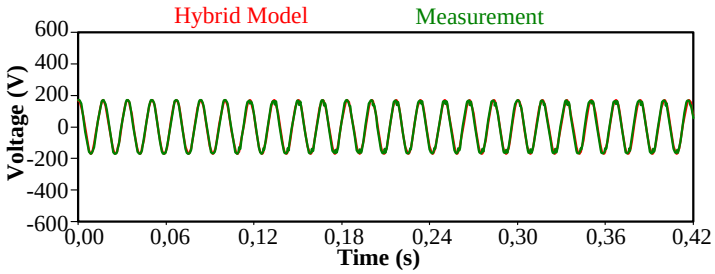

Figure 4.59. Three-phase transformer validation case 5: Phase A.

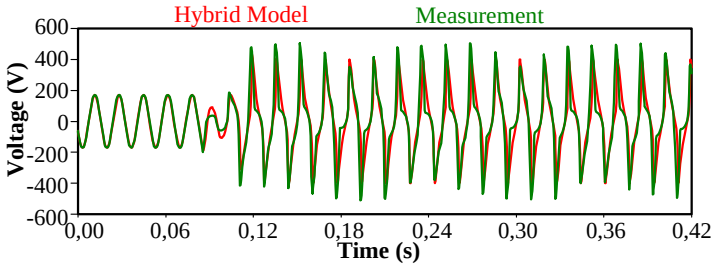

Figure 4.60. Three-phase transformer validation case 5: Phase B.

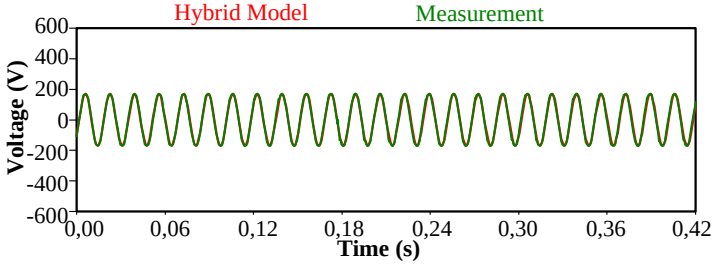

Figure 4.61. Three-phase transformer validation case 5: Phase C.

4.2.7.6 Validation 6

The last case study is based on the transformer coded as Tri_12. Its data is shown below.

Table 4.27: Transformer Tri_12 main data

Phases	Three	*Power(kVA)*	45	*High Voltage side (V)*	13200
Core type	5-Legged	*Connection Grup*	Dyn5	*Low Voltage side (V)*	214

The data for the configuration of the Hybrid model is shown below:

Table 4.28: Case 6 - Hybrid transformer configuration data

V%	Loss kW	Iav %
39.4055048	0.020690	0.11970909
60.2009061	0.046550	0.18011276
79.9387312	0.082750	0.2399673
99.525474	0.139000	0.45742051
102.304309	0.150300	0.56504886
103.86909	0.157200	0.649614
106.243241	0.167600	0.84949523
107.996875	0.176800	1.09248271
109.669572	0.187000	1.43293975
112.583302	0.206900	2.33460178
114.876516	0.227800	3.31067015
116.684108	0.248700	4.29744644

Saturation

IMP(%)	POW(MVA)	PLOSS(kW)
3.453	0.045000	0.643292

Resistance and Inductance

IMP(%)	POW(MVA)	PLOSS(kW)
16.42	0.045000	0.643292

Zero sequence

V (%)	Loss(kW)	Iav(%)
0.6361	0.0106	38.49

Zero sequence

HV-LV(nF)	HV-GND(nF)	LV-GND(nF)
0.205	0.7125	1.12

Internal Capacitance

As a final test, a case having a greater dynamic complexity is studied in this case, a chaotic waveform is analyzed. The results from the simulation are shown in Figure 4.62.

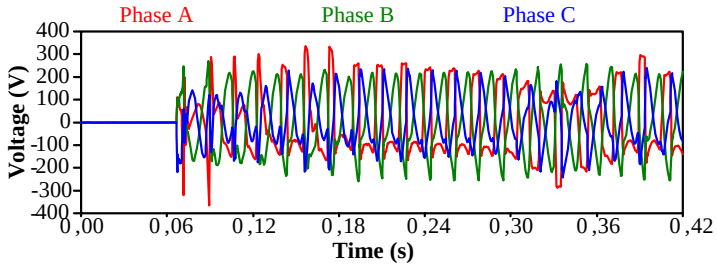

a) Experimental measurement

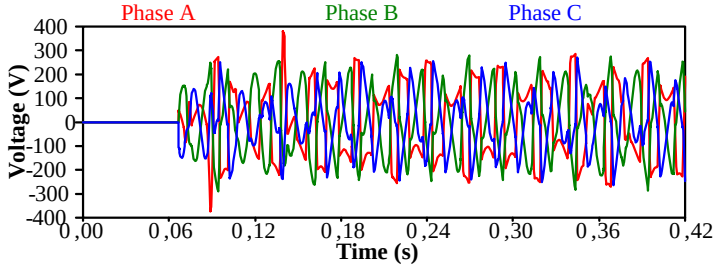

b) Hybrid model simulation

Figure 4.62. Three-phase transformer validation case 6: Waveform analysis.

To get a better assessment of the similarity of the waveforms is better to perform a phase-to-phase analysis. Such comparisons are presented in Figures 4.63 to 4.65.

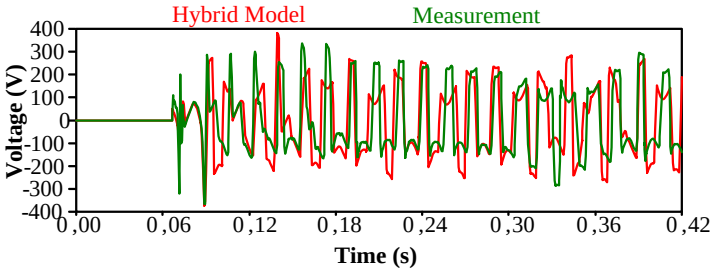

Figure 4.63. Three-phase transformer validation case 6: Phase A.

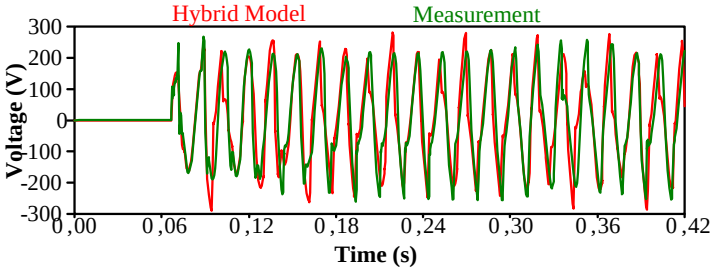

Figure 4.64. Three-phase transformer validation case 6: Phase B.

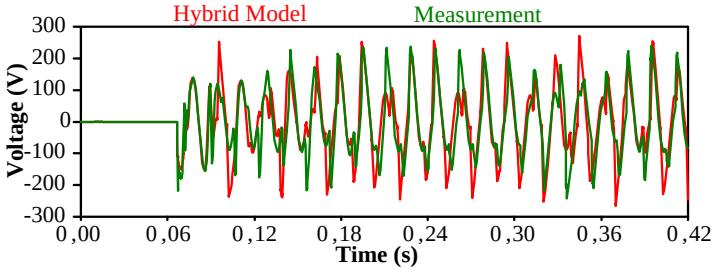

Figure 4.65. Three-phase transformer validation case 6: Phase C.

In the simulation, the Phase *A* presents a chaotic signal where even if the peaks are not all exactly correct, the general dynamics of the event is well represented. For the Phases *B* and *C*, the simulation response is quite similar and with a less error rate in the timeline representation. Again, it is confirm that the degree of precision of the Hybrid model is sufficient enough to known whether ferroresonance is presented in a system or not, however, there exist the need for improvements, mostly, for those cases were waveform representation is important with a high accuracy level.

The study has shown that the effect of the interwinding capacitances cannot be always neglected for three-phase transformers. It has also been proved that the Hybrid model can represent ferroresonance cases with some precision. Differences between measurements and simulation results may be mainly due to: (i) the fact that magnetization curves have been considered identical for each transformer's leg; (ii) the model for the voltage source used in the simulations did not consider any saturation degree; (iii) the hysteresis effect was not included in the transformer magnetization curve. The analysis has also point out the principal aspect to improve within the model: the addition of the hysteresis effect in the representation of the transformer core. Fixing the core saturation, by allowing to introduce individual saturation branches to have individual behaviors in each leg. The use of other transformer models, such as the π model [21], [22], derived also through the Principle of Duality for core representation is another option.

4.3 EFFECT OF THE HYSTERESIS ON THE FERRORESONANCE PHENOMENON: AN INTRODUCTION.

So far, few authors have made serious studies on the involvement of the hysteresis cycle in the phenomenon of ferroresonance. Still, some research can be found, for example [24]-[27], which describes how the residual magnetic flow affects some transients. Although these works are quite extensive, they do not focus on the ferroresonance and its dynamics. Figure 4.66 shows a typical hysteresis cycle.

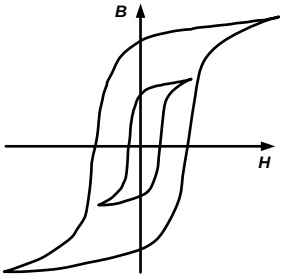

Figure 4.66. Hysteresis cycle.

The lack of studies considering the hysteresis during the ferroresonance phenomenon may possibly be due to the difficulty for obtaining experimental measurements and the lack of specialized equipment for that purpose. Normally, accessing to internal parts of a transformer is rarely possible, since most of commercial transformers show only the external connection terminals and do not allow access to the core. In this regard, it is important to set a precedent, looking into methods to obtain the hysteresis cycle, in such a manner that allows performing a simple test and avoiding the need of expensive or too sophisticated equipment. Two different proposals have been tested, the first one based on the test set out in the *IEEE Std 393-1991* [41], where the geometry of the transformer by using mathematical expressions is considered, and complementing such test using the excitation data.

4.3.1 Hysteresis cycle by direct measurement using the excitation test: Geometrical approach

Here is the procedure to follow:

1) It is assumed that the hysteresis loop is governed by a B-H curve. In this sense, it is necessary to change the data obtained in the excitation test, usually referred to a set of V-I pairs. This requires performing the test excitation incrementally until it reaches a peak that does not exceed 5% harmonic distortion according to [41], [42] to ensure that the supply voltage signal remains sinusoidal. The assay is performed according to Figure 4.67

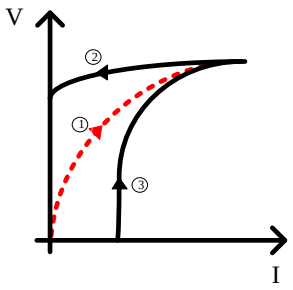

Figure 4.67. Hysteresis cycle: Reversible and irreversible components.

The above figure, (1) represents the first excitation curve, for cases in which the transformer is de-magnetized, (2) stands for the reverse excitation process, and (3) the normal excitation, the last two starting from a point which has residual flux. If the transformer is magnetized, the curve (3) should be obtained first and then (2).

2) Considering the physical relationship between the magnetic flux and the excitation voltage in the form of:

$$\Phi = \frac{V}{4.44\, N\, f} \tag{4.4}$$

where Φ is the magnetic flux, V is the voltage measured during the excitation test, N is the number of turns in the winding, and f is the driving frequency. Now considering the cross section of the column it is possible to determine the magnetic flux density:

$$B_{max} = \frac{\Phi_{max}}{A} \tag{4.5}$$

where B is the magnetic flux density and A the area of the ferromagnetic material. It must be remarked again the need to access the transformer design data, or to request it to the manufacturer.

3) Finally the strength of the magnetic field, H, is calculated analogously to the calculation of the flux. This depends on the excitation current and the topological characteristics of the core.

$$H = \frac{NI}{L} \tag{4.6}$$

where I is the current calculated from the excitation test, and L is the length of the ferromagnetic material. Within the single-phase transformers tested, it was possible to obtain sufficient data to represent the hysteresis for the transformer labeled as Mono_5. The extracted data is summarized in Table 4.30.

As a complement to modeling the hysteresis cycle, and to include it in the π transformer model, design data was requested to the manufacturer. That information is summarized below:

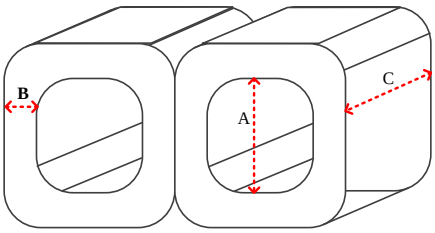

Figure 4.68. Single-phase transformer core.

Table 4.29: Transformer construction data

Nº of turns High voltage high	Nº of turns Low voltage side	A (mm)	B (mm)	C (mm)
3410	62	100	40	150

Table 4.30: Saturation Test

%	V (V)	I (A)	Ploss (W)
60	145,8	0,085	10,52
80	193,6	0,124	18,08
100	241,3	0,656	31,09
102	245	0,796	33,04
104	250	1,008	35,71
106	254	1,187	38,1
108	259,8	1,474	42,94
110	264,4	1,735	46,67
112	269,5	2,05	52,06
114	273,5	2,329	56,12
116	278,4	2,752	63,15
118	283,7	3,228	70,84
120	288,7	3,806	79,62
118	281,8	3,05	67,83
116	275,6	2,518	59,43
114	273,1	2,318	55,9
112	268,1	1,965	50,35
110	264,8	1,766	46,93
108	259,3	1,451	42,25
106	254,5	1,202	38,17
104	249	0,969	34,91
102	243,3	0,742	32,04
100	240,2	0,625	30,55
80	195,8	0,126	18,3
60	146,3	0,083	9,561

In order to calculate the hysteresis cycle, data must be pre-processed. Once the cycle is obtained, a strategy to implement the hysteresis effect in the π model is described below:

1) After calculating the hysteresis loop, create a new model of EMTP inductance. For this, TACS and MODELS from ATPDraw can be used as tools.

2) After checking the correct operation of the inductance, it must be included in the π model as seen in Figure 4.69.

3) Once the π model is working properly with the addition of the hysteresis loop, the results must be validated with data collected experimentally for transformers.

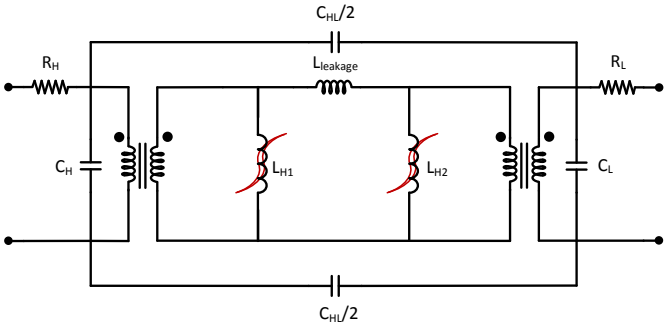

Figure 4.69. Equivalent π model including hysteresis core characteristic.

Three case studies have been carried out using the hysteresis cycle by direct measurement. The more relevant results are presented in Figures 4.70, 4.71 and 4.72. Three different tests have been performed using a 5 kVA 7.62-0.240 kV single-phase transformer: a) Configuration 4 de-energizing the transformer by switching on S2, with a capacitance value for each cable of 5 μF; b) Configuration 4 de-energizing the transformer from steady state, with a shunt capacitance value of 50 μF; c) Configuration 4 de-energizing the transformer from steady state, with a shunt capacitance value of 60 μF.

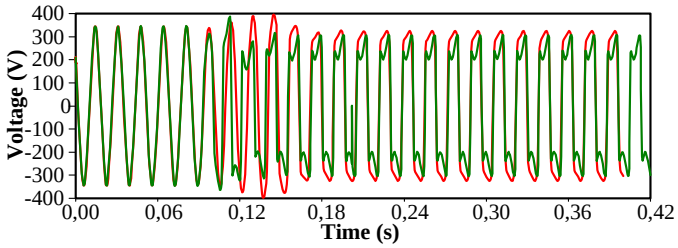

Figure 4.70. Configuration 4, de-energizing with C_s=5 μF.

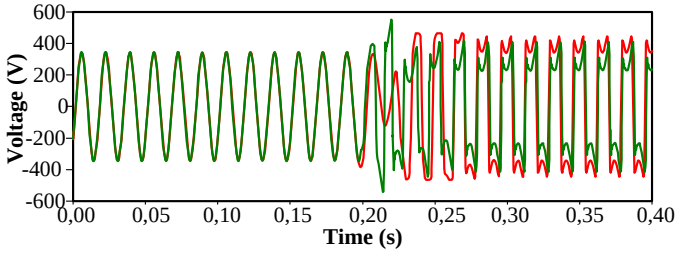

Figure 4.71. Configuration 4, de-energizing with C_s=50 μF.

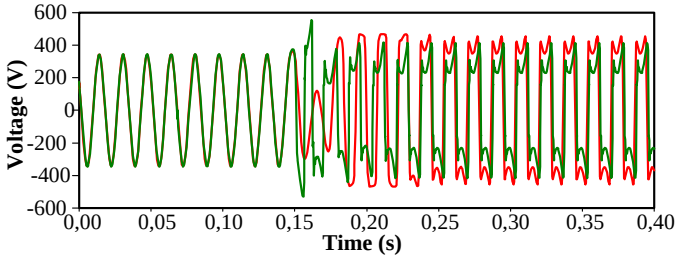

Figure 4.72. Configuration 4, de-energizing with C_s=60 μF.

The goal of this study is not only to observe the effect of the hysteresis loop in the behavior of the ferroresonance, but most importantly to be able to conclude whether the addition of the hysteresis cycle is a priority for ferroresonance modeling or not. It is important to remark that this approach is still dependent on the physical characteristics of the core. In most cases, transformer does not have such information and it is not possible to obtain it from the manufacturer either.

4.3.2 Hysteresis modeling avoiding geometrical data: First approach

The magnetization characteristic of iron core transformers is composed by two main components: (a) a reversible component, known as the anhysteretic curve of the material, which is a single-valued function where each element of the function's domain maps to a single element of its range; (b) an irreversible component, represented by the hysteresis loop. Hysteresis loops are the result of the interaction between domains, anisotropy and pinning forces due to the existence of dislocations, interstices and impurities inside the material [25]. Hysteresis characteristic usually presents a sigmoid shape involving the flux density against the magnetic field intensity, also known as the B/H characteristic of the material. Three different types of hysteresis loops can be observed: (1) the major hysteresis loop, (2) symmetric minor loops, and (3) asymmetric minor loops [41]. The major and the symmetric loops were presented in Figure 4.66.

Test methods are useful to determine transformer characteristics and assist the design, analysis and operation of magnetic cores in many types of applications. Tests for measuring permeability, core loss, apparent core loss, thermal characteristics, and other properties are collected as standard measurements. Most test methods include specific parameter ranges, instrument accuracies, or core sizes. However, hysteresis measurement tests, even if they are collected by international standards, still remain complex. Usually, the standards only consider inductors and its tests are being extended to transformer cores [41], [43].

Over the years several models have been proposed to describe the complex phenomenon of hysteresis [44], [45]. However, these methods are often laborious or require an important amount of parameters. In practice, most of transformer models focus on the simplified representations of the magnetic core. The aim is to come up with a realistic representation and skipping the need of using parameters difficult or impossible to be measured.

Typically, the hysteresis curve is presented as a plotted data matching the flux linkage against the magnetizing current of the winding. It is worth remarking that flux linkage, λ, is a specific property of two-terminal element that can be defined by:

$$\lambda = \int \varepsilon \, dt \tag{4.7}$$

where ε represents the potential difference between the winding terminals. If a long period of both voltage and magnetizing current can be recorded, an approximation to the actual hysteresis curve can be plotted. Based on this property, the following procedure has been used to obtain a hysteresis model:

1) Make a capture of experimental ferroresonance voltage and current waveforms. If possible, a case where maximum saturation is reached should be selected. Voltage and current measurements must be recorded as closest as possible to the transformer physical terminals.
2) The recorded signals are referred to the primary side and exported to MATLAB format. Then, the voltage signal is integrated making sure that any possible offset produced by the integration constant is fixed. In this way, flux linkage is calculated.
3) After an approximation to the actual hysteresis curve has been plotted in MATLAB, the signal is filtered for high harmonic content since the recorded magnetization current could have high frequency ripples.

4) Once the major loop is spotted in MATLAB, a curve fitting approximation is performed individually for each side of the loop (left and right). The resulting fitting curves should have the form of a polynomial expression were current is obtained as a function of the flux linkage.
5) The expressions for the polynomials previously defined are written in the form of TACS code in the ATP environment and used as a nonlinear inductor model within the transformer model.

The implementation and benchmarking of this method is presented in the last Chapter of this thesis, where several ferroresonance cases modeled using this technique are discussed. In here, three different case studies have been documented to illustrate different ferroresonance stages. In all case studies, the hysteresis loop has been calculated avoiding geometrical data.

4.3.2.1 Case Study 1

Three tests have been carried out on a 3 kVA, 7.62/0.240 kV single-phase transformer:

1. De-energization of the transformer from steady state in Configuration 1 by opening Switch S1, being the capacitance value of the breaker 5 μF.
2. De-energization of the transformer from steady state in Configuration 2, with a series capacitance value of 50 μF, and a cable capacitance value of 20 μF.
3. Energization of the transformer using Configuration 3. The Switch S1 is closed while Switch S2 is open. Each cable has a capacitance-to-ground value of 20 μF.

Table 4.6 presented previously shows the data required to implement the transformer using the π model. Figure 4.73 shows the hysteresis cycle, directly derived from lab measurements, for the core representation including the symmetrical minor loops. Capacitive effects between windings were measured for this case. Figure 4.74 shows the comparisons between measured and simulated waveforms for the different tests specified above. Considering hysteresis effects, a good match between simulation and measurements was obtained once ferroresonance did occur. Although energization or de-energization are random processes difficulting the inclusion of initial conditions, the differences between waveforms were not too large. Therefore, it can be concluded that the degree of accuracy provided by the π model including hysteresis effect was quite acceptable. Notice that with Configurations 2 and 3, the model could not follow properly lab measurements when hysteresis was not considered.

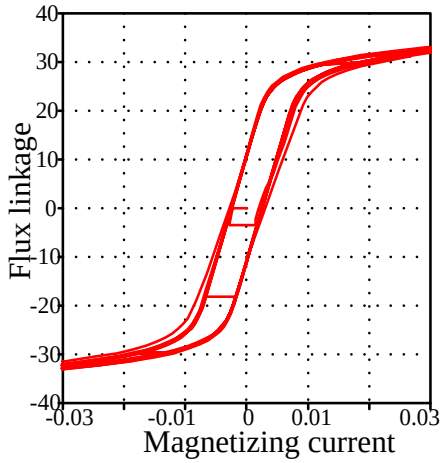

Figure. 4.73 Case Study 1 - Hysteresis loop.

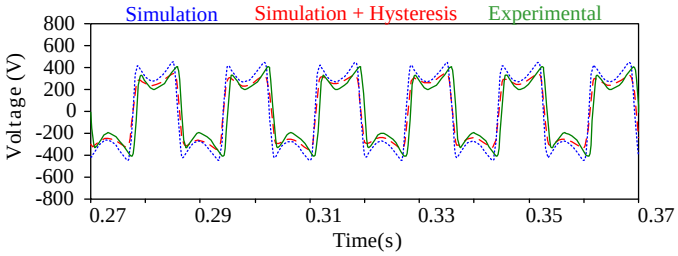

a) Configuration 1 - De-energization

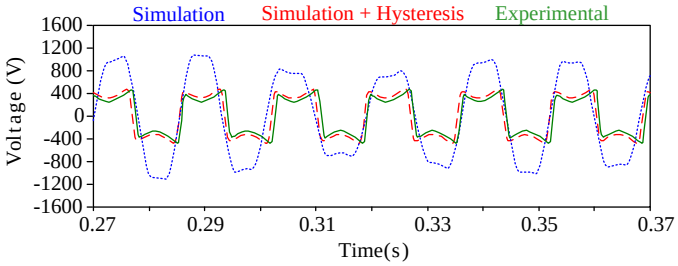

b) Configuration 2 - De-energization

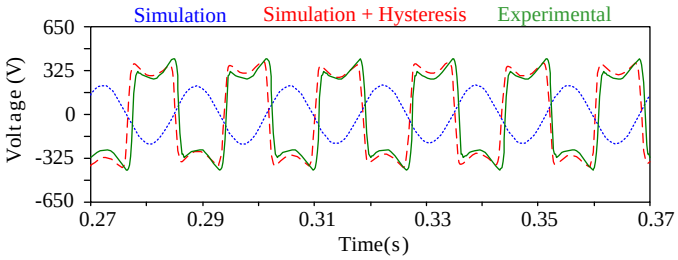

b) Configuration 3 - Energization

Figure 4.74. Case Study 1: Comparison between simulation results and measurements.

4.3.2.2 Case Study 2

Three tests have been carried out on a 37.5 kVA, 7.62/ 0.240 kV single-phase transformer:

1. De-energization of the transformer from steady state in Configuration 1 by opening Switch S1, being the capacitance value of the breaker 10 μF.
2. De-energization of the transformer from steady state in Configuration 2, with a series capacitance value of 20 μF, and a cable capacitance value of 10 μF.
3. De-energization of the transformer from steady state in Configuration 3 by opening Switch S2, being the capacitance value for each cable 83 μF.

Table 4.9 presented previously shows the data required to implement the transformer using the π model. Figure 4.75 shows the hysteresis cycle for the core representation including again the symmetrical minor loops. Capacitive effects between windings were again measured for this case. Simulation results are shown in Figure 4.76. With Configurations 1 and 3, a noticeable discrepancy (i.e. a lag between waveforms) can be found when comparing lab measurements and simulation results. It is believed that this is due to the change in the temperature of the core while performing the ferroresonance test and the routine tests. The lack of representation of non-measureable nonlinear components in other part of the core could also affect the representation (i.e. dispersion fluxes). Notice that the transformer for Configuration 2 was not driven into ferroresonance. However, it is shown here just to verify the model follows correctly the experimental measurements.

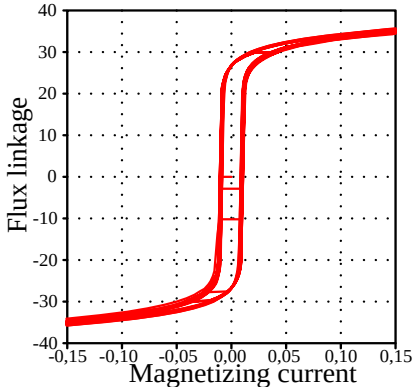

Figure 4.75. Case Study 2 - Hysteresis loop.

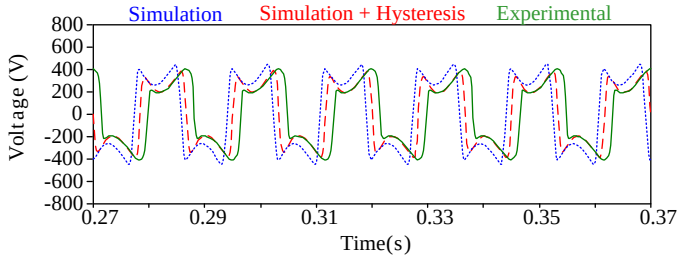

a) Configuration 1 - De-energization

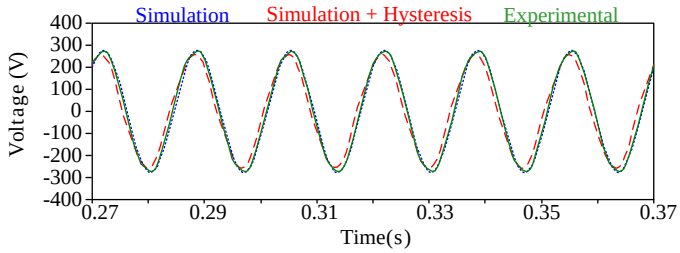

b) Configuration 2 - De-energization

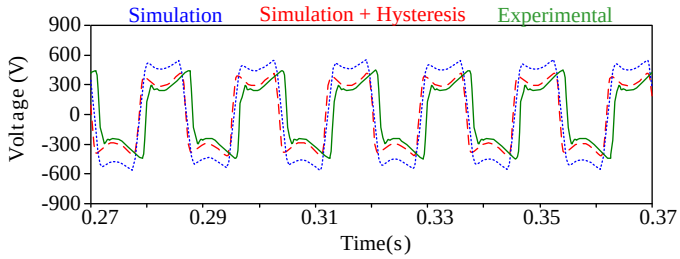

c) Configuration 3 - De-energization

Figure 4.76. Case Study 2: Comparison between simulation results and measurements.

4.3.2.3 Case Study 3

Three tests have been carried out on a 5 kVA, 7.62/0.240 kV single-phase transformer:

1. De-energization of the transformer from steady state in Configuration 1, by opening Switch S1, being the capacitance value of the breaker 2 μF.
2. Energization of the transformer using Configuration 3. The Switch S1 is closed while Switch S2 is open. Each cable has a capacitance-to-ground value of 20 μF.
3. De-energization of the transformer from steady state in Configuration 3 by opening Switch S2, being the capacitance value for each cable 5 μF.

Table 4.12 shown previously presents the data required to implement the transformer

using the π model. Figure 4.77 shows the hysteresis loop for the core representation in this case, including the symmetrical minor loops. Capacitive effects between windings were not measured for this case, so they were not considered in the simulations. Results are shown in Figure 4.78. Conclusions are similar to those ones discussed previously. Notice that although internal capacitive effects were not considered for this case study, a good match between simulation and measurements was obtained again since differences between waveforms were not too large. Therefore, it may be concluded that internal capacitive effects of the transformer are not too decisive for this case.

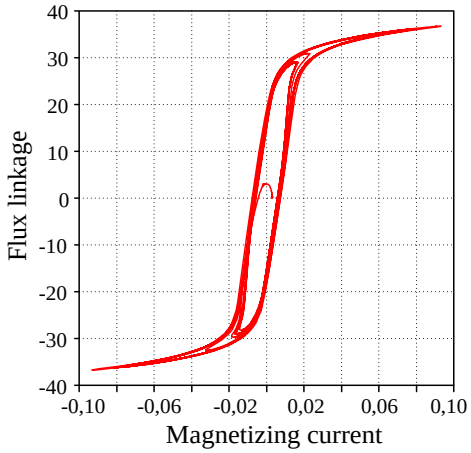

Figure 4.77. Case Study 3 - Hysteresis loop.

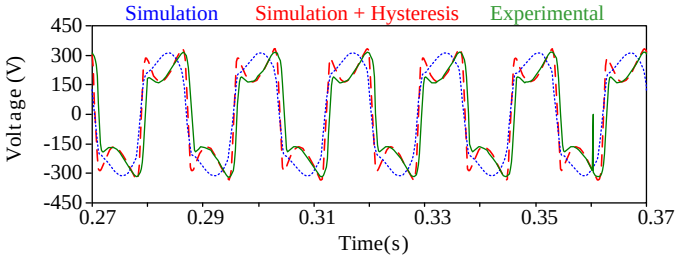

a) Configuration 1 - De-energization

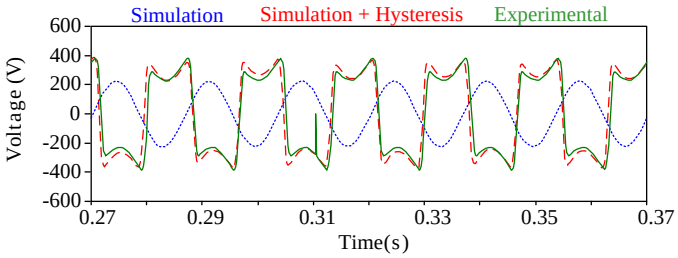

b) Configuration 3 - Energization

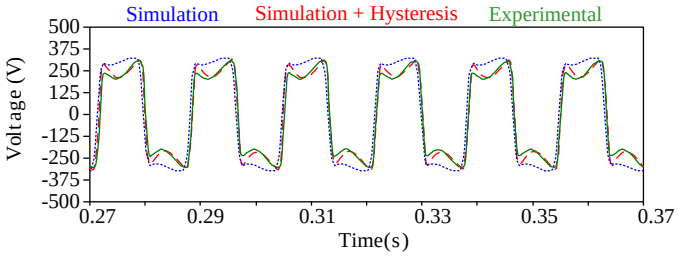

c) Configuration 3 - De-energization

Figure 4.78. Case Study 3: Comparison between simulation results and measurements.

The study of ferroresonance is highly dependent on the models used for representing the main system components, being the transformer the most critical one. Results obtained by means of simulation have been compared to actual lab measurements when using the π model to represent single-phase transformers. This preliminary study has demonstrated the correctness of the π model behavior for ferroresonance analysis. The comparisons show for all the cases studies that, although there can be some differences between simulated and actual waveforms for the initial transient state, the global and dynamic behavior is similar in both cases (i.e., measurements and simulations), and stable ferroresonant states are represented quite well by the π model. The additions of hysteresis effects significantly improve simulation results, and this work has proved that these effects can be crucial: in some case the response was correct only when hysteresis effects were added to the transformer model. Differences between measurements and simulation results may be mainly due to: (i) the no consideration of any saturation degree for the voltage source used in the simulations; (ii) the differences between the temperature of the core during ferroresonance tests and during excitation tests for estimating internal core parameters.

4.4 FERRORESONANCE ANALYSIS FOR CASES INVOLVING DIFFERENT TYPES OF NONLINEAR SOURCES

4.4.1 Ferroresonance in single phase transformer supplied from a nonlinear source

The objective of the coming tests is divided in two parts: 1) Feed the ferroresonant circuit from a nonlinear source with known parameters, 2) Control the shift angle of the switch when energizing/de-energizing the event.

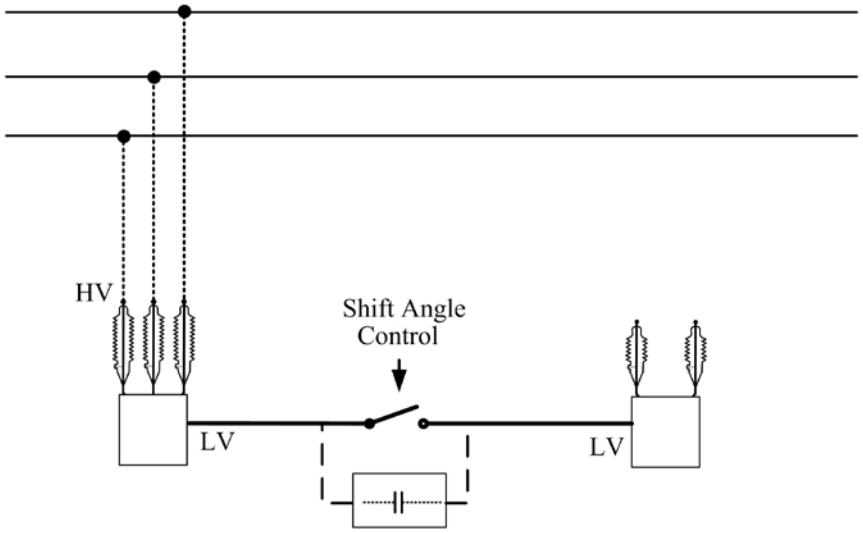

Figure 4.79. Nonlinear source test: General scheme.

Figure 4.79 depicts the scheme used during the essay where the test circuit includes: a Dyn5 three-phase transformer, 45 kVA, 13200/214 V; a switch connected to a zero crossing detector with adjustable switching trigger; an adjustable capacitance bank with a rate of 2-160 μF; and a single-phase transformer 3 kVA, 13200/214 V. The first transformer is connected directly to a 13200 V grid and was used as a source to the test system. The single-phase transformer is leaded to ferroresonance in the low voltage side. Conceptually, the ferroresonance circuit in this essay should replicate the configurations shown in Figure 4.80.

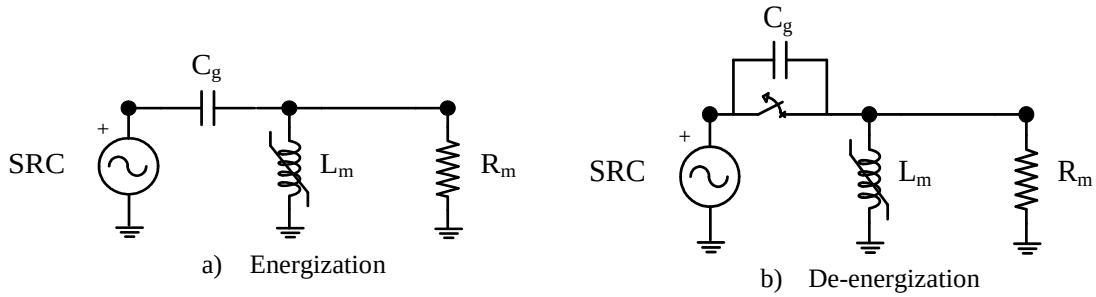

Figure 4.80. Nonlinear source test: Equivalent circuits.

It can be seen on the figure the equivalent circuits including the transformer core, represented by the nonlinear inductance L_m and the core losses R_m. A capacitance is connected in series with the core, representing the grading capacitance of the switch; the value chosen for C_g capacity is 20 μF.

4.4.1.1 Energization

To perform the energization test the two switches methods was used. This method consists in having two synchronized switches, closing one after the other with a controlled time gap. This way, it was possible to control the grading capacitance and the timing to trigger the Switch S2. Figure 4.81 has been varied from the scheme in Figure 4.79, displacing the grading capacitance between the tested transformer and the Switch S2 to have an energization ferroresonance case.

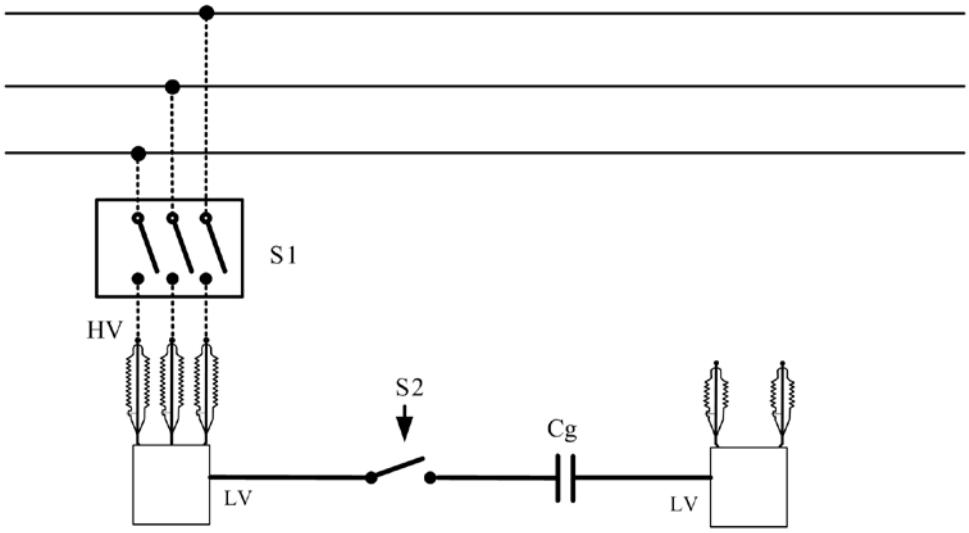

Figure 4.81. Nonlinear source test: Energization scheme.

First, the switch S1 is closed while having S2 open. This will prevent the three-phase transformer inrush current to disturb the test results. After 300 ms, the Switch S2 closes energizing the single-phase transformer and the grading capacitance. At this point, the ferroresonance essay begins, and each signal recorded has a duration of 3 s. Using the zero crossing detector the switch shift angle can be controlled. The initial variation time for the trigger is changed every 0.5 ms which is the equivalent to 10º. The following figures show the sequence obtained in some of the measurements.

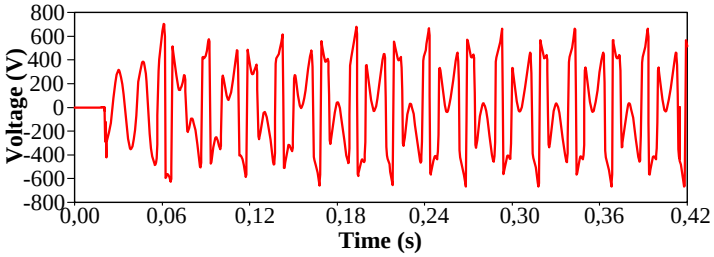

Figure 4.82. Energization case: Ferroresonance signal for a switch shift angle =280º.

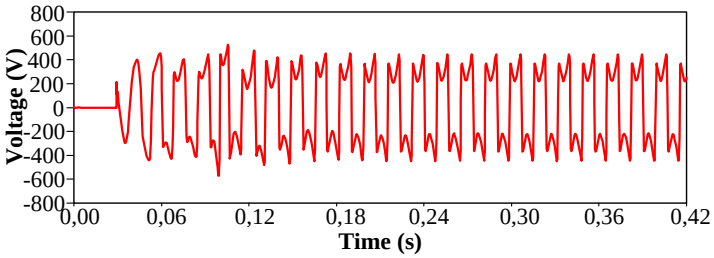

Figure 4.83. Energization case: Ferroresonance signal for a switch shift angle =130º.

In this assay, for the first time, it was possible to obtain a ferroresonance mode different than the fundamental one in a single-phase transformer. The measurements obtained changed from fundamental to chaotic modes when energizing the transformer. The incorporation of a source with a dynamic nature, the three-phase transformer, made ferroresonance to jump to different operation modes. This is because the operating point of the system depends not only on the saturation curve of the affected transformer phase, but also the saturation point from the power supply.

4.4.1.2 De-energization

The process of de-energization is performed using the method of the two switches. The three-phase transformer is energized first, then, after some seconds the single-phase transformer is started too. The experiment is carried out de-energizing the single-phase transformer 3 seconds after every signal was stable. The equivalent arrangement is shown in Figure 4.84.

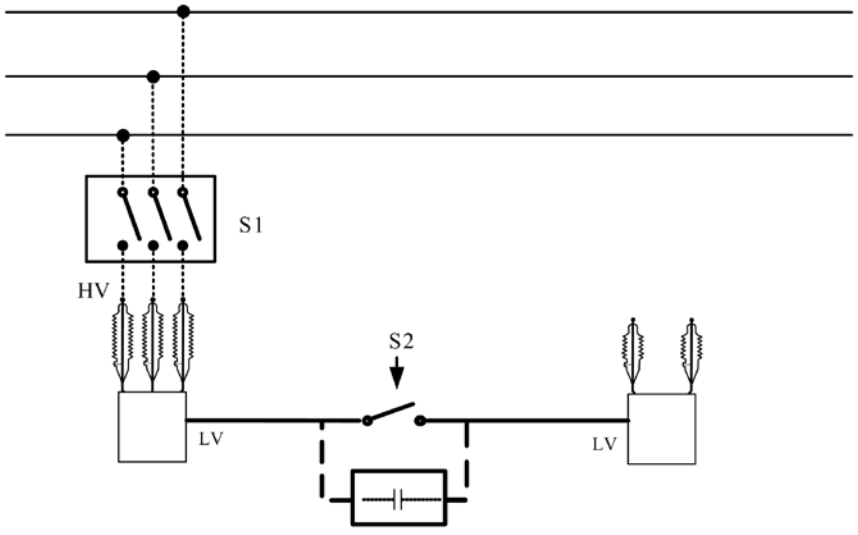

Figure 4.84. Nonlinear source test: De-energization scheme.

The value of the grading capacitance, C_g, is maintained constant at 20 μF while all other conditions are controlled. Waveforms obtained are shown below:

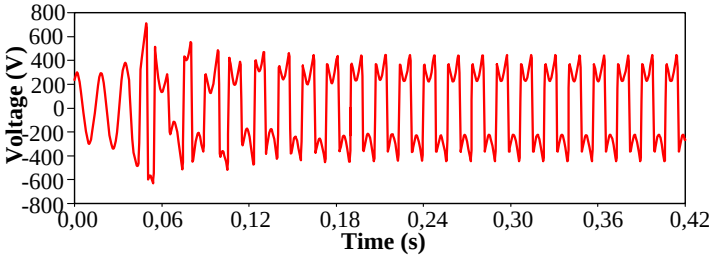

Figure 4.85. De-energization case: Ferroresonance signal for a switch shift angle =0º.

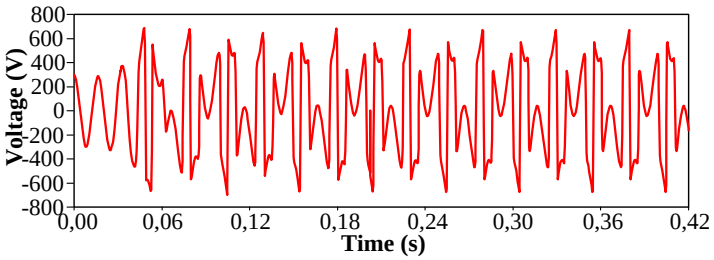

Figure 4.86. De-energization case: Ferroresonance signal for a switch shift angle =30º.

As well known, it is difficult to identify at glance the de-energizing triggering, so to analyze the experimental waveform it is necessary to rely on its rms value. So when this signal undergoes its average value, it can be considered the de-energization time and from there the shift angle is calculated. Again, it was found that the signal dynamics went from ferroresonance fundamental mode to chaotic mode. This, as it was previously contemplated, may be due to the influence of the nonlinearity of the source.

4.4.2 Effect of transformer magnetization over ferroresonance behavior

Magnetization is defined as the state in which a transformer has an amount of residual flux stored in its windings. The interest on the magnetization emerged from endless list of parameter that may affect the ferroresonance. There were some traces that magnetization could affect the initial set up in a ferroresonance case. Previous studies have demonstrate there is an impact over the inrush current [46] and how the experimental technique FRA (Frequency Response Analysis) could help to detect whether a transformer has a significant value of residual flux or not.

The concept of magnetization contains an important internal aspect of complexity. Evidence exists that residual flux in transformer windings can remain stored per days or even months [47]. It is still difficult to know whether a transformer is or not in a magnetization state after its disconnection. This is probably the main reason behind the absent of the residual fluxes during the modeling of real events, since knowing the exact amount of residual flux would be nearly impossible. Despite this, the test was conducted to check whether there was evidence to prove its influence on ferroresonance. In this sense, a strategy to magnetize and to de-magnetize the transformer was raised.

4.4.2.1 Magnetization process

The magnetization process is a complicated procedure, specially because the sine waves of voltage and flow vary with time. Therefore, it is possible to obtain very different amounts of residual flux and still considered magnetized. To avoid this randomness, the shift angle of the switch is controlled when switching off, so voltage and flux angle will be controlled and remain invariant from one test to another as shown in Figure 4.87.

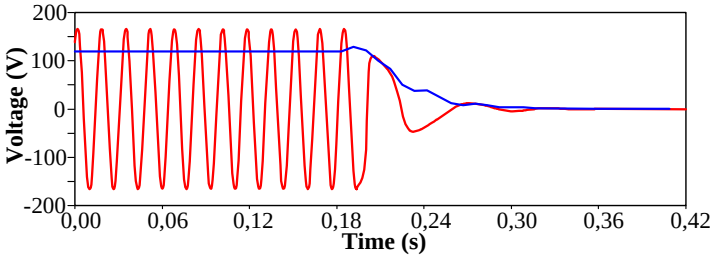

Figure 4.87. Switching shift angle control.

To facilitate the figure reading, a blue line representing the RMS value of the signal has been added. The RMS remains constant during normal operation, its change will precise the time when the switch was open.

4.4.2.2 De-magnetization process

The de-magnetization is a process that is taking great importance in recent times. So much that it is recommended by some manufacturers to run this process before performing any routine tests on a transformer. It is believed that it directs affects any measurement taken, specially when calculating the magnetizing branch elements. In this case, the method proposed by Francisco de León in [47] is used. The method consists on exciting the transformer (preferably the high voltage side) with a DC signal for a period of time t_a, forcing the current to gradually reach its nominal value at a time t_b; this current will also induce a temporary flux. Then suddenly the polarity of the voltage changes until a t_d time. Finally, the polarity is changed again until a time t_e. Thus, the time taken by the current to reach its nominal value going from a positive to a negative polarity is considered the time rate ΔT. If this time rate is measured and divided by two, it is possible to estimate the instant at which the flux passes through its zero value and therefore considered the transformer demagnetized. Figure 4.88 introduces the scheme for the procedure.

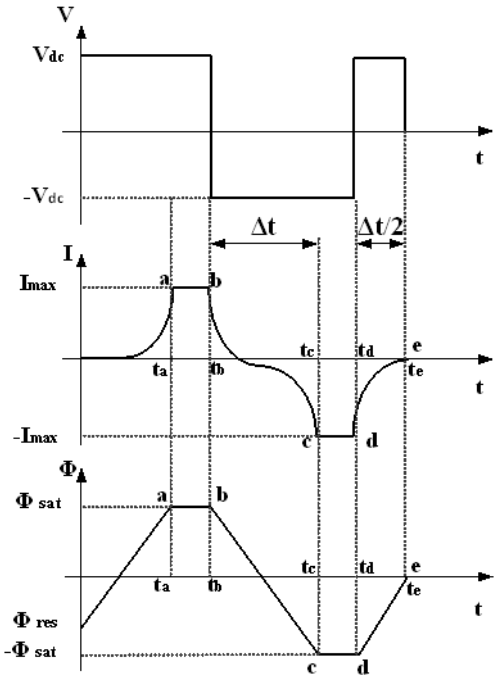

Figure 4.88. De-magnetization: Theoretical process.

The following figures show the variations suffered by the transformer for the magnetized and not magnetized stage. The parameter impedance refers to the (global) internal impedance of the transformer referred to the high voltage side.

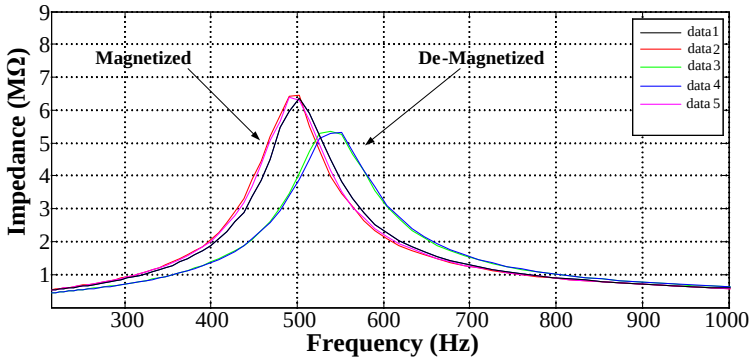

Figure 4.89. De-magnetization: Impedance frequency response.

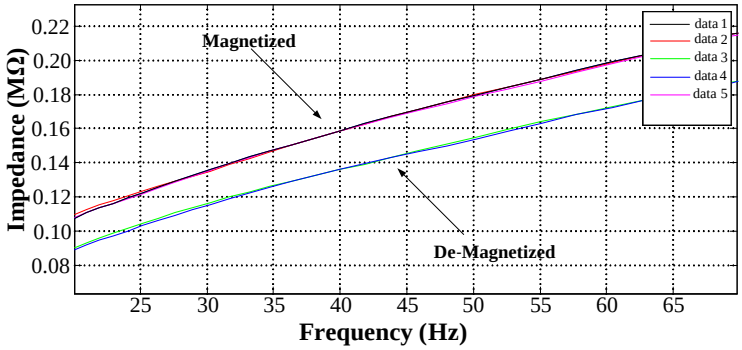

Figure 4.90. De-magnetization: Impedance frequency response in ferroresonance study zone.

The check boxes with the legends data 1 to 5 show the number of samples taken for each case, being three samples for magnetization and two samples for de-magnetization. Figure 4.89 shows the total spectrum analyzed, while Figure 4.90 shows the portion of the frequency spectrum concerning the phenomenon of ferroresonance. The Frequency Response Analysis technique used to obtain Figures 4.89 and 4.90 is essentially a comparative method. It consists on measuring the impedance of the transformer windings over a wide range of frequencies and comparing the results of these measurements with a reference set. This comparison is usually done by graphical inspection and concentrates on identifying changes in overall shape of the response. For the case of Figure 4.89 the general idea was to set a tendency curve when the transformer is magnetized, thus, by using this curve as reference it was possible to distinguish any change in the Frequency Response Analysis when the transformer has been demagnetized. The impact of magnetization and demagnetization over the ferroresonance phenomenon is shown in the Figures below.

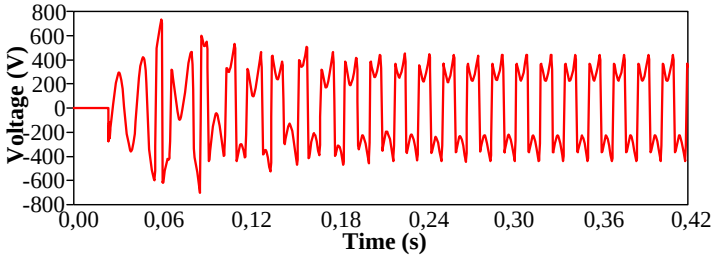

Figure 4.91. Magnetization test: Waveform analysis.

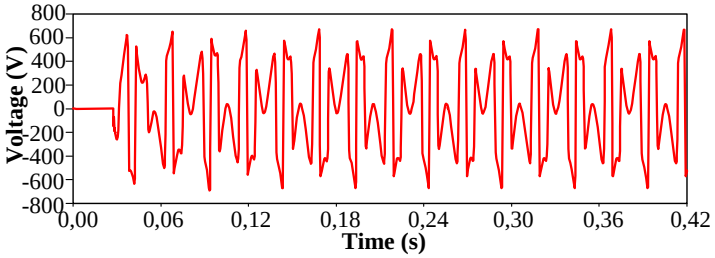

Figure 4.92. De-magnetization test: Waveform analysis.

Figures 4.91 and 4.92 are obtained using the scheme presented in Figure 4.80a, with a capacitance value (C_g) of 20 μF and an angle of 280°, the transformers are the same used for the switch angle study in Section III. This test has only experimental measurement and no simulations, because even when there is evidence of magnetization using the standard test FRA, there is no way to know the actual value of the residual flux. Again, note that this type of study should be performed using a statistical strategy, i.e. obtaining many samples as possible, since simulations can turn into a very complicated process because of the uncertainty of flux parameters. By this experiment has been possible to observe that magnetization has an impact on ferroresonance behavior and its presence can change the mode of the signal even though the rest of the parameter remained constant.

4.4.3 Ferroresonance Analysis on Power Transformers Interconnected to Self-Excited Induction Generators

This research intends to prove by experimental work how ferroresonance can occur between generating systems, based on self-excited induction generator (SEIG), and power transformers. Up to four different paths have been tested under different commutation maneuvers. Ferroresonance appearance can unfold into a dangerous state for machinery and personnel. Several overvoltages can be present in the system by a simple delay in one of the poles responsible for grid connection/disconnection.

In the last few decades extensive changes have occur affecting modern electrical power systems. The massive increase in the price of fossil fuels, the attention to environmental issues and the general consciousness of finite and limited sources of energy on earth, has reveal the importance of distributed generation and the need for the development of renewal and alternative energy solutions [48]. Small-scale hydro-generation and wind-powered systems represent the most firmly established alternative solutions. As a general rule, the sitting of generators using renewable energy sources is determined by the location of the energy resource itself and, occasionally, this location unfolds into remote, unattended, and isolated areas.

The versatility of the squirrel cage induction generator offers advantages for hydro and wind power plants, because of its easy operation as either fixed speed generator or performing as variable speed induction generator [49]. Squirrel cage generators can also work connected to the electrical network or as standing alone machine (self-excited mode). In this last condition, it uses a 3 or 4 wires connection system [50]. However, a need of voltage and frequency controller is mandatory when the system runs isolated from the network to ensure a satisfactory operation [51]. For remote areas, it is often common to have squirrel cage induction machines, performing as a self-excited induction generator [52]. The self-excitation phenomenon occurs when a capacitor bank

is connected across the stator terminals of an induction machine which is driven by an external prime mover [53]. An excitation voltage will be induced at the stator windings. This electromotive force will continue to rise until the steady state condition is attained, influenced by the magnetic saturation of the machine. At this operating point**,** the voltage and current will be stabilized at a given peak value and frequency.

Moreover, switching operations are common in micro power plants. Commutations are often required for interconnection or disconnection from the grid. In self-excited induction generators, commutations are also used to enable the capacitor bank for the excitation process and occasionally to add extra capacitance in order to maintain and control the voltage in the common coupling point [54], [55]. As well known, switching or other type of commutation can lead into a transient state. Until now, several types of transients have been reported in micro energy conversion systems [56]-[58] such as: overvoltage, flicker, distorted ac waveform, sub-synchronous resonance, ferroresonance or power fluctuation.

The test system for this study, tries not only to illustrate the general paths of ferroresonance phenomenon appearance for renewable energy systems [59], but also to test the closeness of a catastrophic situation by a switching missoperation. The topology of the test system represents a micro-hydro or wind system configuration having a self-excited induction generator, a capacitor bank, a three-phase switch and a step-up transformer [60], [61]. Figure 4.93 shows the ferroresonant test path.

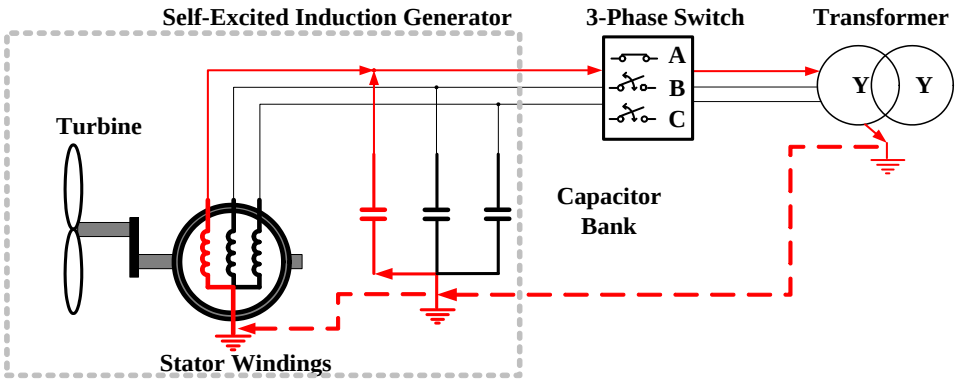

Figure 4.93. Ferroresonance circuit including an induction machine.

4.4.3.1 System description

The great majority of energy sources in the world depend on rotating generators, mainly due to primary energies coming from hydro turbine, wind turbine or internal combustion engines. The system under study is composed by a 4 kW induction machine, 220/380 V, 50 Hz, a 75 µF/650 V capacitor bank, three independent switches, a 3.5 kVA , 220/380 V, 50 Hz, 3-legged, dry-type three-phase transformer and 10 µF capacitors representing the cable capacitance component. The parameters obtained from the test routine performed to the three-legged transformer and to the inductor generator are provided below:

Laboratory routine test induction generator:

Table 4.31: Induction machine parameters

P (kW)	4	J (Kg/m^2)	0.012
V (V)	220/380	Rs (Ω)	1.39
I (A)	15/8.7	Rr (Ω)	1.39
F (Hz)	50	Lls (mH)	5.84
Pole number	4	Llr (mH)	5.84

Laboratory routine test for the three-legged transformer according to [62]:

Table 4.32: Transformer parameters

Load test (85 °C)	
PCC (W)	196.76
I2R (W)	103.92
Additional losses (W)	92.84
UCC (V)	96.09
ZCC (%)	25.27
XCC (%)	24.40
RCC (%)	6.55
Winding resistance (85 °C)	
Primary winding (Ω)	1.48
Secondary winding (Ω)	1.86
No load test (20 °C)	
P0 (W)	24.08
I0 (%)	1.98

Excitation tests:

Table 4.33: Transformer and Induction machine magnetizing curve

Transformer magnetizing curve			**Induction machine magnetizing curve**	
V%	**Loss Kw**	**I %**	**I (A)**	**L (mH)**
40.110	0.004	0.402	0.000	208.000
60.165	0.005	0.621	0.500	250.264
80.221	0.011	1.111	1.000	262.373
100.276	0.023	1.989	1.500	255.792
102.099	0.025	2.358	2.000	239.296
104.834	0.028	2.647	2.500	219.277
107.113	0.030	2.852	3.000	200.059
109.848	0.032	3.217	3.500	184.205
110.760	0.034	3.327	4.000	172.832
115.318	0.39	3.912	4.500	165.920

The studied scenario consists on a case when a self-excited induction generator is connected or disconnected to a step-up transformer. In this manner, a general example can be diagrammed, see Figure 4.93, regardless the origin of the primary mover. The scope of the following tests is pointing out the possibilities of obtaining ferroresonance in systems whose energy source has a non-linear dependence and a limited amount of power. Four different case studies have been documented here to illustrate how prone a hydro or micro-wind energy system is to be lead into ferroresonance. For all cases, ferroresonance phenomenon will be initiated either by energizing or de-energizing the step-up transformer. It is important also to keep in mind that the voltage source has a limited power and not all the cases unfold into ferroresonance condition:

- Case 1: Two tests are presented for Δ-Δ connection: (1) De-energization of the transformer from steady state by opening Switch A, being the capacitor bank value of 75 μF, with no cable capacitance considered. (2) Energization of the

transformer initially deactivated by closing Switches B and C, being the capacitor bank 75 μF, with no cable capacitance considered.

- Case 2: One test is presented on a Y-Y connection: (1) Energization of the transformer, initially deactivated, by closing Switches B and C, being the capacitance bank 75 μF, with no cable capacitance considered.

- Case 3: One test is presented on a Yn-Yn connection: (1) Energization of the transformer, initially deactivated, by closing Switches B and C, being the capacitance bank 75 μF with no cable capacitance considered.

- Case 4: Two tests are presented on a Yn-Yn connection: (1) De-energization of the transformer from steady state by opening Switch A, being the capacitance bank 75 μF, and a cable capacitance value of 10 μF; (2) Energization of the transformer, initially deactivated, by closing Switches B and C, being the capacitance bank 75 μF, and a cable capacitance value of 10 μF.

Besides the cases presented in this study, a wide range of experiments that can unfold into a ferroresonance state were carried out. All performed tests are summarized in Table 4.34.

Table 4.34: System configuration tested

Case	System Connection	Maneuver	Open Phase	Close Phase	Signal obtained
1	Δ-Δ	De-ener.	A	B-C	Ferroresonance
1	Δ-Δ	Energization	A	B-C	Ferroresonance
2	Y-Y	De-ener.	A	B-C	Damped sinusoidal
2	Y-Y	Energization	A	B-C	Damped sinusoidal
3	Yn-Yn	De-ener.	A	B-C	Damped sinusoidal
3	Yn-Yn	De-ener.	B-C	A	Damped sinusoidal
3	Yn-Yn	Energization	A	B-C	Overvoltage
3	Yn-Yn	Energization	B-C	A	Ferroresonance
4	Yn-Yn + Cable	De-ener.	A	B-C	Overvoltage
4	Yn-Yn + Cable	De-ener.	B-C	A	Ferroresonance
4	Yn-Yn + Cable	Energization	A	B-C	Ferroresonance
4	Yn-Yn + Cable	Energization	B-C	A	Overvoltage

4.4.3.2 Ferroresonance testing and analysis

Up to 4 different sets of system configuration have been performed in order to test all possible paths for ferroresonance, including: energization and de-energization routines, and capacitance effect of cables for wye and delta connections. Grounded and ungrounded connections have been tested for wye configuration. It is important to remark that only delta-delta or wye-wye configurations are a valid connection between the induction machine and the step-up transformer. The voltage parity to operate the system can only be obtained in such a way. Another important aspect in this study is the location of the capacitance involved in the ferroresonant event. As seen in Figure 4.93, the capacitor bank is placed prior to the commutation switch that separates the IG and the step-up transformer. This system set up is different from the typical ferroresonance cases, where the capacitors involved in the ignition of the phenomenon are placed closer to the transformer and after the commutation switch. Figure 4.94 presents the induction generator self-excitation process.

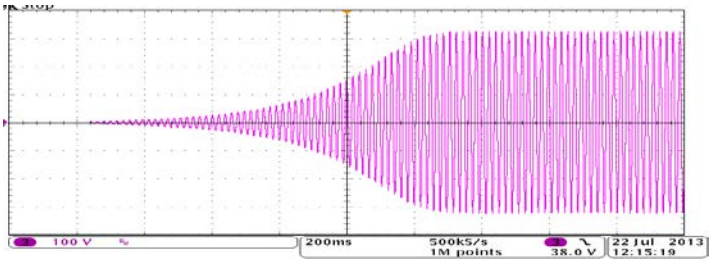

Figure 4.94. Voltage growth during self-excitation of the induction generator.

As shown in the Figure 4.94, the self-excitation of the induction generator is quickly acquired; the voltage amplitude and frequency are stable and corresponds to the desired levels. Figure 4.95 shows the steady state generated voltage V_{IG} and the excitation current of the transformer I_0.

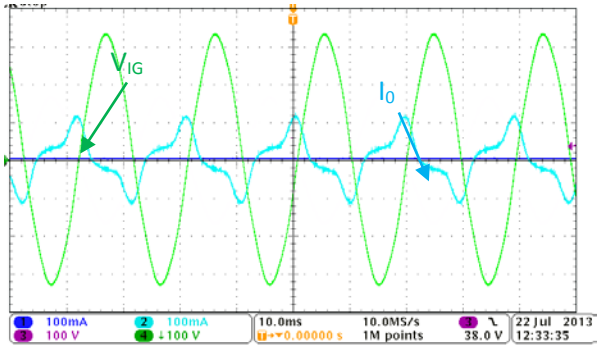

Figure 4.95. Steady state waveforms.

The experimental system has been confirmed to fulfill the steady state expected condition. Experimental cases are discussed in the upcoming sections presenting different conditions that can lead into ferroresonant states.

4.4.3.3 Case study 1

The self-excitation of an induction machine is a process requiring an interaction between the nonlinearity of the machine and a physical capacitor bank. In this case, a delta connection was used for the stator winding and the capacitor bank to produce that interaction. In most cases, ferroresonance phenomenon arises after a fussing or commutation maneuver. In those conditions, two case scenarios can occur: miscoordination on the switch while transformer is being energizated or while the transformer is disconnected, being this second maneuver often referred as de-energization. Both cases will be reviewed in this experiment. Figure 4.96 shows the voltage signal in Phase A after the transformer has been de-energizated while Phases *B* and *C* remain closed. A voltage is being induced in the open Phase A as seen in Figure 4.96a, since the three-phase core of the power transformer provide direct magnetic coupling between phases. Terminal voltage waveform presented in Figure 4.96b is close to that presented as fundamental ferroresonance in [63]. The peak value of the voltage is not bigger that 0.3 p.u. and could be classified as harmless for the equipment. But, in general, applications such distributed generation could be dangerous for maintenance personnel.

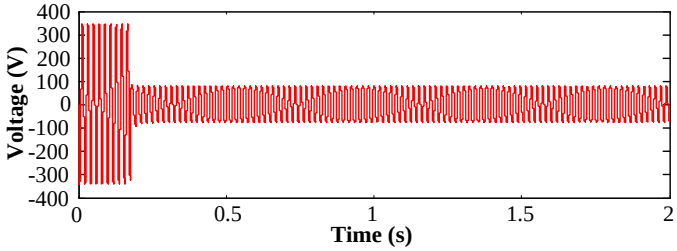

a) Signal dynamic

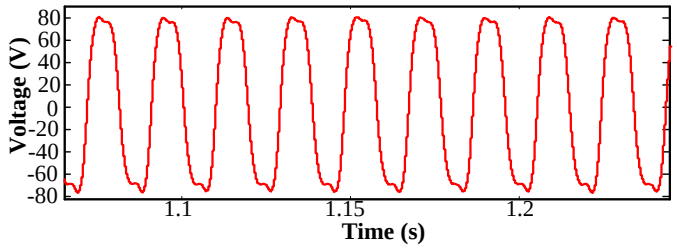

b) Steady state waveform

Figure 4.96. Case 1: De-energization, analysis of voltage Phase A.

The other condition leading into a potential ferroresonant state is that in which a transformer is being energizated and one or more switches remained open. In the next tested case, Phases *B* and *C* get closed while Phase *A* stays open. Figure 4.97 presents the analysis on the voltage signal of Phase *A*.

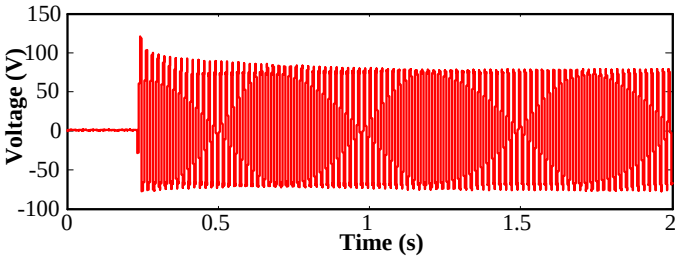

a) Signal dynamic

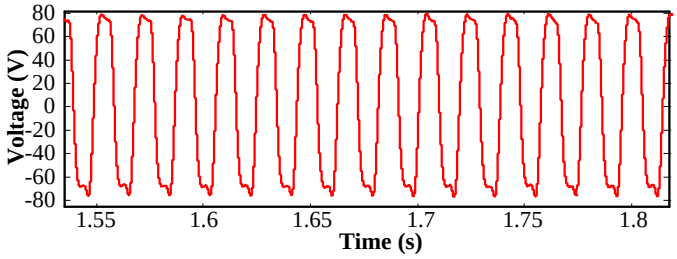

b) Steady state waveform

Figure 4.97. Case 1: Energization, analysis of voltage Phase A.

The maneuver performed can be seen on Figure 4.97a, while the induced voltage waveform on the open phase is shown in Figure 4.97b. The waveform is similar to that presented in the de-energization case, having the first cycles of the signal affected by the inrush current of the transformer. Again, the peak values are smaller than those under normal operation, but its distortion and waveform suggest ferroresonance. Depending on the severity of the ferroresonance phenomenon the stability of the induction machine could be affected, and in the worst case scenario the self excited phenomenon could be loose, leading the machine to stop the generation. The ferroresonance waveform obtained in Figures 4.96 and 4.97 are quite close to those ones presented in [64] for a similar distribution generation system under ferroresonance condition.

4.4.3.4 Case Study 2

During the second experimental test, primary windings of the transformer, induction generator stator windings and capacitor bank connections were changed to an ungrounded wye configuration. The case presented focuses in the energization of the step-up transformer. This maneuver consists on energizing one or two of the switch poles while the other remains open. In this experimental case, Phases *B* and *C* were closed while Phase *A* continued open. Figure 4.98 shows the analysis for Phase *A*.

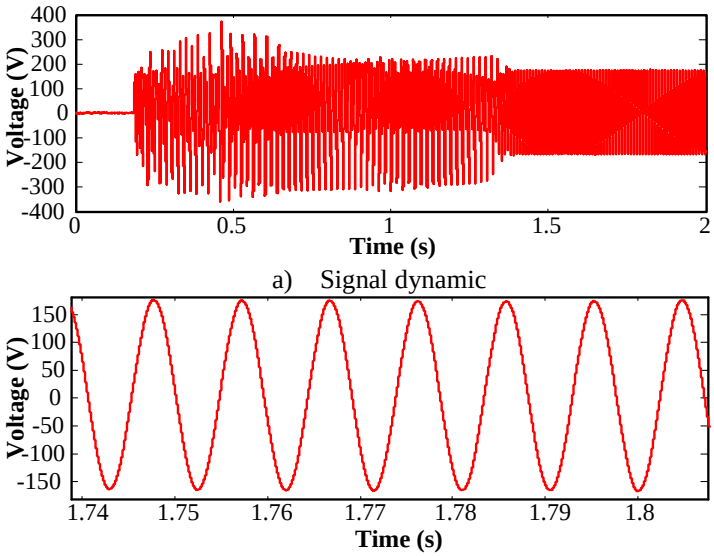

Figure 4.98. Case 2: Energization, analysis of voltage Phase A.

Figure 4.98a presents a large transient happening between the energization and the final sinusoidal state. Figure 4.98b shows the final steady state reached by the system; the sustained oscillations presented cannot be directly related to ferroresonance due to the sinusoidal characteristic of the waveform. But, in any case, the existence of a voltage in a supposedly turned off transformer could result dangerous for the equipment and personnel surrounding the network. Besides, mechanical vibration, audible noise and overheating can be presented aging all the cooper-made components in the induction machine and the transformer.

4.4.3.5 Case Study 3

Most of the distribution generators described in literature uses the grounded wye connection to get the auto-excitation. That said, it is important to verify how prone that connection is from an actual failure condition involving ferroresonance. The first scenario analyzed consists on a multi-branches failure while trying to de-energize the step-up transformer. Phases *B* and *C* get open while Phase *A* remains closed. Figure 4.99 shows the voltage on Phase *B*. As seen in Figure 4.99b, ferroresonance mode is not reached. Even thou, it can be extracted from Figure 4.99a that overvoltages do occur during the initial cycles of the transient. Usually these types of sustained oscillations are accompanied with audible noise and vibration. The last condition arises by having Phases *B* and *C* closed, and opening *A* while the energization process of the transformer is performed, as seen in Figure 4.100a. Ferroresonance can be obtained in this configuration, as seen in Figure 4.100b. Since ferroresonance phenomenon is highly dependent on initial conditions, it is possible to assume that the previous configurations studied having sinusoidal state could as well turn into ferroresonance state with proper initial conditions. At the same time, it has been proved that capacitor banks used for

self-excited process of a generator can involved in the occurrence of ferroresonance oscillations. A case study presented in [65] is similar to the test system presented in this work, concluding that even small overvoltages can unfold harmful results for physical equipment.

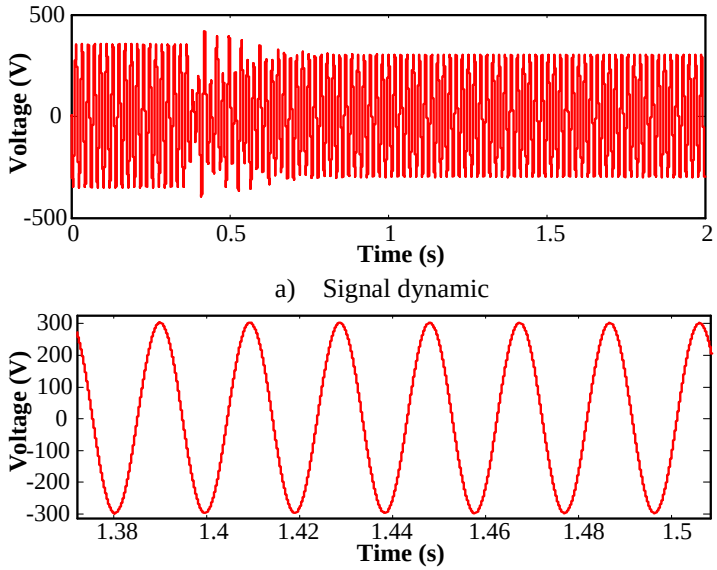

a) Signal dynamic

b) Steady state waveform

Figure 4.99. Case 3: De-energization, analysis of voltage Phase B.

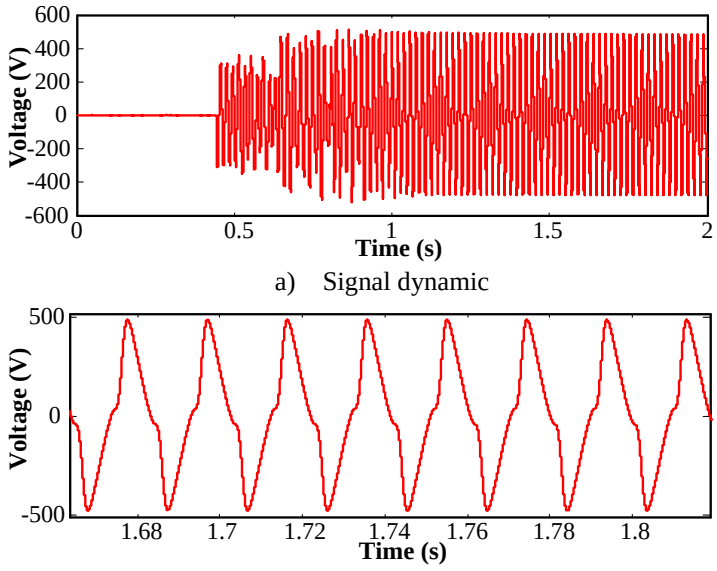

a) Signal dynamic

b) Steady state waveform

Figure 4.100. Case 3: Energization, analysis of voltage Phase A.

4.4.3.6 Case study 4

The last experiment considers most of the parameters included in a real distributed generation system, where the section of cable connecting the main IG with the first transformer substation normally is an underground cable with high capacitive effect. For that purpose, the capacitance provided by the cables between the IG and the transformer is included as a straight capacitance between the ground and each individual cable. Figure 4.101 shows the test system.

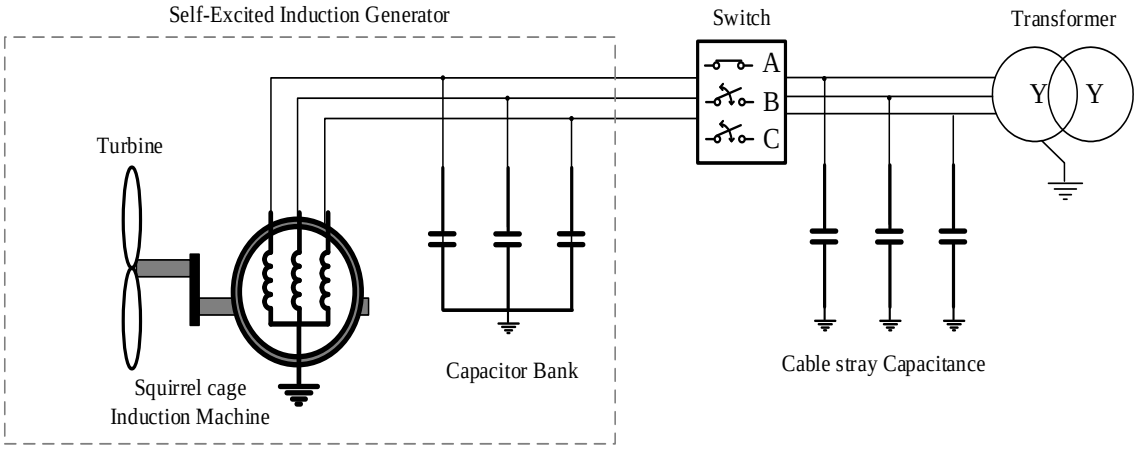

Figure 4.101. Test system.

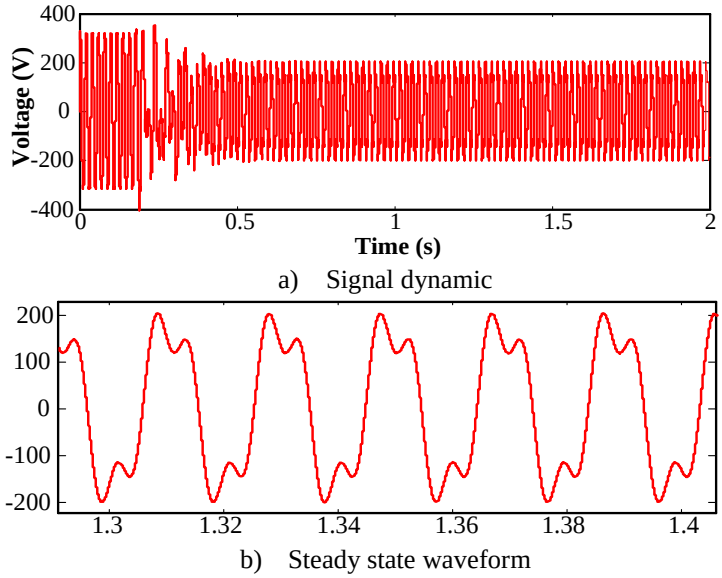

Figure 4.102. Case 4: De-energization, analysis of voltage phase B.

The first test is carried out by implementing a de-energization maneuver opening two of the three Phases *B* and *C*, while Phase *A* continues closed. Figure 4.102a shows the maneuver for Phase *B*. A highly distorted waveform is presented in Figure 4.102b. This type of oscilation corresponds to ferroresonance fundamental mode. It is important to note the big influence of the third harmonic component coming from the unbalance condition of the system. Commonly this type of distortion is followed by physical vibration of the transformer, audible noise and overheating.

A fault in the energization maneuver of a transformer could as well be the origin of ferroresonant oscillations. For that, the system has been tested by introducing a miscommutation fault when the transformer is being energized. Figure 4.103a presents the global behavior of the maneuver performed to the Phase *B* while the energization is only generated by closing Phase *A*. Note that a high distorted voltage in Figure 4.103b is induced to an open phase; this condition is potentially dangerous and unwanted due to the heat produced by the oscillation that will also affect the isolation material of the transformer. The protection equipment, especially arresters, would not work properly and if the fault condition is sustained long enough, permanent damaged will occur.

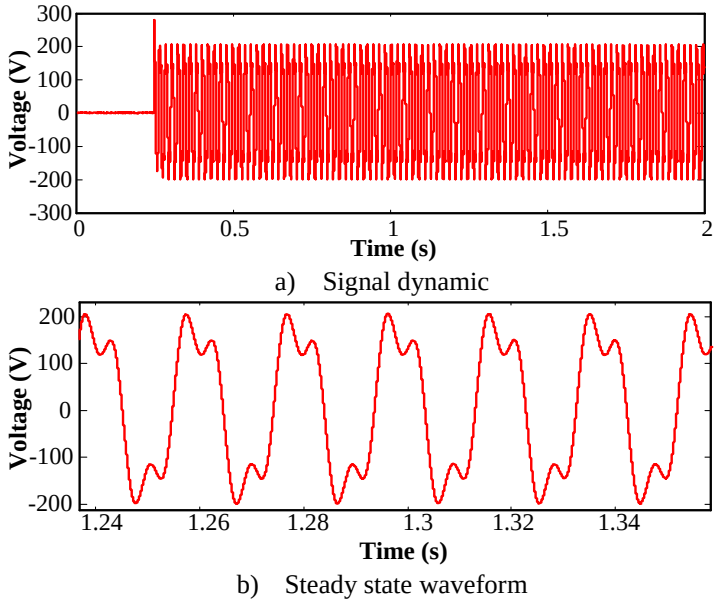

a) Signal dynamic

b) Steady state waveform

Figure 4.103. Case 1: Energization, analysis of voltage phase B.

It is worth to remark when ferroresonance oscillation is obtained in a generation system, the failure condition would affect the entire network resulting in dangerous vibrations in the induction machine, overheating in protection elements and cables, and potentially dangerous spots for personnel. Efforts should be made in order to deeply studying the impact of the phenomenon in this new area of action; for this purpose a simulation model for an isolated generator have been created [66]. Although, deeper parametric analysis must be performed to fully characterize all the electrical and mechanical effects that ferroresonance can cause to an isolated generation network.

Characterization of the signal has been carried out resulting in ferroresonance sub-harmonic and fundamental modes. The fundamental mode is the most frequent case in this study, presumably due to the static nature of the capacitive values. Parametric analysis could reveal more ferroresonance modes for this type of system. Identification of the configurations prone to ferroresonance was performed. For the cases presented here, delta-delta connection seems to be the less affected having damped signal at low peak-to-peak voltages even when ferroresonance stage is obtained; the absence of a physical neutral connection makes difficult to sustain high oscillations. Regarding the most adverse situation obtained in this work, the grounded wye connection accompanied with high capacitive valued wiring (underground cables case) can develop significantly high overvoltages due to the closed loop created by the ground connection that becomes a pure series ferroresonant circuit. It is troubling to identify that the ferroresonant stage is not away for the renewable generation systems and the fact that miscoordination when the system is connecting or being disconnected from the network could unfold into a destructive event as ferroresonance. Several cases involving ferroresonance have been studied in the literature, but none of them have been directly pointed into the interaction of self-excited process in generators. Therefore in this sense, the contribution of this work is to facilitate the possible paths in which the capacitor of the self-exciting process can interact with the nearest transformer in the system in a manner that obtaining ferroresonance will be inevitable. At the same time, precaution should be taking into consideration due to the high vibration and heating presented along with the overvoltage oscillation. Several insulation damages can overcome.

4.4.4 Implementation of a Self-Excited Induction Generator Model Using TACS

The ever-growing improvements on distributed generation systems make possible the developing of simulation models an essential necessity for the power system engineers. The computational representation of steady and transient state is the central key of any type of studies. Induction generator is a common component in micro-hydro and wind power systems. Stand-alone units (self-excited mode) are nowadays the perfect solution for systems in remote areas. This section presents the implementation of a self-excited induction generator (SEIG) dynamic model for the EMTP-ATP platform. The modeling is based on Park's transformation and it is implemented through TACS components. This will allow fast simulations, easy interconnection with other elements and easily implementation of control systems.

Induction generators are preferred for electricity generation in isolates areas [50], because they do not need an external power supply to produce the excitation magnetic field. In addition, its versatility allows the generator to work either as fixed speed generator or performing as variable speed induction generator [55]. For small power plants, the induction generator can be connected to the grid or equally serve standing alone (self-excited mode) using a 3 or 4 wires system [51]. However, a need of voltage and frequency controller is mandatory when the system runs isolated from the grid to ensure a satisfactory operation [52].

The electromagnetic transient program (EMTP) is one of the most used software for the power systems studies [67], [68]. The increasing interest in distributed generation systems, make its design, analysis and simulation vital for the modern power system engineers [70]. This Section tries to illustrate the implementation of a self-excited generator into the EMTP environment. The modeling is performed using the Park's transformation for the analytical representation of the SEIG and it is implemented in ATPDraw through the transient analysis of control system modules (TACS) [69]. Every stage of the modeling process would be described, explaining both mathematical implementation as wells as TACS implementation.

4.4.4.1 Transient Analysis of Control System Modules (TACS)

The Transient Analysis of Control Systems (TACS) was introduced to the EMTP program [67] by L. Dube in 1977. The first release of TACS was conceived as a flexible general representation of control systems in EMTP models. Nowadays, due to the improvements realized, it is possible to have an unlimited number of applications that can be created in a friendly to user environment similar to that in SIMULINK. TACS blocks can easily interconnect system elements. Control elements can be in the form of: Transfer functions, algebraic functions, logical expressions and special devices that can be connected in an arbitrary manner to model a given control system [68]. TACS has become important for the study of high voltage direct current transmission systems, static reactive compensators, generators, and more recently for the creation of new models [69]. The solution method used by TACS is also based on the trapezoidal rule [70]. The Figure 4.104 shows the internal order solution given by ATP.

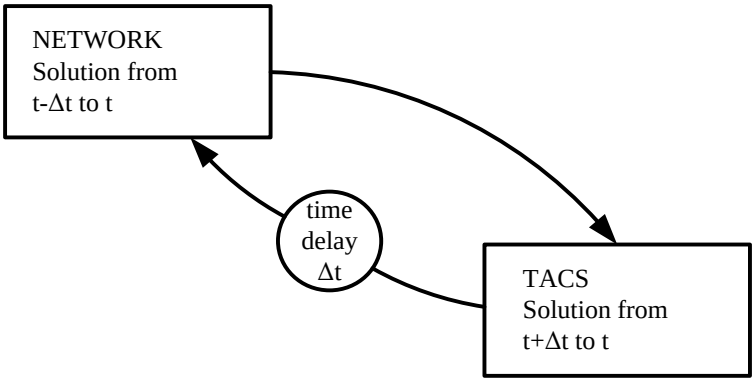

Figure 4.104. Interface between TACS and the electrical network.

It is of great importance to understand the priority given by ATP to the solution of a system that combines electrical network and TACS. First, as shown in Figure 4.104 the state for the all electrical parameter will be calculated and then the TACS solution will be found. In order to improve the efficiency in founding systems solution, ATPDraw has implemented a useful feature for the solutions of TACS systems: The option 'order' and it is available in every TACS command box. The order option is a numeric label that set the sequence in which the block will be arrange in the FORTRAN output file.

4.4.4.2 Self-Excited Induction Generator

The operation of an induction machine as a self-excited generator is a phenomenon well known for most power system engineers. It was first reviewed by Basset and Potter in 1935 [53]. The self-excitation phenomenon occurs when an induction machine which is driven by an external prime mover is connected through its stator terminals to a capacitor bank whose capacitance is equal to, or greater than, the magnetizing reactance requirements of the machine [60]. An excitation voltage will be then induced at the stator windings. This electromotive force will continue to rise until the steady state condition is achieved, influenced by the magnetic saturation of the machine. At this point, the voltage and current will be stabilized at a given peak value and frequency. This is considered the operation point of the SEIG.

Figure 4.105 shows the excitation processes from a graphical point of view. The growing evolution of the voltage and current is depicted in the Figure. It is easy to understand how the voltage originally at some low initial value (V_0) due to residual flux in the machine, starts increasing its magnitude with time until a final operation point is reached in the saturation zone, where the magnetization curve cross the capacitive reactance (X_c) of the capacitor bank. It is worth to remark that for self-excitation to occur, a specific capacitance value will set a corresponding specific speed [71].

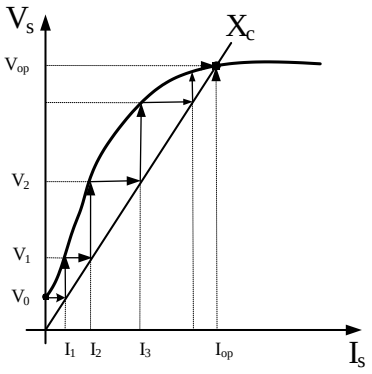

Figure 4.105. Voltage grow of self-excitation process.

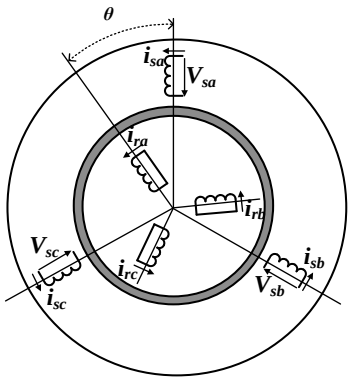

Figure 4.106. Ideal induction machine.

4.4.4.3 Dynamic model of a self-excited induction generator

In order to assist the analysis of a self-excited induction generator, it is essential to derive a mathematical model which allows the calculation of its different parameters, including, both steady state and transient response of the machine. The dynamic model of a three-phase induction machine presented in [72] is suitable for the study of the self-excitation phenomenon. The main considerations in the calculations of the model, as seen in Figure 4.106, are: the rotor is squirrel cage type, it has a constant gap, the machine is constructed symmetrically, it has a sinusoidal distribution of magnetic field in the gap, negligible iron losses, and all variables are referred to the stator. Equations (4.8) to (4.11) define a general mathematical model of an induction machine.

$$v = Ri + \omega \frac{dM(\theta)}{d\theta} i + M(\theta) \frac{di}{dx} \tag{4.8}$$

$$T_e = [i_s]^t \left\{ \frac{\partial M_{sr}(\theta)}{\partial \theta} \right\} i_r \tag{4.9}$$

$$T_e - T_L = J \frac{d\omega}{dt} + B\omega \tag{4.10}$$

$$\omega = \frac{d\theta}{dx} \tag{4.11}$$

Despite the simplifications, the model is still complex and difficult to be solved. To facilitate the calculation a matrix transformation if often performed. This transformation converts the three phase variables (a, b, c) of the stator and rotor to an equivalent system of two axes (d,q). In addition, the new reference frame is rotating at arbitrary speed; this assumption allows removing the dependency of inductances to position *M(θ)*.

4.4.4.4 Reference Frame Theory

A reference frame system is a set of conventions using an external observer to estimate the position of physical quantities over time and space. Perceiving whether an object is moving or not, depends only on the reference system taken. In the late 1920's, R. H. Park [73] develop a technique to change from one reference frame to another. This new approach referred as Park's transformation started a revolution in electric machine analysis. By using Park's transformation it was possible to eliminate all time-varying inductances from the voltage equation of the electrical machine. This was obtained by referring the stator and the rotor variables to a frame reference that may rotate at any angular velocity or remain stationary. Figure 4.107 shows the reference frame calculation from where it is easy to calculate the relationship between the two reference frames. Equation (4.12) and (4.13) shows the mathematical representation of Figure 4.107.

$$\begin{bmatrix} v_d \\ v_q \\ v_0 \end{bmatrix} = K_s \begin{bmatrix} v_a \\ v_b \\ v_c \end{bmatrix} \Leftrightarrow V_{dq0} = K_s V_{abc} \tag{4.12}$$

$$K_s = \frac{2}{3} \begin{bmatrix} \cos\theta & \cos(\theta - \frac{2\pi}{3}) & \cos(\theta + \frac{2\pi}{3}) \\ \sin\theta & \sin(\theta - \frac{2\pi}{3}) & \sin(\theta + \frac{2\pi}{3}) \\ \frac{1}{2} & \frac{1}{2} & \frac{1}{2} \end{bmatrix} \tag{4.13}$$

In the equations, v_a, v_b and v_c represent any set of three-phase signals and the values v_d and v_q represent the values projected on the axes q and d. v_0 is referred to the homopolar or zero sequence component, K_s represents the Park's transformation matrix. Occasionally, Park's transformation is also known as *dq0* transform.

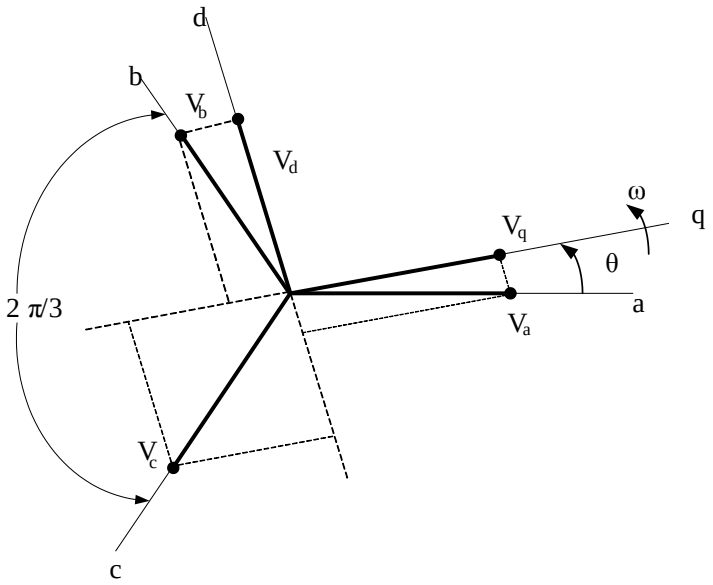

Figure 4.107. dq reference frame transformation.

4.4.4.5 TACS Implementation of the Induction Generator Model

Deriving the model equations in the *dq0* reference can be a simple task if there is certain familiarity with the mathematical representation of the induction machine. For the induction machine case, the flow chart of the model mathematical solution is presented in Figure 4.108.

4.4.4.5.1 Excitation voltage

The first block in the flow chart corresponds to the excitation voltages of the generator. The proper set of this parameter will define the self-excitation process start or not. In practice, the voltage on the capacitor will be a product of the prime mover of the machine. For the simulation case, it is possible to assign an initial condition to the capacitor. Equation (4.14) may be implemented and solved using TACS.

$$\begin{bmatrix} V_d \\ V_q \\ V_0 \end{bmatrix} = \frac{2}{3}\begin{bmatrix} \cos\theta & \cos(\theta-\frac{2\pi}{3}) & \cos(\theta+\frac{2\pi}{3}) \\ \sin\theta & \sin(\theta-\frac{2\pi}{3}) & \sin(\theta+\frac{2\pi}{3}) \\ \frac{1}{2} & \frac{1}{2} & \frac{1}{2} \end{bmatrix}\begin{bmatrix} V_a \\ V_b \\ V_c \end{bmatrix} \tag{4.14}$$

Figure 4.105 shows how the voltage is taken from the circuit and converted to *dq0* reference.

In equation (4.14), the conversion of the reference frame is presented; the angle θ is driven to 0 for stationary reference transformation. Figure 4.109 present an example of how to implement equation (4.14) using TACS components in ATPDraw; the element *coupling to circuit* in the TACS menu has been used to measure the voltage across the excitation capacitors and export it as numerical values to TACS. Those values can be exported by simply calling the node's name. For instance, each part of equation (4.14) can be directly written inside of the *general fortran statement* box, using i.e. the name NOD1_A for V_a

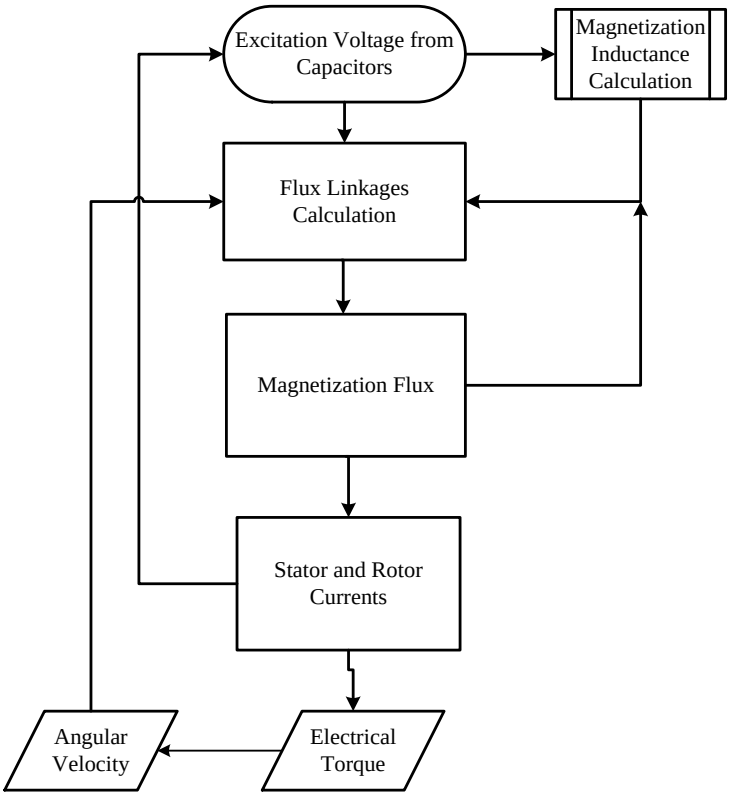

Figure 4.108. Model flow chart.

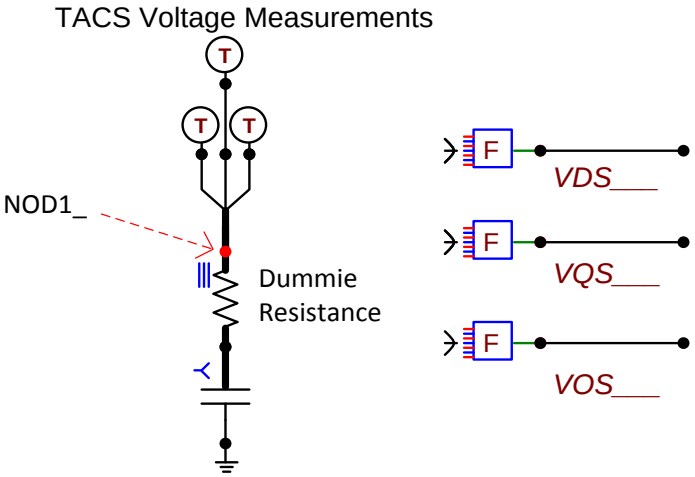

Figure 4.109. TACS implementation of excitation voltage.

4.4.4.5.2 Flux linkage

The flux linkage equations for the dq0 reference are presented as follows. Notice the subindex '*r*' stands for the rotor and the subindex '*s*' represents the stator components.

$$\psi_{qs} = \int (\omega_b (V_{qs} - r_s i_{qs} - \omega \frac{\psi_{ds}}{\omega_b})) \tag{4.15}$$

$$\psi_{ds} = \int (\omega_b (V_{ds} - r_s i_{ds} + \omega \frac{\psi_{qs}}{\omega_b})) \tag{4.16}$$

$$\psi'_{qr} = \int (\omega_b (V'_{qr} - r'_r i'_{qr} - (\omega - \omega_r) \frac{\psi'_{dr}}{\omega_b})) \tag{4.17}$$

$$\psi'_{dr} = \int (\omega_b (V'_{dr} - r'_r i'_{dr} + (\omega - \omega_r) \frac{\psi'_{qr}}{\omega_b})) \tag{18}$$

The implementation using TACS of the flux linkage equations it is easy to understand. The main part of the equation is written inside a *general fortran statement* element and the integral TACS block is added obtaining the Flux solution. It is important to remark that for the ATPDraw internal processor, all variable coming from TACS must have a six character name. If a variable is named with fewer characters, ATPDraw will complete the missing characters with blank spaces. In order to avoid compilation errors is advisable to use the six characters when naming variables, i.e. $\psi_{qs\_\_}$.

4.4.4.5.3 Non-linear inductance

The magnetizing inductance is probably the most important calculation for the case of a SEIG. The operation point and the ignition of the self-exciting process depend directly on this feature. In most cases, the magnetization characteristic is represented by a non-linear curve which relates the inductance as a function of the magnetization current. For the dq0 representation of the induction machine, having an inductance-current curve will imply calculating the current before evaluating the curve. That assumption leads the calculation of the inductance at the end of each iteration. This in a global perspective of the model means that the inductance value is delayed by one iteration.

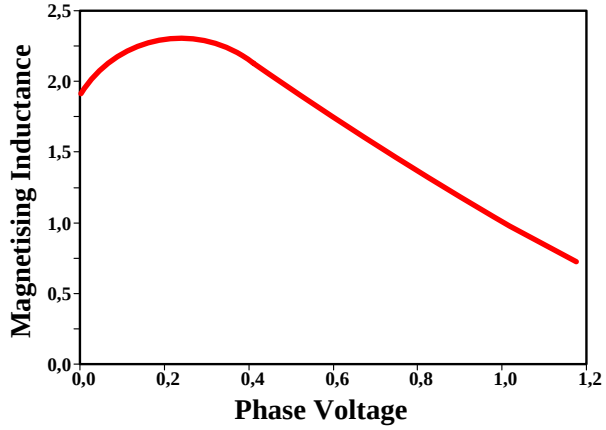

a) Magnetization Curve

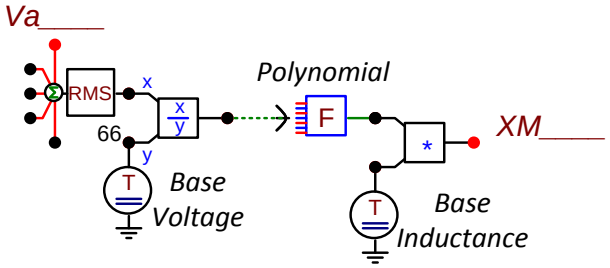

b) TACS implementation

Figure 4.110. Saturation curve and TACS implementation.

Figure 4.110b present the TACS implementation of magnetizing characteristic of the machine. Recent work has shown that an induction-voltage curve can be estimated [54]. This would avoid unnecessary assumptions in the calculation and more important could allow having an updated value of the inductance each iteration. Figure 110a show the form of the Inductance-voltage curve and equation (4.19) presents the mathematical polynomial representation.

$$X_m = -2.9V_a^4 + 10V_a^3 - 12V_a^2 + 4V_a + 1.9 \tag{4.19}$$

Where X_m is the nonlinear characteristic of the machine and V_a is the Phase voltage. The implementation has been performed using a per unit technique, since the model should be for general use and must fit in every set of parameters. A general polynomial characteristic has been set and only base values are asked. Normally, the value of the inductance in steady state is known or can be easily derived. For specific cases, the polynomial expression can be edited if the true characteristic of the machine is known.

4.4.4.5.4 Magnetization flux

The magnetization fluxes are the main components to define the final currents in the stator and rotor. Having previously calculated the magnetizing inductance, the derivation of the fluxes is just a simple task. Equations (4.20) and (4.21) present the calculation of the *dq* components of the flux.

$$\Psi_{Mq} = X_{Ml}\left(\frac{\Psi_{qs}}{X_{ls}} + \frac{\Psi_{qr}}{X_{lr}}\right) \qquad (4.20)$$

$$\Psi_{Md} = X_{Ml}\left(\frac{\Psi_{ds}}{X_{ls}} + \frac{\Psi_{dr}}{X_{lr}}\right) \qquad (4.21)$$

Where, X_{Ml} represents the inverse value of the sum of the reciprocal form of reactance's X_m, X_{ls} and X_{lr}. Since the equations do not imply any integration or derivative just simple algebraic operations, they can be easily implemented in TACS form using the *general fortran statement* element. The equations are edited inside the element dialogue box. In addition, it is important to mention that TACS elements do not need to have physical connection in the simulation prompt. To use the solution of one TACS into another element, writing the full name of the variable is sufficient, since TACS at the end are a method to declare and control variables.

4.4.4.5.5 Stator and rotor currents

The current of the stator and rotor are probably the main output of the model. The stator currents are the only parameters that will be converted from the TACS numerical state back to electrical ATPDraw circuit values. The equations for current calculation are presented as follows.

$$i_{qs} = \frac{\Psi_{qs} - \Psi_{Mq}}{X_{ls}} \qquad (4.22)$$

$$i_{ds} = \frac{\Psi_{ds} - \Psi_{Md}}{X_{ls}} \qquad (4.23)$$

$$i'_{qr} = \frac{\Psi'_{qr} - \Psi_{Mq}}{X'_{lr}} \qquad (4.24)$$

$$i'_{dr} = \frac{\Psi'_{dr} - \Psi_{Md}}{X'_{lr}} \qquad (4.25)$$

The equations representing the current are completely algebraic, so, its implementation in TACS is done using *general fortan statement* block for each equation. In order to transform the calculated currents of the stator back into an electric variable, the inverse Park's transformation should be used. In the circuit, a TACS controlled current source should be used to inject the calculated currents into a ATPDraw circuit.

$$\begin{bmatrix} i_{as} \\ i_{bs} \\ i_{cs} \end{bmatrix} = \begin{bmatrix} \cos\theta & \sin\theta & 1 \\ \cos\left(-\frac{2\pi}{3}\right) & \sin\left(-\frac{2\pi}{3}\right) & 1 \\ \cos\left(\frac{2\pi}{3}\right) & \sin\left(\frac{2\pi}{3}\right) & 1 \end{bmatrix} \begin{bmatrix} i_{qs} \\ i_{ds} \\ i_{0s} \end{bmatrix} \qquad (4.26)$$

The matrix presented in equation (4.26) will generate three equations, and for each equation a

general fortran statement block is assigned. Each block should be properly named, because in the electrical circuit the TACS controlled sources would only respond to a block equally labeled. Now, a better interpretation of the whole model can be depicted in Figure 4.111. Prior to the first iteration, an initial voltage must be given to capacitor bank. That voltage will be turned into a numeric value during the first iteration and the whole set of equations representing the machine would be evaluated, finally, a current will return through the TACS controlled sources charging the capacitor bank for the next iteration. Once this process is started, voltage and current will increase until the SEIG reach its operation point. At this point, any circuit connected to the SEIG will receive a constant value of voltage. The maximum current supplied will depend only of the SEIG power.

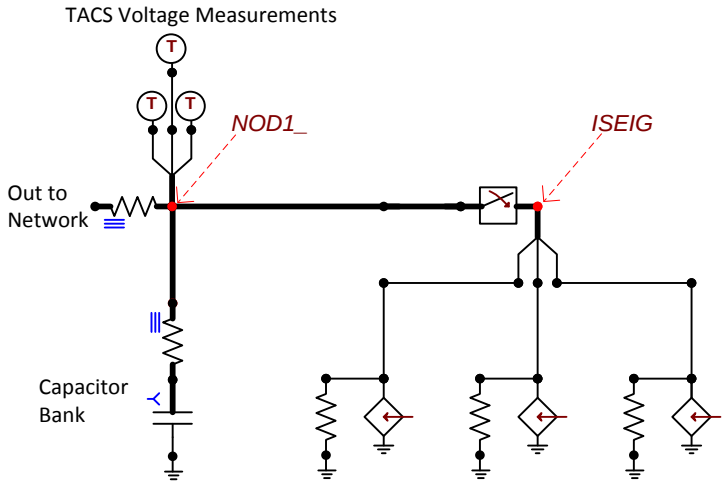

Figure 4.111. TACS current, integration to electrical network.

4.4.4.5.6 Electromechanical toque and angular velocity

Finally, the other two important outputs of the model are the electromechanical torque and the angular velocity of the machine. Neither of the two parameters must be returned to the electrical circuit, the analytical calculation of the TACS component is already a correct output form. Equation (4.27) presents the electromechanical torque, and equation (4.28) presents the angular velocity.

$$T_e = \frac{3P}{4\omega_b}(\psi_{ds} i_{qs} - \psi_{qs} i_{ds}) \qquad (4.27)$$

$$\frac{\omega_r}{\omega_b} = \int \left(\left(\frac{P}{2J\omega_b}\right)(T_e + T_L)\right) \qquad (4.28)$$

In the equations ω_b is the base angular speed, P and J represents the number of poles and the inertia of the machine respectively. The electromechanical torque is an important parameter in any generator. The implementation is easy because most par of the equation is formed by basic algebraic operations; no especial blocks are needed and would be implemented by simply writing the equation in a *general fortran statement*. For the angular velocity calculation there is a couple of details worth to extend. First the implementation is simple, just by adding an integral block to the *general fortran statement* containing the main equation, and finally adding a multiplication block to eliminate the parameter W_b. The important part comes by analyzing the torque. The first parameter T_e has been previously calculated and does not imply any difficulty, but the second parameter T_L refers directly to the torque present in the shaft of the generator. In other words, the torque generated by the prime mover of the machine. For the purpose of this Section, that value comes directly from a PI controller that keeps the main speed of the generator above the nominal value. For a more sophisticated analysis, the T_L value can be easily substituted for instance by a wind model or other type of control.

4.4.4.5.7 Zero sequence components

The zero-sequence components are an important part of the model, mostly when analyzing transient phenomenon. The expressions in *dq0* reference are collected as follows.

$$v_0 = (v_A + v_B + v_C)/3 \tag{4.29}$$

$$\Psi_0 = \int (v_0 - i_o R_s) \tag{4.30}$$

$$i_0 = \Psi_0 / X_{ls} \tag{4.31}$$

The modeling part is implemented in the same manner that has been performed previously Section. Using a *general fortran statement* block for the algebraic parts of the expressions, and for the flux calculation an integral TACS block is added.

4.4.4.5.8 Constant components

Any other parameter presented in the equations is considered constant and it will be modeled in TACS form using a *type 11* DC TACS source. This element generates a constant signal with a given value. The constant parameters involved in the model are listed as follows: Stator resistance (r_s), rotor resistance (r_r), stator impedance (X_{ls}), rotor impedance (X_{lr}), base frequency (f), base electrical angular velocity (ω_B), Inertia (J), and number of poles (P).

4.4.4.6 Experimental Validation of the Self-excitation Process

The self-excitation process has been validated through experimental measurements. A 4 kW induction machine, 220/380 V, 50 Hz, has been initiated as a self-excited machine using a 75 µF/650 V capacitor bank. Figure 4.112 shows the excitation process of the machine. From this Figure, it can be seen that the self-excitation process takes no more than two seconds. The variation between the experimental result and the simulation is not bigger than 200 ms. This difference is acceptable, considering the amount of parameters involved in the ignition of the machine not presented in the model, such as friction or viscosity. Besides, the experimental system uses a dc machine to simulate the prime mover while the simulation uses constant parameters. In addition, the time of the excitation is not as important as the frequency or voltage amplitude, which are accurate in the simulation. One of the main features of the model is the response to load application. For this purpose, the induction machine was connected to an electrical load of the 75% of the nominal capacity. Figure 4.113 shows the results. Voltage drop is a typical response of this kind of generators when facing large loads. Normally the electronic control of the machine will compensate the drop by increasing the capacitance connected to the bank or increasing the speed of the shaft. Figure 4.114 shows the recovery from a voltage drop by increasing the capacity of the bank. Finally, the two mechanical outputs of the model are presented in Figures 4.115 and 4.116, the angular velocity and the electromechanical torque, respectively. The applied load not only affects the electrical response by dropping the voltage but also has a physical impact in the machine by decreasing the rotor speed. After applying the extra capacitance to recover the voltage peak is clear that an increase of the mechanical torque is also needed to keep the voltage magnitude.

A model has been implemented for the analysis of a self-excited induction generator. The use of TACS as a programming tool has been proved. The interactive capabilities of TACS make them suitable for implementation of mathematical models. The model has been implemented in a manner that any third party can improve the control of any variable involved in the calculation. At the same time, the implementation of this model allows improving the studies in distributed generation using EMTP-ATP software.

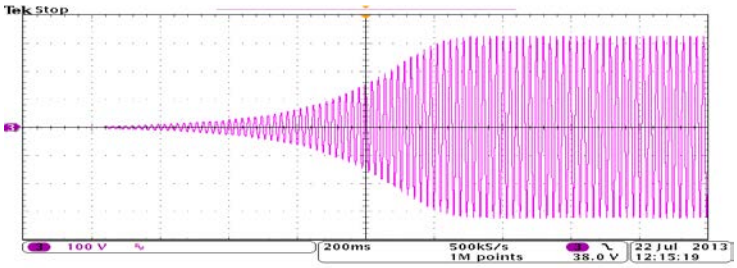

a) Experimental

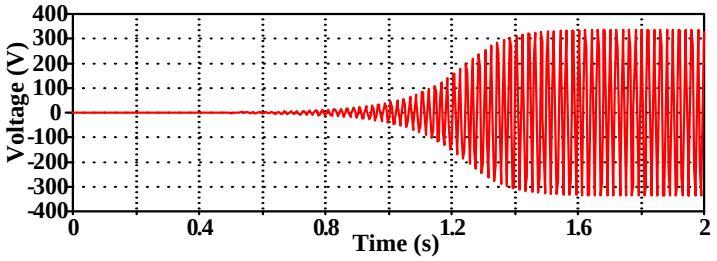

a) Simulation

Figure 4.112. Excitation voltage of a SEIG.

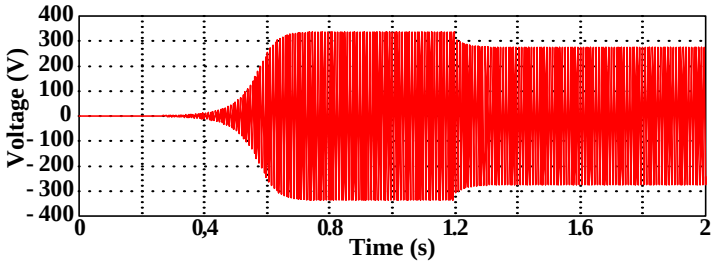

Figure 4.113. Voltage drop due to load application.

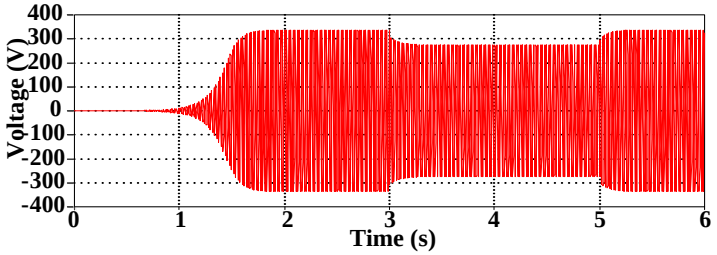

Figure 4.114. Recovery voltage from load application.

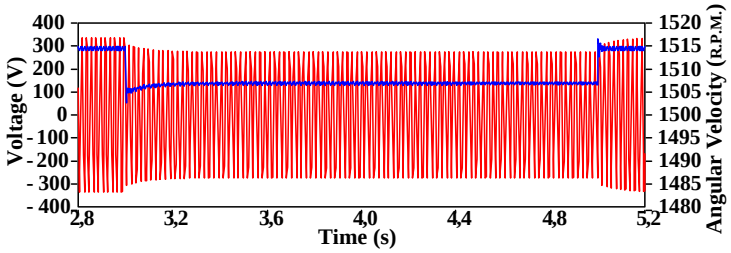

Figure 4.115. Voltage and angular velocity response to load.

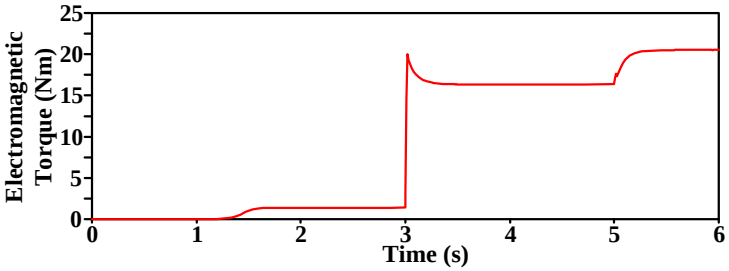

Figure 4.116. Torque response to load application.

4.5 CHAPTER SUMMARY

This Chapter has presented a significant amount of experimental validations for both single- and three-phase transformer models. For the single-phase transformer the π model has been used, analyzing its behavior in different configuration set ups. Besides, the impact of the internal capacitance has been studied determining that for the case of small single-phase transformer it is not conclusive in the final state of ferroresonance. For the case of the three-phase transformer, the Hybrid model has been validated for the first time ferroresonance analysis. The model has been presented in steady state condition in the literature, however, until now it have not been validated for transient analysis. For that the contribution of this thesis is highly relevant. In addition the weak points of the model have been addressed and appointed as future work proposal. The ferroresonance phenomenon has been tested in situations where the power source is highly nonlinear showing the randomly behavior that the phenomenon can present. Finally, the first approach of implementing the hysteresis cycle to the π model has been introduced.

4.6 REFERENCES

[1] M. R. Iravani, A. K. S. Chaudhary, W. J. Giewbrecht, I. E. Hassan, A. J. F. Keri, K. C. Lee, J. A. Martinez, A. S. Morched, B. A. Mork, M. Parniani, A. Sarshar, D. Shirmohammadi, R. A. Walling, and D. A. Woodford, "Modeling and analysis guidelines for slow transients: Part III: The study of ferroresonance", *IEEE Transactions on Power Delivery*, vol. 15, no. 1, pp. 255-265, January 2000.

[2] J. A. Martinez-Velasco and F. Gonzalez, *Temporary Overvoltages in Power Systems*, Ref. E6.39.59, The Encyclopedia of Life Support Systems (EOLSS-UNESCO), 2012.

[3] J. A. Corea-Araujo, F. Gonzalez-Molina, J. A. Martinez-Velasco, J. A. Barrado-Rodrigo, and L. Guasch-Pesquer, "Ferroresonance analysis using 3D bifurcation diagrams", *IEEE Power and Energy Society General Meeting*, Vancouver, Canada, July 2013.

[4] CIGRE Working Group C4.307, Resonance and Ferroresonance in Power Networks and Transformer Energization, *Cigre Technical Brochure no. 569*, February 2014.

[5] D. A. N. Jacobson, "Examples of ferroresonance in a high voltage power system", *IEEE Power and Energy Society General Meeting*, Toronto, Canada, July 2003.

[6] D. A. N. Jacobson, P. W. Lehn, and R. W. Menzies, "Stability domain calculations of period-1 ferroresonance in a nonlinear resonant circuit", *IEEE Transactions on Power Delivery*, vol. 17, no.3, pp. 865-871, July 2002.

[7] M. Val Escudero, I. Dudurych, and M. A. Redfern, "Characterization of ferroresonant modes in HV substation with CB grading capacitors", *Electric Power Systems Research*, vol. 77, no. 1, pp. 1506-1513, October 2006.

[8] J. A. Martinez-Velasco and B. A. Mork, "Transformer modeling for low- and mid-frequency transients - A review", *IEEE Transactions on Power Delivery*, vol. 20, no. 2, pp. 1625-1632, April 2005.

[9] F. de León, P. Gómez, J. A. Martinez-Velasco, and M. Rioual, "Transformers," Chapter 4 of *Power System Transients. Parameter Determination*, J. A. Martinez-Velasco (ed.), CRC Press, 2009.

[10] IEEE Standard, "Test Code for Liquid-Immersed Distribution, Power, and Regulating Transformers", IEEE Std C57.12.90-2010 (Revision of IEEE Std C57.12.90-2006).

[11] IEC Standard, "Power transformers - Part 1: General", IEC 60079-1. Ed. 3. 2011.

[12] J. A. Corea-Araujo, F. Gonzalez-Molina, J. A. Martinez-Velasco, J. A. Barrado-Rodrigo, and L. Guasch-Pesquer, "An EMTP-based analysis of the switching shift angle effect during energization/de-energization in the final ferroresonance state", *International Conference in Power Systems Transients (IPST)*, Vancouver, Canada, July 2013.

[13] B. A. Mork, F. Gonzalez, D. Ishchenko, D. L. Stuehm, and J. Mitra, "Hybrid transformer model for transient simulation-Part I: Development and parameters", *IEEE Transactions on Power Delivery*, vol. 22, no. 1, pp. 248-255, January 2007.

[14] H. K. Høidalen, B. A. Mork, F. Gonzalez, D. Ishchenko, and N. Chiesa, "Implementation and verification of the hybrid transformer model in ATPDraw", *Electric Power Systems Research*, vol. 79, no. 3, pp. 454-459, March 2009, Special issue: papers from the 7th International Conference in Power Systems Transients (IPST).

[15] H. K. Høidalen, N. Chiesa, A. Avendano, and B. A. Mork, "Developments in the hybrid transformer model–Core modeling and optimization", *International Conference in Power Systems Transients (IPST)*, Delft, The Netherlands, June.

[16] P. Ferracci: Ferroresonance, *Cahier Technique no. 190*, Groupe Schneider, 1998.

[17] H. K. Høidalen, L. Prikler, J. Hall, "ATPDraw- Graphical Preprocessor to ATP. Windows version", *International Conference in Power Systems Transients (IPST)*, Budapest, 1999.

[18] G. McPerson and R. D. Laramore, *An Introduction to Electrical Machines and Transformers*, John, Wiley & Sons, 1990.

[19] G. R. Slemon, "Equivalent circuits for transformers and machines including non-linear effects", *Proc. of the IEE-Part IV: Institution Monographs*, vol. 100, pp.129 -143, 1953.

[20] F. de Leon, A. Farazmand, P. Joseph, "Comparing the T and π Equivalent Circuits for the Calculation of Transformer Inrush Currents", *IEEE Transactions on Power Delivery*, vol.27, no.4, pp.2390-2398, October 2012.

[21] E. C. Cherry, "The duality between interlinked electric and magnetic circuits and the formation of transformer equivalent circuits", *Proceeding of the Physical Society. Section B* 62.2, 1949.

[22] S. Jazebi, A. Farazmand, B. P. Murali, F. de Leon, "A comparative study on π and T equivalent models for the analysis of transformer ferroresonance", *IEEE Transactions on Power Delivery*, vol.28, no.1, pp.526-528, January 2013.

[23] J. A. Martinez-Velasco and J. R. Martí, *Electromagnetic Transients Analysis*, *Chapter 12 in Electric Energy Systems: Analysis and Operation*, A. Gomez-Exposito, A. Conejo, and C. Canizares (Eds.), CRC Press, Boca Raton, 2008.

[24] A. Rezaei-Zare, R. Iravani, and M. Sanaye-Pasand, "Impacts of transformer core hysteresis formation on stability domain of ferroresonance modes", *IEEE Transactions on Power Delivery*, vol. 24, no. 1, pp. 177-186, January 2009.

[25] A. Rezaei-Zare and R. Iravani, "On the transformer core dynamic behavior", *IEEE Transactions on Power Delivery*, vol. 25, no. 3, pp. 1606-1619, July 2010.

[26] A. Rezaei-Zare, R. Iravani, M. Sanaye-Pasand, H. Mohseni, and S. Farhangi, "An accurate hysteresis model for ferrorresonance analysis of a transformer", *IEEE Transactions on Power Delivery*, vol. 23, no. 3, pp. 1448-1456, July 2008.

[27] P. Moses, M. A. S. Masoum, and H. A. Toliyat, "Impact of hysteresis and magnetic couplings on the stability domain of ferrorresonance in asymmetric three-phase three-leg transformers", *IEEE Transactions on Power Delivery*, vol. 26, no. 2, pp. 581-592, 2011.

[28] F. De Leon and A. Semlyen, "Complete transformer model for electromagnetic transients", *IEEE Transactions on Power Delivery*, vol. 9, no. 1, pp. 231-239, January 1994.

[29] IEEE Power Eng. Soc. Task Force on Data for Modeling System Transients, "Parameter determination for modeling system transients— Part III: Transformers", *IEEE Transactions on Power Delivery*, vol. 20, no. 3, pp. 2051-2062, July 2005.

[30] Slow Transients Task Force of the IEEE Working Group on Modeling and Analysis of Systems Transients Using Digital Programs, "Modeling and analysis guidelines for slow transients—Part III: The study of ferroresonance", *IEEE Transactions on Power Delivery* , vol. 15, no. 1, pp. 255–265, January 2000.

[31] A. Narang and R. H. Brierley, "Topology based magnetic model for steady-state and transient studies for three phase core type transformers", *IEEE Transactions on Power Systems*, vol. 9, no. 3, pp. 1337-1349, August 1994.

[32] B. A. Mork, "Five-legged wound-core transformer model: Derivation, parameters, implementation, and evaluation," *IEEE Transactions on Power Delivery*, vol. 14, no. 4, pp. 1519-1526, October 1999.

[33] C. M. Arturi, "Transient simulation and analysis of a five-limb generator step-up transformer following an out-of-phase synchronization", *IEEE Transactions on Power Delivery*, vol. 6, no.

1, pp. 196-207, January 1991.

[34] B. A. Mork, "Ferroresonance and Chaos - Observation and Simulation of Ferroresonance in a Five Legged Core Distribution Transformer", Ph.D. Thesis, North Dakota State University, 1992.

[35] J. Rougin and V. Ranjamina, "Modeling of magnetic circuits with EMTP", *EMTP Newsletter*, vol. 7, no. 1, pp. 8-28, March 1987.

[36] P. L. Sorenson, "Simulation of faults and switching in electrical distribution networks", ATV-NESA-Electrical Engineering Department, DTH-DEFU, Industrial Research Project EF186, pp. 1–120, April 1988.

[37] D. L. Stuehm, "Final report—Three phase transformer core modeling", Bonneville Power Administration Award no. DE-BI79-92BP26700, Copies available from BPA, Dept. EOHC, (503) 230-4404. Febuary 1993.

[38] E. J. Tarasiewicz, A. S. Morched, A. Narang, and E. P. Dick, "Frequency dependent eddy current models for nonlinear iron cores", *IEEE Transactions on Power Systems*, vol. 8, no. 2, pp. 588–597, May 1993.

[39] B. A. Mork, D. Ishchenko, F. Gonzalez, and S. D. Cho, "Parameter estimation methods for five-limb magnetic core model", *IEEE Transactions on Power Delivery*, vol. 23, no. 4, pp. 2025-2032, October 2008.

[40] B. A. Mork, F. Gonzalez, D. Ishchenko, D. L. Stuehm, and J. Mitra, "Hybrid transformer model for transient simulation – part II: laboratory measurements and benchmarking", *IEEE Transactions on Power Delivery*, vol. 22, no. 1, pp. 256-262, January 2007.

[41] IEEE Standard, "Test Procedures for Magnetic Cores," *IEEE Std 393-1991*, March 1992.

[42] A. de Blas, "Modelización de la histéresis magnética y su aplicación al cálculo numérico en máquinas eléctricas", Ph.D. Thesis, Universidad Politécnica de Catalunya, 2006.

[43] ASTM Standard, "Test methods for alternating-current magnetic properties of materials using the wattmeter–ammeter–voltmeter method 100 to 10000 Hz and 25 cm", *ASTM Publication* A348/A348M-00.

[44] S. R. Talukdar and J. R. Bailey, "Hysteresis model for system studies", *IEEE Transaction on Power Apparatus and Systems*, vol. 95, no. 4, pp. 1429–1434, 1976.

[45] D.C. Jiles and D.L. Atherton, "Theory of ferromagnetic hysteresis", *Journal of Magnetism and Magnetic Mater*ials, vol. 61, pp. 48–60, September 1986.

[46] N. Abeywickrama, Y. V. Serdyuk, and S. M. Gubanski, "Effect of Core Magnetization on Frequency Response Analysis (FRA) of Power Transformers", *IEEE Transactions on* Power Delivery, vol. 23, no. 3, pp. 1432-1438, July 2008.

[47] B. Kovan, F. de Leon, D. Czarkowski, Z. Zabar, and L. Birenbaum, "Mitigation of Inrush Currents in Network Transformers by Reducing the Residual Flux With an Ultra-Low-Frequency Power Source", *IEEE Transactions on Power Delivery*, vol. 26, no. 3, pp.1563-1570, July 2011.

[48] N. Jenkins, R. Allan, P. Crossley, D. Kirschen, and G. Strbac, *Embedded Generation*, IEE London, 2000.

[49] M. G. Simoes, and F. A. Farret, *Renewable energy systems*, CRC Press Florida, 2004.

[50] S. S. Murthy, B. Singh, P. K. Goel, and S.k. Tiwari, "A comparative study of fixed speed and variable speed wind energy conversion systems feeding the grid," *IEEE International Conference on Power Electronics and Drive Systems*, PEDS'07, Bangkok, Thailand, November 2007.

[51] D. Nishad, D. V. Singh, and D. Singh, "A Review of VF Controller for an Asynchronous Generator Based Wind Energy Conversion System", *International Journal of Engineering Science*, vol. 5, no. 3, pp. 602–608, March 2013.

[52] S. Singh, and A. N. Tiwari, "Voltage and frequency controller for self excited induction generator in micro hydro power plant: review", *International Journal of Advanced Research in Electronics and Communication Engineering*, vol. 2, no. 2, pp 214-219, February 2013.

[53] E. D. Basset, and F. M. Potter, "Capacitive excitation of induction generators", *Transactions of the American Institute of Electrical Engineers*, vol. 54, no. 5, pp. 540–545, May 1935.

[54] D. Seyoum, C. Grantham, and M. F. Rahman, "The dynamic characteristics of an isolated self-excited induction generator driven by a wind turbine", *IEEE Transactions on Industry Applications*, vol.39, no.4, pp. 936-944, July 2003.

[55] M. Steurer, J. Langston, L. Anderson, S. Suryanarayanan, R. Meeker, and P. Ribeiro, "Voltage Sensitivity to Capacitor Switching on an Existing Fixed Speed Induction Generator Wind Farm", *IEEE Power Engineering Society General Meeting*, Tampa, USA, June 2007.

[56] S. Sugiarto, A. Abu-Siada, and S. Islam, "Performance enhancement of grid-connected fixed speed wind energy conversion systems", *IEEE Australasian Universities Power Engineering Conference*, AUPEC, Adelaide, Australia, September 2009.

[57] M. G. Sugirtha, and P. Latha, "Analysis of power quality problems in grid connected wind power plant", *International Conference on Recent Advancements in Electrical, Electronics and Control Engineering* (ICONRAEeCE), Sivakasi, India, December 2011.

[58] R. K. Varma, S. Auddy, and Y. Semsedini, "Mitigation of subsynchronous resonance in a series-compensated wind farm using FACTS controllers", *IEEE Transactions on Power Delivery*, vol.23, no.3, pp.1645-1654, July 2008.

[59] L. Wang, and L. Chen, "Reduction of Power Fluctuations of a Large-Scale Grid-Connected Offshore Wind Farm Using a Variable Frequency Transformer", *IEEE Transactions on Sustainable Energy*, vol.2, no.3, pp.226-234, July 2011.

[60] C. J. Mozina, "Impact of Smart Grids and Green Power Generation on Distribution Systems", *IEEE Transactions on Industry Applications*, vol.49, no.3, pp.1079-1090, May-June 2013.

[61] G. K. Singh, "Modeling and experimental analysis of a self-excited six-phase induction generator for stand-alone renewable energy generation", *Renewable Energy*, vol. 33, pp. 1605–1621, July 2008.

[62] EEE Standard "Test Code for Dry-Type Distribution and Power Transformers", *IEEE Std C57.12.91-2001*, vol., no., pp.1,82. March 2001.

[63] K. Kasal, and B. Singh, "VSC with T-connected transformer based decoupled controller for a pico hydro power generation", *IEEE International Conference on Sustainable Energy Technologies*, Singapore, November 2008.

[64] D. Braun, M. Delfanti, M. Palazzo, and R. Zich, "Harmonic distortion in pwer stations due to ferroresonance", *Asia-Pacific Symposium on Electromagnetic Compatibility*, APEMC, Singapore, May 2012.

[65] H. Molland, and E. Dietmar, "Modelling the system dynamics of islanding asynchronous generators", *10th International Modelica Conference*, Lund, Sweden, March 2014.

[66] J. A. Corea-Araujo, F. Gonzalez-Molina, J. A. Martinez-Velasco, J. A. Barrado-Rodrigo, and L. Guasch-Pesquer, " Implementation of a Self-Excited Induction Generator Model Using TACS", *EEUG Conference*, Sardinia, Italy, September 2014.

[67] H. W. Dommel, "Digital Computer Solution of Electromagnetic Transients in Single and Multiphase Networks", *IEEE Transac*tions *on Power Systems*, vol. PAS-88, pp. 388-399, April 1969.

[68] H. W. Dommel, *EMTP Theory Book*, BPA, Portland, 1986.

[69] R. H. Lasseter, J. Zhou, "TACS enhancements for the Electromagnetic Transient Program", *Power Industry Computer Application Conference*, Arizona, USA, May 1993.

[70] J. A. Martinez-Velasco, "Digital computation of electromagnetic transients in power systems: current status", *IEEE PES Working Group* in *Modeling and analysis of system transients using digital programs*, IEEE PES Special Publication, 1998.

[71] J. M. Elder, J. T. Boys, and J. L. Woodward, "Self-excited induction machine as a small low-cost generator, " *IEE Proceedings C, Generation, Transmission and Distribution*, vol. 131, no. 2, pp. 33–41, March 1984.

[72] P. C. Krause, O. Wasynczuk, S. D. Sudhoff, S. Pekarek, *Analysis of Electric Machinery and Drive Systems*, Wiley-IEEE Press, New York, 2013.

[73] R. H. Park, "Two-reaction theory of synchronous machines generalized method of analysis-part I," *Transactions of the American Institute of Electrical Engineer*s, vol.48, no.3, pp.716-727, July 1929.

5 Improvements and experimental validations of the π transformer model: Addition of hysteresis effects.

5.1 INTRODUCTION

THE transformer is an essential component of power systems. Its privilege position as a bond between power stations and utilization points makes it an indispensable component for electrical networks. A transformer's main functions consist on transferring electrical energy from one circuit to another providing electrical isolation through electromagnetic induction. Voltage level changes upon circuits are allowed without any frequency change [1]. In addition, the magnetic coupling performance will determine if a transformer is labeled as either a step-up or step-down transformer depending on whether the secondary voltage is higher or lower than the primary voltage.

In the last few decades, rapid advancements have taken place in the design, analysis, manufacturing and condition-monitoring technologies of transformers. These technological progresses have been significantly boosted by the exponential grow in computational trends. Hardware and software used to study electrical phenomena have been improved vastly within a decade. Nowadays, complex signal analysis or difficult to represent materials characteristic can be modeled in a virtual environment. Thus, extensive system analysis can be performed by means of several simulation techniques.

The massive growth of power systems has put tremendous responsibilities on the transformer industry to supply reliable and cost-effective transformers [2]. Being the most important component of transmission and distribution systems, transformer accurate modeling is an important task. Since not every characteristic of the transformer plays a part in all transients, the existence of a unique or global model is rather unlikely. The existing models implemented in transient tools are not yet adequate for some scenarios. Several built-in models are currently documented in the literature [3], [4]. In general, users of computational tools can develop their own custom-made models. A very common approach when developing new transformer models is to apply the principle of duality. This principle is a very common approach for developing correct transformer core representation. It was presented by Cherry in 1948 [5], proving that by applying the duality technique to a single-phase transformer, regardless its type of core (core type or shell type), the obtained magnetic model has only one leakage inductance branch in series and two shunt magnetizing branches. This configuration named the π model has proven to be topologically-correct for a single-phase transformer core [6]. In 1952 Slemon presented the equivalent π circuit for a single-phase transformer, including both electrical and magnetic circuits [7].

The focus of this chapter is to present an easy to follow analysis into the description, calculation and validation of the computational representation for a single-phase transformer by using the π model for core representation. The description is done following the general electrical machine theory, the calculation is performed by using the methods depicted by Cherry and Slemon [5][7], and finally, the validation is made by comparing simulation results to actual laboratory measurements. The transformer model has been implemented in ATPDraw [8].

5.2 THE EQUIVALENT Π TRANSFORMER MODEL: COMPUTING AND IMPLEMENTATION

The duality theory was first introduced by Cherry in 1948 [5]. Placing the foundations that would allow changing a magnetic circuit to an equivalent electric one (dual) or vice versa. Duality theory it is still considered as one of the most important contributions to the modeling of complex magnetic devices. It was Slemon in 1952 [6], who implemented duality theory to a single-phase transformer deriving its equivalent electric circuit. The final model included all electrical components and integrated the magnetic core equivalent circuit. This circuit received the name of equivalent π model. In the coming pages, the application of the duality derivation method is presented in detail to calculate such π circuit.

5.2.1 *Formulation of the π transformer model*

In the model developing criteria, there are two important characteristics to value while trying elaborate a transformer model: (1) The equivalent model should include enough information accumulated on the elements that assemble it. For transient phenomena analysis, the model data should be adequate. (2) The model should not be more complex than the problem on hand. Therefore, it should avoid parameters which, from an engineering point of view, are neglected for specific phenomena. Some typical winding and magnetic core arrangement for a power single phase transformer are presented in Figure 5.1. As it is known, the setup of the winding over the iron core gives name to the transformer topology. Figure 5.1a presents the shell type construction; while Figure 5.1b introduces the core-type construction. Both are composed by flat iron laminations commonly referred as the stacking technique. Figures 5.1c and 5.1b shows the wounded core technique consisting on a trip of iron fed through the coils.

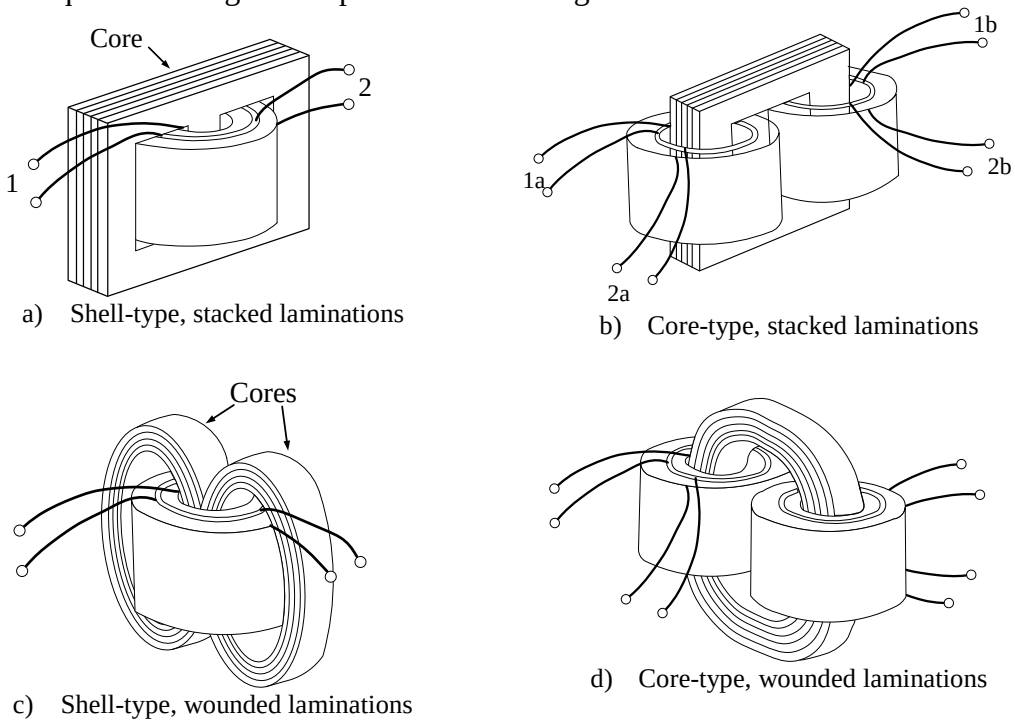

a) Shell-type, stacked laminations

b) Core-type, stacked laminations

c) Shell-type, wounded laminations

d) Core-type, wounded laminations

Figure 5.1. Transformer's winding and core arrangements.

Table 5.1 – Duality transformation pairs

Magnetic Circuit	Electrical Dual
Meshes	Nodes
Nodes	Meshes
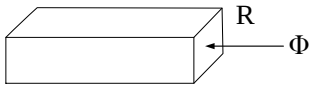	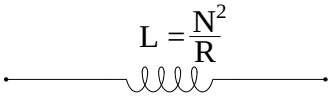
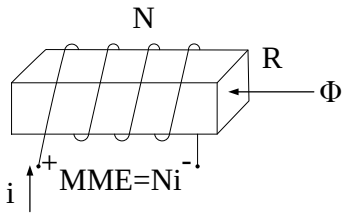	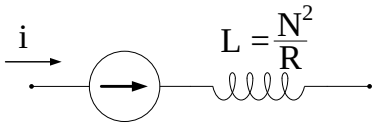

The existing Steinmetz T model is not sufficiently accurate to predict all transformer behaviors. Highly saturated phenomena have been proved to collapse the model, making it to converge into erroneous solutions. A more elaborated model including most of the transformer dynamic characteristics is needed. The methodology used to derive a topologically correct model is implemented here for a core-type stacked single-phase transformer. The duality principles used are presented on Table 5.1. The initial step consists on defining the magnetic flux paths distributed along the physical magnetic core circuit. Figure 5.2 shows the distribution of the flux over the three legs of the transformer.

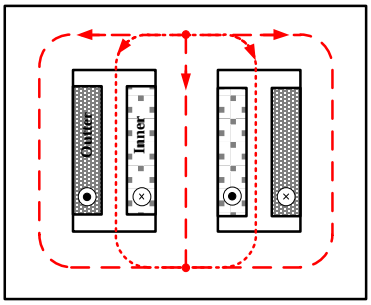

Figure 5.2. Flux distribution over the core.

The second step is to consider a magnetomotive force, *mmf*, comprised over the central leg making the flux move to the outer legs crossing the yokes, where F_{in} and F_{out} are the magnetomotive forces representing the windings. The part of the flux leakage moving in the air, going from the coils to the legs, has been represented with the model proposed by Arturi [4]. Figure 5.3a presents the equivalent magnetic circuit.

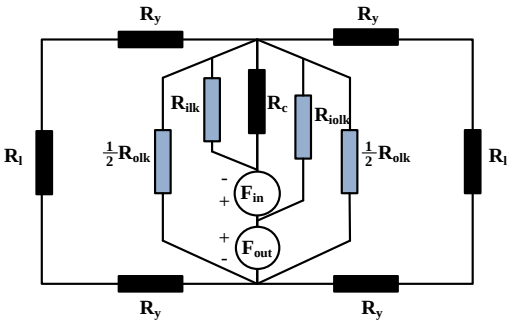

a) Equivalent circuit

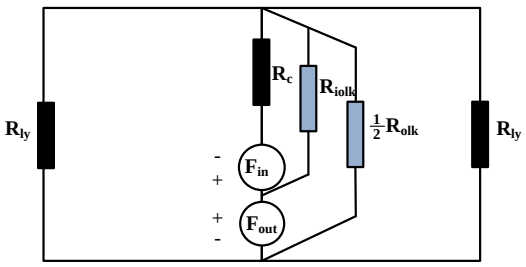

b) Reduced circuit

Figure 5.3. Transformer's magnetic circuit.

According to [3], it is possible to reduce the reluctances on the outer legs (R_y and R_l). Most of the core topologies are constructed symmetrically, thus, these reluctances are crossed by magnetic flux as they were one (R_{ly}). The flux leakage flowing between the core and the inner leg can be neglected (R_{ilk}) and the flux leakage between the core and the outer legs is collected to a single value (R_{olk}). By using these assumptions the magnetic circuit is reduced to that presented in Figure 5.3b. From here, the dual electrical circuit can be computed by applying the duality principle. According to Table 5.1, every mesh in the magnetic circuit has a node equivalent in an electric dual. This change is completed by drawing imaginary the nodes inside each circuit mesh. A label should be given to every individual node (*i.e.* a, b, c). Subsequently, an extra node is added outside the circuit and labeled as node *k*. Finally, a dashed line is drawn connecting every existing node and crossing all elements in the circuit. Figure 5.4 shows the duality transformation first step.

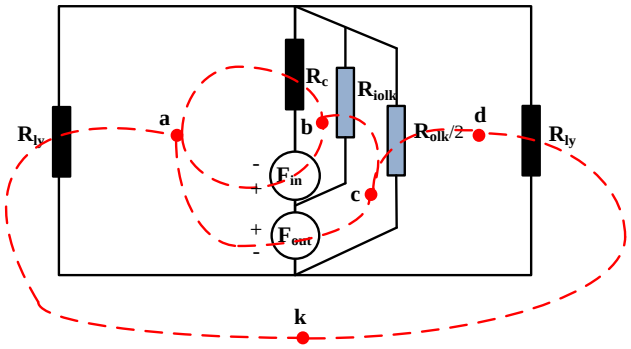

Figure 5.4. Duality transformation: First step.

All dashed trajectories presented in Figure 5.4 represent the equivalent design of the circuit. Figure 5.5a, shows the new structure of the magnetic circuit before changing the reluctances and mmf:

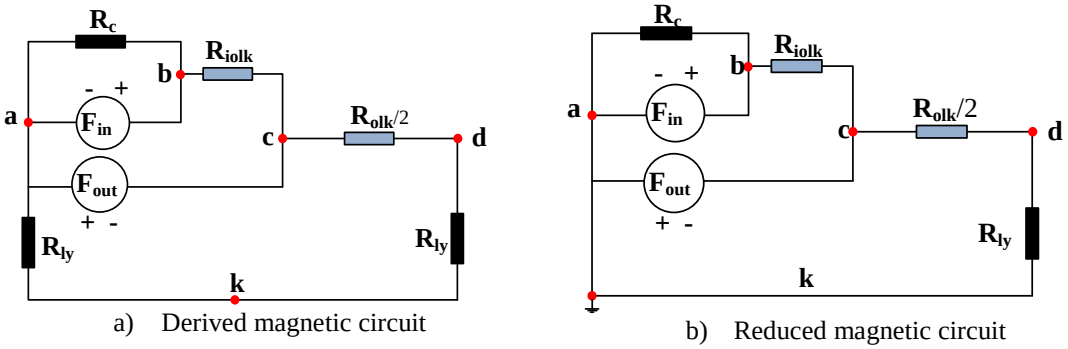

a) Derived magnetic circuit

b) Reduced magnetic circuit

Figure 5.5. Duality transformation: magnetic circuit.

According to Slemon, the physical resemblance of the core makes possible to simplify the circuit by unifying the values of the leg reluctance. Figure 5.5b shows how the π structure is about to be formed. It important to remark, that the flux leakage has been concentrate in the same element R_{iolk} during the whole calculation process. This is considered the most significant characteristic of the π model structure and implies a big advantage over the traditional T Steinmetz model.

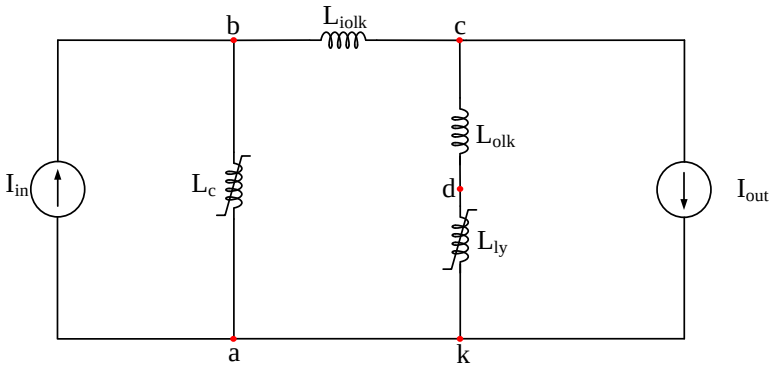

Figure 5.6. Transformer's model representation.

Now, the mmf and all reluctances will be changed to its electrical dual. Consequently, currents sources and inductances will be placed instead. All non-linear elements will keep its characteristic, thus, reluctance representing the core area will turn into non-linear equivalent inductances. Finally, all the current sources are substituted for ideal single-phase transformers. According to the Steinmetz hysteresis approach, every non-linear inductance should have a parallel resistance to correctly represent the saturation effects and the core losses. The value of leakage inductances L_{olk} can be neglected because is really small as compared with L_{ly}.

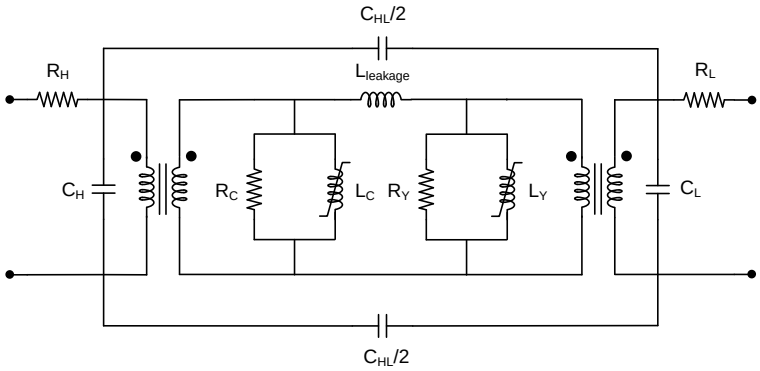

Figure 5.7. Transformer's π equivalent model.

The saturation branches of the model could have different values and behavior for specific cases. However, it would always depend on construction topologies. In most cases transformer cores are constructed symmetrically in terms of area and length of the legs. In general cases, both branches will use the same values. The equivalent relation between data used on T and π models are presented bellow [9].

$$L_{leakage} = L_H + L_L \quad (5.1)$$

$$R_C = 2R_M \quad (5.2)$$

$$L_C = 2L_M \quad (5.3)$$

According to the results presented on [9][10], the π model has better performance when highly saturation phenomena is studied. In those studies a comparison has been presented for inrush current and ferroresonance cases proving that the π model overcomes the traditional T model in those cases.

5.3 HYSTERESIS IMPLICATION INTO THE FINAL FERRORESONANCE STATE: π MODEL IMPLEMENTATION

Nowadays, a large theoretical background is available for the adequate modeling of a transformer subjected to all kind of transients. Regarding voltage transformers, an up-to-date research presented in [9] and [10] proved that the π model can be more accurate than the classical Steinmetz 'T' model for representing transient response under high saturation levels. Figure 5.8 presents the circuit representation for both models.

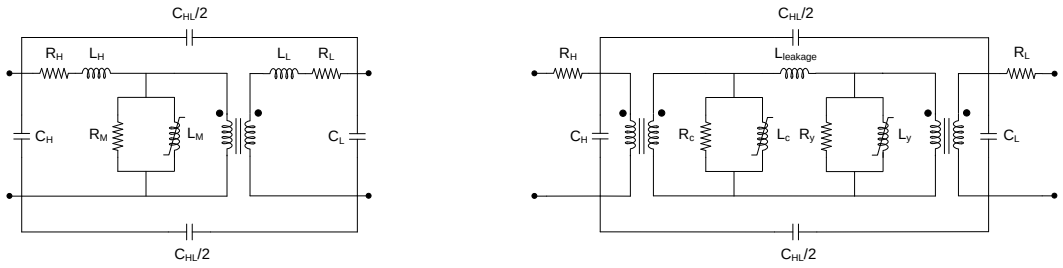

a) T model b) π model

Figure 5.8. Transformer's model representation.

It is common having difficulties when obtaining the necessary data to compute the model parameters. For the voltage transformer case, the magnetic representation of the saturation phenomenon is the most complex to be measured. For low-frequency transients such as ferroresonance, the precision to calculate the magnetizing characteristic of the core will decide whether the computational representation is accurate or not. The work presented en [9] proves the capabilities of the π model to represent the ferroresonance phenomenon. Nevertheless, accuracy and matching between simulation and experimental waveforms are still a matter of study. The existing π model uses only a reversible component based magnetization characteristic. It implies, that both shunt magnetizing branches are formed by a fixed resistor representing the core losses and a non-linear inductor connected in parallel only defined by an anhysteretic curve. However, a comprehensive theoretical basis together with application of modern computational techniques can lead to develop a π model variation that respects the reversible and irreversible magnetic components. Thus, including hysteresis cycle.

5.3.1 *Hysteresis Modeling*

The magnetization characteristic of iron core transformers is composed by two main components: (a) a reversible component, represented by the anhysteretic curve of the material. This curve is a single-valued simplification where for each function's domain value exist only a single element in its range; (b) an irreversible component, represented by hysteresis loops. Hysteresis loops are the result of the interaction between domains, anisotropy and pinning forces due the existence of dislocations, interstices and impurities inside the material [11]. Hysteresis characteristic usually presents a sigmoid shape involving the flux density against the magnetic field intensity, also known as the B/H characteristic of the material. Three different types of hysteresis loops can be observed: (1) the largest loop, which is the hysteresis major loop; (2) symmetric minor loops; and (3) asymmetric minor loops [12]. Figure 5.9 present a full hysteresis cycle.

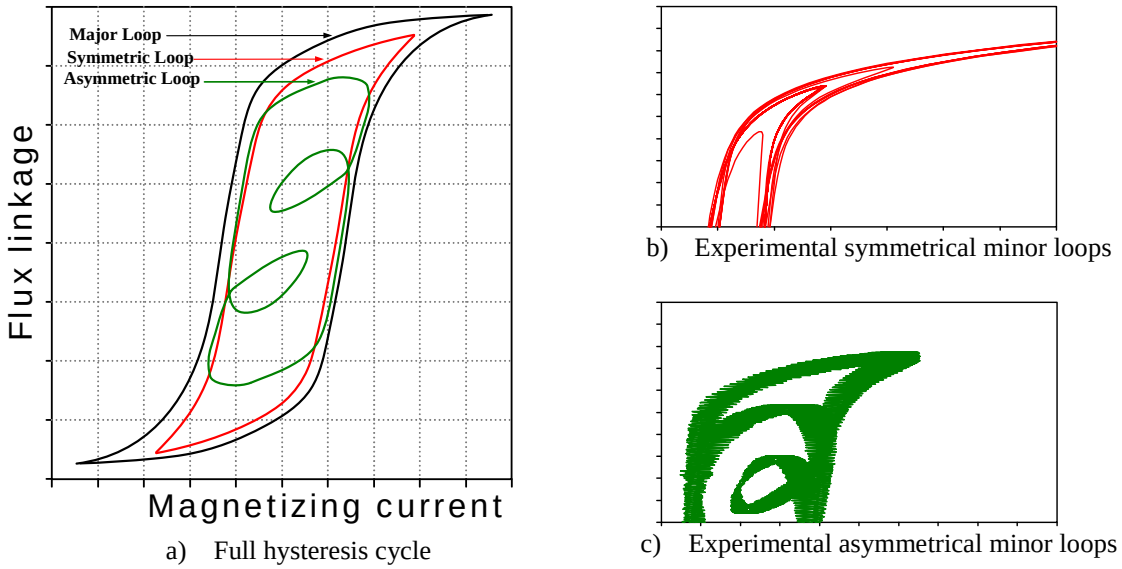

Figure 5.9 Hysteresis cycle.

Experimental testing methods are useful to determine transformer characteristics and assist the design, analysis and operation of magnetic cores in many types of applications. Tests for measuring permeability, core loss, apparent core loss, thermal characteristics, and other properties are collected as measurement standards [13], [14]. Most test methods include specific parameter ranges, instrument accuracies, or core sizes. However, hysteresis measurement tests are collected in external standards due to its complexity and the need to globalize inductors and transformer cores [15], [16].

Over the years several models have been proposed to describe the complex phenomenon of hysteresis [17], [18]. However, these methods are often laborious or require an important amount of parameters. In practice, most of transformer models focus on the simplified representation of the magnetic core. The aim is to come up to a realistic representation and skipping the need of using parameters difficult or impossible to be measured.

5.3.2 *Hysteresis loop approaching from anhysteretic characteristic*

The majority of transformer models available in commercial simulation software are based on the traditional Steinmetz T equivalent circuit model. Literature presents two different approaches to implement the Steinmetz model using only the anhysteretic characteristic: constant core loss model based on fixed resistance, and dynamic core loss model based on nonlinear resistance.

In the constant core losses approach, the transformer iron core is modeled as a circuit shunt branch composed by a nonlinear inductance (with an anhysteretic magnetization characteristic) connected in parallel to a constant resistance that represents fixed core losses. On the other hand, the dynamic core losses approach have been presented in the technical literature, the arrangement of the magnetization branch is proposed as a nonlinear inductance connected in parallel to a nonlinear resistance which varies as function of the core flux or the peak value of the applied voltage. Figure 5.10 presents the circuit representation of the core losses models.

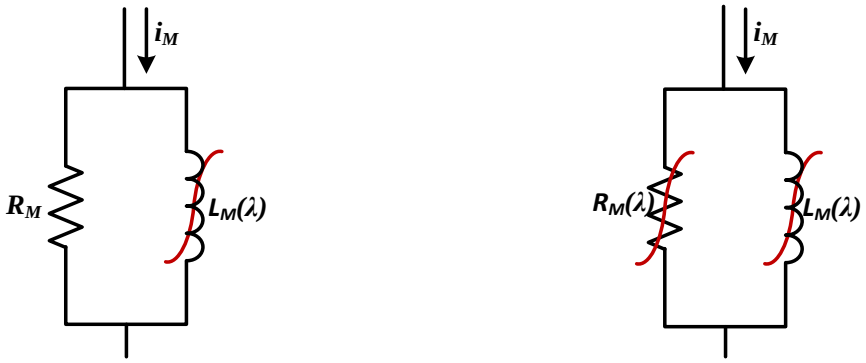

(a) Constant Losses (b) Nonlinear losses

Figure 5.10. Transformer's core representation

From the scheme in Figure 5.10a, an approximated hysteresis loop can be plotted by matching the peak flux linkage presented in the branch versus the branch current (i.e. adding the inductance current and the resistance current). The benefit of using this approach is that requires only routine transformer test information to be modeled. On the other hand, core losses do not remain constant and are highly dependent on the amplitude of the core flux. For the dynamic model presented in Figure 5.10b, the nonlinear resistance can be easily implemented since data required for its calculation is obtained from the same excitation test performed to obtain the nonlinear inductance. According to previous work [19][20], this approach is accurate for symmetric hysteresis loops but it can result in erroneous results under transient conditions where asymmetric flux variations are presented.

5.3.3 *Hysteresis loop approach from actual test data*

Including the hysteresis characteristic of a transformer iron core gives a better representation of the magnetic core behavior. However, implementing this feature is not a simple task. First, the branch circuit used to represent the magnetic core will change from the parallel inductor-resistor set to a parallel current source (i.e. Hysteresis controlled). A dummy resistor (i.e. 100 MΩ) should be added in parallel to give mathematical stability to the model and to avoid any kind of numerical oscillations. Whether the hysteretic characteristic will include the major and minor loops will depend on the information available. Figure 5.11 presents the circuit representation of a core including hysteresis.

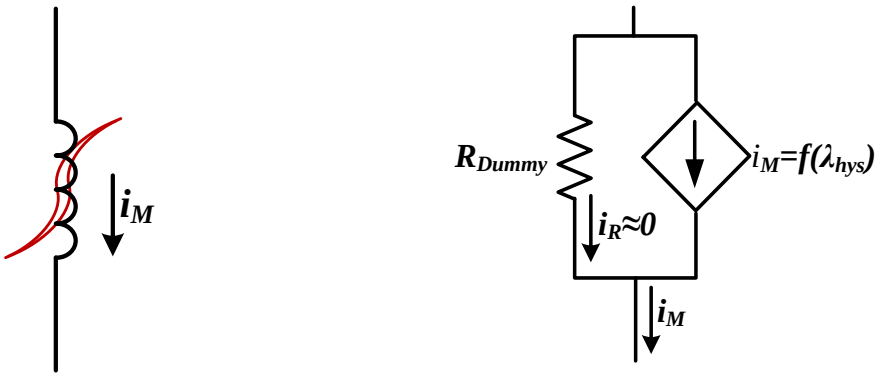

a) Hysteresis inductor b) Equivalent circuit

Figure 5.11. Transformer's hysteresis core representation

Modeling of the major hysteresis loop can be implemented by using curve fitting techniques such the Langevin function or the polynomial approximation [21],[22]. Then, other important hysteresis properties, such as residual and coercive forces can be included by adding control algorithms to complete the fitting. Figure 5.12 shows the main consideration to model the hysteresis loop. The procedure starts by knowing the actual form of the major hysteresis loop which is determined by an experimental measurement [15]. Thus, a curve-fitting approximation is applied to each loop side. The displacement through the '*X*' axis must coincide with the value of the coercive force. The intersection of the fitted curve and the '*Y*' axis is also called the residual flux.

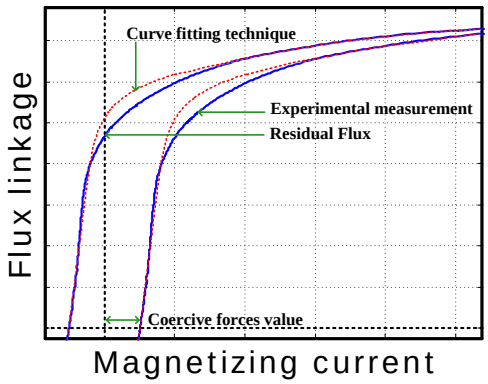

Figure 5.12. Hysteresis fitting technique

In order to generate a polynomial implementation, equation (5.4) can be used. This expression was originally presented in [23]. It has been used through the years in several works to represent anhysteretic properties [22][24][25].

$$i_L(t) = \mathrm{a}\lambda(t) + \mathrm{b}\lambda(t)^{\mathrm{n}} \tag{5.4}$$

where i_L represents the magnetizing current, λ represents the fluxlinked, *a* and *b* are the coefficients for the curve fitting, and *n* is the power of the expression. To add the sigmoid shape produced by the hysteresis cycle, an extra term is needed in Equation (5.4). The time dependent term presented in Equation (5.5) has been inspired in the Steinmetz representation of the core and it fixes the displacement of the curve to the coercive points. In the original Steinmetz model the current produced by a nonlinear inductor was complemented by a sinusoidal current produced as a function of the core losses. In this approach, equation (5.5) complements equation (5.4) in a similar way by adding shape-preserving mathematical term. Such term is a function of the correct coercive force in the hysteresis cycle.

$$i_L(t) = \mathrm{a}\lambda(t) + \mathrm{b}\lambda(t)^{\mathrm{n}} + \mathrm{F_c}\sin(\omega t + \alpha) \tag{5.5}$$

where F_c represents the magnitude of the coercive force. The positive values of the sinus will shift to the right side of the loop while the negative will serve for the left side of the loop formation. To complete the dynamic characteristic of the core, all the trajectories, including the hysteresis major and minor loops should be incorporated in the transformer core model. The major loop is probably the most used term when referring to hysteresis. Commonly, the major loop is depicted as a sigmoid shape closed curve and it is often called just hysteresis loop. The term minor loop is less utilized. It refers to the small trajectories created whenever a saturating maximum field is not achieved. Under periodic excitation, the minor loops shape should follow the form of

the major loop. Each loop maximum point should form part of the anhysteretic curve. Because of the geometrical resemblance of the symmetrical minor loops, its implementation in the control part of the model will require an external variable working as a function of geometrical characteristic. This variable has to work as scale factor controller:

$$i_{Loop} = k_{sf}(i_L) \tag{5.6}$$

Where the parameter k_{sf} represents the control variable. Since the symmetrical minor loops are proportional to the major loop, the factor k_{sf} should be a function of the flux leakage rate:

$$k_{sf} = (\frac{\lambda_{actual}}{\lambda_{max}}) \tag{5.7}$$

The implementation in the model will significantly contribute to a better core representation. Figure 5.13 presents the hysteresis cycle including the symmetrical minor loops as calculated by the model prior described.

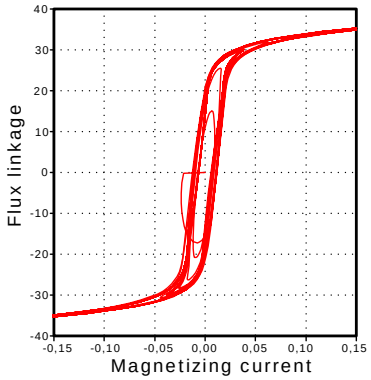

Figure 5.13. Hysteresis cycle including symmetrical minor loops

The transformer model, as considered in this work, has been developed in the form of a mathematical system of equations and logical rules [26]. Those mathematical assumptions have change the model proposed in Figure 5.8b. In order to better understand those changes, Figure 5.14 shows the new proposed model using the hysteresis characteristic of the core implemented in the π transformer model.

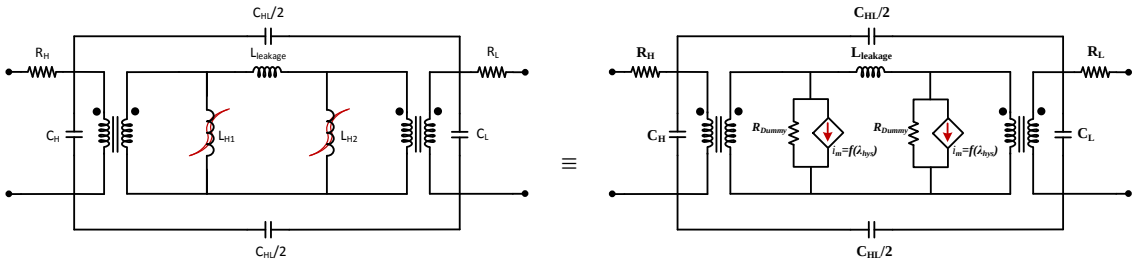

a) π equivalent model with hysteresis characteristic

b) π model with hysteresis for ATPDraw simulation

Figure 5.14. Equivalent π model including hysteresis core characteristic.

The implementation and benchmarking of this method is presented in the upcoming section, where several ferroresonance cases modeled using this technique are discussed.

5.4 MODEL BENCHMARKING

Several factors make transformer modeling a difficult task: transformer's behavior is nonlinear and frequency dependent; many topological variations on core and coil construction are possible; there are many physical attributes whose behavior may need to be correctly represented (self- and mutual inductances between coils, leakage fluxes, skin effect and proximity effect in coils, magnetic core saturation, hysteresis and eddy current losses in core, and capacitive effects) [27].Thus, validating power component models for transient analysis implies carry out numerous experimental procedures either field measurements or laboratory tests in order to obtain sufficient data to successfully guarantee a proper model operation. Following, the standard tests required for a basic transient model are described.

5.4.1 *Routine tests*

Modeling electromechanical components such as transformers implies obtaining experimental data measurements. These data could be in the form of linear and nonlinear inner elements of the transformer. Nowadays, a standard set of tests are presented by international institutions such as IEEE or IEC [14], [15]. These standards are a collection of the experimental routine tests defined for transformers (dry-type or liquid immerse). The name of routine tests are given to those experiments performed to the transformer prior its first start up. There is up to five typical tests to perform: (1) Isolation test, (2) Resistance measurement, (3) Ratio test, (4) No-load losses and Excitation current, (5) Load losses and Impedance Voltage. For models working under steady state, the routine tests supply sufficient information but transient analysis is often highly dependent on those nonlinear parameters and internal capacitive effects, and additional tests are needed.

5.4.2 *Special Tests*

Whenever transient phenomena are analyzed, the transformer model should have the nonlinear characteristic of every leg containing a winding. Often, in ferroresonance analysis cases, not only the nonlinear characteristic of the core is needed but also the zero sequence behavior and the internal capacitive effects. The special tests required in transformers, for a correct representation in computational analysis, are listed as follows: (1) Internal Capacitance measurement, (2) Zero Sequence Impedance, (3) Magnetization curve. In the industry, this type of tests are considered special due to its complexity and because they are not required for transformer installation [15]. In research, special tests are often needed because the amount of information extracted allows exact computational representation of electromechanical equipment.

5.4.3 *Ferroresonance Tests*

Although an actual test for ferroresonance measurements has not been yet considered by international standards, it is possible, however, to find within literature some authors who describe precisely the ferroresonance path and the prone conditions for ferroresonance ignition. It is therefore possible to prepare a sort of tests to measure and capture ferroresonance signals in a controlled environment [28], [29]. In these sense, it is possible to prepare an arrangement of standard ferroresonance circuits and routines to measure and capture its electrical signal in a controlled environment. In addition, commonly used routines to ignite the transformer can be used (i.e. Energization and De-nergization).

5.4.4 *Hysteresis Test*

Throughout the years international power system committees have developed a series of manuals stating general step-by-step instructions about transformers testing. Hysteresis characteristic, as well known, is the most important data required to truly know transformer behavior. Information obtained through the hysteresis loop will give insight idea of the material used to build in the transformer, the losses presented in the core, main electrical information like saturation or maximum flux reachable. The tests described on international standards are designed primarily to be used in determining the magnetic properties of assembled magnetic cores rather than the properties of basic magnetic materials. There are three different strategies presented in the literature: a) The DC based test measurements b) The Direct Measurement of Flux Density and c) Dynamic Hysteresis Loop Measurement. The methods are briefly explained below:

5.4.5 *The DC based test measurements*

The direct current based measurements are methods created in such a form that allows going over the external major hysteresis loop moving point to point by using a series of synchronized polarity changes in the excitation source. There are different approaches to implement DC measurements, some of the most used tests are presented below:

Determination of the Basic Symmetrical Hysteresis Loop

The most convenient procedure to measure the magnetic flux flowing through a physically accessible solid core is to place several turns of wire around the core and measure the time integral of the voltage induced in these turns when the flux level in the core is changed. This procedure is based upon adaptation of one of Maxwell's equations, i.e., $N\Delta\psi = Edt$, where N is the number of turns in a coil through which the flux has been changed by an amount $\Delta\psi$, and E is the resulting voltage induced in these turns. This procedure yields the change of the flux level in a magnetic circuit.

Elementary DC Hysteresis Loop Testing-Major Loop

An elementary tester for obtaining the dc hysteresis loop of a magnetic material is constructed by means of a bipolar current supply and an electronic flux-meter, all levels of excitation and flux density can be obtained for a particular magnetic material. Using this system arrangement an operator can obtain B and H values to construct a dc hysteresis loop. B is read directly from the flux-meter in Gauss, while H is calculated using the relationship $H = 1.26Ni/L_m$, where '*i*' is in Amperes, L_m, is the mean length of the core in Centimeters, and *H* is the magnetic field measured in Oersteds.

Automated Hysteresis Loop Testing-Major Loop

The current delivered by a bipolar current can be controlled either manually or with a function generator. The function generator can deliver sinusoidal, square wave, ramp, or special function signals to the bipolar current supply. These signals can be generated at frequencies from 0.01 Hz to 20 kHz. The current shunt yields a calibrated voltage proportional to the current *I* from the bipolar current supply. A two dimensional X-Y plane can be recorded with an electronic oscilloscope, using the current I and the magnetic flux density B as the axis. A scaling attenuator should be used to scale the shunt signal to satisfy the relationship mentioned in the previous section, that $H = 1.26Ni/L_m$.

The major limitation to use the DC methods is that the hysteresis loop measured does not correspond to a real time operation cycle. Moreover, the measurement equipment

i.e. (flux-meters) are often imprecise because of the three-dimensional behavior of the flux. Such behavior makes difficult to obtain a trustable measurement. In addition, the required point-to-point excitation makes it a tedious task that often turns in the necessity of start over the experiment if any error during polarity change occurs.

5.4.6 *Direct Measurement of Flux Density*

The most common direct-reading flux measuring devices are based on semiconductor sensing elements that, when placed in the presence of a magnetic field, produce a change in their output parameter as a function of the flux density of the magnetic field. The most common sensor is a Hall voltage generator generally constructed of indium arsenide or indium antimonide films. The Hall gauss-meters make use of the Hall generator type of probe to obtain a signal proportional to flux density. This signal is amplified and conditioned be read in terms of flux density, usually gauss. The calibration of these devices is achieved by means of a stable permanent magnet of a known flux density. Hall gauss-meters measure the field within a magnetic material by direct contact. In other words, the probe must be placed among the core laminations. The principal benefit over DC methods is that allows to measure during real time operation of the core. The principal limitation of using the Flux Density measurement is that semiconductor sensors measure only the fields in air regions and cannot directly measure the field within a magnetic material. In addition, structural fragility of the probes is a serious problem as well as the variation of the Hall voltage coefficient with temperature.

5.4.7 *Dynamic Hysteresis Loop Measurement*

The dynamic hysteresis loop may be obtained with two modes of sinusoidal excitation of the core: *Sine Voltage and Sine Current.* If core is excited with sinusoidal voltage source, the output impedance should remain low to minimize distortions caused by the nonlinear exciting current. The total harmonic distortion of the induced voltage should be less than 5% to avoid distortion of the hysteresis loop. In the case the core is excited with a sinusoidal current source, the output impedance should be high to minimize the distortion of the current wave by the voltage induced across the test coil. There are two main considerations that must be taken into account: (1) The excitation winding; when sinusoidal voltage excitation is used, the test winding shall consist of a sufficient number of turns to keep the exciting current within the capability of the voltage source, with a maximum of 5% harmonic distortion; when sinusoidal current excitation is desired, the number of turns is kept to a minimum. (2) Current pickup; the magnetizing current shall be detected as the voltage across a resistor in series with the exciting winding; the resistance shall be selected not significantly altering the conditions of the existing circuit, particularly in the case of sinusoidal voltage excitation. Once the measurements are acquired the magnetic field strength and the exciting current are proportional, following the relation:

$$H = \frac{N \cdot I}{L} \tag{5.8}$$

where: H is the magnetizing field strength, N is number of winding turns, I is the winding current, and L is the effective magnetic path length. In the same way, the instantaneous value of the induced voltage can be escalated to calculate the flux density

$$e = N \cdot A \cdot \frac{dB}{dt} \tag{5.9}$$

Where e represents the instantaneous induced voltage across the winding, N is the number of winding turns, A is the effective core cross-sectional area, and $\frac{dB}{dt}$ is the time rate of change of induction in the core measured in Tesla per second.

The main advantage of this approach is that hysteresis traces can be obtained under the actual operating conditions and environment of the core and as a function of real time. Although this technique has been used primarily with sinusoidal excitation, it is adaptable to excitation of almost any type of waveform.

5.5 MEASUREMENT OF THE TRANSFORMER HYSTERESIS CYCLE USING STANDARD MEASUREMENT

A single phase distribution transformer has been tested. The dry-type transformer has the following characteristic: 5-kVA, 7.62-0.230-kV, and 50 Hz with a core-type structure. The hysteresis measurement has been carried out by means of the dynamic hysteresis measurement. A linear power source has been used to feed the test coil and an electronic scope-meter has been used to capture the current and voltage samples. Figure 5.15 present the hysteresis cycle measured.

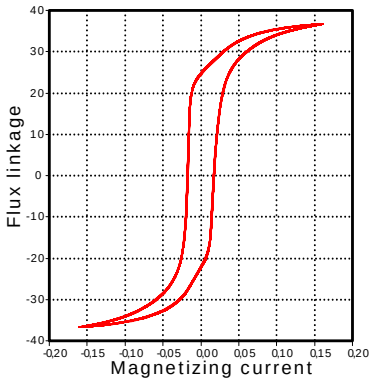

Figure 5.15. Hysteresis major loop calculated by standard measurement

The main advantage of using this approach is the facility of computing the data. Modern electronic equipment has an immense capacity of digitalize and process signals. The noise filtering for high harmonics in the capture probes is easily clean in the built-in software include in such scope-meters. The diversity of functions only depends on the test probes available. Volt-meter or Amp-meter capabilities are included directly in the scope. Data acquisition is one of the most useful tools. All the signals scoped can be quickly digitalized and transferred to a computational environment.

5.5.1 *Determination of Hysteresis using Faraday method*

The hysteresis loop is often expressed in the plot form of the voltage integral as a function of the magnetizing current [30]. It is worth remarking that in two-terminal electromagnetic element the voltage integral is known as the flux linkage and represents a specific magnetic property. The mathematic form is denoted by:

$$\lambda = \int \varepsilon \, dt \tag{5.10}$$

where ε represents the potential difference between the winding terminals. By utilizing this concept, there could be a path to measure the hysteresis of an inductor by integrating the measured voltage feed to the test transformer. Since normal steady state in a transformer does not reach saturation zones, the shape obtained under such operating conditions will not correspond to the major loop of the hysteresis. Nevertheless, in highly saturated phenomena, such as ferroresonance, it is possible to obtain maximum saturation. To implement the method the subsequent steps should be followed: (1) Long experimental time domain captures for voltage and current waveforms should be done. If possible, a case where maximum saturation is reached should be measured; (2) Voltage and current probes should be placed as closes as possible to the transformer physical terminals. It is important to approach as much as possible the measurement to as it was an inductor case instead of a transformer; (3) The post-processing of the recorded signals can be completed in MATLAB format. If the measurement were performed to the low voltage side, it is advisable to refer the data to the primary side; (4) Consequently, the voltage signal should be integrated making sure that any possible offset produced by the selected integration method has been fixed. At this point, an approximation to the actual hysteresis curve can be already plotted; (5) Frequently, filtering the signals to eliminate high order harmonic content is advisable. Recorded magnetization current occasionally could have high frequency ripples due to network or measurement equipment noise. Figure 5.16 shows the hysteresis loop obtained.

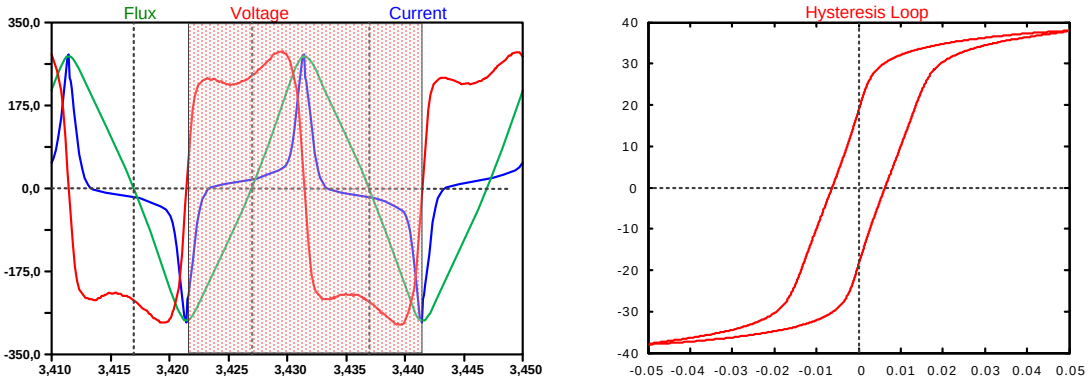

a) Captured Voltage and current waveforms

b) Hysteresis loop

Figure 5.16. Hysteresis loop calculation by Faraday method

Once the major loop is obtained (Figure 5.16b), a curve fitting approximation can be performed individually for each side of the loop (left and right) as stated in the previous sections. The resulting fitting curves are high order polynomial expression that presents the current as a function of the fluxlinked. The implementation of the equations presented in sections 5.3.3 can be done in EMTP-ATP using the TACS elements or MODELS element [31]. It is important to remark, that the calculation of hysteresis by the Faraday method is only a technique to obtain the magnetic branch of the core. In other words, is the data required for an inductor model. This inductor model should as well run within an actual transformer model such as the π model.

5.5.2 *Dual curve approximation*

As it was mentioned before, a better representation of hysteresis can be obtained if the left and right side of the loop are considered as not symmetric to each other. Then, two individual fitting can be prepared. Most of the methods used for representing hysteresis

are based on fitting approximations that take symmetry for granted. That's implies that the hysteresis loop behave the same in each quadrant. The proposal presented in this section tries to prove that using two different curves fitted to each side of the hysteresis loop would improve the core representation. Consequently, the model will give better representations to transient phenomena such ferroresonance. The two curves can be broken in four sub sections; this will permit having control of almost the whole formation of the current waveform. Figure 5.17a presents the hysteresis cycle using the broken dual curve approximation. Figure 5.17b presents how the current created manipulates the formation of the voltage waveform.

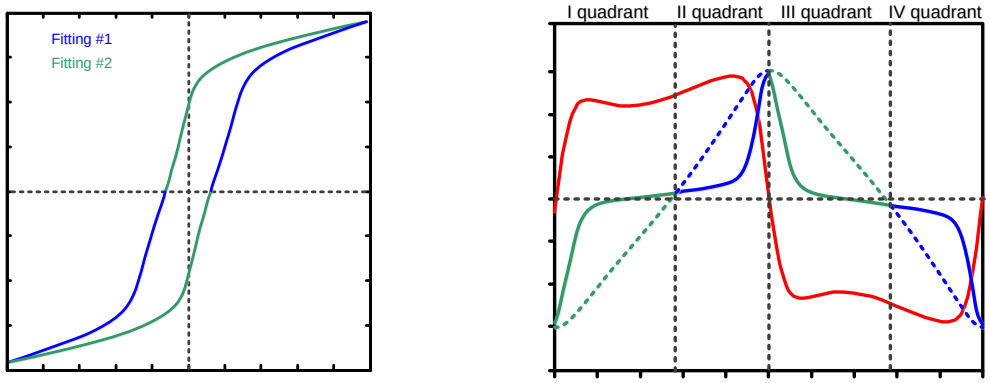

a) Clipping the curves b) Influence zones of the curves

Figure 5.17. Hysteresis dual curve technique implementation

The technique described before can be implemented in EMTP-ATP, several tools and design strategies can assist the modeling. It is worth to remark that the hysteresis technique will be a complement to the transformer model selected. In this case the π transformer model will include the hysteresis characteristic implemented through a TACS and MODELS arrangement.

5.5.3 *Experimental studies and validation*

Different experimental data has been collected from ferroresonance cases involving single-phase transformers. Figure 5.18 shows the configurations prone to ignite ferroresonance.

The objective of those configurations is to analyze some possible situations prone to the ferroresonance phenomenon containing different ferroresonant modes, where capacitive effects interacting with the transformer could be found in series (C_g), parallel (C_s), or a combination of both. It is needed to remain the purpose of each configuration: Configuration 1 represent those cases where ferroresonance has been ignited by a grading capacitance. Configuration 2 represents cases where besides the grading capacitance, the capacitive effect among the supply cable are significant enough to contribute in ferroresonance formation. Configuration 3 is a special case based on the fact that most of distribution transformers generally are fed through two phases, instead of one phase and the neutral. In that case, there can be a capacitance (C_s) connected in parallel to each phase. For all configurations, ferroresonance phenomenon will be initiated either by energizing or de-energizing the transformer. It is important also to keep in mind that the voltage source is connected to the low voltage secondary side.

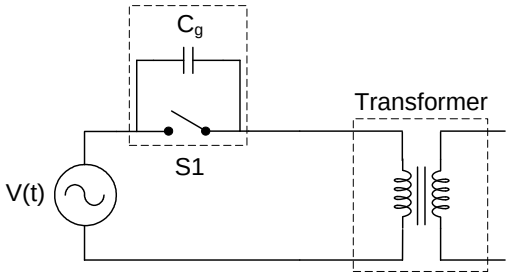

a) Configuration 1

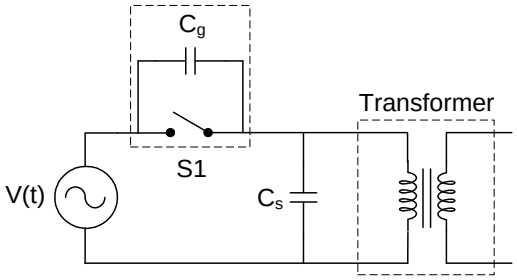

b) Configuration 2

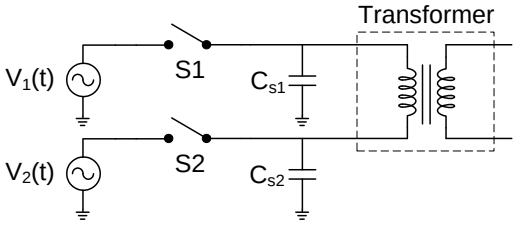

c) Configuration 3

Figure 5.18. Laboratory tests for ferroresonance analysis.

5.5.4 *Dual curve model benchmarking: Oil immerse transformer*

It is important to evaluate the operation of the model based on the *dual curve approximation* with those models presented in a previous work [32]. Three different tests have been carried out using a 5 kVA 7.62-0.240 kV 60 Hz single-phase transformer connected using Configuration 3. The three cases differ by its shunt capacitance value: a) 5 μF, b) 50 μF, c) 60 μF. This parameter is of interest because it represents the capacitive effect presented in the cable feeding the transformer. In addition, changing the value will lead to a change in the way ferroresonance is presented, having different transient and amplitude in its final state. Table 5.2 shows the data required to implement the transformer using the π model. Figure 5.19 shows the hysteresis curve for the core representation. Capacitive effects between windings were not measured for this case, and they were not considered in simulations.

Table 5.2: data for π model implementation

Resistances and linear inductances			
R_H (Ω)	R_L (Ω)	$L_{leakage}$ (mH)	R_{core} (Ω)
86.038966	0.077426	386.984804	3949114.557

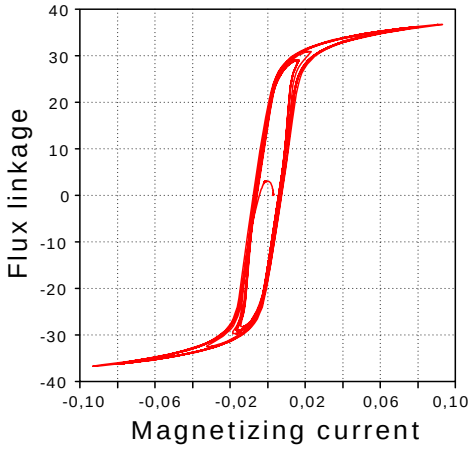

Figure 5.19. Case Study 3 - Hysteresis loop.

5.5.4.1 Case A: C_s=5 μF

The first case deals with the de-energizing voltage transformer using Configuration 3 while having a shunt capacitance value of 5 μF. Figure 5.20 presents the evaluation of the steady state condition of the signal produced by the dual curve model against the different approximations made until this moment.

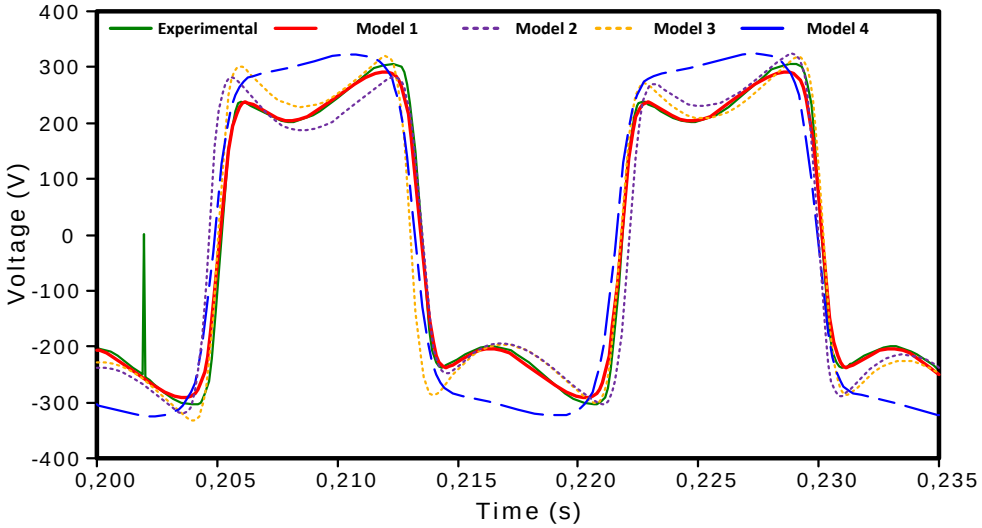

Figure 5.20. Case Study A - Comparison between models response.

The specific descriptions of the waveforms are as follow: The Model 1 is the *Dual Curve model*. The Model 2 represented by a dotted purple line proceed from the Hysteresis π model when considering only the major loop. The Model 3 marked as a dotted yellow line is obtained using the Hysteresis π model including minor loops [32]. The Model 4 is presented by a dashed blue line produced by means of the Hysteresis π model using the hysteresis cycle measured by the standard measurement [15]. It is evident from Figure 5.20 that the dual curve model gives the neatest result, therefore, it is the only model considered for the rest of the waveforms analysis. Figure 5.21 presents the complete waveform obtained during the de-energization of the transformer. The simulated results using the dual core mode have been overlapped to the experimental measurement to have a clear comparison.

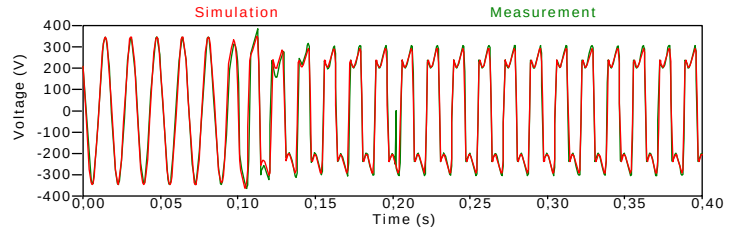

a) Ferroresonance waveform

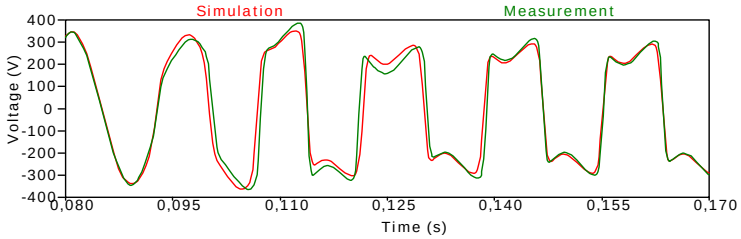

b) Transient state

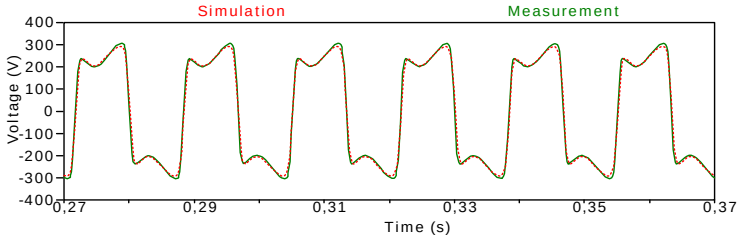

c) Ferroresonance final State

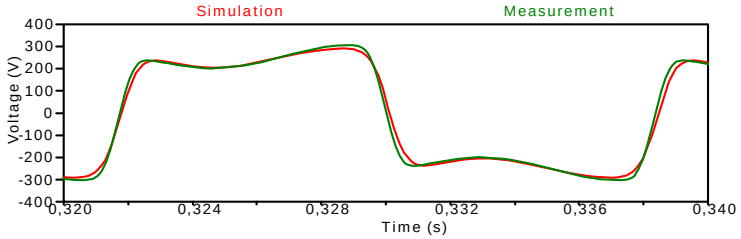

d) Cycle close-up

Figure 5.21. Case Study A - Configuration 3 – De-energization: Comparison between simulation results and laboratory measurements using the Dual Curve model.

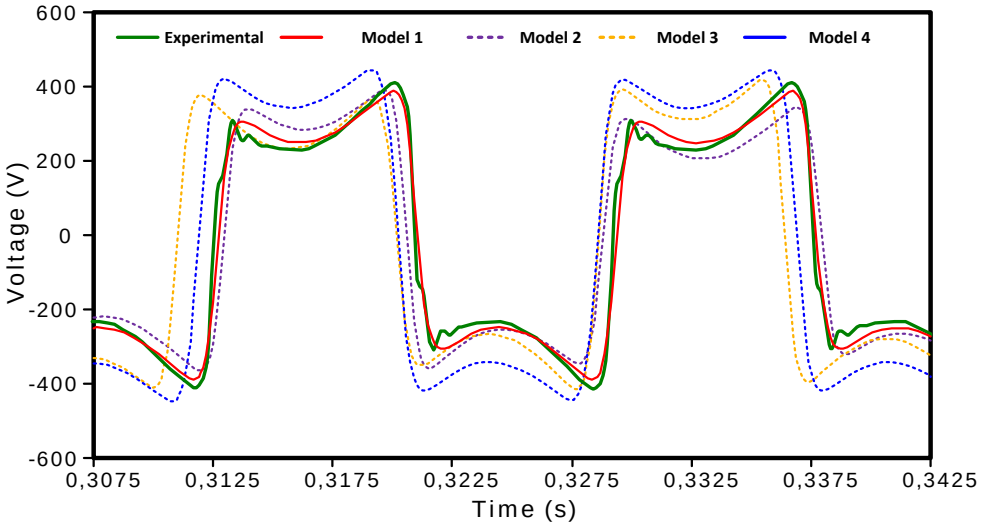

Figure 5.22. Case Study B - Comparison between models.

The Dual Curve model is an improved version of the π model and overcome any other single phase transformer models used previously. The simulation result in the transient state come notably near to the experimentation waveform and taking into consideration how unpredictable a transient can be, it means an important step forward in the voltage transformer modeling.

5.5.4.2 Case B: C_s=50 μF

For the second case the shunt capacitance values has been changed to 50 μF. The evaluation goes by comparing the results given by the computational model against the experimental waveforms. Figure 5.22 presents the comparative between different model approximations to the experimental result in the steady state.

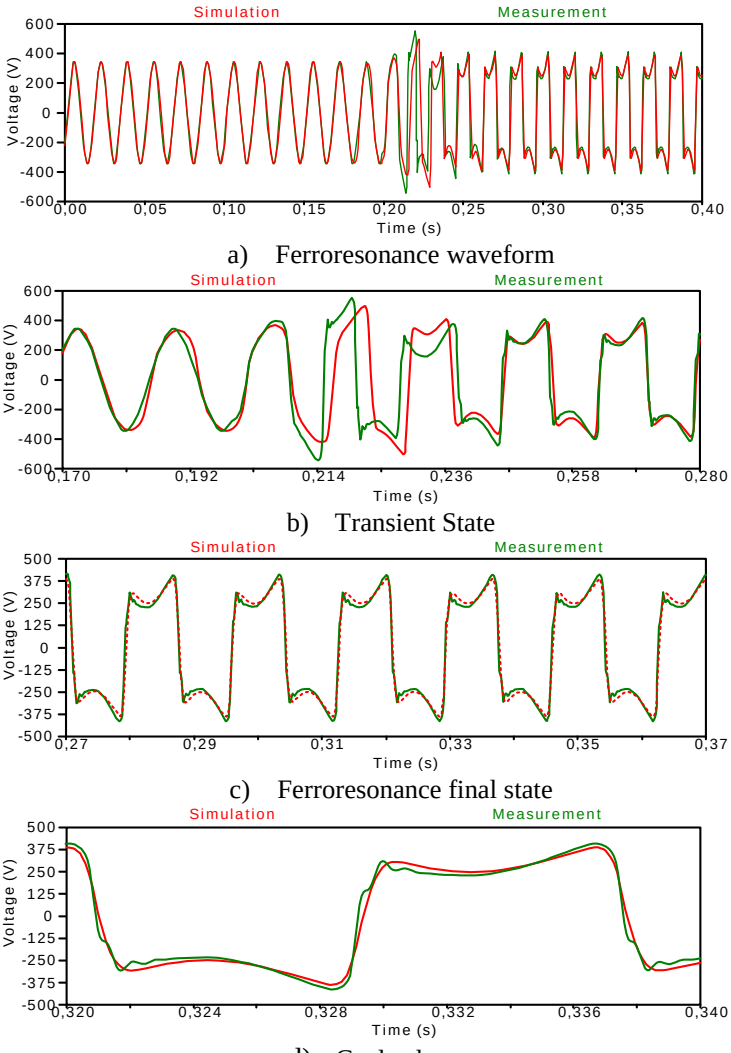

Figure 5.23. Case Study B - Configuration 3 - De-energization: Comparison between simulation results and laboratory measurements using the Dual Curve model.

The models used have been described in the previous section. Since the π is the based on all the models used, ferroresonance is correctly predicted by all of them. Nevertheless, the accuracy changes depending on the technique used to represent the core. Drawbacks such as phase-shift or amplitude inaccuracies have been proved to depend on the hysteresis model used. It is clear that the Dual Curve model approaches most to the experimental measurement. For this reason, in Figure 5.23 only the Dual Curve model is considered.

In this particular case, the experimental signal has been affected by a high order harmonic distortion coming from the network while the test was made. That distortion made its validation really difficult when using the π model with any core representation studied in the previous chapters. However, the Dual Curve model has come really close to represent the waveform behavior of the ferroresonance. This could lead to inquire that a good core representation is more valuable to ferroresonance simulation than the unusual parameter coming from the network.

5.5.4.3 Case C: C_s=60 μF

The last comparison contrast the results given by the Dual Curve model against the experimental measurements. The shunt capacitance has been changed to 60 μF. Before ongoing deeper in the analysis, Figure 5.24 presents a steady state comparative between different models to a ferroresonance experimental signal.

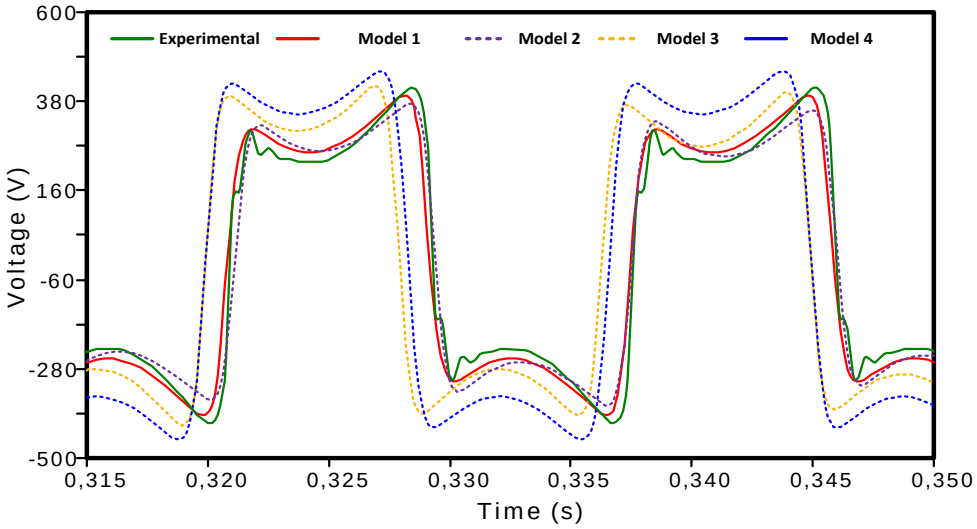

Figure 5.24. Case Study C - Comparison between models.

Besides Model 1, the rest of the models have been missing accuracy in the waveform representation. As it has been stated, the formation of the minor loops plays an important role in the depiction of waveforms whose amplitude differs with respect to its sinusoidal state. Since Model 2 uses a technique in which the creation of minor loops is concurrent to the flux amplitude the waveform construction has become more precise. Figure 5.25 presents the complete waveform obtained during the de-energization maneuver and the corresponding comparison to the Dual Curve model.

Notice that although internal capacitive effects were not considered, a good match between simulation and measurements was obtained, since differences between waveforms were not too large. It may be concluded that internal capacitive effects for the transformer are not too decisive in the benchmarking. On the other hand, once again, better hysteresis representation has proven to be a dominant parameter. It's been concluded that current waveform is highly dependent on the hysteresis shape. Indirectly, hysteresis characteristic form will also affect the ferroresonance waveform, because of the influence current waveform has over ferroresonance signal formation.

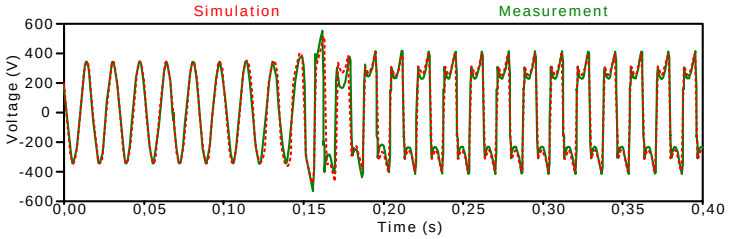

a) Ferroresonance Waveform

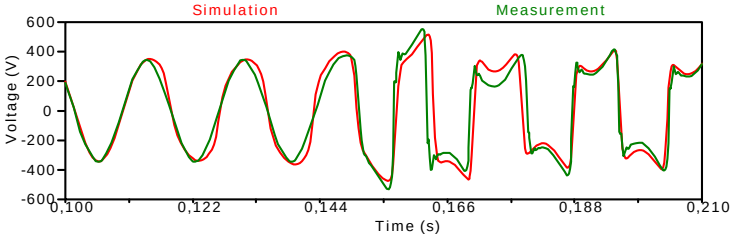

b) Transient State

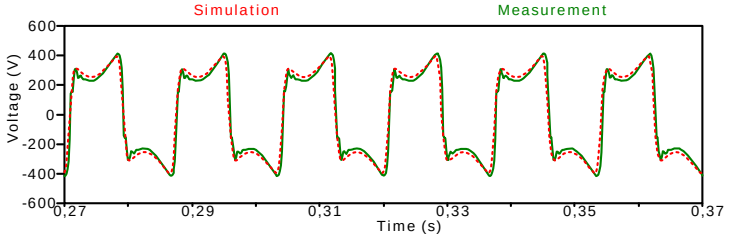

c) Ferroresonance final state

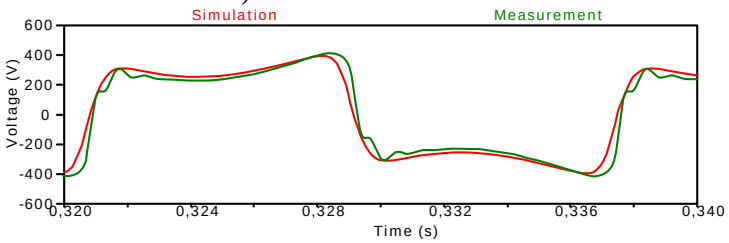

d) Cycle close-up

Figure 5.25. Case Study C - Configuration 3 – De-energization: Comparison between simulation results and laboratory measurements using the Dual Curve model.

5.5.5 *Dual curve model benchmarking: Dry-type transformer*

Several essays have been carried out on a 5-kVA, 7.62-0.230-kV, and 50 Hz single-phase transformer. The purpose of the tests is to back up the theory for Dual Curve Hysteresis model. Each test has a different configuration set of parameters. Hence, the capacitance values presented in the circuit are changed and also the circuit topology used to ignite the ferroresonance phenomenon. Table 5.3 resume the circuit parameter used to configure the transformer model. Figure 5.26 shows the hysteresis cycle implemented in the model using the dual curve approximation.

Table 5.3: data for π model implementation

Resistances and linear inductances			
R_H (Ω)	R_L (Ω)	$L_{leakage}$ (mH)	R_{core} (Ω)
70.385861	0.062964	409.305244	1297659.635

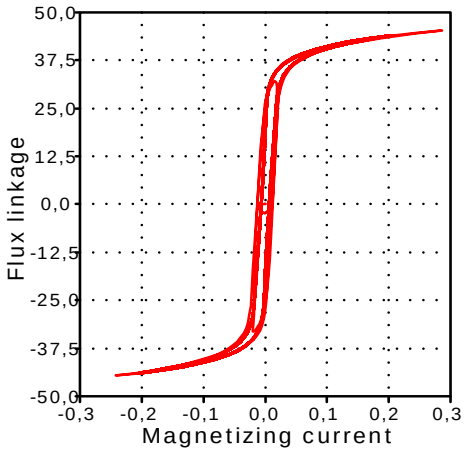

Figure 5.26. Dual Curve model benchmarking - Hysteresis loop.

All tests performed to the transformer have been executed on the low voltage side through a 230 V, 5 kVA linear source. The experiments are organized as follows:

A. De-energization of the transformer connected in Configuration 1 and having a grading capacitance value of 17 μF.

B. Two different energization cases were considered to a transformer connected in Configuration 1 and having grading capacitance values of 17 and 20 μF, respectively.

C. Two cases of de-energization maneuver were made, both having Configuration 2 with a fixed parallel capacitance value of 10 μF and a series capacitance value changing from 17 to 20 μF, respectively.

D. Two energization cases with Configuration 2 were carried out. A fixed parallel capacitance value of 10 uF was considered for both cases. The series capacitance value was changed from 15 μF in the first case to 17 μF for the last case.

5.5.5.1 Case Study A

The intention of the case study is to establish the feasibility of the Dual Curve model in the representation of the ferroresonance phenomenon. For that purpose, simulation results are compared to experimental measurement; the results are presented in Figure 5.27.

It was only possible to obtain a single experimental sample for the de-energization case of Configuration 1. However, the comparison gives a clear sight on the improvement of the model. The steady state waveform generated with the model has a high accuracy percentage and nearly overlaps to that waveform experimentally acquired.

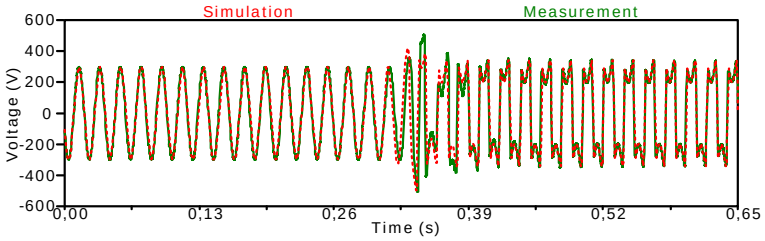

a) Ferroresonance waveforme

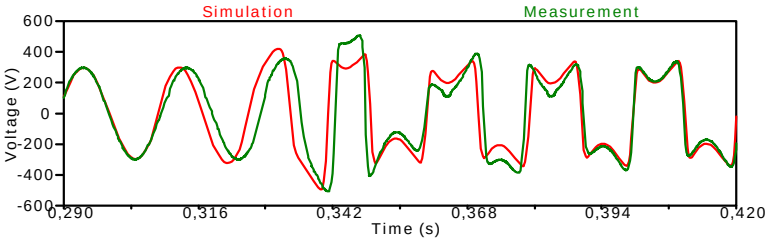

b) Transient State

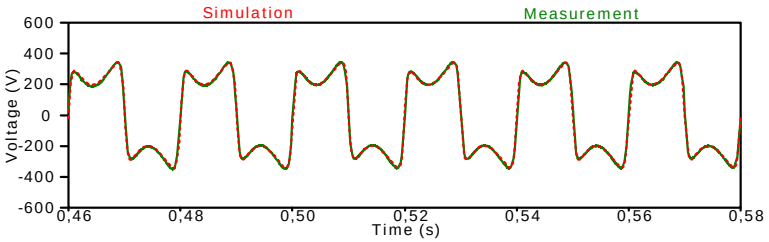

c) Ferroresonance final state

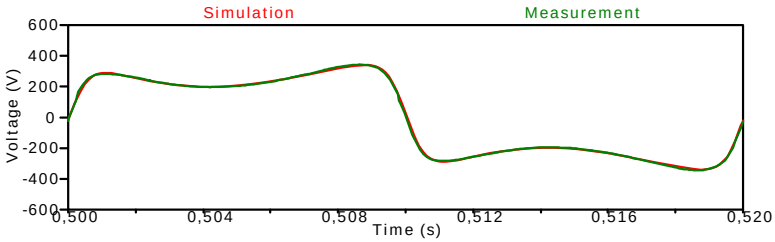

d) Signal Close-up

Figure 5.27. Case Study A - Configuration 1 – De-energization: Comparison between simulation results and laboratory measurements using the Dual Curve model.

5.5.5.2 Case Study B

For this case study, two different grading capacitance values were tested. The results for the circuit operating with a capacitance value of 17μF are presented below. Figure 5.28 show the waveforms comparison.

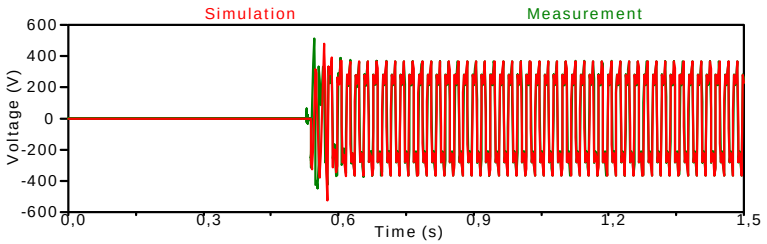

a) Ferroresonance waveforme

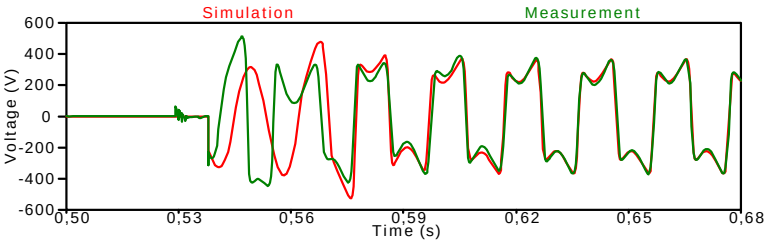

b) Transient State

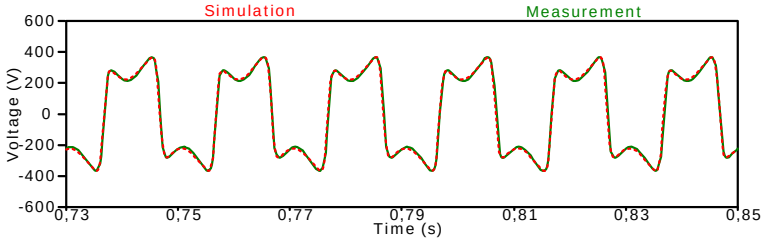

c) Ferroresonance final state

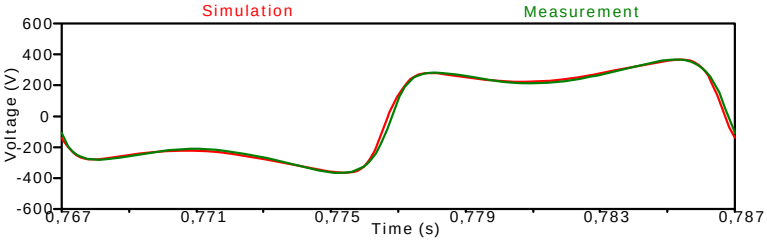

d) Waveform Close-up

Figure 5.28. Case Study B - Configuration 1 - Energization: Comparison between simulation results and laboratory measurements using the Dual Curve model.

Results obtained with the model are really good. Comparison in the ferroresonance final state from Figure 5.28c and 5.28d are really close in form. The transient part seems to be a little distorted but it is acceptable considering its unpredictability in form and how quickly it gets in track to change to the steady state.

The second energization case was made to the transformer connected in Configuration 1; the grading capacitance value was changed to 20 μF. Figure 5.29 presents the waveform analysis.

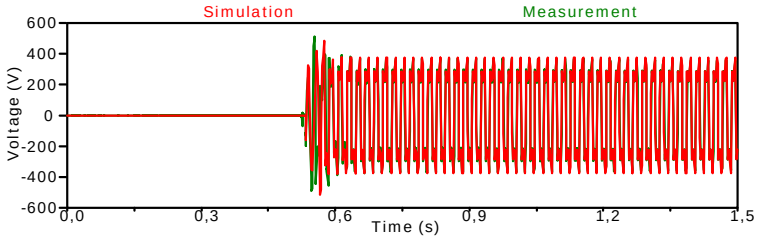

a) Ferroresonance waveform

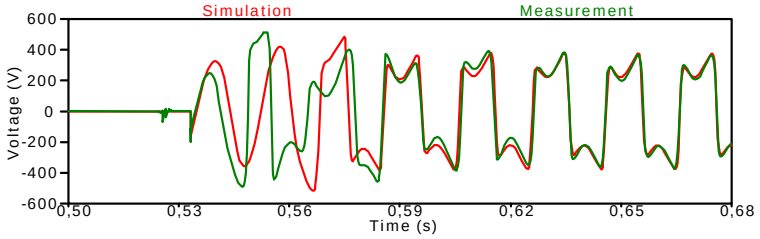

b) Transient State

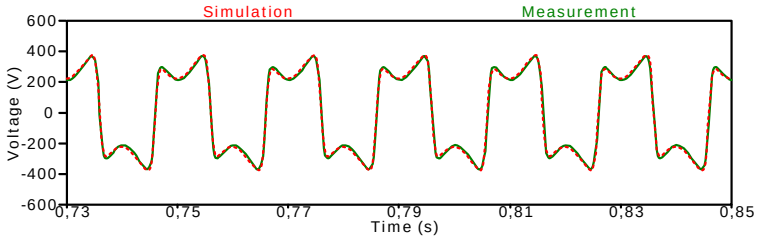

c) Ferroresonance final state

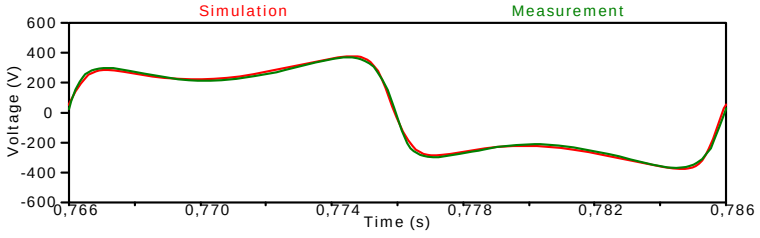

d) Waveform Close-up

Figure 5.29. Case Study B - Configuration 1 - Energization: Comparison between simulation results and laboratory measurements using the Dual Curve model.

5.5.5.3 Case Study C

The third case study was carried out using Configuration 2. The ferroresonance circuit created for this configuration has two different capacitive effects. Two cases have been considered. The first one presented below has a series capacitance value of 17 μF and a parallel capacitance value of 10 μF. Figure 5.30 presents the waveform analysis on the maneuver performed to the circuit.

As it can be seen in Figure 5.30, the model representation has a high precision level. The transient state depiction in Figure 5.30b has a quite accurate correspondence to the experimental measurement.

The second test in this case study presents a series capacitance of 20 μF and a parallel capacitance of 10 μF. Figure 5.31 presents the comparison with the experimental measurement.

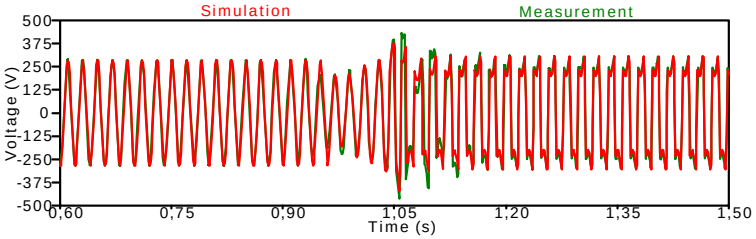

a) Ferroresonance waveform

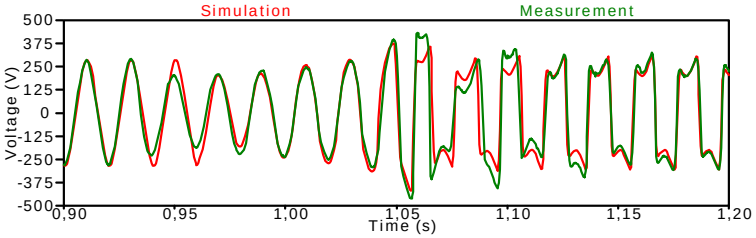

b) Transient State

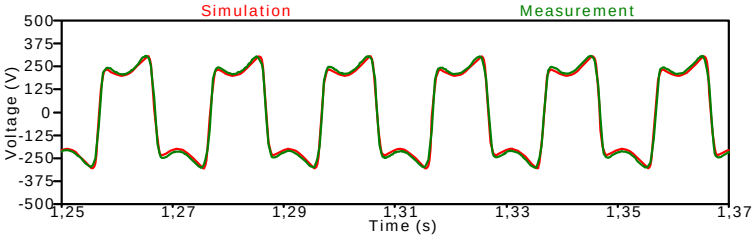

c) Ferroresonance final State

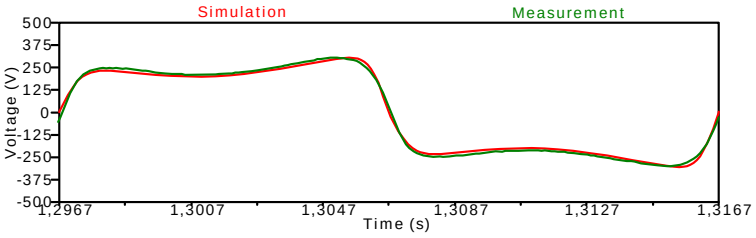

d) Waveform Close-Up

Figure 5.30. Case Study C - Configuration 2 – De-energization: Comparison between simulation results and laboratory measurements using the Dual Curve model.

For this case, it has been settled that the Dual Curve model has the capability not only to represent ferroresonance steady state correctly but also to reach an acceptable matching during the transient state. This characteristic means an important improvement over the π transformer model considered in previous chapters. In the same way, reaffirm the theory that ferroresonance waveform main dependence relies in the core hysteretic representation.

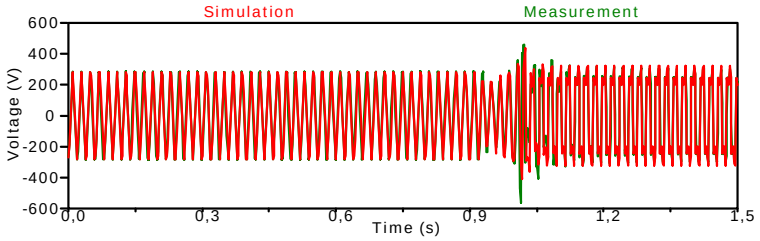

a) Ferroresonance waveform

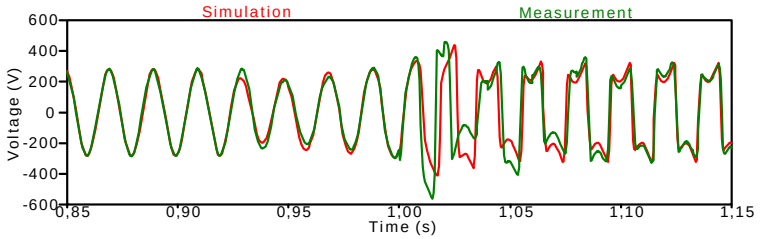

b) Transient State

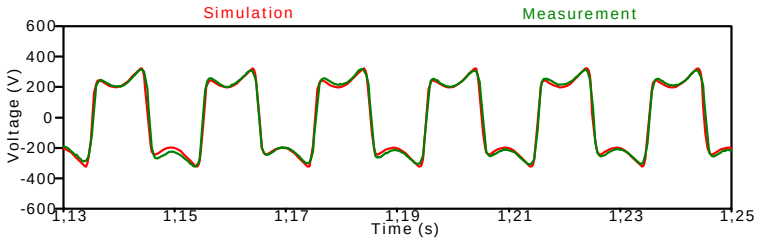

c) Ferroresonance final state

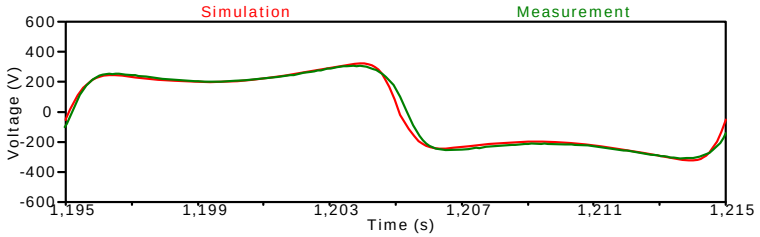

d) Waveform Close-up

Figure 5.31. Case Study C - Configuration 2 – De-energization: Comparison between simulation results and laboratory measurements using the Dual Curve model.

5.5.5.4 Case Study D

The last case study evaluates two different situations for the energization maneuver. In the first test, the series capacitance value is 15 μF and the parallel capacitance value is 10 μF. Figure 5.32 presents the signal analysis.

Transient state of an energization case is certainly a more complex condition than those transient obtained in a de-energization case. Not having a previous sinusoidal state as reference makes the energization initial transient an unpredictable stage because the model has to be initiated directly into a fault state. Nevertheless, the Dual Core model has proven to appropriately represent energization case in all its stages. On the last part of the study, again a Configuration 2 circuit is used to energize the voltage transformer. The series capacitance value is 17 μF and the parallel capacitance value is 10 μF. Figure 5.33 presents the waveform analysis.

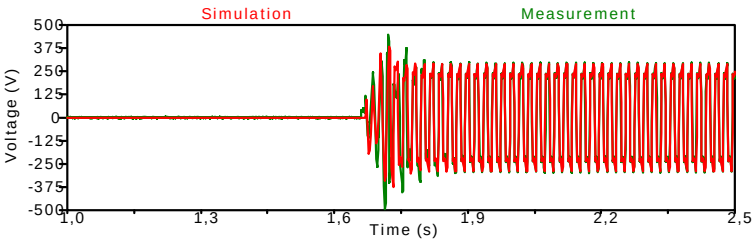

a) Ferroresonance waveform

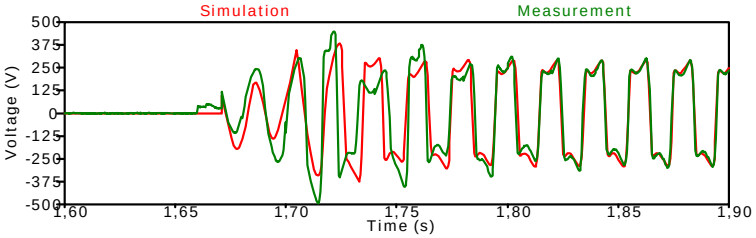

b) Transient State

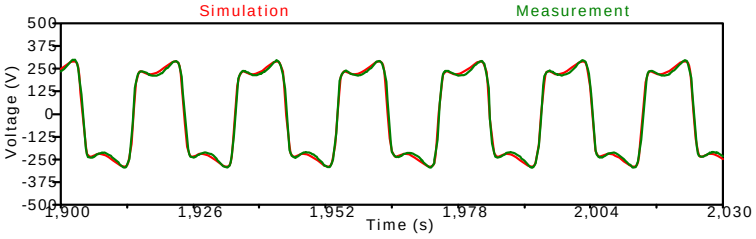

c) Ferroresonance final state

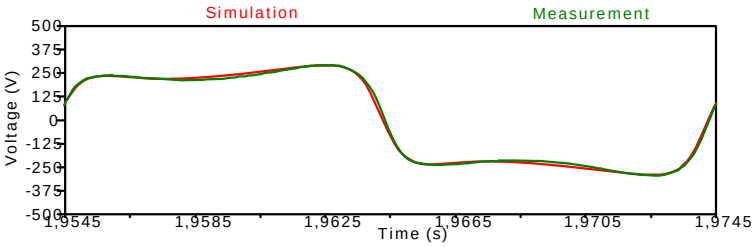

d) Waveform Close-up

Figure 5.32. Case Study D - Configuration 2 - Energization: Comparison between simulation results and laboratory measurements using the Dual Curve model.

This case presents a longer transient stage. However the model response is in good agreement with the experimental waveforms and the result obtained is significantly good.

It can be concluded that, up to seven different ferroresonance cases have been studies and validated to benchmark the Dual Curve Hysteresis model. The results obtained have been conclusive over the feasibility of the model to properly represent the ferroresonance phenomenon. Some important improvement has been shown in comparison to the previous π model presented. The matching during the transient period gives an important insight of the model properly working for different ferroresonance waveforms. The obtained precision in the ferroresonance steady state is sufficient to validate the model and to concludes that the results significantly overcomes any result obtained with previous models.

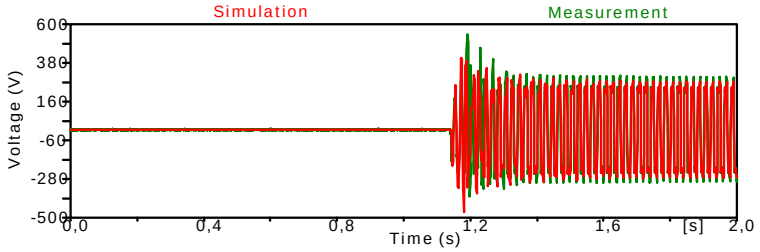

a) Ferroresonance waveform

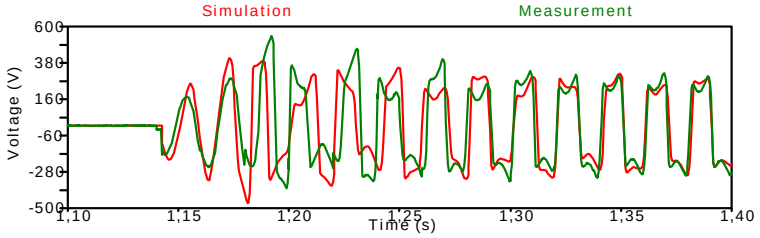

b) Transient State

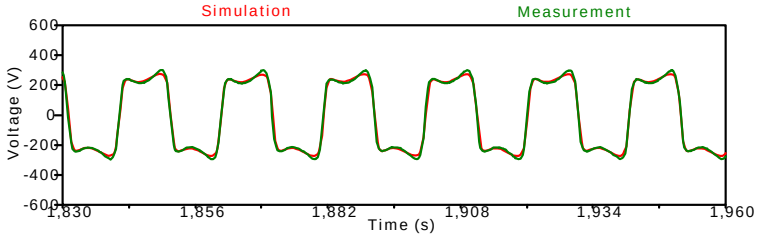

c) Ferroresonance final state

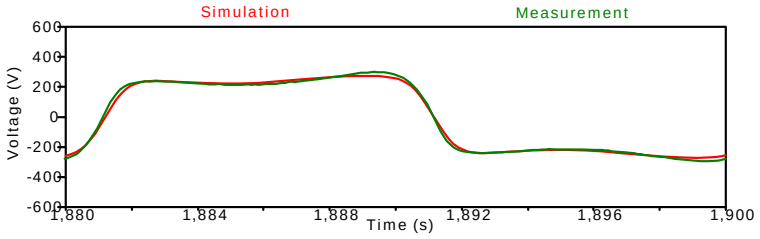

d) Waveform Close-up

Figure 5.33. Case Study D - Configuration 2 - Energization: Comparison between simulation results and laboratory measurements using the Dual Curve model.

5.6 HYSTERESIS DYNAMIC BEHAVIOUR UNDER DIFFERENT FERRORESONANCE MODES

Ferroresonance phenomenon has been described in the literature as an electrical resonance condition associated with the saturation of a ferromagnetic device, such as a transformer through capacitance. [33]. By definition ferroresonance gets directly influenced by the actions of ferromagnetic materials. Thereby, accurate representation of magnetic behavior will directly means having a more realistic representation of ferroresonance [34]. Accurate core models for true hysteresis behavior including major and minor loop effects are crucial for reliable ferroresonance predictions [35]. Hysteresis is the central feature magnetic cores and its dynamic behavior has been proved to impact the stability domains of the formation of ferroresonance modes [36].

In other words, if hysteresis cycle keeps a symmetrical behavior, ferroresonance waveform will also maintain a symmetrical formation.

As it is widely known, the magnetic core characteristic is composed by all the reversible and irreversible components presented in the iron. Probably the most important of the core nonlinear characteristic is the hysteresis cycle. Within the literature it is possible to find the exact theoretical composition of the hysteresis phenomenon [19],[35]. This is, in all ferromagnetic materials three different types of loops can be observed: 1) The largest loop which is the hysteresis major loop; 2) Symmetric minor loops; and 3) Asymmetric minor loops. Fundamentally, all this hysteresis features form the referred dynamic behavior of an iron core. Currently the existing transformer models, even the topology-based models which provide the most accurate representations of the iron core [3], [37]–[40], represent the core based on one of the following approaches:

- *Constant core loss resistance-based core models*
- *Dynamic core loss resistance-based core models*
- *Frequency-dependent core models*

Nowadays, there are several limitations associated with every core representation. Problems related to the instantaneous core loss modeling are known to be the origin of inaccuracies while representing a transient state. In such stages, the hysteresis loop width (coercive forces) is stretching in and out as the amplitude of the excitation current varies rapidly. These conditions, in a core model that do not consider dynamic losses representation, will make impossible to represent a transient accurately. Other limitations associated to the non-symmetric properties of the hysteresis are presented in the actual core models. The asymmetric effect on hysteresis has been widely demonstrated to be caused by the nature of the excitation waveform [41]-[45]. In transformer modeling, this principle works in the opposed direction. A core model that includes the non-symmetrical characteristic will be able to replicate non-periodic waveforms. However, the majority of current models do not consider such effects due to its complexity making the simulation of non-periodic waveforms a tricky assignment.

A series of six experiments have been developed to study those dynamic changes made by the core characteristic of a transformer when a non sinusoidal excitation is induced. The experiments have been carrying out by taking into account periodic and non periodic signal. A pseudo-ferroresonance waveform has been created using a linear power source 0-300 V 5 kVA 0-5000 Hz with the capability of designing desired waveforms though a Fourier analysis. Once the test signal is created, the new voltage waveform is supplied to a 5 kVA, 7.62-0.230 kV for a few seconds with the intention of replicate the same stress generated by a real ferroresonance case, then the dynamic hysteresis can be measured. It is worth to remark that all the waveform created has been based on real ferroresonance signals.

5.6.1 *Waveform Study 1*

A typical periodic ferroresonance signal has been created and fed to the transformer. The hysteresis cycle continues to preserve the sigmoid shape as in the case of sinusoidal excitation. Figure 5.34 presents the details.

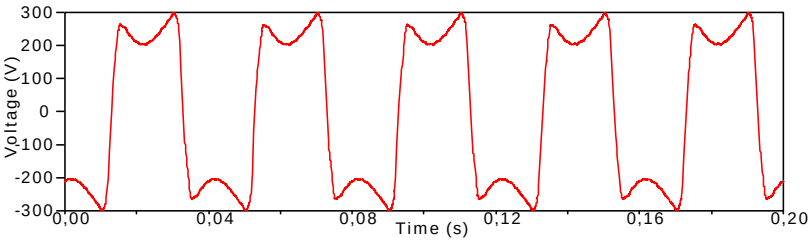

a) Voltage waveform

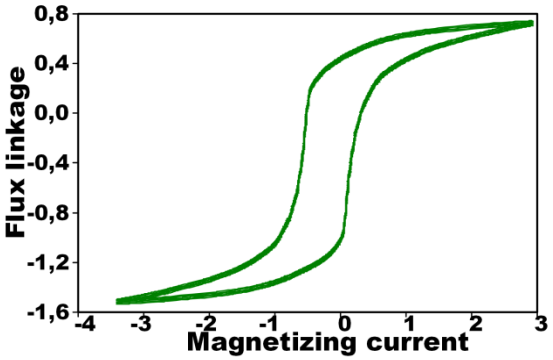

b) Hysteresis cycle

Figure 5.34. Waveform Study 1 - Periodic ferroresonance signal.

5.6.2 *Waveform Study 2*

A period-1 ferroresonance signal has been created and implemented. The harmonic distortion in this waveform is significantly bigger that the one presented in the Study 1. Figure 5.35b presents the distortion in the hysteresis cycles which starts to lose the smoothness in the residual flux zones and losing the sigmoid shape.

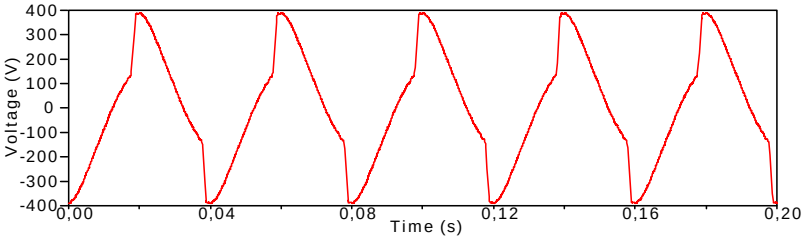

a) Voltage waveform

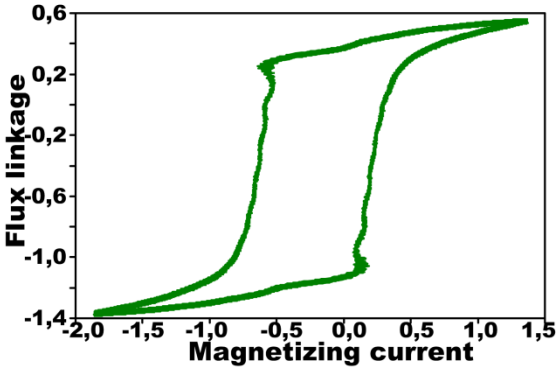

b) Hysteresis cycle

Figure 5.35. Waveform Study 2 – Period-1 ferroresonance signal.

5.6.3 *Waveform Study 3*

A ferroresonance period-2 has been supplied to the transformer. Figure 5.36b shows the coexistence of two separated loops. It is worth to remark that for this case the dynamic part of hysteresis cycle happens inside the third quadrant.

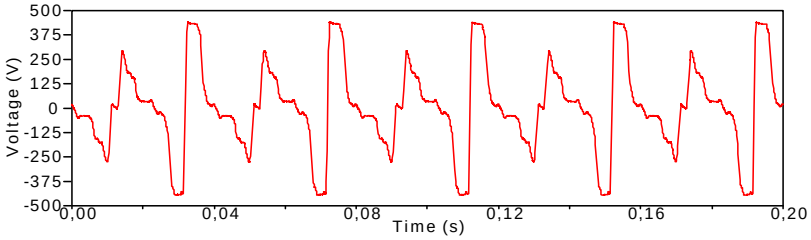

a) Voltage waveform

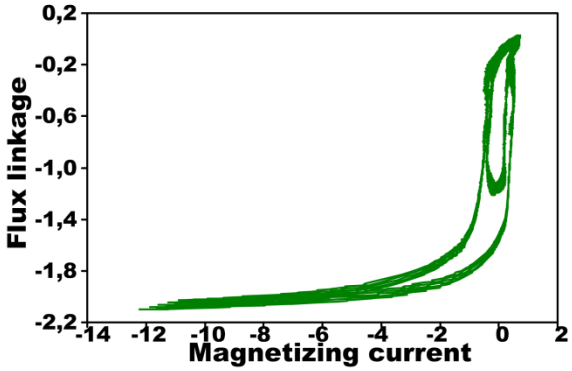

b) Hysteresis cycle

Figure 5.36. Waveform Study 3 - Period-2 ferroresonance signal.

5.6.4 *Waveform Study 4*

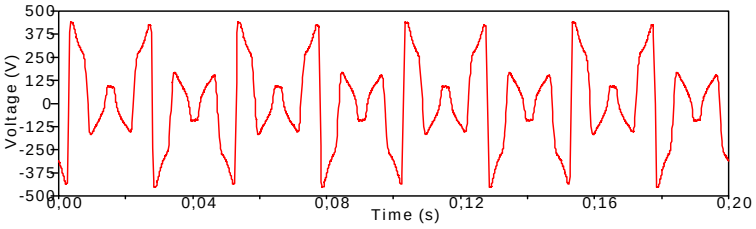

a) Voltage waveform

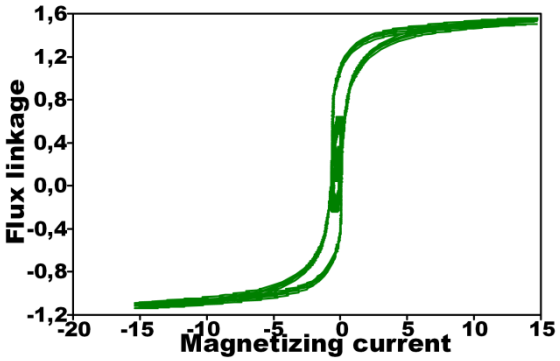

b) Hysteresis cycle

Figure 5.37. Waveform Study 4 - Period-3 ferroresonance signal.

A period-3 ferroresonance signal is presented. Figure 5.37b presents how three clear orbits have been formed in the hysteresis cycle. This type of waveforms are still in the domain of normal hysteresis core models because the internal loops formed are symmetrical and do not implies a distortion to the major loop.

5.6.5 *Waveform Study 5*

Sub-harmonic state is common in ferroresonance cases, mostly when more than one capacitance effect is presented in the circuit that ignites the phenomenon. It is clear in Figure 5.38b that the major loop has been distorted and strange trajectories are creating the cycle. The majority of core models presented in the literature do not consider this type of dynamics.

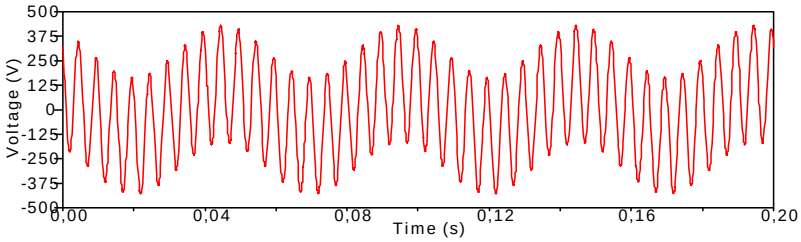

a) Voltage waveform

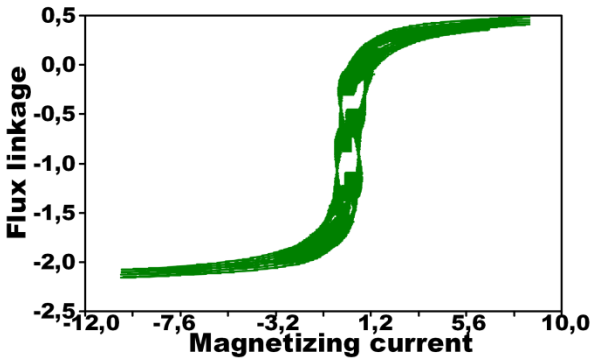

b) Hysteresis cycle

Figure 5.38. Waveform Study 5 - Sub-harmonic ferroresonance signal.

5.6.6 *Waveform Study 6*

Finally, a close to chaotic state was tried to be represented. A chaotic state is a complicated region to be defined but generally it implies having as many responses as possible within a period. Figure 5.39b shows how the cycle got into an asymmetrical dynamic. The minor loops are not following the sigmoid shape that, however, the major loop follows. This complex behavior is not easy to be represented in a mathematical approach and will result in a complex simulation resolution of any model. In addition, it should be remarked that this type of behavior resemblance closely to those transient states obtained between sinusoidal state and periodic ferroresonance.

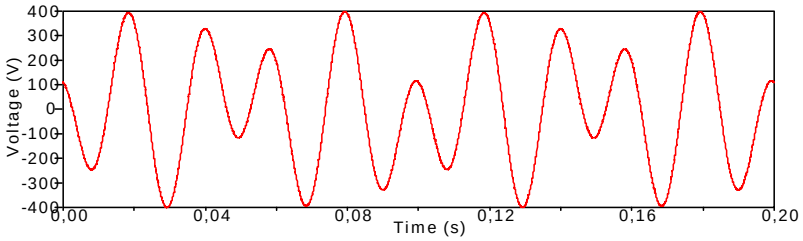

a) Voltage waveform

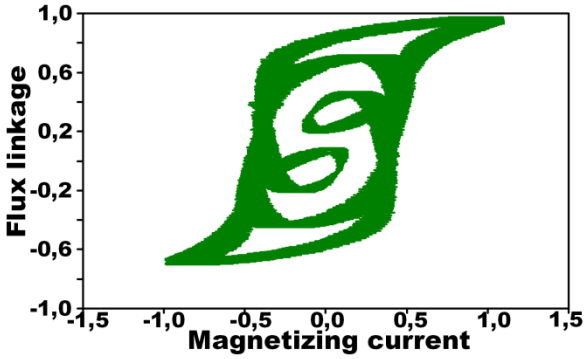

b) Hysteresis cycle

Figure 5.39. Waveform Study 6- Chaotic ferroresonance signal.

As it has been seen, ferroresonance cases where the 'excitation' becomes frequency independent and the harmonic distortion level is over 50%, will be almost impossible to reproduce. In a way, it may be reasonable not considering such hysteresis dynamics, since its computational representation requires an important mathematical implementation, as well as the vast amount of data that could be necessary to execute it and solving it [46][47]. Nevertheless, it is essential to try characterizing those dynamic behaviors and adapt them to transformer modeling.

On the other hand, it is important to remember that an ideal transformer model should always dwell in a zone where its solution remains fast, reliable and easy to understand. Nowadays, it is still difficult to find a model that accurately and generally describe all the phenomena involved in true core nature [48],[49]. In general, preparing a mathematical model that includes most of the behaviors that the hysteresis cycle can present may be a remarkable task.

5.7 CHAPTER SUMMARY

This chapter has proposed a new method for hysteresis calculation based in Faraday's theory. Even though, the approximation obtained is not the actual *B-H* curve is completely valid for transformer modeling. A new technique for implementation of the hysteresis cycle is also proposed in the Chapter, explaining clearly the steps to follow to include it in the π equivalent model. Finally, several validations are performed demonstrating the enhancement in the model response when the hysteresis is included. In the last part of the Chapter, dynamical behavior of the hysteresis is studied briefly with the intention to draw the line to follow for future work.

5.8 REFERENCES

[1] S. V. Kulkarni, and S. A. Khaparde. *Transformer engineering: design and practice*, CRC Press, 2004.

[2] C. McLyman, *Transformer and inductor design handbook*, CRC press, 2011.

[3] J.A. Martinez-Velasco and B.A. Mork, "Transformer modeling for low- and mid-frequency transients - A review," *IEEE Transactions on Power Delivery*, vol. 20, no. 2, pp. 1625-1632, April 2005.

[4] F. de León, P. Gómez, J.A. Martinez-Velasco, and M. Rioual, "Transformers," Chapter 4 of *Power System Transients. Parameter Determination*, J.A. Martinez-Velasco (ed.), CRC Press, 2009.

[5] E.C. Cherry, "The duality between interlinked electric and magnetic circuits and the formation of transformer equivalent circuits," *Proc. of the Physical Society, section B*, vol. 62, pp.101-111, 1949.

[6] L. F. Blume, A. Boyajian, G. Camilli, T. C. Lenox, S. Minneci and V. M. Montsinger, *Transformer Engineering: A Treatise on the Theory, Operation, and Application of Transformers*, Wiley, 1951.

[7] G.R. Slemon, "Equivalent circuits for transformers and machines including non-linear effects," *Proc. of the IEE-Part IV: Institution Monographs*, vol. 100, pp.129 -143, 1953.

[8] H.K. Høidalen, L. Prikler, J. Hall, "ATPDraw- Graphical Preprocessor to ATP. Windows version," *International Power System Transient conference IPST*, Budapest, 1999.

[9] F. de Leon, A. Farazmand, P. Joseph, "Comparing the T and π equivalent circuits for the calculation of transformer inrush currents," *IEEE Transactions on Power Delivery*, vol.27, no.4, pp.2390-2398, October 2012.

[10] S. azebi, A. Farazmand, B.P. Murali, F. de Leon, "A Comparative Study on π and *T* Equivalent Models for the Analysis of Transformer Ferroresonance," *IEEE Transactions on Power Delivery*, vol.28, no.1, pp.526-528, January 2013.

[11] F.C.F. Guerra, W.S. Mota, "Magnetic core model, " *IET Science, Measurement & Technology*, Vol. 1, no.3, pp. 145-151, 2007.

[12] A. Rezaei-Zare, R. Iravani, "On the transformer core dynamic behavior during electromagnetic transients," *IEEE Transaction on Power Delivery*, vol.25, no.3, pp.1606-1619, July 2010.

[13] IEEE Standard, "Test Code for Liquid-Immersed Distribution, Power, and Regulating Transformers," *IEEE Std C57.12.90-2010* (Revision of IEEE Std C57.12.90-2006), October 2010.

[14] IEC International Standard, "Power transformers - Part 1: General," *IEC 60079-1*, 2011.

[15] IEEE Standard, "Test Procedures for Magnetic Cores," *IEEE Std 393-1991*, March 1992.

[16] ASTM Standard, "Test methods for alternating-current magnetic properties of materials using the wattmeter–ammeter–voltmeter method 100 to 10000 Hz and 25 cm," *ASTM Publication* A348/A348M-00.

[17] D.C. Jiles, D.L. Atherton, "Theory of ferromagnetic hysteresis," *Journal on Magnetism Magnetic Materials*, Vol. 61, pp. 48–60, 1986.

[18] S.R. Talukdar, J.R. Bailey, "Hysteresis model for system studies," *IEEE Transactions on Power Apparatus and Systems*, Vol. 95, no. 4, pp. 1429–1434, 1976.

[19] A. Rezaei-Zare, R. Iravani, "On the transformer core dynamic behavior during electromagnetic transients," *IEEE Transaction on Power Delivery*, vol.25, no.3, pp.1606-1619, July 2010.

[20] A. Gaudreau, P. Picher, L. Bolduc, A. Coutu, "No-load losses in transformer under overexcitation/inrush-current conditions: Tests and a new model," *IEEE Transactions on Power Delivery*, vol. 17, no. 4, pp. 1009–1017, Oct. 2002.

[21] D.C. Jiles, J.B. Thoelke, M.K. Devine, "Numerical determination of hysteresis parameters for the modeling of magnetic properties using the theory of ferromagnetic hysteresis," *IEEE Transactions on Magnetics*, Vol.28, no.1, pp. 27–35, 1992.

[22] D.A.N. Jacobson, P.W. Lehn, and R.W. Menzies, "Stability domain calculations of period-1 ferroresonance in a nonlinear resonant circuit," *IEEE Transactions on Power Delivery*, vol. 17, no.3, pp. 865-871, July 2002.

[23] J.R. Marti, A.C. Soudack, "Ferroresonance in power systems: fundamental solutions," *IEE Proceedings C Generation, Transmission and Distribution*, vol.138, no.4, pp.321-329, July 1991.

[24] M. Moradi and A. Gholami, "Harmonic balance based stability domain analysis of period-1 ferroresonance," *Electric Power Components and Systems*, vol. 39, no. 12, 2011.

[25] S. Mozaffari: *Chaotic ferroresonance in power transformers*, Ph.D. Thesis, University of British Columbia, 1996.

[26] Z. Stojkovic, *Computer-aided Design in Power Engineering: Application of Software Tools*, Springer Science & Business Media, 2012.

[27] J.A. Martinez-Velasco, *Power system transients: parameter determination*, CRC press, 2009.

[28] P. Ferracci, Ferroresonance, *Cahier Technique no. 190*, Groupe Schneider, 1998.

[29] F. de León, P. Gómez, J.A. Martinez-Velasco, M. Rioual, "Transformers," Chapter 4 of *Power System Transients. Parameter Determination*, J.A. Martinez-Velasco (ed.), CRC Press, 2009.

[30] A. Gaudreau, "No-load losses in transformer under overexcitation/inrush-current conditions: tests and a new model," *IEEE Transactions on Power Delivery*, vol. 17, no. 4, pp.1009-1017, 2002.

[31] H.W. Dommel: *EMTP Theory Book*, BPA, Portland, 1986.

[32] J.A. Corea-Araujo, F. Gonzalez-Molina, J.A. Martinez-Velasco, J.A. Barrado-Rodrigo, L. Guasch-Pesquer "Single-Phase Transformer Model Validation for Ferroresonance Analysis Including Hysteresis," *IEEE Power and Energy Society General Meeting*, Denver CO, United States, July 2015.

[33] *IEEE Standard Definitions for Power Switchgear*, IEEE Std. *C37.100-1992*

[34] J.C. Lacerda Ribas, et al. "Modeling ferroresonance phenomena with a flux-current Jiles-Atherton hysteresis approach," *IEEE Transactions on Magnetics*, pp 1797-1800, 2013.

[35] P. Moses, M.A.S. Masoum, H.A. Toliyat, "Impact of hysteresis and magnetic couplings on the stability domain of ferrorresonance in asymmetric three-phase three-leg transformers," *IEEE Transactions on Power Delivery*, vol. 26, no. 2, pp. 581-592, 2011.

[36] A. Rezaei-Zare, R. Iravani, M. Sanaye-Pasand, "Impacts of transformer core hysteresis formation on stability domain of ferroresonance modes," *IEEE Transactions on Power Delivery*, vol. 24, no. 1, pp. 177-186, January 2009.

[37] F. De Leon, A. Semlyen, "Complete transformer model for electromagnetic transients," *IEEE Transactions on Power Delivery*, vol. 9, no. 1, pp. 231–239, January 1994.

[38] IEEE Power Eng. Soc. Task Force on Data for Modeling System Transients, "Parameter determination for modeling system transients— Part III: Transformers," *IEEE Transactions on Power Delivery*, vol. 20, no3, pp. 2051–2062, July 2005.

[39] A. Rezaei-Zare, R. Iravani, M. Sanaye-Pasand, H. Mohseni, S. Farhangi, "An Accurate Hysteresis Model for Ferroresonance Analysis of a Transformer," *IEEE Transactions on Power Delivery*, vol.23, no.3, pp.1448-1456, July 2008.

[40] P.S. Moses, M.A.S. Masoum, H.A. Toliyat, "Dynamic Modeling of Three-Phase Asymmetric Power Transformers With Magnetic Hysteresis: No-Load and Inrush Conditions," *IEEE Transactions on Energy Conversion*, vol.25, no.4, pp.1040-1047, December 2010.

[41] D. Mayergoyz, *Mathematical Models of Hysteresis and Their Applications*, Elsevier, New York 2003.

[42] S. Lizon-Martinez, B. Tellini, R. Giannetti, G. Robles, "Measurement of Asymmetric Minor Loops in Soft Ferrites Up to Medium Frequencies," *IEEE Proceedings of Instrumentation and Measurement Technology Conference, IMTC.*, pp. 1-3, May 2007.

[43] B. Tellini, R. Giannetti, G. Robles, S. Lizon-Martinez, "New method to characterize magnetic hysteresis in soft ferrites up to high frequencies," *IEEE Transactions on Instrumentation and Measurement*, vol.55, no.1, pp.311-315, February 2006.

[44] M. Marracci, B. Tellini, "Characterization of Asymmetric Loops of Soft Magnetic Materials via the Induction Method", *Proceedings of the 12th WSEAS International Conference on Electric Power Systems, High Voltages, and Electric Machines*, Prague, Czech Republic, 2012.

[45] E. Cardeffi, R. Giannetti, B. Tellini, "Numerical characterization of dynamic hysteresis loops and losses in soft magnetic materials," *IEEE Transactions on Magnetics*, vol.41, no.5, pp.1540-1543, May 2005.

[46] N. Chiesa, H. K. Høidalen,. "Modeling of nonlinear and hysteretic iron-core inductors in ATP". *European EMTP-ATP Conference*. 2007.

[47] D. C. Jiles, "A self consistent generalized model for the calculation of minor loop excursions in the theory of hysteresis", *IEEE Transactions on Magnetics*, pp. 2602-2604. 1992.

[48] P. S. Moses, M. A. S. Masoum. "Modeling and analysis of the suppression of ferroresonance in nonlinear three-phase three-leg transformers." *IEEE Power and Energy Society General Meeting*, September 2011.

[49] B. Patel, et al., "Simulation of ferroresonance with hysteresis model of transformer at no-load measured in laboratory", *IEEE Region 10 Conference TENCON*, Hyderabad, India, November 2008.

6. General Conclusions

This doctoral thesis has illustrated the study of ferroresonance by going through different interesting areas such as: (1) Analyzing case studies of system level impacts, (2) improving analytical and prediction methods, (3) improving transformer models. Each area studied has contributed with relevant information about ferroresonance analysis, modeling and prediction. Chapter 2 has assisted to conclude that ATPDraw is a valid platform to develop power systems under ferroresonance situations. The software allows deep analysis of the phenomenon and also permits creating new analysis tools to assist the global understanding of ferroresonance.

This thesis has also presented the elaboration of computational tools for ferroresonance analysis enhancing the waveform classification and assisting the summarization of long parameter studies. The development of these tools is made in such a way that permits its easy implementation in any EMTP-like software. It also shows clearly and concisely the steps to follow for each implementation.

In Chapter 2, it is also possible to find the development of predictions techniques using high dimensional strategies. Such tools can identify the zones for each mode under a parameter variation. The 2D diagram is helpful for understanding the implication of some parameters in the final behavior of ferroresonance. The 3D diagram allows a better comprehension of the behavior of a power system while driven into a ferroresonant state; it also can be used to establish the roadmap of a hypothetical ferroresonant situation, pointing the safe zones in which the parameter under study should be selected. The 4D diagrams are presented as an approach to generate a general tool to characterize and predict any ferroresonance state in a given power system. While developing these techniques, it has been also possible to take advantage of the great computational power offered by parallel computing systems. With this last technique has been possible to summarize millions of simulations in a reasonable amount of computational time.

At the end of Chapter 2 some strategies are presented for the improvement of long parametric analyses. Those techniques have proved that the veracity of a parametric analysis involving any system value related to load or capacitances, among others, can be significantly affected just by changing the set up in the switch event, so much of the responsibility of the transient relies on the switching shift angle. In order to obtain the most precise representation of such cases, some effort should be addressed to approach the correct moment of the energization/de-energization event. It has also been demonstrated that The Harmonic Balance Method can be used as a predictive tool. Its capability to describe the behavior tendency of a system prone to ferroresonance makes it a powerful technique. At the same time, its simplicity makes it suitable to substitute large parametric analysis avoiding extensive time-domain simulations.

Several laboratory measurements have been obtained and compared to simulation models providing some insights on how the different ferroresonance modes can appear through energization and de-energization processes, and demonstrating the correctness of the Hybrid Transformer Model behavior for ferroresonance analysis. It has been conclude that the Hybrid Model is able to represent ferroresonance cases. However, some critical aspects have been located for the improvement in the accuracy of

waveform representation. Features such as individual leg nonlinearities representation can be enhanced in the model.

Situations where ferroresonance involves nonlinear sources have been addressed, and it has been proved that the oscillations presented in a ferroresonance event are highly dependent on the amount of power fed by the supply. In cases where the source can also be saturated, the unpredictability of the phenomenon increased. There is not a typical behavior and fundamentals waves can easily co-exist with highly chaotic waveforms. In addition, a model for a self-excited generator has been created, tested and validated with the purpose of having a nonlinear source to inquiring into the effects that ferroresonance may have in situations where to nonlinear inductor are presented in a system.

A novel technique has been introduced to obtain and implement the hysteresis cycle as a function of the linked flux. The uses of such technique facilitate greatly the inclusion of a deeply nonlinear effect in a single-phase transformer model, but, at the same time, keeping the simplicity of the traditional piecewise models, where sophisticated experiments are avoided. The implementation of the new hysteresis model is addressed to EMTP as any other technique presented in this thesis, however, it is explained in such a way that exporting it to any other computational software is possible.

The recently introduced π equivalent model has been enhanced with the inclusion of the hysteresis characteristics. The accuracy on waveform representation of the model has increase significantly allowing reproduce ferroresonance cases with sufficient precision. Several cases studies have been presented and analyzed involving ferroresonance ignition in a single-phase transformer. The cases consist of different situations and different maneuvers. Each case study has been used to validate the π equivalent model with the hysteresis characteristic by contrasting experimental results with the simulated ones obtained from the model.

In general, the topics addressed in this thesis mark a roadmap for researchers interested in the study of ferroresonance phenomenon ranging from complex power system modeling through nonlinear dynamic analysis to improving transformer modeling for ferroresonance representation. One of the main characteristic of the thesis is the flexibility in the system and methods implemented which, in spite of being implemented in ATPDraw, can be easily exported to any other software or mathematic analyzer such MATLAB or PSCAD.

There is still a wide list of tasks to do. The future work can be separated by areas:

(1) In modeling techniques, for both single- and three-phase transformer models there is still work to do. Single-phase models should improve even more the hysteresis representation to take into account the asymmetric loops. The three-phase model should consider two cases: the first one including the hysteresis representation, and the second one implementing a new topology of the core based in the π model structure.

(2) The prediction techniques have proven to be valid for ferroresonance analysis, however, they are still time consuming. It would be meaningful to apply an optimization technique in order to reduce the computation process and the time invested in the calculation of the maps.

(3) It is important to apply all the information collected in this thesis in developing mitigation techniques. For instance, the guidelines obtained from nonlinear analysis could help to create tools to damps the ferroresonance signal. Besides, the prediction maps such as the 3D and 4D can also be used to find the values in which the ferroresonance result in a damped oscillation. Thus a mitigation tool could move the system parameter to those safe zones when ferroresonance is igniting.